IChF
Institute of Physical Chemistry PAS

Institute of Physical Chemistry Polish Academy of Sciences
Kasprzaka 44/52
01-224 Warsaw, Poland

ICTER
International Centre for Translational Eye Research

International Centre for Translational Eye Research
Skierniewicka 10a
01-230 Warsaw, Poland

Ph.D. thesis

Structural characterization and conformational changes of Retinol Binding Protein 3

Luca Gessa

Supervisor: prof. dr. hab. Maciej Wojtkowski
Auxiliary supervisor: dr. Humberto Fernandes

Warsaw, September 2025

IChF
Institute of Physical Chemistry PAS

Institute of Physical Chemistry Polish Academy of Sciences
Kasprzaka 44/52
01-224 Warsaw, Poland

ICTER
International Centre for Translational Eye Research

International Centre for Translational Eye Research
Skierniewicka 10a
01-230 Warsaw, Poland

Ph.D. thesis

Structural characterization and conformational changes of Retinol Binding Protein 3

Luca Gessa

Supervisor: prof. dr. hab. Maciej Wojtkowski
Auxiliary supervisor: dr. Humberto Fernandes

Warsaw, September 2025

Funding and cooperation acknowledgment

This thesis was conducted at the International Centre for Translational Eye Research (ICTER).

The International Centre for Translational Eye Research (MAB/2019/12) project is carried out within the International Research Agendas programme of the Foundation for Polish Science co-financed by the European Union under the European Regional Development Fund.

This work has been supported by iNEXT-Discovery, grant number 871037, funded by the Horizon 2020 program of the European Commission.

Some of the results presented in this thesis have been realized with the support of the Institute of Biochemistry and Biophysics of the Polish Academy of Science (IBB PAS). My sincere gratitude goes to the International Institute of Molecular and Cellular Biology (IIMCB) and, in particular, to dr. Mariusz Czarnocki-Cieciura, for negative staining and cryoEM grid preparation. CryoEM grid screening was performed at the *Centre for New Technologies at the University of Warsaw (CeNT)*. CryoEM and cryoET datasets were acquired at the Central European Institute of Technology (CEITEC). TEM imaging has been performed at Nencki Institute of Experimental Biology (Nencki). Circular Dichroism measurements were performed at the European Molecular Biology Laboratory (EMBL) in Hamburg. CryoSXT data were collected at Diamond Light Source (Oxfordshire, UK).

Acknowledgment

Before showing any scientific results presented in this thesis, I feel mandatory to give thanks to all the people who helped me and made this possible.

I want to express my gratitude to prof. Maciej Wojtkowski for giving me the opportunity to pursue a PhD at ICTER.

I owe a huge thanks to my scientific mentor, dr. Humberto Fernandes, leader of the ISB group, not only for his ability to pass his knowledge, but especially for his constant guidance, support, patience, and readiness to help me.

Part of the results presented in this thesis have been possible thanks to the training I received in prof. Krzysztof Palczewski's lab and the help of the colleagues from the CTVR lab at the University of California, Irvine.

A big help came from the coordinators of the ISB group: dr. Joanna Krwawicz, dr. Magdalena Pieczynska-Kovacs, dr. Justyna Czarnecka and all the current and past members of the ISB group.

A very special thank you goes to dr. Vineeta Kaushik, my PostDoc senior, but most importantly, a close friend who stood by me through many challenges in the last 5 years. Her support, both scientifically and personally, has meant a great deal to me during this PhD.

My gratitude also goes to Poland and Warsaw, for warmly welcoming me and for this wonderful experience, thank you very much.

Let me use this space to give thanks also to all the previous mentors and high school teachers who contributed to shape my scientific mind set and reasoning: prof. Pål Falnes and dr. Jędrzej Małecki, my supervisors during my master degree at the University of Oslo, dr. Paolo Mereu, who supervised me during my bachelor thesis at University of Sassari, prof. Mario Arcamone and prof. Nicola Comerci, my mathematics and philosophy teachers, whose teaching profoundly influenced the way I think and reason.

Thanks also to all the members of the ISB group and all the new friends I met here, especially those who helped me when I broke my face with the scooter: Nelam, Arvind, Stefania, Abhishek, Shakeel, Lukasz, Swaraj, Behdokht. Besides the new friends, I cannot forget the old friends, in particular: Salvatore, Anthony, Luigi, Daniele, Antonio, Natalia, Fabio, and especially my best friend Giovanni.

Of course, I cannot fail to acknowledge all the staff- Doctors, nurses, and healthcare assistants- of the Nephrology Department of Sassari Civil Hospital Santissima Annunziata. My special thanks go to dr. Giovanna Serra and dr. Giacomina Loriga.

A huge thanks goes to my parents, my brother, and all my family members for their endless unconditional love and for believing in me even when I found it hard to believe in myself. A particular thought is for my Godchildren: Marco, Silvia, and Emanuele, if I managed to get a PhD, you can achieve much more.

The final thanks is for the St Paul's English Speaking Catholic Parish, which nourished my faith in God, the most important thing in my life.

Publications

1. Kaushik V, **Gessa L**, Kumar N, Fernandes H. Towards a New Biomarker for Diabetic Retinopathy: Exploring RBP3 Structure and Retinoids Binding for Functional Imaging of Eyes In Vivo. Int J Mol Sci. 2023 Feb 23;24(5):4408. doi: 10.3390/ijms24054408. PMID: 36901838; PMCID: PMC10002987.

2. Kaushik V, Dąbrowski M, **Gessa L**, Kumar N, Fernandes H. Corrigendum: Two-photon excitation fluorescence in ophthalmology: safety and improved imaging for functional diagnostics. Front Med (Lausanne). 2025A Feb 19;12:1572630. doi: 10.3389/fmed.2025.1572630. Erratum for: Front Med (Lausanne). 2024 Jan 03;10:1293640. doi: 10.3389/fmed.2023.1293640. PMID: 40046924; PMCID: PMC11881446.

3. Kaushik V*, **Gessa L***, Kumar N, Pinkas M, Czarnocki-Cieciura M, Palczewski K, Nováček J, Fernandes H. CryoEM structure and small-angle X-ray scattering analyses of porcine retinol-binding protein 3. Open Biol. 2025B Jan;15(1):240180. doi: 10.1098/rsob.240180. Epub 2025 Jan 22. PMID: 39837501; PMCID: PMC11750400.
   ***Equal first authors**

Abstract

Vision, perhaps the most crucial sense for human life, is a remarkably complex process that requires a tight orchestration of all the tissues, cells, and biomolecules of the eye. Specifically, the retina, located at the back of the eye, is the region where the light stimulus is converted into electrical impulses that the brain can interpret. The biochemical pathway responsible for this vital process that occurs in the photoreceptors is known as the phototransduction cascade. This process occurs when a photon hits the 11-cis retinal chromophore bound to rhodopsin, causing the conversion of 11-cis retinal into all-trans retinal, ultimately leading to the activation of the enzyme PDE6, hyperpolarization, and extension of the photoreceptors. In order to sustain vision, this biochemical pathway requires constant replenishment of the chromophore. This function is provided by the retinoid visual cycle, which occurs between the Retinal Pigment Epithelium and the photoreceptors through the Interphotoreceptor Matrix. Within the Interphotoreceptor matrix resides a protein known as RBP3, which is involved in the transport of the 11-cis retinal and other retinoid molecules between the photoreceptors and the Retinal Pigment Epithelium. In mammals, RBP3 consist of a single peptide chain of ~1300 amino acids. Since the RBP3 gene has undergone a quadruplication event, within the single peptide chain, it is possible to identify four homologous repeats known as Modules. Each of the Modules represents a functional unit capable of binding retinoids. Despite the important protective role in the retina's physiology, due to its ability to bind retinoids, the proper structural characterization of RBP3 has remained elusive. The target of the thesis is to provide a high-resolution structure of the protein in order to reveal the mechanism through which RBP3 is capable of maintaining a healthy retina. In order to achieve the target, two strategies were used. Given the size and the high flexibility of the protein and the unlikelihood to obtain suitable crystals, the first approach consisted in the study of the full-length protein through CryoEM in order to obtain a high-resolution structure of the entire architecture of the protein. The RBP3 high flexibility allows for conformational changes of the protein, and Small Angle X-ray Scattering was used to investigate the relationship between the ligand binding and the conformational changes in solution. The second approach consisted of the production of recombinant truncated versions of the protein (e.g., Modules), for crystallization in complex with the ligand in order to identify the retinoid binding sites.

Streszczenie

Wzrok, prawdopodobnie najważniejszy zmysł w ludzkim życiu, to niezwykle złożony proces, który wymaga ścisłej koordynacji wszystkich tkanek, komórek i biocząsteczek oka. Siatkówka, położona w tylnej części oka, to obszar, w którym bodziec świetlny jest przekształcany w impulsy elektryczne, które mózg może interpretować. Szlak biochemiczny odpowiedzialny za ten kluczowy proces zachodzący w fotoreceptorach, znany jest jako kaskada fototransdukcji. Proces ten zachodzi, gdy foton uderza w chromofor 11-cis retinalu związany z rodopsyną, powodując przekształcenie 11-cis retinalu w retinal all-trans, co ostatecznie prowadzi do aktywacji enzymu PDE6, hiperpolaryzacji i wydłużenia fotoreceptorów. Aby utrzymać widzenie, ten szlak biochemiczny wymaga stałego uzupełniania chromoforu. Funkcja ta jest zapewniana przez cykl wzrokowy retinoidów, który zachodzi pomiędzy nabłonkiem barwnikowym siatkówki a fotoreceptorami poprzez macierz międzyfotoreceptorową (Interphotoreceptor Matrix). W macierzy międzyfotoreceptorowej znajduje się białko znane jako RBP3, które bierze udział w transporcie 11-cis retinalu i innych cząsteczek retinoidów pomiędzy fotoreceptorami a nabłonkiem barwnikowym siatkówki. U ssaków RBP3 składa się z pojedynczego łańcucha peptydowego o długości ~1300 aminokwasów. Ponieważ gen RBP3 uległ czterokrotnej replikacji, w obrębie pojedynczego łańcucha peptydowego możliwe jest zidentyfikowanie czterech homologicznych powtórzeń znanych jako moduły. Każdy z modułów reprezentuje jednostkę funkcjonalną zdolną do wiązania retinoidów. Pomimo ważnej roli ochronnej w fizjologii siatkówki, ze względu na jej zdolność do wiązania retinoidów, właściwa charakterystyka strukturalna RBP3 pozostaje nieuchwytna. Celem pracy jest przedstawienie struktury białka o wysokiej rozdzielczości, aby odkryć mechanizm, dzięki któremu RBP3 jest w stanie utrzymać zdrową siatkówkę. Aby osiągnąć ten cel, zastosowano dwie strategie. Biorąc pod uwagę rozmiar i wysoką elastyczność białka oraz mało prawdopodobne uzyskanie odpowiednich kryształów, pierwsze podejście polegało na badaniu białka o pełnej długości za pomocą CryoEM w celu uzyskania struktury o wysokiej rozdzielczości całej architektury białka. Wysoka elastyczność RBP3 pozwala na zmiany konformacyjne białka, a rozpraszanie promieni rentgenowskich pod małymi kątami zostało wykorzystane do zbadania związku między wiązaniem ligandu a zmianami konformacyjnymi w roztworze. Drugie podejście polegało na produkcji rekombinowanych, skróconych wersji białka (np. modułów) do krystalizacji w kompleksie z ligandem w celu identyfikacji miejsc wiązania retinoidu.

List of abbreviations

µg, Microgram;

µm, Micrometer;

µl, Microliter;

µM, Micromolar;

11cRAL, 11-cis retinal;

11cROL, 11-cis retinol;

Å, Ångström;

A2E, N-retinylidene-N-retinylethanolamine;

ABCA4, ATP-binding cassette sub-family A member 4;

ATP, Adenosine Triphosphate;

atRAL, All-trans retinal;

atROL, All-trans retinol;

AWAT2, Acyl-CoA wax alcohol acyltransferase 2;

BRB, Blood-Retinal Barrier;

bp, Base pair;

Ca^{2+}, Calcium ion;

CC, Connecting Cilium;

CCO, Carotenoid Cleavage Oxygenase;

CD, Circular Dichroism;

CNS, Central Nervous System;

cGMP, Cyclic Guanosine Monophosphate;

CHAPSO, 3-(3-[Cholami dopropyl]dimethylammonio)-2-hydroxy-1-propanesulfonate;

CNGA1 channel, Cyclic Nucleotide-Gated Channel alpha-1;

CNGCs, cGMP-gated ion channels;

ConA, Concanavalin A;

CRALBP, Cellular retinaldehyde-binding protein;

CRBP1, Cellular Retinol Binding Protein 1;

CRX, Cone-Rod Homeobox;

CryoEM, Cryo Electron Microscopy;

CryoET, Cryo Electron Tomography;

CTF, Contrast Transfer Function;

DES1, Dihydroceramide desaturase-1;

DH5α, Douglas Hanahan 5-alpha;

DHA, Docosahexaenoic acid;

Dmax, Maximum particle dimension;

DNA, Deoxyribonucleic Acid;

DR, Diabetic retinopathy;

dNTP, Deoxynucleotide triphosphate;

DTT, Dithiothreitol;

E, Embryonic;

ELM, External Limiting Membrane;

ELISA, Enzyme-Linked Immunosorbent Assay;

ER, Endoplasmic Reticulum;

ERG, Electroretinogram;

FBS, Fetal Bovine Serum;

FSC, Fourier Shell Correlation;

FT, Flow Through;

Fuc, Fucose;

GAF domains, cGMP-dependent phosphodiesterases (PDEs), Anabaena adenylyl cyclases, and E. Coli FhlA domains;

Gal, Galactose;

GC, Guanylate cyclase;

GCAPs, Guanylyl Cyclase Activating Proteins;

GCL, Ganglion Cell Layer;

GDP, Guanosine Diphosphate;

GlcNAc, N-acetylglucosamine;

GLUT1, Glucose Transporter 1;

GMP, Guanosine Monophosphate;

GPCR, G-Protein Coupled Receptor;

GRK1, G protein-coupled receptor kinase 1 (aka rhodopsin kinase)

GST, Glutathione S-Transferase;

G_t, Transducin;

$G_{\alpha t}$, Transducin α subunit;

GTP, Guanosine Triphosphate;

GTPase, Guanosine Triphosphatase;

HEPES, 4-(2-hydroxyethyl)-1-piperazine ethanesulfonic acid;

HFCS, Hybridoma Fusion and Cloning Supplement;

HRP, Horse Radish Peroxidase;

iBRB, inner Blood-Retinal Barrier;

ILM, Internal Limiting Membrane;

IMPG1, Interphotoreceptor Matrix ProteoGlycan 1;

IMPG2, Interphotoreceptor Matrix ProteoGlycan 2;

INL, Inner Nuclear Layer;

IPL, Inner plexiform layer;

IPM, Interphotoreceptor Matrix;

IPTG, Isopropyl β-D-thiogalactopyranoside;

IRBP, Interphotoreceptor Retinoid Binding Protein;

IS, Inner Segment;

kb, Kilobase;

kDa, Kilodalton;

L, load;

LB, Lysogeny Broth;

LRAT, Lecithin Retinol Acyltransferase;

mAb5, Monoclonal Antibody 5;

MDM, Methyl α-D-mannopyranoside;

mm, Millimeter;

mM, Millimolar;

ml, Milliliter;

mRNA, Messenger Ribonucleic Acid;

mV, Millivolt;

NADH, Nicotinamide Adenine Dinucleotide (Reduced);

NADPH, Nicotinamide Adenine Dinucleotide Phosphate (Reduced);

ng, Nanogram;

nm, Nanometers;

NMR, Nuclear Magnetic Resonance;

NEAA, Non Essential Amino Acid;

NetNGlyc, Neural networks for prediction of N-linked Glycosylation;

NFL, Nerve Fiber Layer;

NP-40, Nonidet P-40;

OA, Oleic acid;

oBRB, outer Blood-Retinal Barrier;

OCT, Optical Coherence Tomography;

OD600nm, Optical Density at 600 nanometers;

ONL, Outer Nuclear Layer;

OPL, Outer Plexiform Layer;

ORF, Open Reading Frame;

ORG, Optoretinography;

OS, Outer Segment;

OTX2, Orthodenticle homeobox 2;

P, Post-natal;

PBS, Phosphate Buffered Saline;

PBST, Phosphate Buffered Saline Tween 20;

PCR, Polymerase Chain Reaction;

PDB ID, Protein Data Bank unique identifier;

PDE6, Phosphodiesterase 6;

PE, Phosphatidylethanolamine;

PEG, Polyethylene Glycol;

PMFS, Phenylmethylsulfonyl Fluoride;

PP2A, Protein Phosphatase 2A;

P(R), Pair-distance distribution function;

PR/EZ: Photoreceptor layer/ellipsoid zone (inner and outer photoreceptor segment junction);

PVDF, Polyvinylidene difluoride;

R9AP, RGS9 anchor protein;

RBP3, Retinol Binding Protein 3;

RBP4, Retinol Binding Protein 4;

RCF, Relative Centrifugal Force;

RDH, Retinol Dehydrogenase;

RetGC, Retinal guanylyl cyclases;

Rg, Gyration radius;

RGR, Retinal G-protein-coupled receptor;

RGS9, Regulator of G-protein Signaling 9;

RMSD, Root Mean Square Deviation;

RNFL, Retinal Nerve Fiber Layer;

ROS, Rod Outer Segment;

RPE, Retinal Pigmented Epithelium;

RPE65, Retinal Pigment Epithelium 65 kDa protein;

SAFT, Sample Application Flow Through;

SAXS, Small-Angle X-ray Scattering;

SDS, Sodium Dodecyl Sulfate;

SDS-PAGE, Sodium Dodecyl Sulfate Polyacrylamide Gel Electrophoresis;

SEC, Size-Exclusion Chromatography;

CryoSXT, Cryo Soft X-ray Tomography;

SPA, Single Particle Analysis;

SPACR (IMPG1), SialoProtein Associated with Cones and Rods;

SPACRAN (IMPG2), SialoProtein Associated with Cones and Rods Proteoglycans;

STRA6, Stimulated by Retinoic Acid 6;

T4, Bacteriophage T4;

TAE, Tris-acetate-EDTA;

TB, Terrific Broth;

TEM; Transmission Electron Microscopy;

TNF, Tumor Necrosis Factor Alpha;

TTR, Transthyretin;

U, Units of enzyme;

UV, Ultraviolet;

VEGF, Vascular Endothelial Growth Factor;

WT, Wild-Type;

Table of contents

1 Introduction

The vision is one of the most important senses in vertebrate animals; therefore, the eye is a critical organ for any aspect of the life of those animals. The human eyes are paired organs, presenting a slightly asymmetrical spheroid form with a diameter of 24 millimeters (mm) (Bron et al., 1997). According to a topographic division, the eye can be divided into the anterior segment and the posterior segment (Figure 1.1) (Anastasi et al., 2007).

1.1 Anatomy of the eye

The coat of the eyeball consists of three concentric tunics: the fibrous tunic, which represents the external delimitation of the eyeball, consists of the anterior and posterior portions. The anterior portion belongs to the anterior segment, which is named the cornea, while the posterior portion, which is part of the posterior segment, takes the name of the sclera (Castano et al., 1999). Internally to the fibrous tunic is located the vascular tunic (uvea), consisting of the choroid, ciliary body, and iris. The nervous tunic (the retina) is adherent to the choroid, from which it receives trophic support (Castano et al., 1999; Bill, 1984).

The anterior segment represents one-third of the eye, and it contains two main chambers: the anterior chamber, which is filled by the aqueous humor, is delimited by the cornea and the iris. The posterior chamber, which includes the crystalline lens and the ciliary body, is separated from the anterior chamber and the vitreous chamber by the iris and the zonular apparatus, respectively (Anastasi et al., 2007; Cioffi, 2020). The cornea is a transparent membrane consisting of five layers: the epithelium, which is separated by the stroma by the Bowman's membrane, and the endothelium, which is separated from the stroma by the Descemet's membrane (Gandhi and Jain, 2015). The crystalline is a biconvex transparent lens formed by three different tissues: capsule, anterior subcapsular epithelium, and lens substance (Kasturi and Matalia, 2017). It plays a crucial role in the accommodative process by which the eye changes its refractive power to keep an object in focus as it changes distance from the eye (Ruan et al., 2020). The cornea, together with the crystalline lens, constitutes the ocular dioptric system, responsible for the correct formation of the image in the retina (Caporossi, 2017).

The posterior segment represents two-thirds of the organ (Cioffi, 2020), and its major component is represented by the vitreous humor: a gelatinous mass consisting mainly of water with a minor portion of glycosaminoglycans and collagen fibrils (Standring, 2020). The vitreous is adherent to the retina, and it is essential for the maintenance of the proper shape of the organ and to provide mechanical support to the retina (Lee et al., 1992).

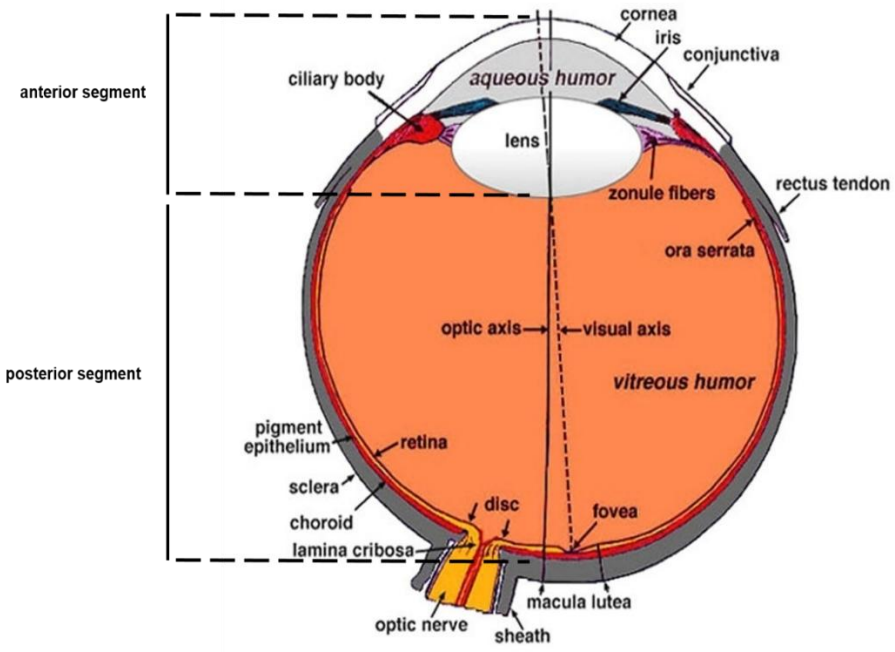

Figure 1.1: General anatomy of the human eye. Schematic representation of the main components involved in vision and segmentation of the eye. Picture taken and modified from (Kolb et al., 2005). http://webvision.med.utah.edu/

1.2 Anatomy of the retina

The retina is a sheet of different types of cells (epithelial, neural, and glial) that lies between the choroid and the vitreous humor. It covers the majority of the posterior segment, terminating at the level of the ora serrata (Standring, 2020), and it is the anatomical region where the light signals, thanks to the photoreceptor cells (rods and cones), are converted into electrical stimuli (Hall and Hall, 2021).

From the embryological and anatomical point of view, the retina is considered a part of the Central Nervous System (CNS) since it is derived from the optic vesicle, and it is considered an extension of the diencephalon (Barbieri and Carinci, 1997).

The retina is not homogenous throughout its extension since it is possible to identify specialized regions capable of performing specific functions in a more efficient way than the rest of the retina (Moore et al., 2017). Within those areas, in the human, it is possible to identify a central region known as macula lutea ("yellow spot") (Figure 1.2A), which contains a special region of the retina known as fovea (Fitzgerald et al., 2012). The fovea is a small depression at the centre of the eye (Figure 1.2B), presenting an extremely high density of cone cells (Fitzgerald et al., 2012), and it is the area with the highest visual acuity (Willmer, 1949). The concentration of cones, extremely high especially

in the foveola (the central part of the fovea, and completely rod-free), progressively decreases toward the peripheral retina, as does the vision acuity. In contrast, the ability to detect dim light stimuli is increased thanks to the higher sensitivity of the rod photoreceptors at the periphery (Purves et al., 2001) (Figure 1.2C).

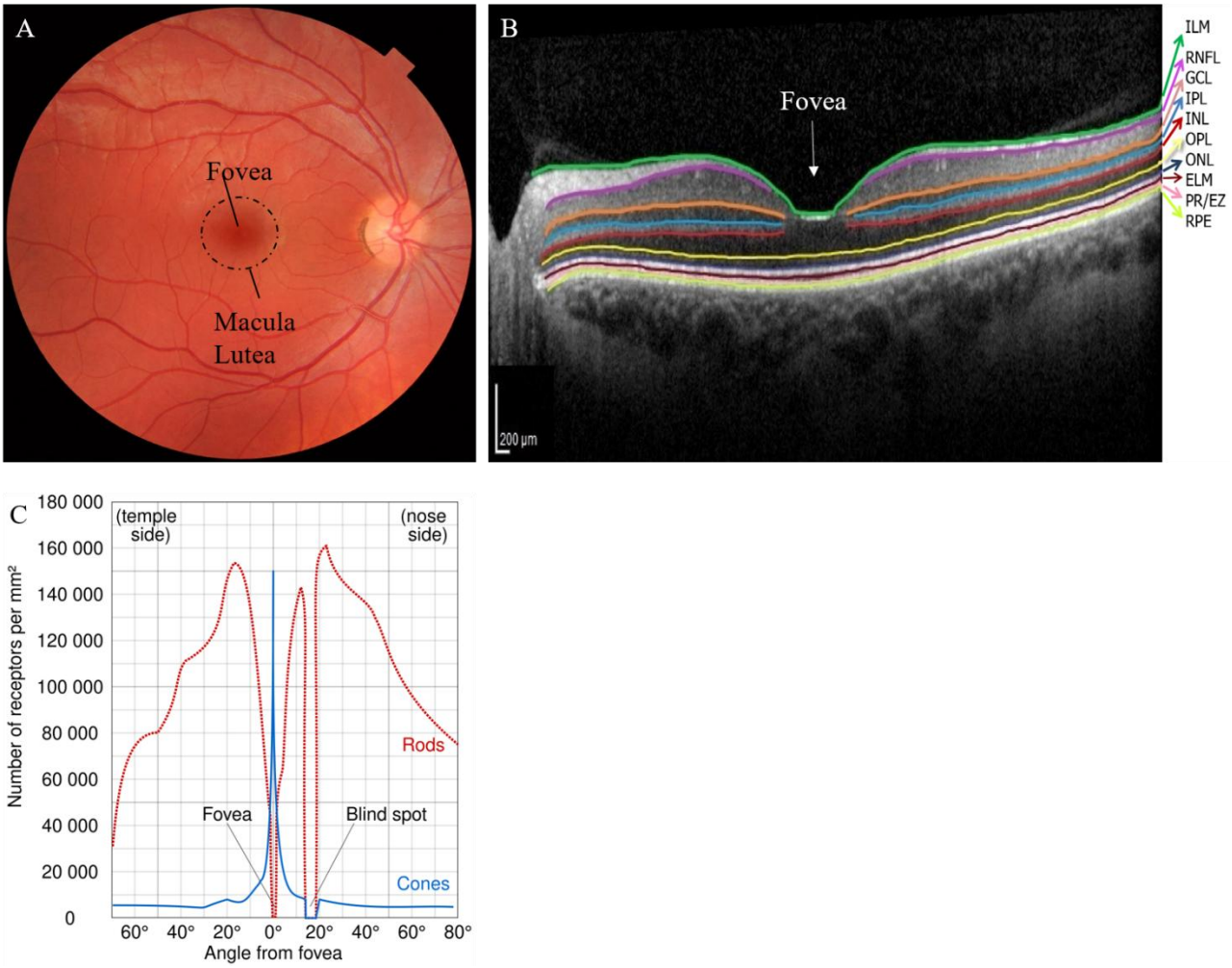

Figure 1.2: Eye fundus, retina layers, and photoreceptors distribution. *A) Fundus of the human retina, the circle encloses the macula lutea with the fovea at the center. Picture modified from Häggström (2014), public domain. B) Imaging of the retinal layers and the central depression (fovea) obtained with Optical Coherence Tomography (OCT), (ILM: Internal limiting membrane; RNFL: Retinal nerve fiber layer; GCL: Ganglion cell layer; IPL: Inner plexiform layer; INL: Inner nuclear layer; OPL: Outer plexiform layer; ONL: Outer nuclear layer; ELM: External limiting membrane; PR/EZ: Photoreceptor layer/ellipsoid zone (inner and outer photoreceptor segment junction; RPE: Retinal pigment epithelium). Picture taken from Ţălu and Nicoara 2021 under the licence CC BY-NC 4.0. C) Distribution of rod and cone densities in the retina. Picture taken from Cmglee 2019 – Own work, CC BY-SA 3.0, https://commons.wikimedia.org/w/index.php?curid=29924570.*

The blood required for the functioning of the retina (one of the most metabolically intensive tissues in the body) is provided by the central retinal artery, which irrorates the internal portion of the retina adherent to the vitreous body, and the short posterior ciliary artery which supply the outer layer of the retina comprising the Retinal Pigmented Epithelium (RPE) and the photoreceptors (Kiel, 2010; Uhl et al., 2020). In order to understand how the retina operates, it is necessary to examine its

multilayer architecture. The retina can be divided into the neural retina, containing the photoreceptors, and the RPE, which, although it is not considered a part of the neural retina, is in a tight relationship with it from a metabolic point of view (Ross and Pawlina, 2016; Kanow et al., 2017). The neural retina is separated from the blood circulation by the Blood-Retinal Barrier (BRB), which consists of an inner Blood-Retinal Barrier (iBRB), formed by the endothelial cells of the choroid, and an outer BRB (oBRB) formed by the RPE and the Bruch's membrane (Campbell and Humphries, 2013).

In total, 10 different layers can be identified in the whole retina (Figure 1.3) (Mescher, 2018). Starting from the outermost layer:

1. Retinal Pigmented Epithelium (RPE): a monolayer of epithelial cells required for the maintenance and shedding of the photoreceptors (Bok, 1993; Kevany and Palczewski, 2010) and other functions (Straus, 2005).
2. Photoreceptor layer: In this layer are localized the outer segments of rods and cones responsible for the detection of light stimuli and their conversion into electric stimuli (Pugh and Lamb, 1993).
3. External Limiting Membrane (ELM): It separates the extracellular spaces between photoreceptor inner segments and their nuclei (Chen et al., 2012A).
4. Outer Nuclear Layer (ONL): It is formed by the nuclei of rods and cones (Lujan et al., 2015).
5. Outer Plexiform Layer (OPL): The layer of the retina where photoreceptors form synapses with bipolar cells (Furukawa et al., 2020).
6. Inner Nuclear Layer (INL): Consists of the nuclei of several cells, mainly bipolar cells and horizontal cells (Remington, 2012).
7. Inner Plexiform Layer (IPL): It is the region where the bipolar cells form synapses with ganglion cells; this is also the operative region of the amacrine cells (Remington, 2012).
8. Ganglion Cell Layer (GCL): It is the layer where the nuclei of the ganglion cells are located (Koeppen and Stanton, 2018).
9. Nerve Fiber Layer (NFL): In this layer, the axons of the ganglion cells form the nerve fiber layer before converging to form the optic nerve (Standring, 2020).
10. Internal Limiting Membrane (ILM): It is the last layer and it separates the retina from the vitreous body (Heegaard et al., 1986; Standring, 2020).

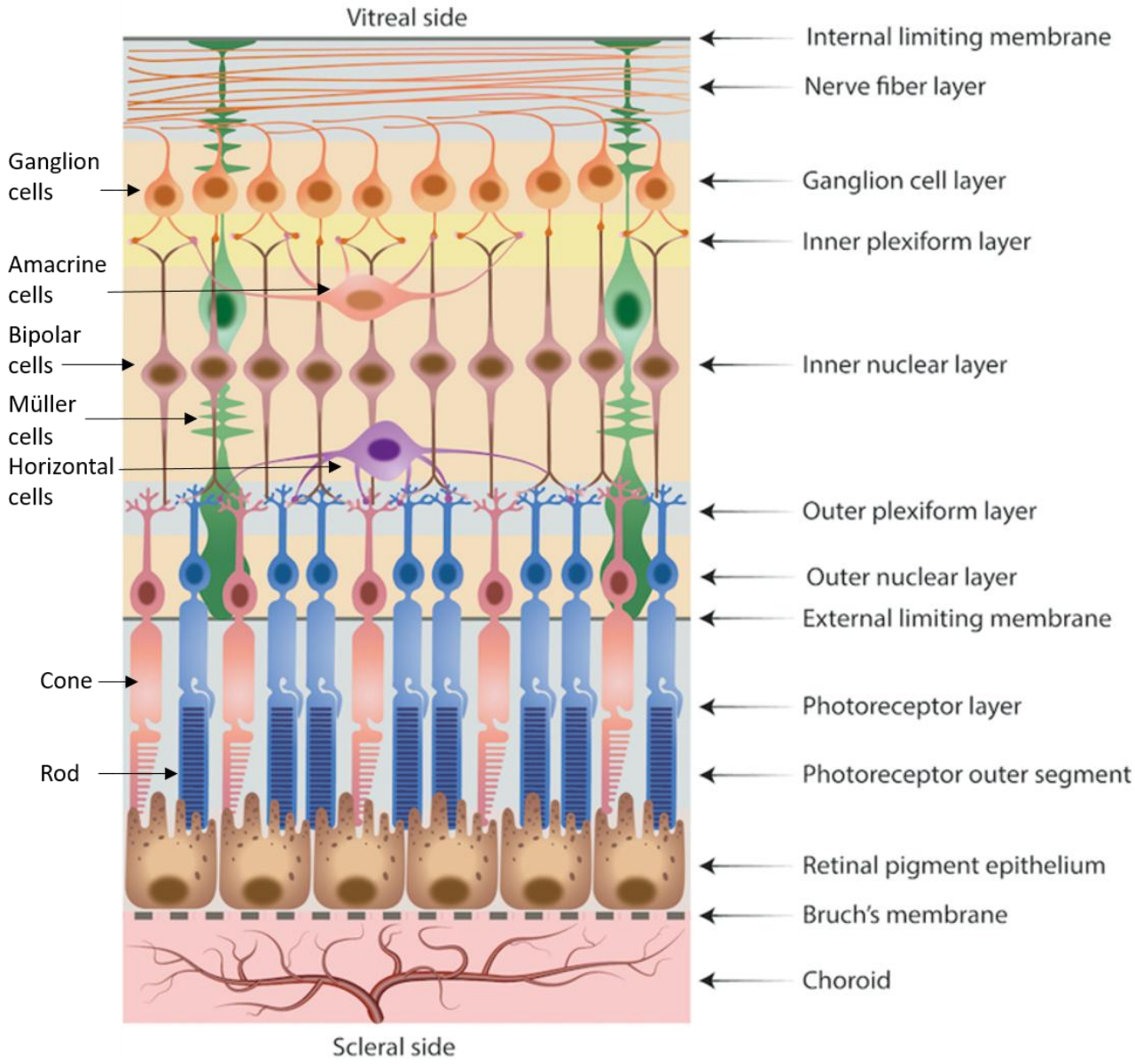

Figure 1.3: Schematic representation of the histological organization of the retina and its layer subdivision. Picture taken and modified from Ferrara et al., 2021 under the licence CC BY 4.0.

Given the inverted disposition of the retinal layer (Wirth et al., 1984), the photoreceptors lie on the opposite side of the light entrance; for this reason, the light must pass through all the retinal layers before hitting the outer segment of the photoreceptors (Figures 1.1 and 1.3).

Although the retina contains approximately fifty-five different cell types (Masland, 2001), considering the histology of the neural retina, it is possible to affirm that the most relevant cell types are the following: photoreceptors (rods and cones), bipolar cells, ganglion cells, amacrine cells, horizontal cells, and Müller cells (Figure 1.3). The photoreceptors and their nurturing RPE cells will be described in detail in the next sections; in this section, the focus will be on other cell types mentioned above, with brief descriptions.

Bipolar cells are interneuron cells; they consist of a soma from which departs one axon that connects with ganglion and amacrine cells and, in the opposite direction, one dendrite that forms synapses with the photoreceptors (Kaneko, 1979). According to the way the bipolar cells respond to the light stimulus, they can be divided into ON and OFF bipolar cells. The ON bipolar cells are active when light increases, and the OFF cells are activated when light decreases; this division is essential in object recognition (Ichinose and Habib, 2022).

Ganglion cells are the final receiver of the electric signal generated by the photoreceptors (Kerschensteiner, 2022). The dendrites of the ganglion cells can form synaptic connections with ON bipolar cells or OFF bipolar cells; thus, they can be distinguished in ON- and OFF-center (Van Wyk et al., 2009).

Horizontal cells are interneurons; although their soma is localized in the inner nuclear layer, they can establish synapses with photoreceptors at the outer plexiform layer (Standring, 2020). The activity of the horizontal cells is essential for the regulation of the photoreceptor response through inhibitory feedback (Chapot et al., 2017).

Amacrine cells are a broad group of cells classified as interneurons; their soma resides in the inner nuclear layer, and they are able to establish contacts with ganglion cells, bipolar cells, and other amacrine cells as well (Standring, 2020; Kolb et al., 1995). Importantly, they play an essential role in the regulation of the signal coming from the bipolar cells (Masland, 2012; Eggers et al., 2013).

Müller cells are the most abundant glial cells in the retina, although their nuclei localize in the inner nuclear layer, their extensions span from the internal limiting membrane to the external limiting membrane (Standring, 2020; Kadomoto et al., 2021). Müller cells are essential in retina physiology since they exert numerous functions, including mechanical support, metabolic support, antioxidant activity, and blood flow regulation (Coughlin et al., 2017; Reichenbach and Bringmann, 2013; Kobat and Turgut, 2020; Standring, 2020).

1.3 Retinal Pigment Epithelium and Interphotoreceptor Matrix

The retinal pigment epithelium consists of a single layer of cuboidal cells (12 micrometers (μm) height × 14 μm diameter) located between the photoreceptor layer and the Bruch's membrane, in close connection with the underlying choroid (Figure 1.3) (Standring, 2020). It is essential to take into consideration the embryological origin of RPE and the neural retina in order to understand the intertwined relationship between the RPE and the photoreceptors (Strauss, 2005) (Figure 1.4). The invagination process of the optic vesicle leads to the formation of the optic cup consisting of an inner

layer, whose cells will give rise to the neural retina, and an outer layer that will develop to form the RPE, with the space between the inner and outer layer later becoming the Interphotoreceptor Matrix (IPM) (Figure 1.4 and 1.5) (Bales et al., 2025; Edward and Kaufman, 2003; Strauss, 2005).

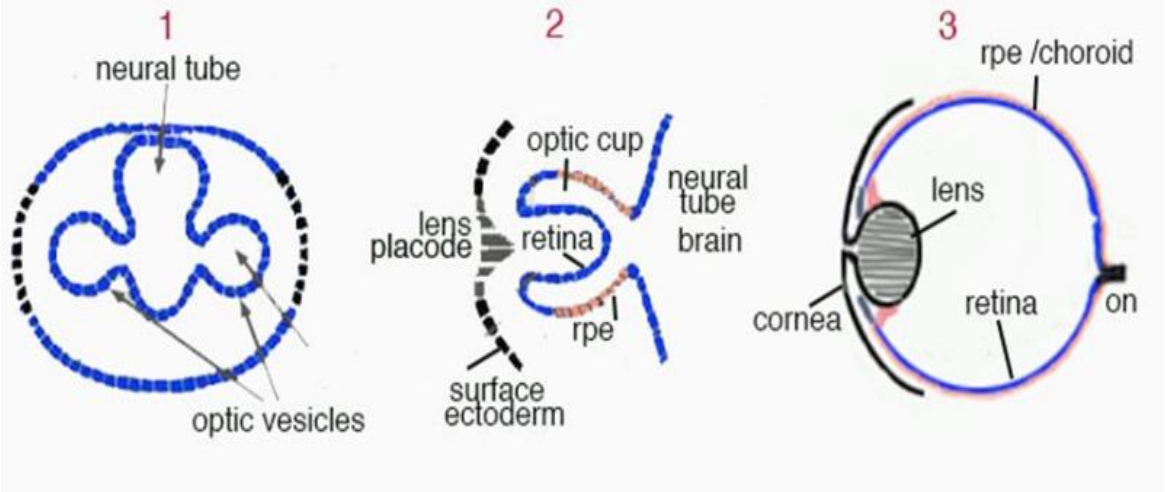

Figure 1.4: Cartoon representation of optic cup development. (Aliancy and Mamalis, 2017). Formation process of the optic cup (1) and its development leading to the formation of the RPE and inner retina, separated by a space that will become the IPM (2). Final formation of the eye (3). http://webvision.med.utah.edu/

The RPE cuboidal cells are a clear example of polarized cells with striking differences between the basal and the apical surface (Marmorstein, 2001). The first difference easily identifiable between the apical and the basal side of RPE cells is the morphology, the apical side of the membrane presents small extroflection of the plasma membrane known as microvilli which extend from the soma of the cell and infiltrate the photoreceptor layer to occupy the space between the outer segments of the photoreceptors (Figure 1.5) (Bonilha et al., 2006). The basal membrane of the RPE is not completely adherent to Bruch's membrane but presents small invagination known as "basal infoldings" that are essential to increase the cell surface area involved in the transport of various molecules with the choroid (Bonilha et al., 1999; Hayes et al., 2019). The lateral side of the RPE plasma membranes presents tight junctions that form a belt-like structure between adjacent cells, creating a continuous barrier that prevents the paracellular movement of molecules between the RPE cells (Rizzolo et al., 2011). This feature is essential for the proper functioning of the BRB (Figure 1.5) (Campbell and Humphries, 2013).

RPE plays several critical functions in retina physiology, including:

1. Light absorption: RPEs are equipped with specific organelles known as melanosomes, which have a high content of melanin, providing RPE with the ability to absorb light and prevent photodamage of the retina (Herman and Steinberg, 1982; Boulton et al., 2001).

2. Epithelial transport: As previously mentioned, the RPE is part of the BRB, and the passage of molecules and ions can occur only through the transcellular path; therefore, the RPE acts as a selective barrier regulating the transport of various solutes (Strauss, 2014).
3. Retinoid transport and regeneration: the RPE plays a crucial role as a receiver of all-trans retinol from the bloodstream as well as its recycling from photoreceptors and its conversion into 11-cis retinal required for phototransduction (Kiser et al., 2014).
4. Photoreceptor shedding: The constant exposure to light causes oxidative stress to the photoreceptor's discs, which need to be constantly renewed and regenerated. The RPE is essential in the phagocytosis of the outer segment of the photoreceptors (Xu et al., 2024; Kevany and Palczewski, 2010).
5. Secretion: The RPEs are involved in the secretion of several proteins important for the proper functioning of the retina, like growth factors, and inhibitors of matrix metalloproteases (Strauss, 2005).
6. Immune privilege: the RPE has the ability to synthesize molecules that regulate the immunological activity contributing to the immune privilege of the retina (Taylor et al., 2021).

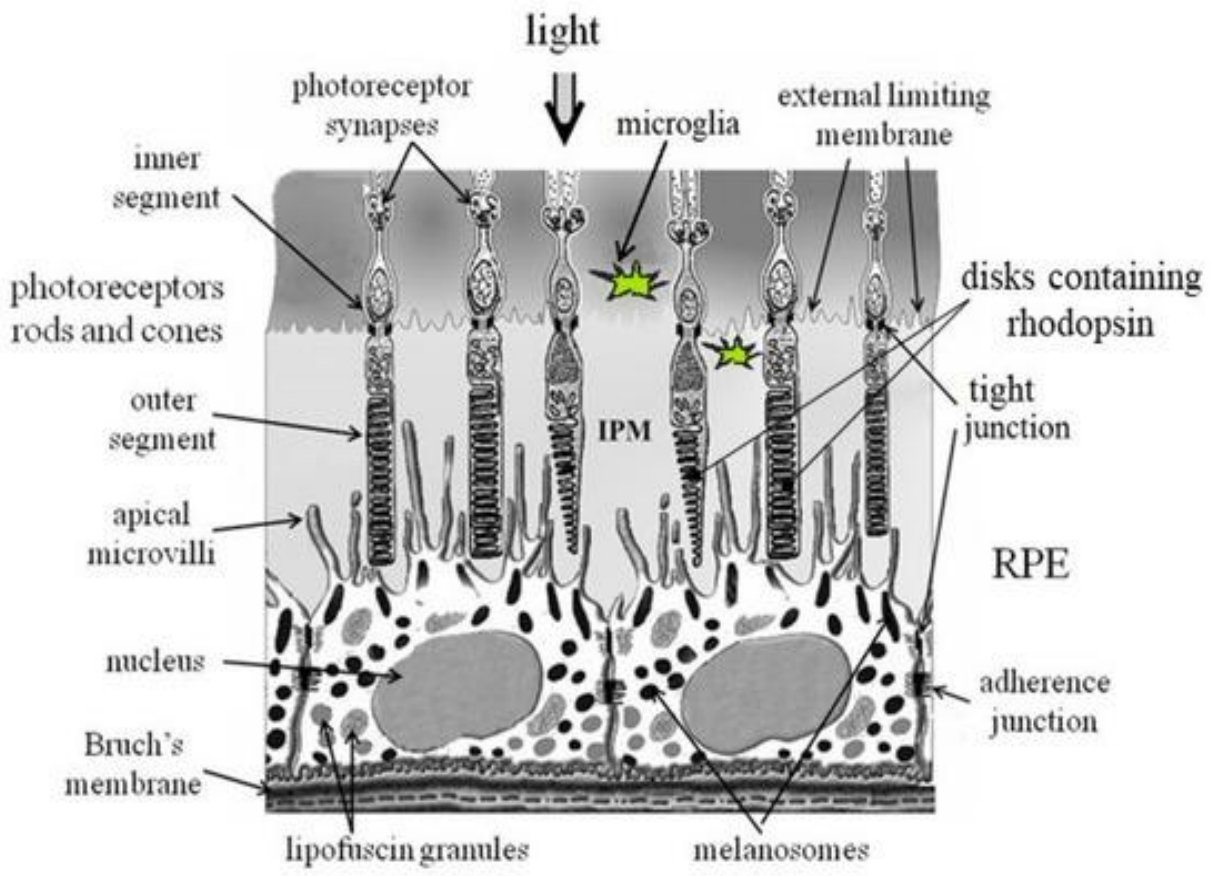

Figure 1.5: Schematic representation of RPE and photoreceptor complex. Picture taken from Dontsov and Ostrovsky, 2024. Creative Commons Attribution (CC BY) license (https:// creativecommons.org/licenses/by/ 4.0/).

The space between the RPE microvilli and the photoreceptor's outer segment, known as the subretinal space, is filled by the IPM (Johnson et al., 1986). The most representative molecular components of the IPM are: glycoproteins, growth factors, chondroitin sulfates, glycosaminoglycan, and proteoglycan (Ishikawa et al., 2015). Amongst the several soluble proteins present in the IPM, the most abundant is Retinol Binding Protein 3 (RBP3), also known as Interphotoreceptor Retinoid Binding Protein (IRBP), which plays an important role in the retinoid visual cycle (Cunningham et al., 1999). Other important components are the SialoProtein Associated with Cones and Rods (SPACR) (encoded by the Interphotoreceptor Matrix ProteoGlycan 1(IMPG1) gene), an important sialoprotein associated with cones (Acharya et al., 1998), and SialoProtein Associated with Cones and Rods proteoglycan (SPACRAN) (encoded by the Interphotoreceptor Matrix ProteoGlycan 2 (IMPG2) gene), a chondroitin sulfate proteoglycan that can bind hyaluronan (Acharya et al., 2000). The IPM also presents high levels of hyaluronan and sulfated molecules such as chondroitin sulfates and heparan sulfates (Clark et al., 2011). Overall, the IPM plays an essential role in mediating the interactions between the RPE and the photoreceptors and in nutrient transport (Ishikawa et al., 2015).

1.4 Photoreceptors

The term "photoreceptors" is used to indicate two different groups of sensory neurons: rods and cones. These cells are required for the first steps of the conversion of the light stimulus into an electrical signal in the process known as phototransduction (which will be described in detail in the next section). Cones are responsible for the photopic vision and allow the color perception, while rods are instead activated by low levels of light and allow the scotopic vision (Boron and Boulpaep, 2016). Although rods and cones respond to light differently, these polarized cells present a similar segmentation in which it is possible to identify five different common components: Outer Segment (OS), Connecting Cilium (CC), Inner Segment (IS), cell body, and synaptic terminal (Figure 1.6) (Molday and Moritz, 2015).

The OS is the photoreceptive portion of the cells; in rods, it consists of a thin cylindrical-shaped tube containing a series of carefully aligned membranous flattened discs originating from evagination of the plasma membrane (Ding et al., 2015; Pugh Jr, 2015; Pöge et al., 2021), with all the necessary proteins to complete the phototransduction cascade. Although functionally similar, the cone OS presents differences from the rod counterpart; first of all, as the name suggests, they present a cone shape, and since they consist of parallel folding of the plasma membrane, the continuity of the plasma membrane is not interrupted (Mustafi et al., 2009). The renewal process of OS is equal for rods and

cones; the discs are formed at the level of the connecting cilium, and their tips are constantly phagocytized by the RPE (Mustafi et al., 2009).

The OS is connected to the IS through the CC, a narrow structure homologous to the transition zone of the motile cilia (Röhlich, 1975; Besharse and Horst, 1990). This portion of the photoreceptor, being the only connection between the photosensitive part and the rest of the cell, plays several critical roles. In particular, the CC regulates the delivery of enzymes and photosensitive membranes to the OS, and it acts as a gate that regulates the compartmentalization of the opsin (Spencer et al., 1988; Besharse and Horst, 1990).

In the IS, it is possible to identify two sub-regions known as the ellipsoid and the myoid region (Wensel et al., 2016). The ellipsoid region presents an abundance of mitochondria, which are the region that provides energy to the rest of the cell (Yordi et al., 2024). The myoid region presents the endoplasmic reticulum (ER), the Golgi apparatus, and free ribosomes, and it is the region of the cells where the proteins are synthesized (Hart, 2009). Overall, the inner segment is the region that contains the majority of ion channels involved in the setting of the membrane potential that modulates the signal coming from the phototransduction (Baker and Kerov, 2013).

In a more distal position from the IS lies the soma of the cell, which contains the nucleus. It is interesting to note that the organization of the chromatin is different between diurnal and nocturnal species. In diurnal animals, the heterochromatin is located at the periphery of the nucleus, while the euchromatin is located toward the center. In nocturnal ones, this disposition is inverted (Solovei et al., 2009; Wensel et al., 2016).

The synaptic terminal portion of the photoreceptor lies in the OPL of the retina, where it forms synapses with the bipolar cells and horizontal cells. The main feature of both cones' and rods' synaptic terminals is the presence of an electron-dense structure named synaptic ribbon, which is necessary to keep a continuous tonic-graded neurotransmission during light conditions (Mercer and Thoreson, 2011). Both photoreceptors release glutamate as a neurotransmitter (Zang and Neuhauss, 2021).

While the human retina contains only one type of rod, the cones can be classified into three distinct subtypes according to the different opsins they express and therefore the different spectral sensitivity (Figure 1.6). In particular, it is possible to distinguish the cones in the S cone, which expresses S-opsin showing a peak sensitivity at 420 nanometers (nm), the M cone, which expresses M-opsin showing a peak sensitivity at 534 nm, and the L cone, which expresses L-opsin and has a peak sensitivity at 564 nm (Hussey et al., 2022).

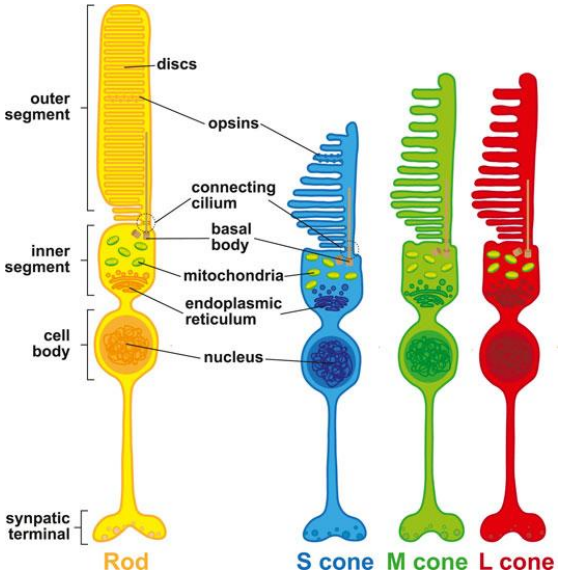

Figure 1.6: Photoreceptor morphology and different cone subtypes. Depicted are the Rod photoreceptor and the three (S, M, and L) human Cone photoreceptors. Picture taken from Hussey et al., 2022 under the license: creative commons attribution license (CC BY).

1.5 Phototransduction

Phototransduction is the name used to indicate the series of biochemical reactions that convert the light stimulus into an electric signal. These reactions occur in the outer segment of the photoreceptors, on the disc surfaces, and will cause changes in the membrane potential of the plasma membrane, leading to the hyperpolarization of the photoreceptor (Figure 1.7) (Kramer, 2015).

The principal molecular components of this cascade are the following (Kramer, 2015):

- 11-cis retinal: the chromophore responsible for the absorption of the photon and opsin activation.
- Opsin: rhodopsin in rods and cone opsin in cones are G-Protein Coupled Receptor (GPCR) proteins activated by light (Peng et al., 2024).
- Transducin: a protein that mediates the signal coming from the opsin to the phosphodiesterase
- Phosphodiesterase 6 (PDE6): degrades cGMP.
- cGMP-gated ion channels (CNGCs): closure causes hyperpolarization of the cells.
- Guanylate cyclase (GC) and Guanylyl Cyclase Activating Proteins (GCAPs): restore the cGMP levels.
- Arrestin: required for the inactivation of rhodopsin.

The term cone opsins refers to a group of visual pigments responsible for photopic vision. They can be further divided according to their responsive wavelength into long-, medium-, and short-

wavelength cone opsins. Although structurally similar to rhodopsin, small variations in the amino acid sequence alter their spectral sensitivity (Peng et al., 2024). Rhodopsin consists of ~ 350 amino acids organized

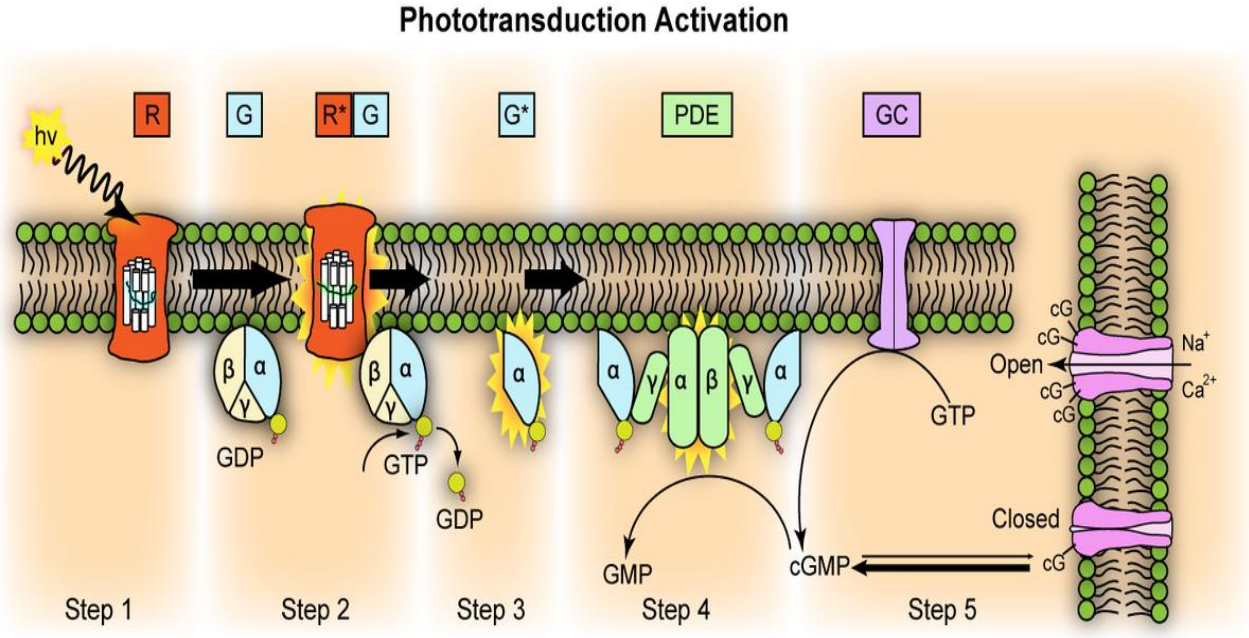

*Figure 1.7: Phototransduction cascade activation in light conditions. R stands for Rhodopsin, G for Transducin (with its α, β, and γ subunits), PDE6 for phosphodiesterase 6 (with its α, β, and γ subunits), and GC for Guanylate cyclase. * stands for activated, hv photon energy, GMP Guanosine Monophosphate, cGMP Cyclic Guanosine Monophosphate, GDP Guanosine Diphosphate, GTP Guanosine Triphosphate, Na^+ Sodium ion, and Ca^{2+} Calcium ion. Picture taken from: Jason J. Corneveaux, http://en.wikipedia.org/wiki/File:Phototransduction.png under the license: creative commons attribution license CC BY 3.0.*

in seven transmembrane α-helices and several post-translational modifications, including glycosylation, palmitoylation, and acetylation (Filipek et al., 2003). In dark conditions, the 11-cis retinal is bound to the lysine residue 296 of rhodopsin through a Schiff base (Palczewski et al., 2000). In this condition, the 11-cis retinal acts as an inverse agonist, preventing rhodopsin from triggering the other proteins of the phototransduction (Kono and Crouch, 2010; Kramer, 2015). Once a photon hits the chromophore, it leads to isomerization of the chromophore into the all-trans retinal state, and rhodopsin will undergo a series of conformational changes: bathorhodopsin, lumirhodopsin, metarhodopsin I, to finally reach the active state of metarhodopsin II (Zhou et al., 2012). Once reached the active state, metarhodopsin II will interact and activate Transducin (Hargrave et al., 1993). Transducin (G_t) is a heterotrimeric G protein consisting of α, β, and γ subunits capable of binding GDP and GTP (Fung, 1983). In dark conditions, the three subunits are united in a tight complex with GDP bound to the α subunit. After the light stimulus, the activated metarhodopsin II will elicit the exchange of GDP with GTP, leading to the dissociation and activation of $G_{\alpha t}$ (Transducin α subunit) (Ivey et al., 2010; Noel et al., 1993; Kramer, 2015). The last protein involved in the phototransduction cascade is PDE6. PDE6 is a heterotetrameric protein that is present in two different isoforms for cones

and rods. It consists of two inhibitory γ subunits and two catalytic subunits. In rods, the catalytic core of the protein is formed by an αβ heterodimer, while in cones it is a homodimer of two α' subunits (Majumder et al., 2015; Cote et al., 2022; Singh et al., 2025). Each subunit of the catalytic core contains two, cGMP-dependent phosphodiesterases (PDEs), Anabaena adenylyl cyclases, and *E. Coli* FhlA (GAF) domains (GAFa and GAFb) and a catalytic domain at the C-terminal; however, of the two GAF domains, only GAFa is capable of binding a cGMP molecule (Singh et al., 2025; Cote et al., 2022), as an allosteric regulator of the catalytic domains that bind cGMP and convert it to GMP. Transducin and PDE6 are classified as peripheral membrane proteins since they are attached to the lipid bilayer through prenylation, which is essential for their proper functionality (Lai et al., 1990; Moakedi, 2024). Two activated molecules of $G_{\alpha t}$ GTP bound will interact with the γ subunits and the catalytic core of PDE6, leading to its activation and starting cGMP hydrolysis (Gao et al., 2020). The activity of PDE6 leads to a decrease in cGMP concentration and subsequently the closure of the Cyclic Nucleotide-Gated Channel alpha-1 (CNGA1) channel, blocking the influx of calcium and sodium, ultimately causing a decrease in the membrane potential from -40 milliVolts (mV) up to -70 mV according to the intensity of the light stimulus (Kramer, 2015). When the calcium concentration is reduced, the interaction between the membrane proteins of the glutamate vesicle and the plasma membrane is inhibited, blocking the fusion and the exocytosis of the glutamate vesicle (Morgans, 2000). Once the light stimulus is terminated, the membrane potential must immediately return to the resting state. This target is achieved through the following mechanisms (Kramer, 2015):

- Rhodopsin deactivation through phosphorylation and interaction with arrestin (Wilden, 1995).
- Hydrolysis of the GTP molecules bound to activated $G_{\alpha t}$ (Sagoo and Lagnado, 1997).
- PDE6 deactivation (Kramer, 2015).
- Restoration of cGMP concentration level through the activity of retinal guanylyl cyclases (RetGC) and re-opening of the CNGA1 channels (Ames, 2022).

Rhodopsin deactivation is an essential mechanism that is required to switch off the phototransduction cascade. Rhodopsin deactivation is obtained through two steps: phosphorylation and arrestin binding (Xu et al., 1997; Mendez et al., 2000). Rhodopsin phosphorylation is catalyzed by G protein-coupled receptor kinase 1 (GRK1) in multiple serine and threonine residues, leading to a reduced catalytic activity, but more importantly, facilitating arrestin binding and completely stopping rhodopsin activity (Hurley et al., 1998; Vishnivetskiy et al., 2007; Berry et al., 2016). Arrestin binding to phosphorylated rhodopsin, in turn, facilitates the dephosphorylation of rhodopsin catalyzed by the Protein Phosphatase 2A (PP2A), bringing rhodopsin to the ground state (Kolesnikov et al., 2017; Hsieh et al., 2022). Another essential step required to switch off the phototransduction cascade is the

inactivation of transducin, which is obtained through the hydrolysis of $G_{\alpha t}$-GTP into $G_{\alpha t}$-GDP-bound (Kramer, 2015). The hydrolysis of the GTP is partially achieved through the intrinsic GTPase activity of transducin itself; however, the complete shutdown of transducin activity requires the presence of the GTPase activating complex formed by Regulator of G protein Signaling 9 (RGS9), Gβ5, and RGS9 anchor protein (R9AP), which enhances the GTP hydrolysis (Gospe et al., 2011; Shim and Chen, 2012). Deactivation of transducin is an essential step since it leads to deactivation of PDE6 and consequent stoppage of cGMP hydrolysis. The complete restoration of the intracellular cGMP level is achieved by the activation of the RetGCs, which catalyze the conversion of GTP into cGMP (Kramer, 2015). RetGCs are transmembrane proteins in which it is possible to distinguish six structural domains: extracellular domain, transmembrane domain, juxtamembrane domain, kinase homolog domain, dimerization domain, and catalytic domain (Koch and Dell'Orco, 2015). RetGC's activity is regulated by GCAPs, which in dark conditions (with high calcium levels) bind calcium atoms and keep the retGCs in the inactive form. After the light stimulus and the subsequent decrease in calcium level, the bound calcium atoms are replaced by magnesium, leading to activation of the retGCs and thus restoration of the cGMP levels (Ames, 2021; Avesani et al., 2021).

1.6 Retinoid visual cycle

As previously described in the phototransduction section, the 11-cis retinal is the essential chromophore required to trigger the phototransduction cascade, since with light stimulus it is converted into all-trans retinal. Thus, a constant supply and recycling is needed in order to sustain the vision. This function is provided by the retinoid visual cycle, which exists in two forms: the canonical visual cycle (Figure 1.8) between the RPE and the photoreceptors, and the cone-specific retina visual cycle, which involves the Müller cells (Figure 1.9) (Sato and Kefalov, 2024). In mammals, the sources of retinoid are represented by the absorption from the diet of vitamin A and pro-vitamin A carotenoids, with β,β-carotene being the most relevant (Kiser et al., 2014). After conversion into all-trans retinol, it will form a complex with the Retinol Binding Protein 4 (RBP4) (D'ambrosio et al., 2011; Cioffi, 2020; Steinhoff et al., 2021). RBP4 is a 21 kiloDalton (kDa) protein showing a β-barrel core capable of binding one molecule of all-trans retinol. The binding of all-trans retinol induces a conformational change in RBP4, increasing its affinity for the protein Transthyretin (TTR) and allowing the formation of the complex holo RBP4-TTR (Newcomer and Ong, 2013; Steinhoff et al., 2021). TTR is a 55 kDa protein consisting of four identical subunits. Its association with RBP4 is essential to form the complex all-trans retinol-RBP4-TTR. The increased molecular weight of the complex prevents the removal of RBP4 from the blood circulation by glomerular filtration (Kanai et

al., 1968; Liz et al., 2020; Yadav et al., 2025). For the intracellular uptake of all-trans retinol, the interaction of the RBP4-TTR complex with the transmembrane receptor known as Stimulated by Retinoic Acid 6 (STRA6) (Cioffi, 2020), present in the basal side of RPE cells, it is required. *Danio rerio* STRA6 is a symmetric dimer; the monomers present 9 transmembrane α-helices and one intramembrane α-helix.

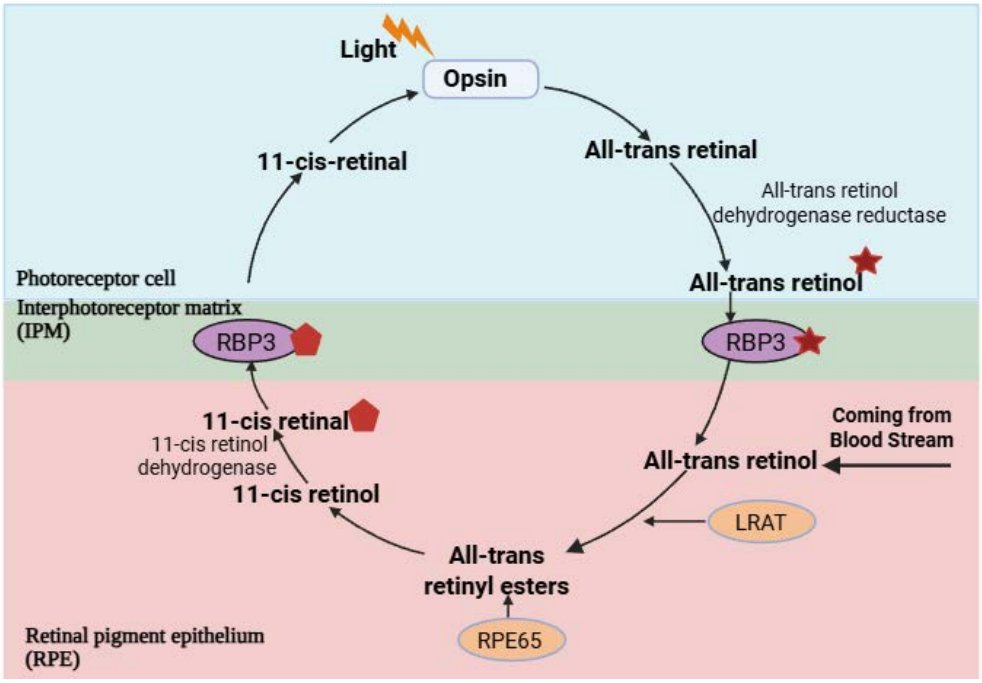

Figure 1.8: Classical retinoid visual cycle. The blue, green, and pink backgrounds represent the Photoreceptors, IPM, and RPE cells, respectively. All-trans retinol first enters the cycle through the bloodstream, and is later recycled through the visual cycle. Picture taken from Kaushik et al., 2023 under the license CC BY 4.0 (https://creativecommons.org/licenses/by/4.0/).

Interestingly, each monomer, at the cytosolic side, is associated with one calmodulin molecule (Chen et al., 2016). With the entrance of all-trans retinol into RPE cytosol being facilitated by the association of STRA6 with Cellular Retinol Binding Protein 1 (CRBP1) and Lecithin Retinol Acyltransferase (LRAT), the classical retinoid visual cycle can begin (Kawaguchi et al., 2011; Cioffi, 2020) (Figure 1.8). CRBP1 binds all-trans retinol within a cavity formed by two β-sheets, each consisting of five antiparallel β-strands (Napoli, 2016). CRBP1 is essential for the storage and protection of all-trans retinol from degradation and for the regulation of its metabolism since the association of holo CRBP1 with LRAT allows the esterification of all-trans retinol into retinyl esters, while apo CRBP1 inhibits LRAT activity (Napoli, 2016). LRAT is a 25 kDa membrane protein localized in the ER, with its catalytic domain exposed toward the cytosolic side. It is able to catalyze the esterification of all-trans retinol with phosphatidylcholine, leading to the formation of retinyl esters (Moise et al., 2007). The retinyl esters produced by the activity of LRAT can be stored in lipid droplets known as retinosomes or used directly by the Retinal Pigment Epithelium 65 kDa protein (RPE65) (Imanishi et al., 2004).

Being localized in the ER and associated with LRAT and Retinol Dehydrogenase 5 (RDH5), RPE65 is a crucial enzyme in the retinoid visual cycle since it is responsible for the isomerization of all-trans retinyl ester into 11-cis retinol (Cioffi, 2020). From the evolutionary point of view, RPE65 is classified as a Carotenoid Cleavage Oxygenase (CCOs); however, it does not show oxygenase activity (Kiser et al., 2014). RPE65 consists of a seven-bladed β-propeller; all of the blades have a residue that coordinates with the same iron cofactor, which is essential for the catalytic activity (Kiser et al., 2009). The 11-cis retinol molecule produced by RPE65 must be further oxidized to 11-cis retinal in order to form a Schiff base with rhodopsin (Palczewski and Kiser, 2020). The oxidation of the alcohol group to an aldehyde is obtained through the activity of RDH5 and RDH11 (Cioffi, 2020). Unfortunately, there are no experimental structures deposited for these two proteins, limiting the understanding of the structure-function relationship, however, although they both catalyze the oxidation of 11-cis retinol to 11-cis retinal, biochemical studies highlighted several differences between these two proteins relative to the cofactor used (RDH11 prefer Nicotinamide Adenine Dinucleotide Phosphate Reduced (NADPH) while RDH5 uses Nicotinamide Adenine Dinucleotide Reduced (NADH)) and substrate specificity (RDH5 can recognize only cis retinoids while RDH11 can oxidize also all-trans retinoids) (Parker and Crouch, 2010). The 11-cis retinal molecule is promptly bound by an intracellular protein named cellular retinaldehyde-binding protein (CRALBP) (Kiser et al., 2014). CRALBP is a 36 kDa protein capable of binding only retinoids in the cis isomer form (11-cis retinoid and 9-cis retinoid) in a hydrophobic cavity, which is formed by five β-strands opposed to three α-helices (Saari and Crabb, 2005; He et al., 2009). CRALBP activity is essential to protect and transfer the chromophore from the RPE to the IPM, where it can be bound by RBP3 and transported to the photoreceptor discs through a non-completely understood mechanism (Cioffi, 2020; Santos et al., 2025). Once the 11-cis retinal chromophore has reached the photoreceptor, it can form a Schiff base with opsin and start the phototransduction previously described. Once a photon hits the chromophore, it will trigger its isomerization to all-trans retinal. Given its cytotoxic effect and its ability to form bisretinoid products, all-trans retinal needs to be recycled in order to preserve the health of the retina. This task is performed by two proteins, namely ABCA4 (ATP-binding cassette sub-family A member 4) and RDH8 (Sparrow et al., 2010; Sparrow et al., 2012; Chen et al., 2012B). The all-trans retinal has the ability to form a Schiff base with the phosphatidylethanolamine (PE), forming the N-retinylidene-PE (Sparrow et al., 2010). N-retinylidene-PE is recognized by a protein localized in the rims of the outer segment disc membranes named ABCA4 (Beharry et al., 2004). ABCA4 is a single polypeptide chain of 256 kDa that can be divided into two homologous halves. In each half, it is possible to identify an exocytoplasmic domain oriented in the lumen of the disc, a transmembrane domain, a cytoplasmic nucleotide-binding domain, and a regulatory domain,

both localized in the cytoplasm (Liu et al., 2021). Using the energy derived from Adenosine Triphosphate (ATP) hydrolysis, ABCA4 is capable of translocating the N-retinylidene-PE from the disc lumen to the cytoplasmic side; therefore, after the hydrolysis of the N-retinylidene-PE to all-trans retinal and PE, all-trans retinal is accessible to the activity of RDH8 (Cioffi, 2020; Xie et al., 2021). Although the experimental structure of RDH8 is not available, biochemical studies determined its importance for the reduction of all-trans retinal to all-trans retinol, showing a preference for NADPH as a cofactor (Parker and Crouch, 2010).

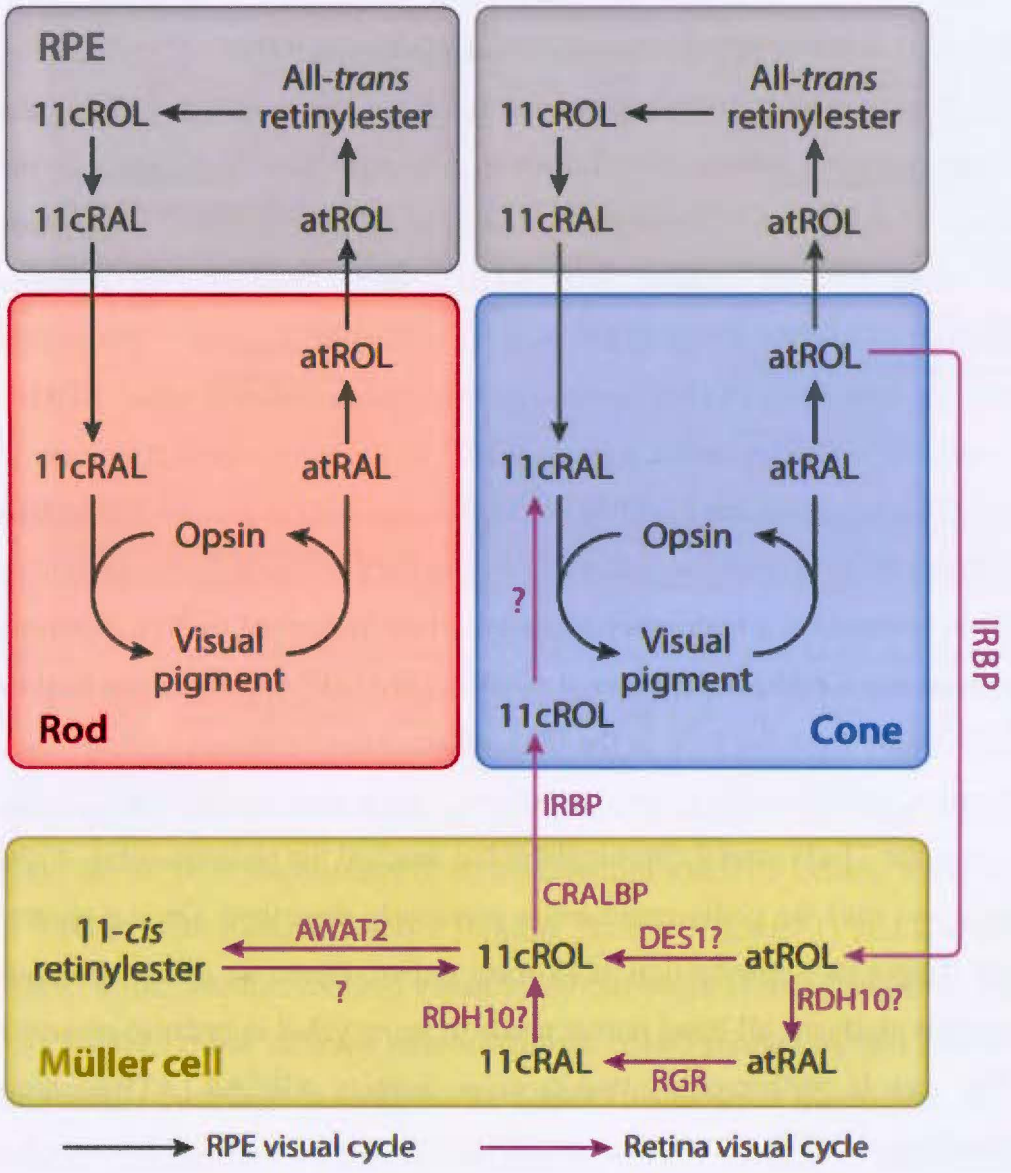

Figure 1.9: Metabolic pathway scheme of the canonical and cone-specific visual cycle. The cone-specific cycle relies on Müller cells' proteins and IRBP. 11cRAL stands for 11-cis retinal, 11cROL 11-cis retinol, atRAL all-trans retinal, and atROL all-trans retinol. CRALBP stands for cellular retinaldehyde-binding protein, AWAT2 Acyl-CoA wax alcohol acyltransferase 2, DES1 Dihydroceramide desaturase-1, RDH10 Retinol Dehydrogenase 10, and retinal G-protein-coupled receptor (RGR). Picture taken from Sato and Kefalov, 2024, under the license: Creative Commons Attribution License (CC BY 4.0).

The all-trans retinol regenerated by RDH8 can leave the cone cells and can be sequestered by RBP3 in the IPM and return to the RPE to restart the classical cycle (Kiser et al., 2014). Alternatively, the

all-trans retinol released by the photoreceptors can be delivered to the Müller cells for the cone-specific visual cycle, where it can be isomerized to 11-cis retinol and subsequently delivered to the cones, where it is oxidized to 11-cis retinal, completing the regeneration of the chromophore independently of the RPE (Figure 1.9) (Sato and Kefalov, 2024).

1.7 Retinol Binding Protein 3

1.7.1 RBP3: discovery, localization, transcription, expression, and ligand binding

Also known as Interstitial Retinol Binding Protein or Interphotoreceptor Binding Protein (IRBP), RBP3 was first isolated in the early eighties during studies aimed at the characterization of the IPM proteins (Adler and Klucznik, 1982). Its glycosylation nature was clearly evident due to RBP3's ability to bind Concanavalin A (ConA), a lectin, while initial gel-filtration analysis misled the correct determination of molecular weight. Its potential to form dimers, which was subjected to debate, ended when cross-linking experiments failed to detect such dimerization, and RBP3 is now widely recognized as a monomeric glycoprotein of ≃ 140 kDa (Liou et al., 1982; Adler and Evans, 1983; Saari et al., 1985). This glycoprotein is predominantly expressed by rods, but cones are also responsible for the expression of a lower amount of RBP, however the RBP3 messenger RiboNucleic Acid (mRNA) expression levels are reversed in cone dominant retinas, interestingly, low levels of RBP3 mRNA were also detected in bipolar cells (Hollyfield et al., 1985A; Porrello et al., 1991; Getz et al., 2024). Besides the retina, RBP3 is also expressed by the pinealocytes in the pineal gland; this finding is not surprising given the high similarities between pinealocytes and rods, the function of RBP3 in the pineal gland is not known; however, given the presence of retinoids in the pineal gland, it is possible to speculate that its role is related to its ability to interact with retinoids (Rodrigues et al., 1986; Phillips et al., 1989). Considering the photoreceptor as the main producer of RBP3, it is not surprising that the major amount of RBP3 is confined in the IPM, while a very minor portion can be detected in the vitreous and aqueous humor through an Enzyme-Linked Immunosorbent Assay (ELISA) (Wiggert et al., 1986). RBP3 is synthesized in the inner segments of the photoreceptors, and after glycosylation in the Golgi apparatus, it is secreted in the IPM at the level of the connecting cilium (Schneider et al., 1986; Carter-Dawson and Burroughs, 1992). Experiments with colloidal gold particles allowed the understanding that the distribution of RBP3 in the IPM is not homogeneous, but it appears mainly associated with the plasma membranes of photoreceptor outer segments and the apical microvilli of the RPE cells (Hollyfield et al., 1985B). Relative to the fraction of RBP3 associated with the photoreceptors' plasma membranes, the area adjacent to the rods shows a higher concentration, while its presence around cones is lower (Carter-Dawson and Burroughs, 1989).

Although a good amount of RBP3 can be extracted by a simple saline rinse of retinas, studies on *Gallus domesticus* show that a fraction of RBP3 adjacent to the cones' plasma membrane is "wash-resistant", suggesting a tight association with the cones' membranes, and further studies suggested the role of the Müller microvilli and cones' pericellular matrix as a binding domain for RBP3 (Garlipp et al., 2012; Garlipp and Gonzalez-Fernandez, 2013). The preferential association of RBP3 to the plasma membranes has also been observed in cultured photoreceptor neurons (Politi et al., 1989). Although the majority of RBP3 is extracellular, an important fraction of RBP3 (18% circa) is localized in RPE phagosomes, formed by photoreceptor shedding, and RPE endosomes formed by a different endocytic pathway, furthermore, also photoreceptors present intracellular RBP3 up-taken from the matrix and targeted to degradation pathway (Hollyfield et al., 1985B; Cunningham and Gonzalez-Fernandez, 2003). Interestingly, the distribution of RBP3 in the rat IPM is dependent on dark/light conditions (Uehara et al. 1990). Under the light stimulus, RBP3 appears associated with the plasma membranes of the cells delimiting the IPM, while in dark conditions it shows a uniform distribution throughout the IPM (Uehara et al., 1990). This change was, however, not observed in *Danio rerio* retina (Cunningham and Gonzalez-Fernandez, 2000). It is clear that the amount of RBP3 present in the IPM is dependent on the rate of its synthesis and secretion and on its degradation and internalization rate through the previously mentioned pathways. Interestingly, the RBP3 mRNA levels are regulated by the circadian rhythm with a higher transcription rate during light conditions, while during dark conditions, the RBP3 transcription rate decreases and it is restricted to the S cones in *Danio rerio* retina (Rajendran et al., 1996). A similar circadian transcription regulation has also been observed in *Gallus gallus domesticus* (Stenkamp et al., 2005). However, the transcription and the translation of RBP3 are regulated independently, and despite the circadian variation of mRNA levels, the amount of RBP3 protein in the IPM is kept constant independently of light and dark conditions (Liou et al., 1998; Cunningham and Gonzalez-Fernandez, 2000). The secretion and internalization processes determine a fast turnover of RBP3, which is measured to be $\simeq$ 7 hours in *Danio Rerio* and $\simeq$11 hours in *Xenopus laevis;* both values are much faster compared to opsin turnover (Cunningham et al., 1999; Cunningham and Gonzalez-Fernandez, 2000).

In order to better understand the biological role of RBP3, several studies related to the expression of RBP3 in development were performed, analyzing the detection and the quantification of RBP3 mRNA during the retina's development in different animals. In cultured cells, the transcription of RBP3 is prompted by the hypomethylation of the first exon and CpG island in the promoter, with Cone-Rod Homeobox (CRX) and Orthodenticle homeobox 2 (OTX2) being the main transcription factors (Albini et al., 1990; Chen et al., 1997; Fong and Fong, 1999). The coincidence between hypomethylation and RBP3 transcription was experimentally confirmed also in mouse retina, where

the hypomethylation and RBP3 mRNA were detected at the embryonic (E) day 11, the mRNA level rapidly increases at E13 until reaching a plateau at Post-natal (P) day 20 (Liou et al., 1994). The RBP3 content is, however, regulated independently from its transcription; for this reason, RBP3 is detected at E17; however, until P7, it remains located intracellularly, and its concentration in the IPM sharply increases at P10 and reaches its maximum after P50 (Carter-Dawson et al., 1986; van Veen et al., 1988). Post-natal expression studies of RBP3 mRNA were also conducted in rats, where two RBP3 mRNAs with differences in the 3' untranslated region were detected (Gonzalez-Fernandez et al., 1993). In rats, RBP3 mRNA is easily detected at P1, and it reaches its maximum at P9; however, the protein content is detected at P2 and it undergoes a marked increase from P10 until P50, reaching a plateau only at P90 (Eisenfeld et al., 1985; Gonzalez-Fernandez et al., 1985; Gonzalez-Fernandez and Healy, 1990). Interestingly, the levels of RBP3 mRNA decrease in dark conditions, but the protein content is not affected by light/dark conditions, suggesting once again independent transcription and regulation mechanisms (Gonzalez-Fernandez et al., 1985; Kutty et al., 1994). In all the studies mentioned above, RBP3 is detected before the beginning of the visual cycle, as mouse eyes open only at ~P13–P14, suggesting RBP3 plays an important role in retina development.

RBP3 has shown the ability to bind several endogenous retinoids, including: 11-cis retinol, 11-cis retinal, all-trans retinol, all-trans retinal, and retinyl esters and other hydrophobic molecules that are not involved in the visual cycle, including retinoic acid, cholesterol, and α-tocopherol (Fong et al., 1984A; Alvarez et al., 1987; Adler and Spencer, 1991). Importantly, the composition of the different endogenous retinoids bound to RBP3 is profoundly affected by light/dark conditions since light conditions lead to a drastic decrease of 11-cis retinal and an important increase in all-trans retinol, these changes are reversed in dark conditions, on the other hand 11-cis retinol, all-trans retinal and retinyl esters do not show any significant changes during light/dark shift (Saari et al., 1985; Lin et al., 1989; Adler and Spencer, 1991). The affinities of RBP3 for the various endogenous retinoids are as follows: 11-cis retinal > all-trans-retinol > all-trans-retinal > 11-cis retinol (Chen and Noy, 1994). RBP3 also has the ability to bind endogenous fatty acids, such as docosahexaenoic acid (DHA), oleic acid (OA), palmitic acid, stearic acid, linoleic acid, and palmitoleic acid, with OA and palmitic acid being the most abundant and DHA being the least abundant (Bazan et al., 1985).

1.7.2 RBP3 gene evolution

In order to better understand the binding properties of RPB3, it is necessary to consider its gene architecture and the implications for the protein structure. *Homo sapiens* RBP3 gene consists of one large and three small exons, which, after splicing, will result in an mRNA that encodes for 1262 amino acids. In the amino acidic sequence, it is possible to identify four repeats (also known as

modules) which present a percentage identity oscillating between 33-38% (Figure 1.10) (Fong and Bridges, 1988; Liou et al., 1989).

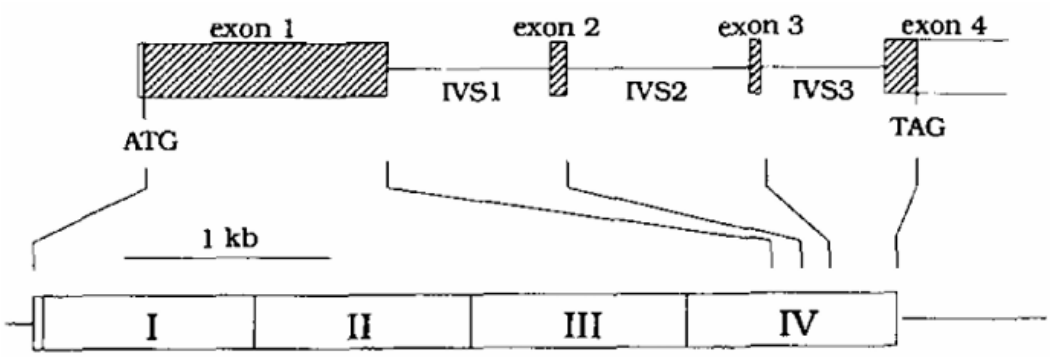

Figure 1.10: Homo sapiens RBP3 gene architecture and its division into four homologous repeats. Boxes represent exons, and connecting lines are introns. Picture taken from Liou et al., 1989 under the license CC BY.

A possible model to explain the evolution of the *Bos taurus* RBP3 gene (which presents an organization similar to the human one) was proposed by Borst and colleagues in 1989, in which an ancestral RBP3 gene consisting of four small exons encoding a ≃ 300 amino acid protein (Borst et al., 1989). According to the model, after the splicing, the mRNA was retrotranscribed and inserted at the 5'end of the ancestral gene, and two subsequent unequal crossover events generated the four-module architecture (Figure 1.11) (Borst et al., 1989).

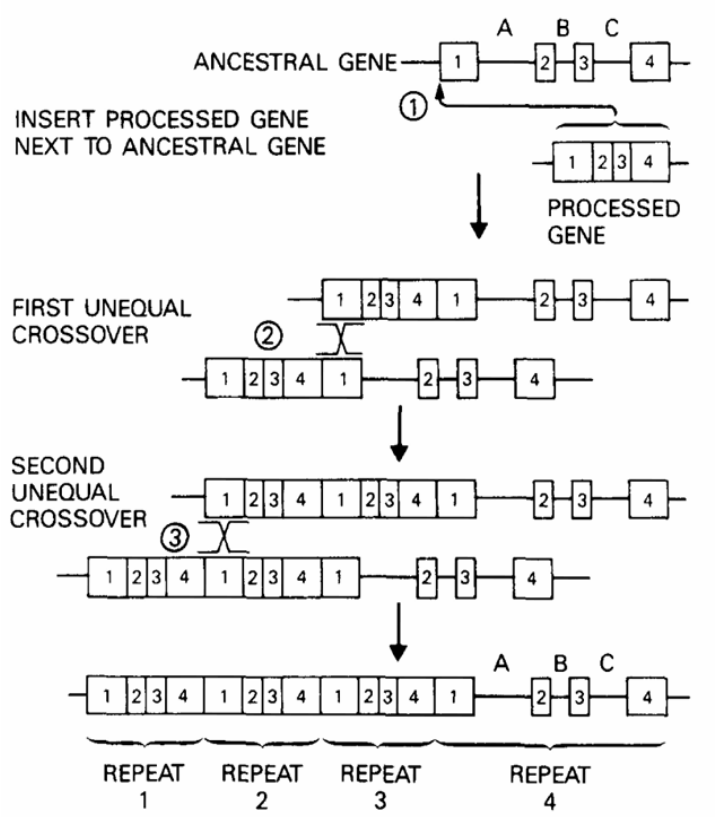

Figure 1.11: Evolutionary model proposed for the explanation of the Bos taurus RBP3 gene evolution (Borst et al., 1989). Boxes represent exons, and connecting lines are introns. Picture taken from Borst et al., 1989 under the license CC BY.

This model, however, cannot be used to explain the phylogenetic relationship amongst the four module of RBP3 in several animals since the modules 2 and 4 are more closely related to each other than to module 1 and 3 (Figure 1.12), for this reason another evolutionary model was proposed by Gonzalez-Fernandez and colleagues in which the mRNA of the ancestral RBP3 gene was retrotranscribed and inserted at the 5'end of the exon 1 generating a gene encoding for a two modules RBP3, after the first duplication event the amino acids sequence of the two modules diverged and a second duplication event generated the four module sequence (Figure 1.13) (Gonzalez-Fernandez et al., 2007).

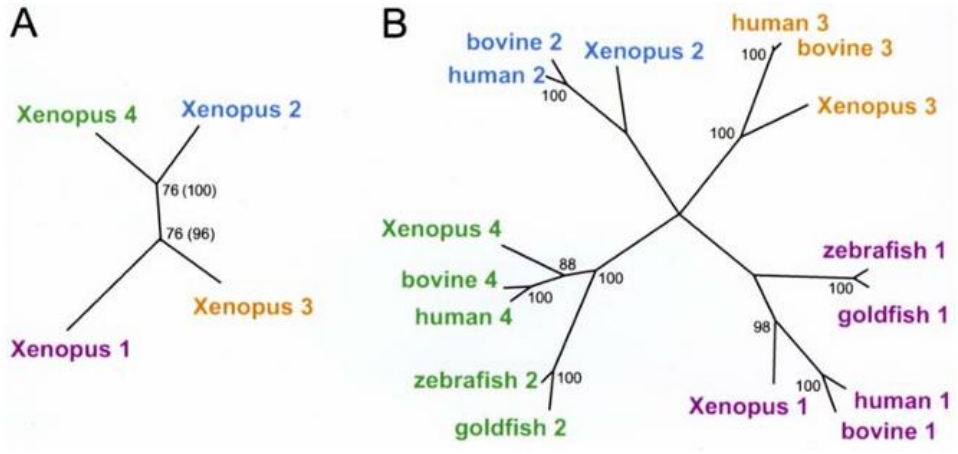

Figure 1.12: Phylogenetic relationships of the four RBP3 modules. A) Phylogenetic tree of Xenopus laevis modules, the tree is rooted using module 4 as the ancestral protein. B) Unrooted phylogenetic tree of RBP3 modules in various animals. Picture taken from Gonzalez-Fernandez et al., 2007 under the license CC BY.

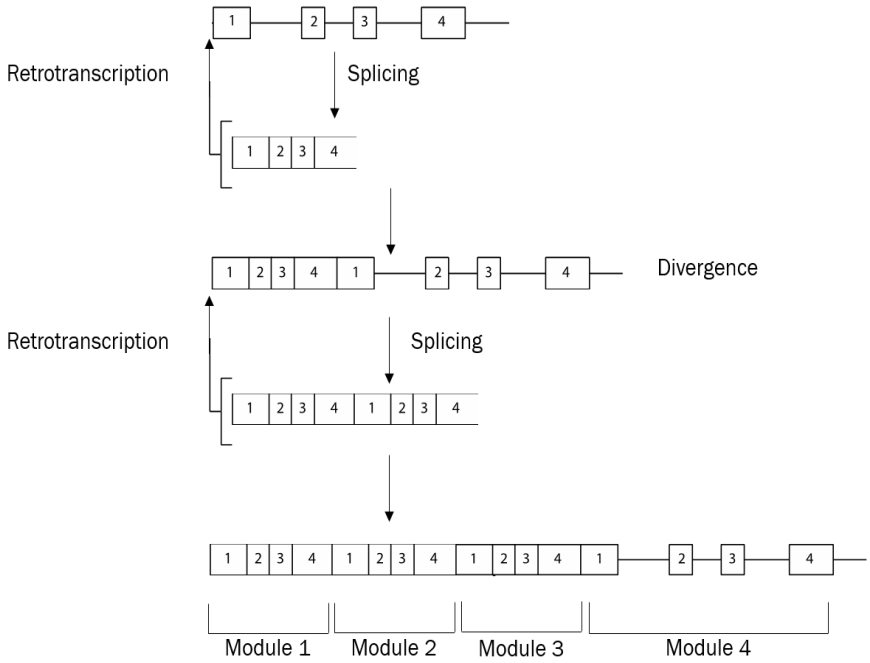

Figure 1.13: Evolutionary model for the RBP3 gene proposed by Gonzalez-Fernandez et al., 2007. The picture is a re-elaborated version of Gonzalez-Fernandez et al., 2007 evolutionary model, using the graphic inspired by the scheme proposed by Borst et al., 1989.

Importantly, the teleost presents an RBP3 structure consisting of only two modules since the middle Modules 3 and 4 were lost during evolution (Wagenhorst et al., 1995; Nickerson et al., 2006; Gonzalez-Fernandez et al., 2007). Considering the evolution of the RBP3 gene, it is clear that each module represents a functional unit of the protein capable of binding retinoids; therefore, considering the size and the complexity of the full-length protein, it represented an interesting tool to facilitate structural and functional characterization (Baer et al., 1998).

1.7.3 RBP3 structural characterization

The structural characterization of full-length RBP3 has been challenging due to its size, complexity, and flexibility. The first study that allowed a rudimentary visualization of the protein was published by Adler and colleagues in 1987, in which, through Transmission Electron Microscopy (TEM) (using rotary shadowing), it was possible to determine the "pi" bent shape of the protein, furthermore they described an extended "straight" conformation after ligand binding (Adler et al., 1987). Because of the technical difficulties encountered in full-length RBP3 crystallization, likely due to the protein's intrinsic flexibility, the efforts have been focused on the single modules. The first crystal structure of module 2 of Xenopus laevis under the Protein Data Bank unique identifier (PDB ID): 1J7X was published in 2002, and a second crystal structure of *Danio rerio* RBP3 module 1 in complex with OA (PDB ID: 4LUR) was published in 2015 (Figure 1.14) (Loew and Gonzalez-Fernandez, 2002; Ghosh et al., 2015).

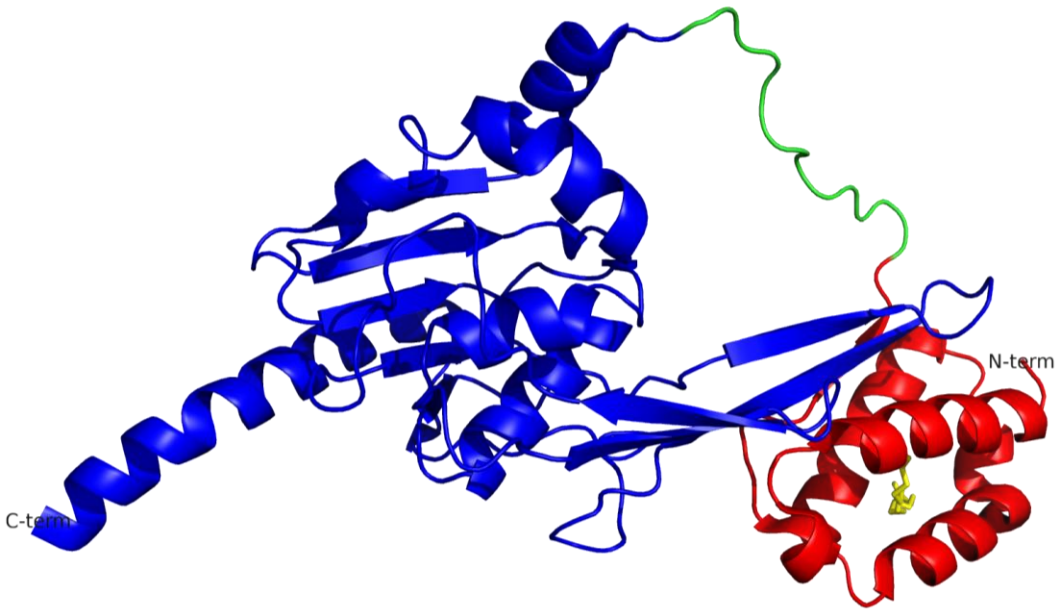

Figure 1.14: Crystal structure of Danio rerio Module 1 (PDB ID: 4LUR). Red: Domain A, green: flexible loop, blue: Domain B, yellow: OA. Picture realized using the software PyMol (Schrödinger, LLC).

Thanks to the crystal structures mentioned above, it is possible to affirm that each module consists of two domains (Domain A and Domain B) connected to each other with a flexible random coil stretch.

The Domain A consists of three α-helices followed by a short β-strand that, together with two β-strands extending from Domain B, forms a hydrophobic cavity (Loew and Gonzalez-Fernandez, 2002; Ghosh et al., 2015). The Domain B presents a β-sheet consisting of five parallel β-strands and one antiparallel β-strand sandwiched between four α-helices on one side (α4, α5, α6, α7) and one C-terminal α-helix. Altogether, the main β-sheet and the four α-helices that form the principal hydrophobic cavity share a similar topology with CRALBP (PDB ID: 3HY5) (He et al., 2009; Kiser et al., 2014). Besides the two β-strands (β9, β10) that extend from Domain B and complete the hydrophobic cavity of Domain A, Domain B presents two other β-strands (β5, β6) forming a loop between α6 and β7. The β-strands (β5, β6) are the contacting area between Domain A and Domain B (Loew and Gonzalez-Fernandez, 2002; Ghosh et al., 2015). The first structure of the full-length *Bos taurus* RBP3 in complex with the Fab fragment of the monoclonal antibody (mAb-5), obtained by Cryo Electron Microscopy (CryoEM), was published in 2020 by Sears and colleagues (PDB ID: 7JTI). Despite the limited resolution, 7.4 Ångström (Å), it was possible for the first time to understand the connection and the three-dimensional orientation of the four modules in space (Figure 1.15) (Sears et al., 2020).

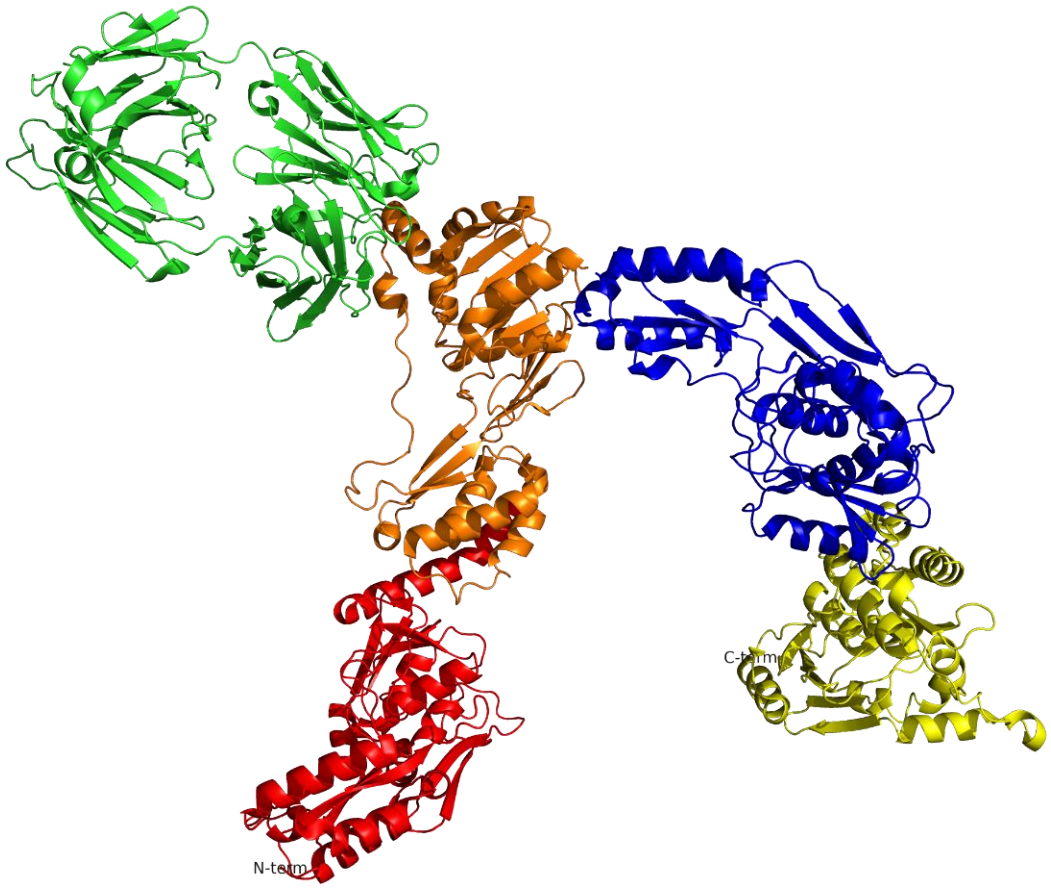

Figure 1.15: CryoEM structure for Bos taurus RBP3 (PDB ID: 7JTI) divided by modules: Module 1 in red, Module 2 in orange, Module 3 in blue, Module 4 in yellow, mAb5 Fab fragment in green (Sears et al., 2020). Picture realized using the software PyMol (Schrödinger, LLC).

Interestingly, Sears and colleagues were not able to observe the straight conformation described by Adler and colleagues in 1987 (Sears et al., 2020). Although the full-length structure gives information relative to the connection between the modules, the low resolution impedes details relative to the possible binding sites in the modules connecting regions of the protein.

1.7.4 RBP3 binding sites

The lack of detailed structural characterization of RBP3 has hindered the functional mechanism and has not allowed a proper quantification of the possible binding sites, which have so far remained elusive. Given the lack of an appropriate structural characterization, fluorescence spectroscopy, in particular, retinol fluorescence enhancement and tryptophan quenching were the main techniques used to investigate the binding properties of RBP3 (Chen et al., 1993). These two different techniques were applied to the study of native full-length RBP3 as well as the recombinantly expressed modules, leading to contradictory results (Chen et al., 1993; Lin et al., 1997). In the studies conducted by Adler and colleagues in 1985 and Okajima and colleagues in 1989 it was claimed that full-length RBP3 possesses one binding site while in the studies conducted by Saari and colleagues 1985 and Chen and colleagues of Noy research group in 1993, two retinol binding sites with different affinities were detected (Adler et al., 1985; Saari et al., 1985; Okajima et al., 1989; Chen et al., 1993). The latest results were confirmed again by the Noy group in a paper published in 1997; however, in a paper published by the same research group in 2001, three retinoid binding sites were described (Tschanz and Noy, 1997; Shaw and Noy, 2001). These discrepancies were exacerbated when the same fluorescence spectroscopic techniques were applied to investigate the retinoid binding properties of the recombinantly produced single modules, since all four modules of *Homo sapiens* RBP3 were capable of binding retinoids (Lin et al., 1997; Nickerson et al., 1998). Another study performed on recombinant *Xenopus laevis* module 4 proposed that the single module 4 contains two distinct binding sites (Baer et al., 1998). Thus, the debate relative to the number of RBP3 binding sites remains open. Importantly, also the localization of the putative binding sites is still unresolved, the first hypothesis was proposed in 2001 by Rengarajan and colleagues, in which through photoaffinity labelling, it was possible to identify the amino acids of the β-strands number 4 (β4) as the binding site of retinoic acid in recombinant *Homo sapiens* RBP3 Module 1, interestingly, this region correspond to the hydrophobic cavity of Domain B (Rengarajan et al., 2001). However, the docking studies performed on the crystal structure of *Xenopus Laevis* Module 2 suggested that the hydrophobic patch located between Domain A and Domain B is the best candidate for a putative binding site, while another possible binding site is located in a narrow cavity of Domain B (Loew et al., 2002; Gonzalez-Fernandez et al., 2007). Another tryptophan fluorescence quenching study, using mutated recombinant *Xenopus laevis* Module 2, showed the hydrophobic cavity of Domain B as the main

binding site for all-trans retinol and 11-cis retinal (Gonzalez-Fernandez et al., 2009). Module 1 of *Danio rerio* was, however, co-crystallized with OA bound to a small cavity of Domain A (Ghosh et al., 2015). Despite the fact that these studies are not conclusive, they all underlie the importance of the hydrophobic interactions in the stabilization of retinoid binding (Tschanz and Noy, 1997). Although the fluorescence spectroscopic studies failed to give a definitive answer to the number of binding sites present on RBP3, it still allowed for some information relative to the interactions between fatty acids and retinoids, since the presence of fatty acids leads to the displacement of retinoids (Chen et al., 1993). Amongst the various fatty acids, RBP3 shows a high affinity for OA, the biological meaning of the high affinity for OA has not been understood yet; on the other hand, it has been demonstrated that DHA causes the release of 11-cis retinal from RBP3 binding sites (Chen et al., 1996; Semenova and Converse, 2003). Importantly, the apical plasma membrane of the RPE cells is rich in palmitic acid and poor in DHA; conversely, the photoreceptor plasma membranes are rich in DHA and poor in palmitic acid (Wolf, 1998). It has been proposed that the differences between DHA and palmitic acid can regulate the loading and unloading of the various retinoids between the RPE and the photoreceptors, in particular the presence of palmitate can trigger a conformational change of RBP3 causing the release of all-trans retinol from and the binding with 11-cis retinal, once the 11-cis retinal RBP3 complex reaches the photoreceptor plasma membrane, the presence of DHA lead to the displacement of 11-cis retinal and the loading of the all-trans retinol (Wolf, 1998).

1.7.5 Glycobiology of RBP3

Glycobiology is not a well-known aspect of RBP3; this post-translational modification is present in *Homo sapiens*, *Bos Taurus*, *Sus scrofa*, *Macaca mulatta*, *Macaca fascicularis*, *Gallus gallus domesticus* (Gonzalez-Fernandez et al., 1984; Wiggert et al., 1984; Fong et al., 1984A; Fong et al., 1984B; Stenkamp et al., 2005; Kaushik et al., 2025B). NetNGlyc-based predictions indicate the majority of the vertebrates' RBP3 homologues present at least two N-Glycan chains linked to the *Homo sapiens* RBP3 homologue asparagine residues 205 and 515; however, the *Carassius auratus* RBP3 homolog is not glycosylated, suggesting that other fish may have a non-glycosylated RBP3 (Bridges et al., 1986; Gupta and Brunak, 2002). *Bos taurus* RBP3 glycan chain sequence was demonstrated to be bi-antennary N-glycans containing sialic acid, Galactose (Gal), N-Acetyl-Glucosamine (GlcNAc), Fucose (Fuc), in which sialic acid residues, located at the non-reducing end of the glycan chain, are linked to the atoms 2 and/or 3 of galactose through α-glycosidic linkage (Figure 1.16) (Fong et al., 1985; Taniguchi et al., 1986).

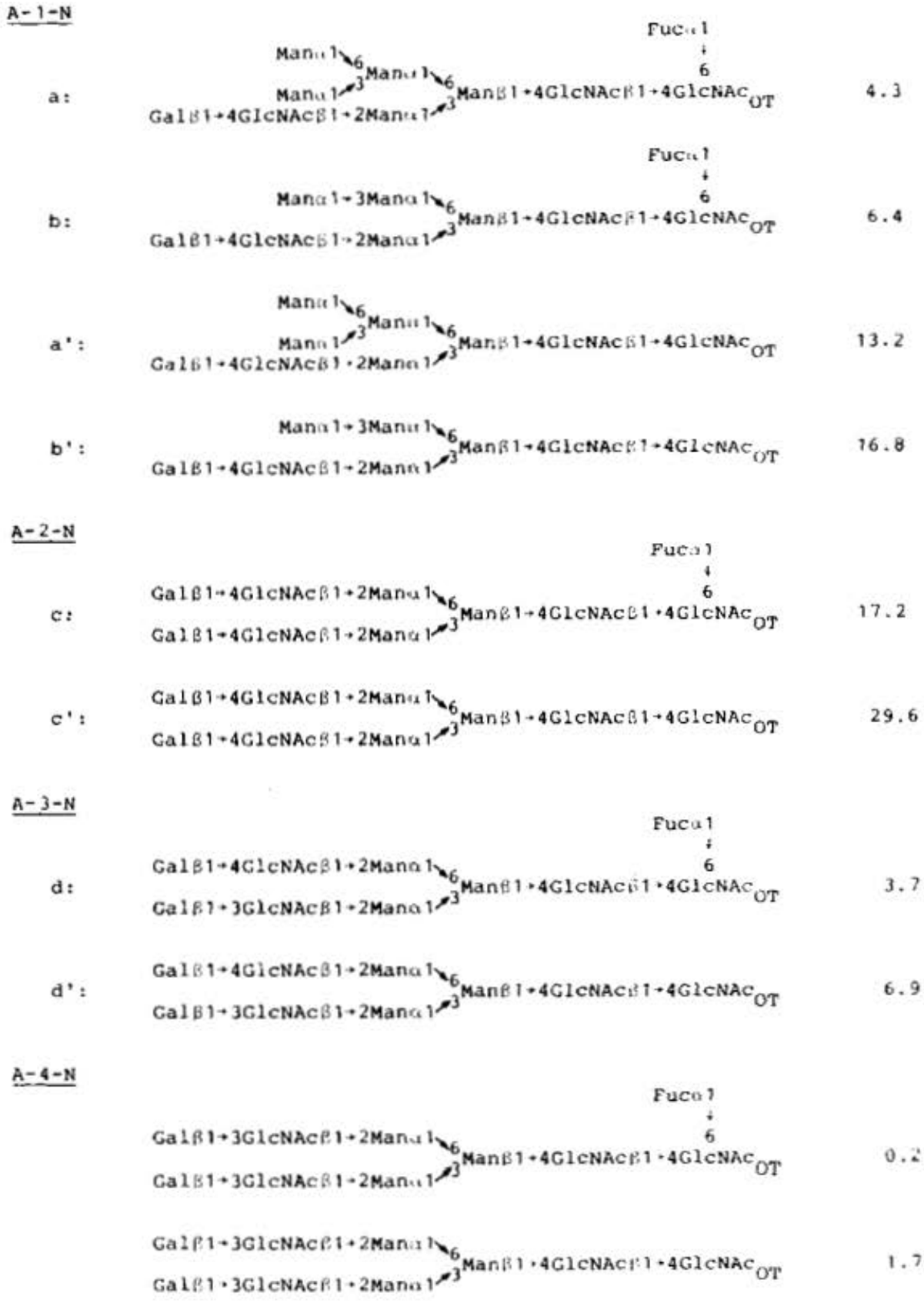

Figure 1.16: Bos taurus glycan chains fractions and their relative percentages on the right. All these fractions were obtained after removal of sialic acid through sialidase digestion. Picture taken from Taniguchi et al., 1986 under the license CC BY.

Using crosslinking and mass spectrometry, Sears and colleagues determined the asparagine residues (of *Bos taurus* RBP3) to which the fractions described in Figure 1.16 could be attached (Sears et al., 2020), and they are Asn107, Asn161, Asn205, Asn513, and Asn1114. Despite the fact that the sequence of RBP3 glycans is characterized, their function is still not known since they are not required for the secretion into the extracellular environment (Fong et al., 1984A), or whether the attachment sites are strictly conserved. The glycan chains give RBP3 the ability to bind ConA, and notably, two different isoforms of RBP3 exist, known as IRBP I and IRBP II, with the latter one capable of being phosphorylated, showing higher binding affinity for ConA (Wiggert et al., 1988; Qtaishat et al., 2005).

1.7.6 RBP3 function

The ability of RBP3 to bind 11-cis retinal and all-trans retinol, and the fact that the amount of 11-cis retinal and all-trans retinol carried by RBP3 changes according to light and dark conditions, coupled with the localization of RBP3 in the IPM, immediately led to the hypothesis that the major function of RBP3 was related to the solubilization and shuttling of retinoids between the RPE and the photoreceptors, in the already described visual cycle (Adler and Evans, 1985; Okajima et al., 1989; Carlson and Bok, 1992). The *ex vivo* experiments using *Bufo marinus* retinas and other experiments performed on detached retinas of *Raja erinacea* and *Raja ocellata* showed higher rates of rhodopsin regeneration in the presence of RBP3, thus furtherly supporting the hypothesis of RBP3 as a retinoid transporter protein in the visual cycle (Okajima et al., 1990; Duffy et al., 1993). However, other *in vitro* experiments questioned the role of RBP3 in the visual cycle since the transfer of all-trans retinol between the Rod Outer Segment (ROS) membrane and the liposome can occur in the aqueous phase, and the presence of RBP3 slows down this movement (Ho et al., 1989). The strong evidence that challenged the role of RBP3 as a retinoid shuttle was, however, provided by Palczewski and colleagues in 1999 and Ripps and colleagues in 2000. In both studies, the RBP3 gene ablation did not prevent the retinoid visual cycle, clearly demonstrating the dispensability of RBP3 in the retinoid visual cycle (Palczewski et al., 1999; Ripps et al., 2000). Considering the ability of RBP3 to bind endogenous 11-cis retinol, it was hypothesized that RBP3 plays a role in the transport of 11-cis retinol from the Müller cells to the cone photoreceptors for the cone-specific visual cycle (Lin et al., 1989; Parker et al., 2011). However, experimental results obtained on RBP3 knockout mice showed normal regeneration of the pigment in M/L cones, clearly demonstrating the dispensability of RBP3 in the delivery of 11-cis retinol to the cones (Kolesnikov et al., 2011). Although the presence of RBP3 is not required for the cone-specific visual cycle, its absence causes a decrease in cones' electroretinogram (ERG) response, likely due to the fact that RBP3 enhances the uptake of all-trans retinol and the release of 11-cis retinal by the Müller cells (Parker et al., 2009; Betts-Obregon et al.,

2014). Although the role of RBP3 in the visual cycle is questionable, its presence is essential for the physiological function of the retina since it is able to remove all-trans retinol and 11-cis retinal from RPE and photoreceptors membranes respectively, however unlike with the Müller cells, it does not facilitate the uptake of all-trans retinol by the RPE (Carlson and Bok, 1992; Edwards and Adler, 2000; Qtaishat et al., 2005; Wu et al., 2007). These abilities of RBP3 affect the kinetics of the visual cycle, allowing a faster regeneration of the chromophore and a faster clearance of all-trans retinol (Jin et al., 2009).

Considering the fact that the amount of endogenous all-trans retinal bound to RBP3 is almost constant in light and dark conditions (Adler and Spencer, 1991), the importance of all-trans retinol clearance can be understood considering the non-favorable thermodynamic aspect of the conversion of all-trans retinal to all-trans retinol. The constant removal of all-trans retinol is probably essential to shift the reaction equilibrium toward the formation of all-trans retinol, thus preventing the accumulation of all-trans retinal in the ROS. All-trans retinal is directly toxic to the photoreceptors since it can react with PE through a Schiff-base formation, generating bisretinoid products such as N-retinylidene-N-retinylethanolamine (A2E). Its accumulation in RBP3 knockout mice causes oxidative stress, mitochondrial dysfunction, an increase of Tumor Necrosis Factor Alpha (TNF) levels, an increase of necrosis and apoptosis, ultimately leading to photoreceptor loss (Sato et al., 2013; Lee et al., 2016; Chen et al., 2017; Palczewska et al., 2023). Importantly, all the retinoids involved in the visual cycle can be photodegraded by light, causing the formation of cytotoxic molecules. Retinoid binding by RBP3 represents a protection from light radiation, avoiding the formation of such products (Gonzalez-Fernandez et al., 2015). In summary, the main function of RBP3 resides in its ability to bind retinoid, which is essential to maintain low levels of cytotoxic products and prevent retinal damage.

Besides its role in protecting the retinoids from photodegradation and avoiding the formation of cytotoxic products, RBP3 also plays a protective role in mitigating the effects of oxidative stress. This specific RBP3 ability is due to the presence of several cysteine residues, which remain in the reduced form and are not involved in the formation of disulfide bonds, although they can cause protein aggregation, giving RBP3 the ability to act as a free radical scavenger, thereby contributing to the mitigation of oxidative stress (Gonzalez-Fernandez et al., 2014).

1.7.7 RBP3 in diseases

Given the essential protective role of RBP3, not surprisingly, its malfunction has been associated with several diseases (Zeng et al., 2020). Pan-retinal degeneration was the first disease found to be associated with RBP3, followed by retinitis pigmentosa, exaggerated eye growth, and myopia (den

Hollander et al., 2009; Wisard et al., 2011; Li et al., 2013; Arno et al., 2015, Markand et al., 2016; Georgiou et al., 2024). It is of particular interest that the link between diabetic retinopathy (DR) and RBP3, since it counteracts the symptoms of hyperglycemia on retinal endothelial cells and Müller cells (Yokomizo et al., 2019). The retinas and the vitreous of individuals with severe DR present lower levels of RBP3 compared to those of non-diabetics. The protective effect of RBP3 in DR is probably due to its ability to bind the receptor Glucose Transporter 1 (GLUT1) and the Vascular Endothelial Growth Factor (VEGF), limiting their activities (Yokomizo et al., 2019). Since the concentration of RBP3 correlates with the severity of the DR, it can be considered a good candidate as a biomarker for DR (Kaushik et al., 2023). A possible strategy for the detection of RBP3 in a non-invasive way can be achieved by exploiting the recent advances in functional imaging, providing a useful diagnostic tool in ophthalmologic care (Palczewska et al., 2023; Kaushik et al., 2025A). This is especially relevant after recent advances in the technology and the noninvasive optical biopsy of retinal fluorophores and separating their individual two-photon signatures employing phasor analyses (Palczewska et al., 2020), and the efforts in making the technology safe for human eye imaging (Palczewska et al., 2018; Boguslawski et al., 2022).

1.8 PDE6 as a potential driver of morphological changes of photoreceptors upon light stimulus

Optoretinography (ORG) is a powerful imaging system capable of detecting optical signals generated by changes in photoreceptor morphology (Ni et al., 2024). Unfortunately, the biomolecules responsible for such changes are unknown, thus limiting the diagnostic power of ORG. At the same time, there is clear evidence that photoreceptors undergo a change in their length after light stimulus; however, the biomolecules responsible for this phenomenon are unknown (Bownds and Brodie, 1975). On the other hand, there is growing evidence that PDE6, the last enzyme of the phototransduction cascade localized in the photoreceptor disc, changes conformation during its activation/inactivation cycle and may be the responsible protein for the change in photoreceptor length (Tomczewski et al., 2025). The hypothesis that PDE6 conformational changes are responsible for the change in photoreceptor morphology can now be tested through Cryo Electron Tomography (CryoET). Although the techniques do not allow to reach the high resolution typical for single particle CryoEM analysis, they allow for testing the behavior of PDE6 in its natural environment (Appendix 2). The detailed knowledge of the mechanism responsible for the morphological changes in photoreceptors may have implications for therapeutics, diagnostics, and the functional imaging of photoreceptor physiology.

1.9 Aim of the thesis

RBP3 involvement in the visual cycle, its retinal protective role, and its ability to maintain the retina free of cytotoxic products, resides in its retinoid binding capacity. Despite its importance, a detailed structural biology characterization of RBP3 has been elusive. A high-resolution structure of the full-length protein is missing, as well as a detailed mapping of the ligand binding sites.

The present thesis has three principal targets:

- Identification of the retinoid binding sites at high resolution through crystallography.
- Structural characterization at high resolution of the full-length protein through cryoEM.
- Investigation of the relationship between the ligand binding event and the conformational changes in solution through Small-Angle X-ray Scattering (SAXS).

The identification of the ligand binding site, the high-resolution structural characterization, coupled with an improved comprehension of conformational changes caused by the ligand binding events it would enhance our understanding of the retinoid visual cycle and retina's biochemistry. Besides the academic interest, the knowledge of the above mentioned aspects would be beneficial under a translational point of view, since it (i) would provide an important information for the synthesis of small molecules that could modulate RBP3 activity, thus regulating the kinetic of the visual cycle, (ii) exploration of RBP3 as a possible drug deliver to photoreceptors or RPE cells, and (iii) offer potential new avenues of research in DR.

1.10 Author's contribution

To achieve the above-mentioned target, two main approaches were implemented. First, I produced truncated recombinant proteins to form protein-ligand complex crystals in order to identify the ligand binding sites at high resolution. The second approach involved the purification of the full length RBP3 protein from the native sources and its structural analysis through cryoEM and SAXS.

To implement the above-mentioned strategies, I performed the following tasks:

- Molecular cloning of several constructs of the RBP3 modules, and testing their expression and purification process.

  For this task, I did all the steps. For cloning, I did bioinformatics analysis to identify the RBP3 module boundaries, designed primers, performed PCRs and ligations, and validated the inserts. For protein expression, I tried different vectors (with different tags), *E. coli* strains, and expression conditions. For protein purification, I tested different protocols and chromatographic techniques (Pages: 45-51, 124-133).
- Purification of *Sus scrofa* and *Bos taurus* full-length RBP3 using different chromatographic techniques.

  For this task, I helped to establish the protocols used now routinely in our lab. I did thousands of eye dissections and retina isolations in dark conditions, and optimized the three necessary chromatographic steps to obtain highly pure and homogeneous RBP3 samples (Pages: 57-59, Kaushik et al., 2025B).
- Biophysical characterization of the purified proteins through Circular Dichroism and Fluorescence spectroscopy.

  I participated in the biophysical characterization of the purified proteins, on my own, for Circular Dichroism done at IChF and at EMBL-Hamburg (I also performed Differential Scanning Fluorimetry assay that are not reported in this thesis), and I performed the Fluorescence spectroscopy assays at IChF and IBB (Pages: 51-52, 59-60, Kaushik et al., 2025B).
- Anti-RBP3 antibody expression, purification, and validation.

  I participate in the cell culturing of the hybridoma line that produces anti-RBP3. I was also part of the team that optimized its purification in our laboratory, and validated its cross reaction with RBP3 of different origins by western blotting (Pages: 54-57).
- Preparation of cryoEM grids, initial screening, and data analysis.

  I was part of the team that troubleshooted the cryoEM grid preparation done over several visits to IIMCB. I was also at the microscope when the initial screening was designed and performed

at CeNT. I then analyzed the RBP3 cryoEM structure done at CEITEC, in particular validating its refinement, looking for Module breakpoints and potential stability issues, implications in diseases, and relevance of glycosylation attachment sites (Pages: 61-72, Kaushik et al., 2025B).

- Molecular docking

  As part of the analysis of the RBP3 structure, I tested different docking protocols, and after choosing one for extensive analysis, I ran the predictions and analyzed the results. Such results were then also carefully compared with information available for other retinol binding proteins (Pages: 72-78, Kaushik et al., 2025B).

- Soft X-Ray Tomography and cryoET

  I participated in ROS deposition in cryoEM grids troubleshooting performed at IIMCB and CEITEC, and after conditions had been optimized, and I was part of the team that visited Diamond Light Source and contributed to that data collection strategy and analysis of the images (Pages: 134-136)

- In solution, RBP3 conformational changes upon ligand binding

  I was preparing the protein and ligands used for SAXS measurements in PetraIII P12 beamline, EMBL-Hamburg. I was on-site establishing the protocols for data collection, and participated to data analysis (Pages: 79-84, Kaushik et al., 2025B).

- Literature explorations

  I was constantly reading and searching RBP3-related literature. In addition to being important for experimental protocols optimization, and writing this thesis introduction, it was very useful and relevant for the writing of two manuscripts, which I am an author of, and that look into the possibility of RBP3 be used as a diabetic retinopathy early biomarker, and also about the usage of two-photon imaging to extract such information from living eyes (Kaushik et al., 2023, Kaushik et al., 2025A).

- Internship at the University of California, Irvine at prof. Krzysztof Palczewski's lab

  I used my internship at Irvine to perform mass spectrometry on RBP3 samples (Page: 59). I also tested recombinant expression of RBP3 modules, protocols for removing endogenous ligands that remain attached to recombinant and native RBP3 after purification (not reported on this thesis). During the 5 weeks' internship in Krzysztof Palczewski's lab, I also practiced ROS isolation (Page 134), PDE6 purification (which I trained ISB lab members on, and is now routinely used in our lab).

2 Materials and methods

2.1 *Bos taurus* RBP3 modules

2.1.1 Molecular Cloning

The term molecular cloning refers to a set of procedures designed to generate a fragment of recombinant Deoxyribonucleic Acid (DNA) used for the insertion into an appropriate vector. Those vectors can be used for the genetic modification of a host organism, allowing the replication of multiple copies of such a construct. During these procedures, an Open Reading Frame (ORF) is amplified through Polymerase Chain Reaction (PCR) and inserted into a plasmid through a ligation-dependent procedure. The generated recombinant plasmids are verified through double restriction digestion and, if positive, sent for sequencing to confirm the proper sequence of the construct.

2.1.1.1 Polymerase Chain Reaction (PCR)

The DNA sequences of the four modules of *Bos taurus* RBP3 were amplified through PCR (Appendix 1) using a synthetic *Bos taurus* RBP3 gene as a template. PCR reactions were performed using primers containing restriction enzyme sites recognized by BamH1 and Xho1(Thermo fisher scientific). Each PCR reaction contained: 0.5 micromolar (µM) forward and reverse primers, 200 µM each deoxynucleotide triphosphate (dNTP), recombinant Taq polymerase 0.025 Units of enzyme (U)/microliter (µl), 0.5 ng/µl of template, 1X Taq buffer (Thermo fisher scientific), for a total volume of 100 µl. After an initial denaturing step of 4 minutes at 98°C the PCR cycle was as follows: denaturing temperature 95°C (30 seconds), annealing temperature oscillating around the value of 60°C was set according to the Tm temperature of the selected primers (Appendix 1) for 30 seconds, extension temperature 72°C, with the time for extension of 1 minutes and 30 seconds, according to the expected size of amplified ORF (10 sec /1000 bp). Each cycle was repeated 30 times; the last cycle was followed by a final extension step of 6 minutes at 72°C.

2.1.1.2 Agarose gel electrophoresis

In order to check the successful outcome of the PCR, and prepare the material for the next cloning step, the band sizes of the PCR products were validated through agarose gel electrophoresis. The PCR products were loaded on a 1% agarose gel in Tris-acetate-EDTA (TAE) buffer, with Gel Red as intercalating agent to stain DNA bands. The electrophoresis was run in 1x TAE buffer at 100V until the loading dye reached the anodic end of the gel. The band's size was checked under Ultra Violet (UV) light and compared with the SM0311 GeneRuler 1 kb DNA Ladder (Thermo Scientific™) for size determination. The bands showing the expected size were excised from the gel under UV light and isolated using the A&A biotechnology Gel-Out kit according to the manufacturer's instructions.

The only deviation from the protocol was represented by the elution step, in which 50 µl of nuclease-free water pre-heated at 50°C was used for the elution of the DNA fragments.

2.1.1.3 Restriction enzyme digestion

The pGEX-6P-1 plasmid (kind gift from Professor Bochtler's lab) was linearized through double digestion using FastDigest BamH1 and FastDigest Xho1 (Thermo fisher scientific). The reaction was set as follows: 1 microgram (µg) of plasmid, 1 µl of FastDigest BamH1 and 1 µl of FastDigest Xho1, 1X FastDigest buffer for a total volume of 20 µl. The reaction was incubated at 37°C for 30 minutes. The successful outcome of the reaction was checked by agarose gel electrophoresis, and the band corresponding to the linearized plasmid was excised from the agarose gel using the A&A biotechnology Gel-Out kit according to the manufacturer's instructions using the same procedure described for the isolation of the PCR products. For the PCR product, in total, 40 nanograms (ng) (20 ng/µl) of material, containing the restriction enzyme recognition sites added in the primers, were subjected to restriction digestion using the same procedure described for the plasmid linearization; however, the digestion was stopped by thermal inactivation at 80°C for 5 minutes according to the manufacturer's instructions.

2.1.1.4 Ligation

To complete the cloning, the ligation reaction was performed by mixing the PCR product with the linearized plasmid in a 5:1 ratio, respectively, 1X bacteriophage T4(T4) DNA ligase buffer, 1 µl Polyethylene Glycol (PEG), 0.035 Units of enzymes (U)/µl T4 DNA ligase (Thermo Scientific™), in a total volume of 30 µl. The reaction was incubated at room temperature overnight.

2.1.1.5 Transformation

The ligation mixture (30 µl) was mixed with 50 µl of *Escherichia coli* Douglas Hanahan 5-alpha (DH5α) competent cells and incubated on ice for 30 minutes. After incubation, the mixture was subjected to heat shock at 42°C for 30 seconds and placed back on ice for 2 minutes. 1 milliliter (ml) of Lysogeny Broth (LB) media preheated at 37°C was added to the mixture and it was then incubated at 37°C for 30 minutes on shaking for the recovery step. The cells were then centrifuged at room temperature at 5000 RCF for 5 minutes, 800 µl of supernatant was removed, and the pellet was resuspended in the remaining 200 µl of supernatant. The mixture was then plated on an agar plate containing ampicillin (100 µg/ml) and incubated at 37°C overnight.

2.1.1.6 Plasmid isolation

The colonies developed overnight on the ampicillin agar plates were inoculated in 5 ml of LB media with ampicillin (100 µg/ml) at 37°C, shaking overnight. After centrifugation at 7000 RCF for 10

minutes at 4°C, the supernatant was discarded and the pellet was used for plasmid isolation using the kit "Plasmid Mini" from A&A biotechnology according to the manufacturer's instructions. The only deviation from the protocol was represented by the elution step in which 50 µl of nuclease free water pre-heated at 50°C were used for the elution of the isolated plasmids. After isolation, in order to check the successful outcome of ligation, the plasmids were subjected to double restriction digestion and run on an agarose gel in order to confirm the presence of the insert. The concentration was measured spectrophotometrically using NanoDrop (Thermo Scientific™), and the plasmids were then sent to NexBio external service for sequencing.

2.1.2 Protein expression and purification

For the protein expression, the plasmid pGEX-6-P-1 containing an ORF encoding for the protein of interest fused with the Glutathione S-Transferase (GST) -tag and PreScission protease recognition site at the N-terminus, was inserted through the transformation procedure previously described in *Escherichia coli* strain C43. A single colony was inoculated in 5 ml of LB media containing ampicillin (100 µg/ml) was incubated at 37°C on shaking overnight. The day after, the 5 ml of LB media were inoculated into 1 litre of LB media containing ampicillin (100 µg/ml) and incubated at 37°C on shaking for ~3 hours, until Optical Density at 600 nm (OD600nm) reached a value between 0.8 and 1.2. Next, the flasks containing the cell culture were transferred to 4°C for 30 minutes, and 0.01 mM Isopropyl β-D-thiogalactopyranoside (IPTG) was added to induce overexpression of the protein of interest. The cell culture was then incubated at 18°C on shaking overnight. The day after the bacterial culture was centrifuged at 10 000 RCF, the supernatant was discarded and the bacterial pellet was stored at -80°C for at least 24 hours.

2.1.2.1 Affinity chromatography

The first step in the purification of the protein of interest is represented by the GST-tag affinity chromatography. The affinity chromatography was performed using a 50 ml gravity column containing 5 ml of Glutathione Sepharose™ 4B resin from Cytiva. The column was washed with 50 ml of MilliQ water to remove the ethanol storage solution and equilibrated with 50 ml of equilibration buffer (50 milli molar (mM) Tris HCl, pH 8.0, 300 mM NaCl, 10% glycerol, 2 mM Dithiothreitol (DTT)). After equilibration, the column was activated with 20 ml of elution buffer (50 mM Tris HCl, pH 8.0, 300 mM NaCl, 10% glycerol, 2 mM DTT, 20 mM L-Glutathione reduced) and equilibrated again with 50 ml of equilibration buffer. The frozen pellet is thawed and mixed with 50 ml of lysis buffer (50 mM Tris HCl, pH 8.0, 300 mM NaCl, 10% glycerol, 0.1 mM phenylmethylsulfonyl fluoride (PMSF), 2 mM DTT, 0.5% Nonidet P-40 (NP-40)) and incubated on ice for 10 minutes. The

cells were disrupted by sonication using a pulse protocol of 10 seconds on and 15 seconds off at 30% amplitude, for a total pulsing time of 5 minutes. The procedure was performed on ice using a Qsonica Q125 Sonicator equipped with a 1/4" diameter probe. After sonication, the mixture was centrifuged at 20 000 RCF for 25 minutes at 4°C to remove cell debris. The supernatant is applied to the previously equilibrated column and left for 2 hours on a rocker at 4°C for binding. After the binding step, the flow through was collected and the column was washed with 50 ml of equilibration buffer for the removal of non-bound proteins. Another 20 ml of equilibration buffer are added to the column, the PreScission protease (kind gift from Professor Bochtler's lab) was added at a concentration of 0.1 mg/ml. The column was left overnight on the rocker for the in-column cleavage step. The day after, the flow through (cut *Bos taurus* RBP3 constructs (bRBP3)) of the cleavage step was collected, and the column was washed with 3 batches of equilibration buffer, 15 ml each, and collected. The elution was obtained using 20 ml of elution buffer (tagged PreScission protease and remaining uncut GST-bRBP3). The entire procedure was performed at 4°C.

2.1.2.2 Anion exchange chromatography

The fractions from the cleavage flow through and the washing flow through were pooled together, desalted, and concentrated to 5 ml using Amicon®Ultra Centrifugal Filter of 10 kDa cut-off, the centrifugation was performed at 1200 RCF at 4°C. The previously desalted 5 ml of protein sample were loaded on the column Mono Q™ 5/50 GL previously equilibrated with anion equilibration buffer M4(50 mM Tris HCl pH 8.0, 2 mM DTT) for anion exchange chromatography. Washing was performed using 10 ml of anion equilibration buffer, while elution was performed using anion elution buffer M4(50 mM Tris HCl pH 8.0, 2 mM DTT, 1M NaCl). The elution was carried out gradually increasing the proportion of the anion elution buffer M4 (linear gradient), reaching 100% over a total volume of 25 ml. Absorbance at 280 nm was used to monitor protein elution; fractions of 1 ml were collected automatically through peak-based fractionation. The entire procedure was performed at 4°C.

2.1.2.3 Size exclusion chromatography

The purest fraction obtained from the anion exchange chromatography was furtherly purified through Size Exclusion Chromatography (SEC). In the final purification step, Superdex™ 75 Increase 10/300 GL was equilibrated with SEC buffer (50 mM Tris HCl pH 8.0, 2 mM DTT, 100 mM NaCl). Elution was carried out at a constant flow rate of 0.7 mL/min, and absorbance at 280 nm was monitored to detect protein peaks. The entire procedure was performed at 4°C.

2.1.2.4 SDS-PAGE

After each chromatography step, the purity of the eluted fraction was assessed through Sodium Dodecyl Sulfate Polyacrylamide Gel Electrophoresis (SDS-PAGE). This electrophoretic technique

resolves the proteins according to their size, allowing for the determination of the number of protein species and their relative quantity present in a sample. The eluted fraction was mixed with 5X SDS loading dye buffer (250 mM Tris HCl pH 6.8, 10% SDS, 200 mM DTT, 50% glycerol, 0.5% bromophenol blue) in a ratio 1:4, heated at 95°C for 5 minutes and loaded on a SDS-PAGE gel with acrylamide concentrations ranging from 8% to 15%. The size of the proteins was compared with PageRuler^{TM} Plus Prestained Protein Ladder.

2.1.2.5 Circular dichroism

The correct folding and secondary structures of the recombinant proteins were tested through circular dichroism (CD). The protein sample was prepared in 10 mM Tris-HCl pH 8.0, 2 mM DTT, 50 mM NaCl at a concentration of 0.2 mg/ml. The CD spectra were measured using a Chirascan^{TM} CD Spectrometer (Applied Photophysics) in the wavelength range between 190 and 260 nm. Measurements were performed at room temperature using a quartz cuvette of 0.1 cm path length. The resulting spectra were analysed using the software BeStSel in order to estimate the content of secondary structures (Micsonai et al., 2018).

2.1.2.6 Retinol fluorescence enhancement

In order to confirm the functionality of the recombinant protein, a retinol fluorescence enhancement assay was performed. The measurements were performed using a 1 μM protein solution in SEC buffer, increasing the concentration of all-trans retinol from 0 to 10 μM. The titration was performed on an Edinburgh FS5 spectrofluorometer; the excitation and emission slit were set at 2 nm, the excitation wavelength was 330 nm, and emission spectra were collected every 5 nm in the range between 400 and 500 nm using a 1-second dwell time. The all-trans retinol was delivered in ethanol, which concentration was kept below 2%. After every addition of 1 μM all-trans retinol, 30 seconds of incubation time were given before taking the measurement.

2.2 Full-length RBP3

2.2.1 IPM isolation

Sus scrofa or *Bos taurus* eyes were bought from local slaughterhouses and kept on ice. The dissections were performed under dim red-light conditions, the detached retinas were first place on ice, then flash frozen in liquid nitrogen and stored at -80ºC for further use. For IPM isolations, a volume of roughly 100 ml of retinas was mixed with an equal volume of Buffer A (50 mM 4-(2-hydroxyethyl)-1-piperazine ethanesulfonic acid (HEPES) HCl, pH 8.0. 300 mM NaCl, 0.1 mM PMSF, 1 mM DTT), for 60 min at 4 ºC. The mixture was then centrifuged at 10 000 RCF for 25 min at 4°C for the

separation of the IPM. After centrifugation, the following components: $CaCl_2$, $MgCl_2$, $MnCl_2$ were added to the separated supernatant reaching the final concentration of 1mM for each component. The supernatant was then filtered through a glass wool-lined funnel. The filtered solution was then centrifuged at 20 000 RCF for 90 minutes at 4℃, and the resulting supernatant was filtered through a 0.45 μm syringe filter.

2.2.2 ConA affinity chromatography

The first step in the purification of the full-length RBP3 is represented by the affinity chromatography, which is performed exploiting the glycosylated states of *Bos taurus* and *Sus scrofa* RBP3 using the Concanavalin A (ConA)-Sepharose 4B (Cytiva) resin. The column was equilibrated with Buffer C (50 mM HEPES HCl, pH 8.0, 300 mM NaCl, 0.1 mM PMSF, 1 mM DTT, 1 mM $CaCl_2$, 1 mM $MgCl_2$, 1 mM $MnCl_2$). After equilibration, the previously mentioned supernatant (IPM isolate) was poured into the column and left on the rocker for three hours binding. After the binding step, the resin was washed using 100 ml of Buffer C. The elution of the glycosylated proteins from the column was obtained using 50 ml of methyl α-D-mannopyranoside (MDM) elution buffer (50 mM HEPES HCl, pH 8.0, 0.1 M NaCl, 400 mM methyl α-D-mannopyranoside,1 mM DTT). The entire procedure was performed at 4℃. Finally, the purity of the samples was analysed by SDS-PAGE.

2.2.3 Anion exchange chromatography

The purest fractions obtained from the ConA purification step were pulled down together, desalted, and concentrated to a final volume of 5 ml. The Amicon®Ultra Centrifugal Filter retentate was then loaded on the AKTA system for anion exchange chromatography as an intermediate purification step using HiTrap Q HP 1 ml column (Cytiva). The column was then washed with 10 ml of anion washing buffer (50 mM HEPES HCl, pH 8.0, 1mM DTT) The elution was performed by gradually increasing the proportion of the anion elution buffer (50 mM HEPES HCl, pH 8.0, 1 mM DTT, 1 M NaCl) (linear gradient), reaching 100% over a total volume of 10 ml. Absorbance at 280 nm was used to monitor protein elution; fractions of 1 ml were collected automatically through volume fractionation. The entire procedure was performed at 4℃. Finally, the purity of the samples was analysed by SDS-PAGE.

2.2.4 Size exclusion chromatography

The purest fraction obtained from anion exchange chromatography was loaded onto a Superdex 200 Increase 10/300 GL column (Cytiva) on an AKTA system for SEC as the last polishing purification step in order to separate the oligomeric state of the protein. Elution was performed with RBP3 SEC buffer (50 mM HEPES HCl, pH 8.0, 300 mM NaCl, 1 mM DTT, 0.01% n-dodecyl β-D-maltoside).

Absorbance at 280 nm was used to monitor protein elution; fractions of 700 µl were collected automatically through volume fractionation. The entire procedure was performed at 4°C. Finally, the purity of the samples was analysed by SDS-PAGE.

2.2.5 Deglycosylation

The deglycosylation reaction consisted of 450 µl of RBP3 (0.2 mg/ml) in RBP3 SEC buffer mixed with 50 µl of 10X GlycoBuffer (500 mM Sodium Phosphate pH 7.5) containing Peptide: N-Glycosydase F (PNGase F) from *Elizabethkingia meningoseptica* (Sigma Aldrich). The solution described above was incubated for 14 hours at room temperature on shaking. In order to confirm the successful outcome of the procedure, an 8% SDS-PAGE gel was run.

2.2.6 Western blotting

After SDS-PAGE, Western blot was run in order to confirm the identity of RBP3 and the cross-reactivity of our antibodies against RBP3 purified from different species. A polyvinylidene difluoride (PVDF) Immobilon-FL membrane was washed in absolute methanol and subsequently immersed in MilliQ water. The membrane was then equilibrated in transfer buffer (25 mM Tris HCl, pH 8.0, SDS 0.25% (m/vol), 192 mM glycine, 20% methanol (vol/vol)). The equilibrated PVDF membrane was placed on the resolved SDS-PAGE and placed between two layers of filter papers previously equilibrated with transfer buffer. The transfer was performed at 25 V for 30 minutes using a Trans-Blot® SD Semi-Dry Transfer Cell (Bio-Rad). After transfer, the PVDF membrane was incubated in blocking solution (5 % Non-fat dry milk, 137 mM NaCl, 2.7 mM KCl, 10 mM Na_2HPO_4, 1.8 mM KH_2PO_4, 0.1 % Tween-20) at room temperature for 1 hour on a rocker in order to saturate the unoccupied binding sites. The membrane was then washed three times with Phosphate Buffered Saline Tween 20 (PBST) buffer (137 mM NaCl, 2.7 mM KCl, 10 mM Na_2HPO_4, 1.8 mM KH_2PO_4, 0.1 % Tween-20) on the rocker at room temperature for 10 minutes each time and subsequently incubated with primary antibody (mAb5) for 1 hour on the rocker at room temperature. The membrane was then subjected to 3 serial washes of 10 minutes each with PBST on the rocker at room temperature. The primary antibody labelled protein was allowed to interact with the secondary antibody (goat anti-mouse IgG conjugated to Horse Radish Peroxidase (HRP)) by incubating on the rocker for 1 hour at room temperature. Subsequently, the unbound fraction of secondary antibody was removed by 3 serial washes of 10 minutes each with PBST on the rocker at room temperature. For the detection 5 ml of the solution A (250 mM luminol, 90 mM *p*-coumaric acid, 100 mM Tris HCl, pH 8.5) and B (5 mM H_2O_2, 100 mM Tris HCl, pH 8.5) were mixed together and poured over the membrane, the excessive solution was removed from the blot and the membrane was incubated in dark condition for 1 minute and the blot was developed by chemiluminescence.

2.2.7 Tryptophan fluorescence quenching

In order to confirm that RBP3 functionality was not impaired during the purification process, a tryptophan fluorescence quenching assay was performed. A solution of 4.4 μM of *Sus scrofa* or *Bos taurus* RBP3 maintained in a quartz cuvette in dark conditions was analyzed using the Perkin Elmer instrument Varian Cary Eclipse Fluorescence Spectrophotometer. The excitation and emission slit were set at 2 nm, the excitation wavelength was 280 nm, and emission spectra were collected every 5 nm in the range between 300 and 500 nm using a 1-second dwell time. Titrations (0−20 μM) of all-trans retinol or 11-cis retinal were performed at room temperature in 50 mM HEPES HCl buffer, pH 8.0, containing 300 mM NaCl, 0.1 mM DTT, 5% glycerol (v/v). The all-trans retinol and 11-cis retinal were delivered in ethanol, which concentration was kept below 2%. The assay was conducted at room temperature.

2.2.8 CryoEM and data collection

For CryoEM data collection, 3 μl of *Sus scrofa* RBP3 at a concentration of 0,8 mg/ml containing 0.5% 3-(3-Cholami dopropyl-dimethylammonio)-2-hydroxy-1-propanesulfonate (CHAPSO), were blotted on a Quantifoil R2/1 200 mesh grid (EM Sciences). For the preparation of the protein ligand complex, *Sus scrofa* RBP3 at a concentration of 0.9 mg/ml containing 0.5% CHAPSO was mixed with three different concentrations (2, 8, 12 μM) of all-trans retinol, 11-cis retinal, or DHA. The solutions were blotted using a Vitrobot Mark IV (ThermoFisher) system for 4 seconds at 4°C, 95% humidity, applying 0 blot force. The grid was then plunge-freeze in liquid ethane. The quality of the grid was assessed using a 200 kV Talos Arctica (Thermo Fisher) CryoEM microscope featuring a K2 Summit direct electron detector and Bioquantum Imaging filter. The grids that displayed the best behavior were analysed on a Titan Krios G1 microscope (Thermo Scientific) operated at 300 kV, aligned for fringe-free imaging, and equipped with a K3 direct electron detector and a BioQuantum Imaging Filter (Ametek). The data collection was performed in electron-counting mode at 105,000× magnification, corresponding to a pixel size of 0.8336 Å, with the energy slit width set to 10 eV. The software SerialEM was used for the data acquisition (Mastronarde, 2005). Using a dose diffraction mode, 23 971 movies were recorded with each movie comprising 40 frames with an exposure of 1 e $Å^{-2}$ per frame, resulting in an overall dose of 40 e $Å^{-2}$ across a 2-second exposure.

2.2.9 Image processing and model building

The CryoSPARC package software was used to process the collected CryoEM data (Structura Biotechnology) (Punjani et al., 2017). The motion correction was performed using full-frame motion correction, and the Contrast Transfer Function (CTF) was then estimated using CTFFIND4 (Rohou et al., 2015). Only the micrographs with CTF fits better than 4.5 Å and astigmatism below 400 Å

were retained. Blob picking was performed on a subset of micrographs for particle extraction, which, after several rounds of two-dimensional classification yielded 176 000 particles used for the generation of a low-resolution initial model and two-dimensional templates. Template picker was used to identify 7 462 000 particles that were subsequently analyzed by multiple rounds of two-dimensional classifications. In total, 1 903 572 particles showed clear secondary structure features and were selected for further processing for iterative hetero refinement with multiple initial volume progressively 3D classifying and decreasing the number of particles after each run. Local refinement was performed after each hetero refinement, allowing the generation of a coulomb potential map. The highest quality map was generated from 611 246 particles after three cycles of refinement. The procedure resulted in a sharpened map with a B-factor of −179.4 Å² and resolved to 3.67 Å (Fourier Shell Correlation (FSC) = 0.143). Due to their high flexibility, the N-terminal and C-terminal portions of the protein appeared smeared; for this reason, they were reconstructed using the three-dimensional flex algorithm in order to generate a better consensus map. The predicted *Sus scrofa* RBP3 Alphafold model was fitted into the generated *Sus scrofa* RBP3 CryoEM map. Multiple rounds of manual model building cycles were performed with COOT software, followed by real-space refinement using PHENIX, resulting in the final model of *Sus scrofa* RBP3 (Emsley et al., 2010, Liebschner et al., 2019). The software MolProbity was used to check the quality of the structure (Williams et al., 2018).

2.2.10 Small-Angle X-ray Scattering (SAXS)

The SAXS experiments were performed at the undulator beamline P12 of the Petra III storage ring at DESY (Hamburg, Germany). A solution of *Sus scrofa* RBP3 at 0.3 mg/ml (2.22 μM in 50 mM HEPES-HCl buffer, pH 8.0, supplemented with 300 mM NaCl and 0.1 mM DTT). The titration with various retinoids and fatty acids (all-trans retinol, 11-cis retinal, DHA, OA) was performed increasing the concentration of the analyzed ligand from 0 to 20 μM. The protein-ligand complexes were prepared by pipette resuspension and subsequently measured at the beamline. The ligands were solubilized and delivered in ethanol, which concentration was kept below 2% v/v of the total sample volume. The measurements were performed at 20°C, acquiring 40 frames of 1 s per sample. The buffer scattering profile was recorded and subtracted from the sample profiles. The data processing was carried out using the software Primusqt embedded in ATSAS 2.8.1 (Franke et al., 2017). The gyration radius (R_g) and the forward scattering intensity I(0) of each titration step were determined using AUTOGNOM, the same that software provided the molecular size estimate showing the pair-distance distribution function P(R). The P(R) function describes the shape of the particle in real space, reaching the value of zero at the maximum particle dimension (Dmax). The I(0) and the P(R) function values provided by AUTOGNOM served as input for the generation of 10 *ab initio* models using the software DAMMIF and Gasbor (Franke et al., 2017).

2.2.11 Docking

The non-flexible portion of *Sus scrofa* RBP3 structure, ranging from the glutamate residue 417 to proline 1191, was used as a receptor while the all-trans retinol, 11-cis retinal, OA, and DHA were used as ligands. CB-Dock2 was used for docking simulations; in total, 20 potential cavities were screened for each ligand using the prepared libraries (Liu et al., 2022). In order to precisely identify the binding position, AutoDock Vina predictions were used for each ligand (Trott and Olson, 2010; Eberhardt, et al., 2021).

2.3 Cell culture and monoclonal antibody production

The Hybridoma F3F5 cells used for the production of the mAb5 antibody were gifted to ISB lab by Palczewski's lab. The cells were thawed in a water bath at 37°C and transferred to a 15 ml conical tube with 3 ml of Mixed Medium previously warmed at 37°C. The Mixed Medium consisted of 75% of DMEM-based Hybridoma Medium (DMEM medium, 10% Fetal Bovine Serum (FBS), L-glutamine 2 mM, Penicillin-Streptomycin 50 U/ml, 1X Hybridoma Fusion and Cloning Supplement (HFCS)) and 25% Hi-Growth Hybridoma Medium (RPMI-1640 medium, 10% FBS, L-glutamine 2 mM, Penicillin-Streptomycin 50 U/ml, 1X HFCS, 10% NCTC-109 medium (Gibco™), 1X Non Essential Amino Acid solution (NEAA) (Gibco™). After resuspension, the solution was centrifuged at 166 RCF for 5 minutes at room temperature, supernatant was discarded, and the pellet was resuspended in 3 ml of Mixed Medium and incubated in a 50 ml flask at 37°C, 5% CO_2 for 24 hours. Culture volume was progressively increased by the addition of fresh Mixed Media, reaching a final volume of 500 ml. In order to induce the cellular stress required for the production of the mAb5 monoclonal antibody, the cells were centrifuged at 166 RCF for 5 minutes at room temperature. Next, pelleted cells were carefully washed in 30 ml Phosphate Buffered Saline (137 mM NaCl, 2.7 mM KCl, 10 mM Na_2HPO_4, and 1.8 mM KH_2PO_4) (PBS), and the cells were centrifuged at 166 RCF for 5 minutes at room temperature. The pelleted cells were resuspended in 500 ml of RPMI-based medium (RPMI-1640, 2 mM L-glutamine, 50 U/ml Penicillin-Streptomycin) and incubated at 37°C, 5% CO_2. After 4 days of incubation, 500 ml of cell culture were centrifuged at 10 000 RCF for 5 minutes at 4°C. The supernatant was collected and filtered through a 0.2 µM filter. The filtered supernatant containing the mAb5 monoclonal antibody was concentrated using a 10 kDa cut-off Amicon®Ultra Centrifugal Filter at 3000 RCF at 4°C until a final volume of 15 ml was reached and stored at 4°C.

The affinity chromatography technique was used to purify the mAb5 monoclonal antibody as suggested by Sears and colleagues (Sears et al., 2020). In total, 5 ml of the previously concentrated

supernatants were applied to the HiTrap Protein G HP 1 mL column (Cytiva), and the column was then washed with 20 ml PBS. The elution was performed using 5 ml of 100 mM Glycine pH 2.5. The eluted fractions of 0.5 ml were collected into tubes containing 25 µL of 1 M Tris HCl pH 9.5, and the tubes were gently mixed immediately after elution in order to neutralize pH. Absorbance at 280 nm was used to monitor protein elution. The entire procedure was performed at 4°C. Finally, the purity of the fractions corresponding to the elution peak in the chromatogram was analysed by SDS-PAGE.

3 Results

3.1 *Bos taurus* RBP3 modules

3.1.1 *Bos taurus* RBP3 modules cloning and purification

One of the scopes of the present research project, together with the determination of the full-length RBP3 structures is the identification of the retinoid binding sites on RBP3. Although the crystallization of full-length RBP3 is difficult to achieve (Gonzalez-Fernandez et al., 2014), likely due to the intrinsic flexibility of this protein, the single modules are more likely to tolerate being crystallized. In fact, the *Danio rerio* RBP3 module was crystallized in complex with the OA (Ghosh et al., 2015). Even if this approach (using protein fragments) is potentially less informative, since it causes a loss of context and potential binding sites located between modules, rather than the study of the full-length protein, is nonetheless expected to be effective in the identification of the amino acids involved in the retinoid binding site for binding sites fully located within the boundaries of the single modules. Moreover, crystallography is the technique that allows to achieve the highest possible resolution, and as a rule of thumb more stable/rigid is the construct, the higher the probability to produce structures of higher resolution. An attempt to produce the single modules (M1, M2, M3, M4) and the tandem duplets (M1M2, M2M3) in fusion with a terminal 6x histidine tag was not successful, however, leading to the production of insoluble inclusion bodies (data not shown). In order to increase the solubility of the constructs, the single modules (M1, M2, M3, M4) and the tandem duplets (M1M2, M2M3, M3M4) were produced recombinantly and cloned into the pGEX-6P-1 plasmid with a GST tag (Schäfer et al., 2015) at the N-terminus and a cleavage site between the tag and the protein of interest (Appendix 1). To verify that the cloning was successful, the recombinant plasmids were subjected to double restriction digestion to confirm the presence of the gene of interest between the selected restriction sites (BamH1, Xho1). All the constructs (Table 1) prepared showed a band of the expected size in the agarose gel electrophoresis (Figure 3.1).

Construct name	Expected size in base pairs (bp) / amino acid range	Sequencing result
GST-bRBP3M1 (Module 1)	969 / amino acids 20 to 323	OK
GST-bRBP3M2 (Module 2)	945 / amino acids 318 to 632	OK
GST-bRBP3M3 (Module 3)	912 / amino acids 631 to 935	Mutated
GST-bRBP3M4 (Module 4)	903 / amino acids 931 to 1232	OK
GST-bRBP3M1M2 (Module 1+2)	1896 / amino acids 20 to 632	OK
GST-bRBP3M2M3 (Module 2+3)	1854 / amino acids 318 to 935	OK
GST-bRBP3M3M4 (Module 3+4)	1803 / amino acids 631 to 1232	OK

Table 1: List of bRBP3 recombinant constructs.

After double restriction digestion, the recombinant plasmids were furtherly checked by Sanger sequencing. After analysing the chromatogram results (data not shown), all the constructs, with the exception of the plasmid encoding for Module 3, were in frame and no mutation was detected in their nucleotide sequences.

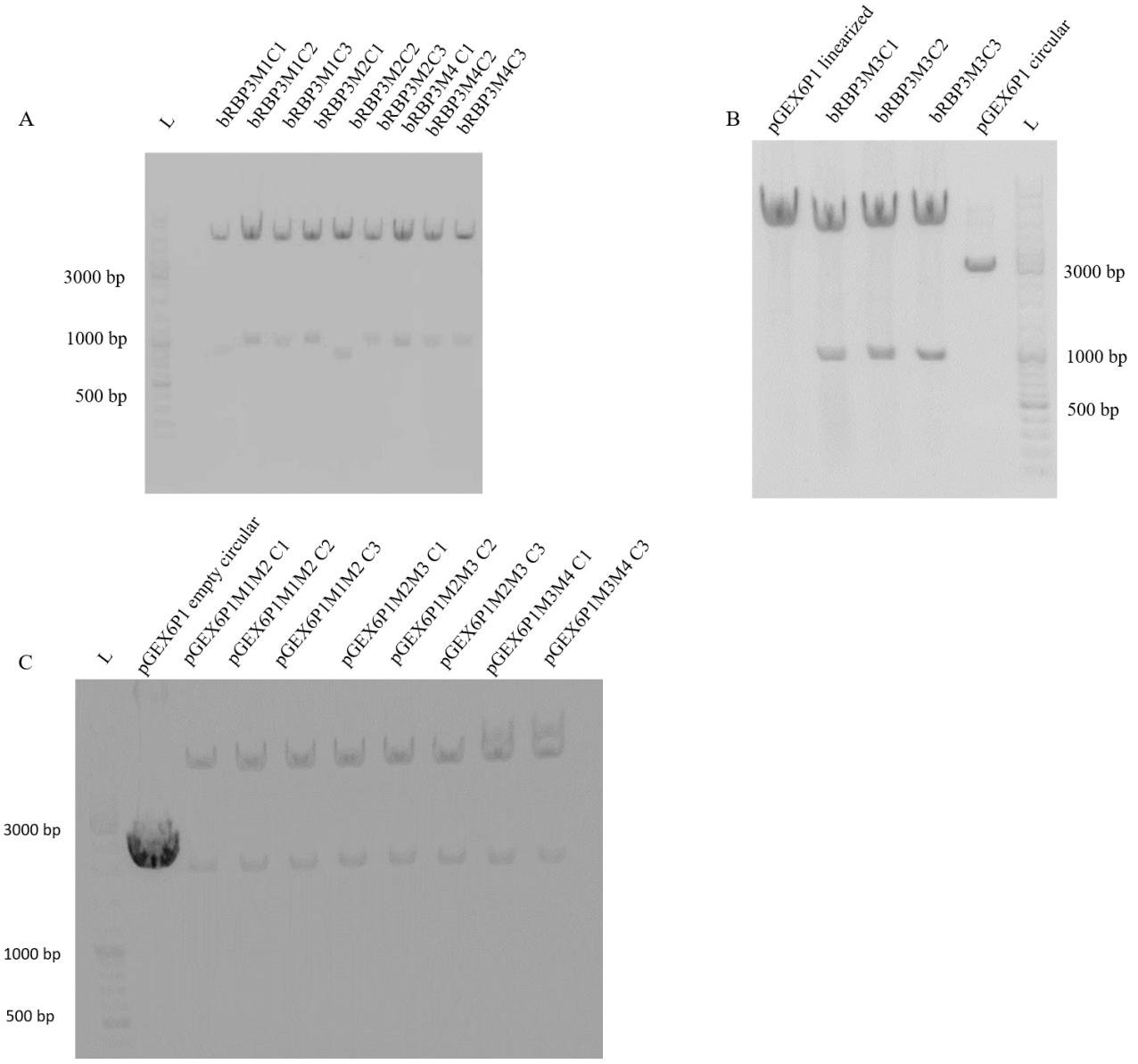

Figure 3.1: Agarose gel electrophoresis after double digestion of recombinant plasmids. A) Constructs encoding for bRBP3 Module 1, Module 2, and Module 4. B) Constructs encoding for Module 3. C) Constructs encoding for tandem modules M1M2, M2M3, M3M4.

After sequencing validation, the plasmids encoding for M1, M2, M3, M4, and M1M2, M2M3, M3M4 were transformed into *Escherichia coli* (*E. coli)* C43(DE3). The cultures were grown in LB and Terrific Broth (TB) media; no significant differences in expression levels and solubility were detected. The protein expression was induced using 50 μM of IPTG at OD600nm = 1. Different

concentrations of IPTG (0.1 mM, 0.5 mM, 1mM) were tested, and 0.1 mM IPTG was found to be sufficient to obtain a good protein expression level (Figure 3.2 and 3.3). To test the solubility of the constructs, the samples were sonicated and centrifuged, supernatant and pellet were then analysed through SDS-PAGE. All the recombinant proteins expressed were forming inclusion bodies; the only exception was represented by GST-bRBP3M4 which was partially soluble (Data not shown).

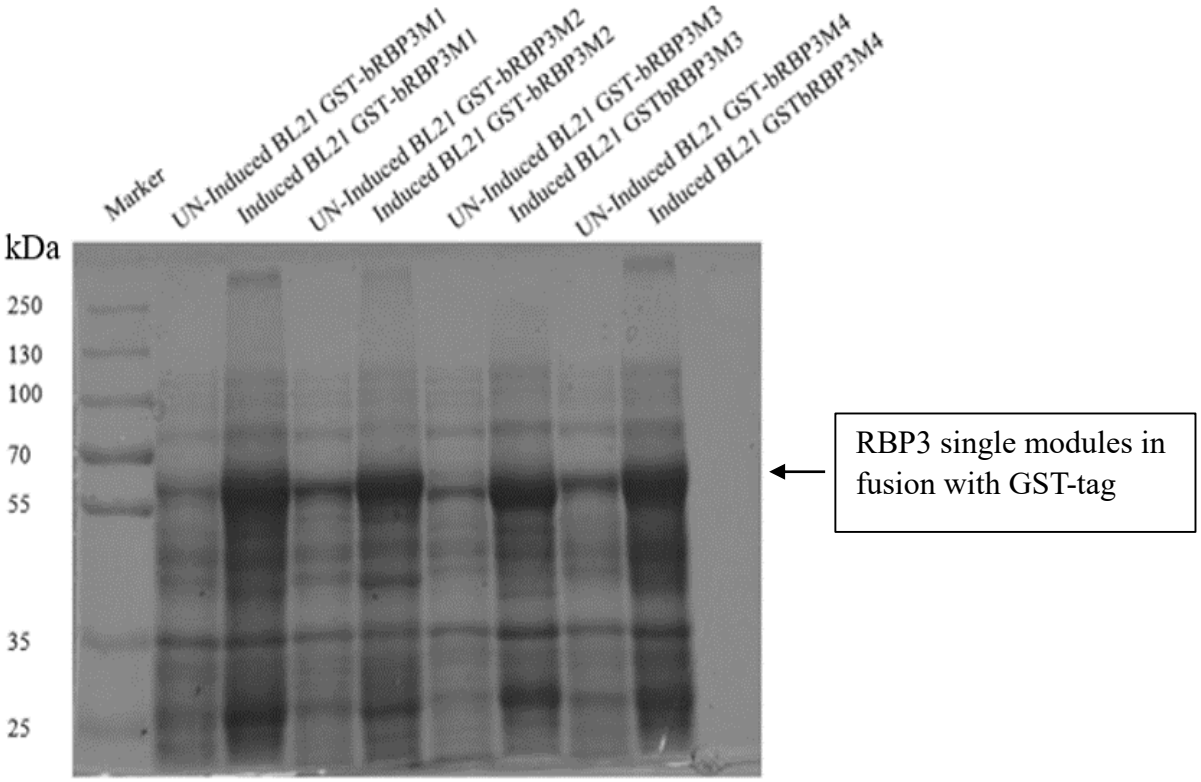

Figure 3.2: Expression of bRBP3 single modules. 15% SDS-PAGE analysis of recombinant expression trials of different bRBP3 modules in BL21(DE3).

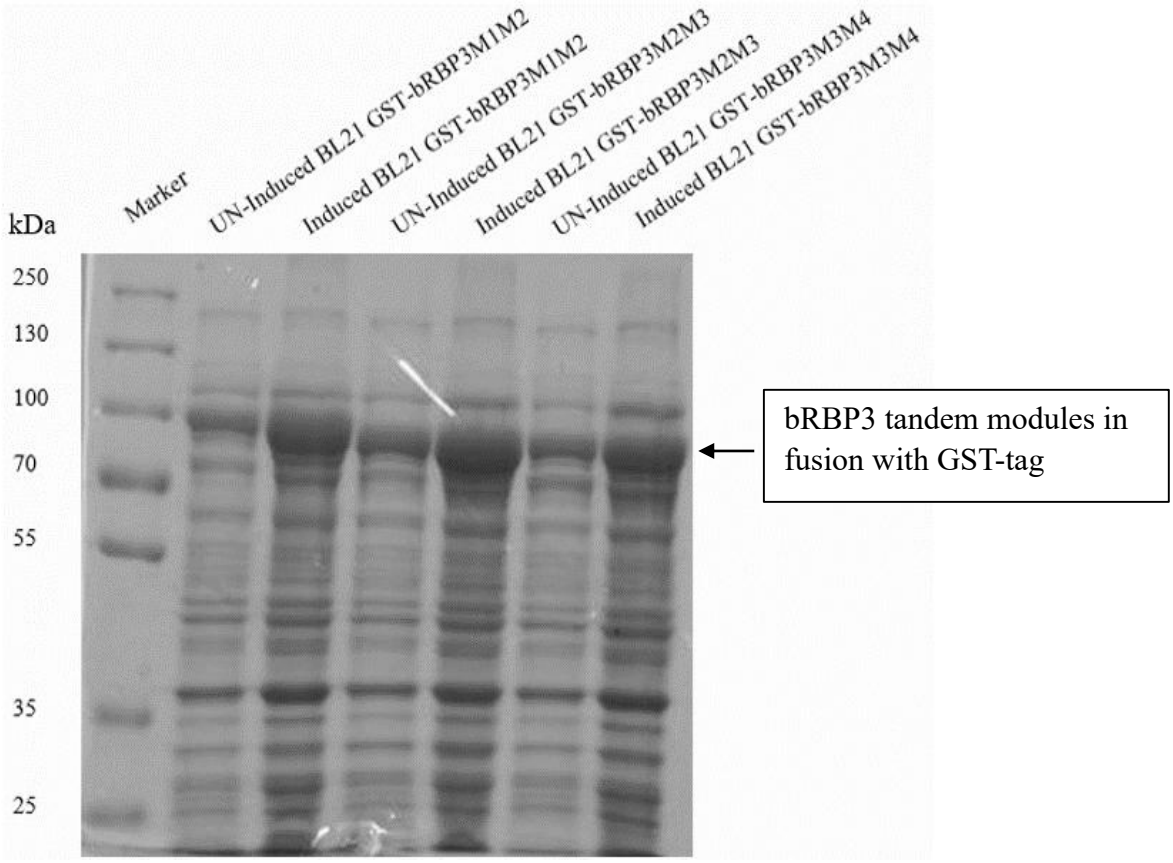

Figure 3.3: Expression of bRBP3 tandem modules. 15% SDS-PAGE analysis of recombinant expression trials of different bRBP3 tandem modules in BL21(DE3).

Due to the fact that it is difficult to completely restore the functionality and the binding ability of the RBP3 modules recovered from inclusion bodies (Baer et al., 1998), no further attempts were made in order to restore the misfolded proteins from inclusion bodies, instead, a subsequent effort was focused only on the partially soluble construct GST-bRBP3M4 and to maximize its yeld.

The purification of bRBP3M4 was obtained through three chromatographic steps. The first step is performed by exploiting the GST tag attached at the N-terminus of the protein to retain the bRBP3M4 construct to the GST resin. During this step, the GST tag is cleaved using the PreScission protease (Kind gift from Professor Bochtler) (Figure 3.4). First the GST-bRBP3M4 (59 kDa) protein present in the load (L) is retained by the resin, while all the other bacterial proteins, unable to bind to the resin, are washed away in the Sample Application Flow Through (SAFT) and the Washing Flow Through (FT). After the addition of the PreScission protease, the cleaved bRBP3M4 (33 kDa) is eluted in the cleaved fraction (Cleavage FT) and in the Washing 1 and 2 fractions. The elution buffer leads to the release of the un-cleft GST-bRBP3M4 (59 kDa), PreScission protease (45 kDa), residual bRBP3M4 (33kDa), and GST tag (26 kDa).

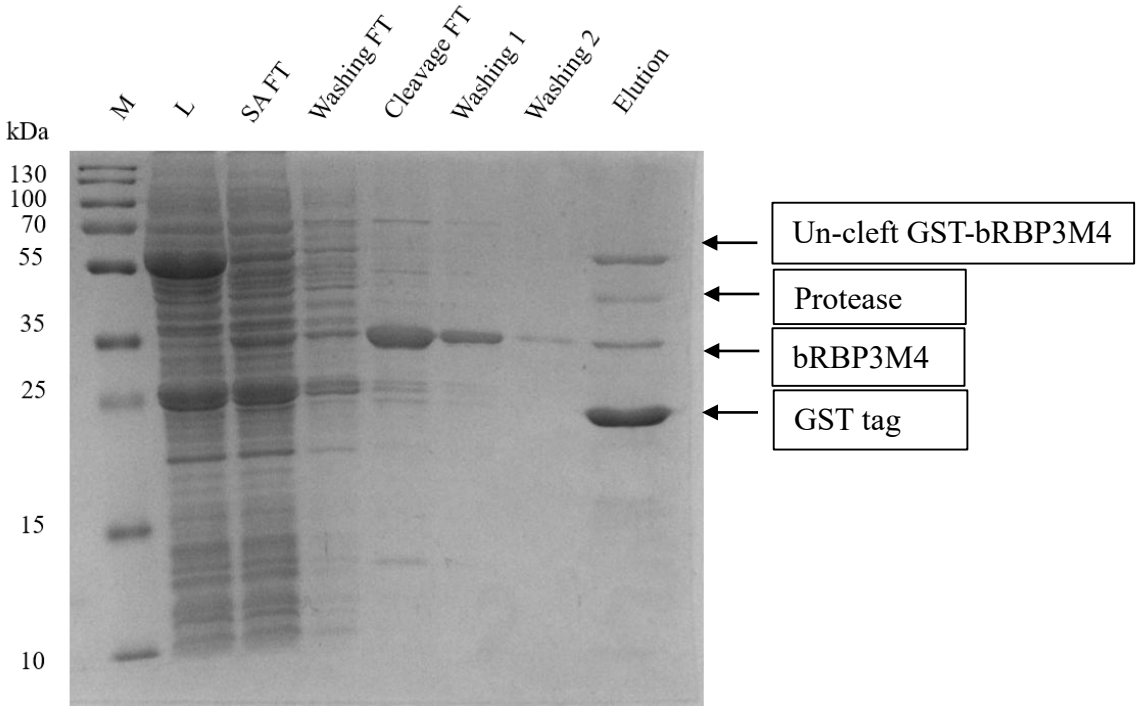

Figure 3.4: SDS-PAGE for bRBP3M4 after affinity chromatography. 15% SDS-PAGE analysis of affinity chromatography purification of GST-bRBP3M4. M stands for Marker, L stands for Load, SAFT stands for Sample Application Flow Through, FT stand for Flow Through.

The fractions "cleavage FT" and "Washing 1" were pulled together, concentrated, desalted, and furtherly purified through anion exchange chromatography Mono Q^{TM} 5/50 GL column (Figure 3.5 and 3.6).

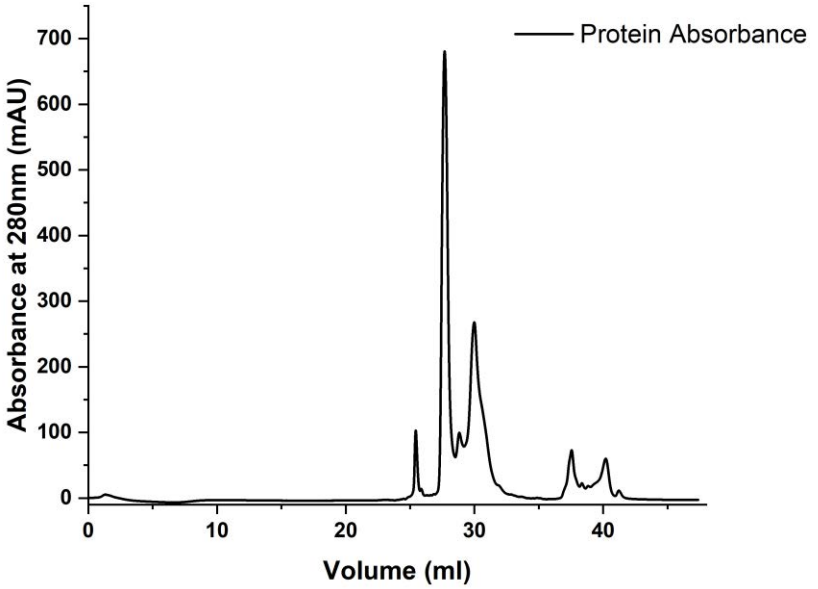

Figure 3.5: Anion exchange chromatogram for bRBP3M4. Chromatogram of the bRBP3M4 using a Mono Q^{TM} 5/50 GL column.

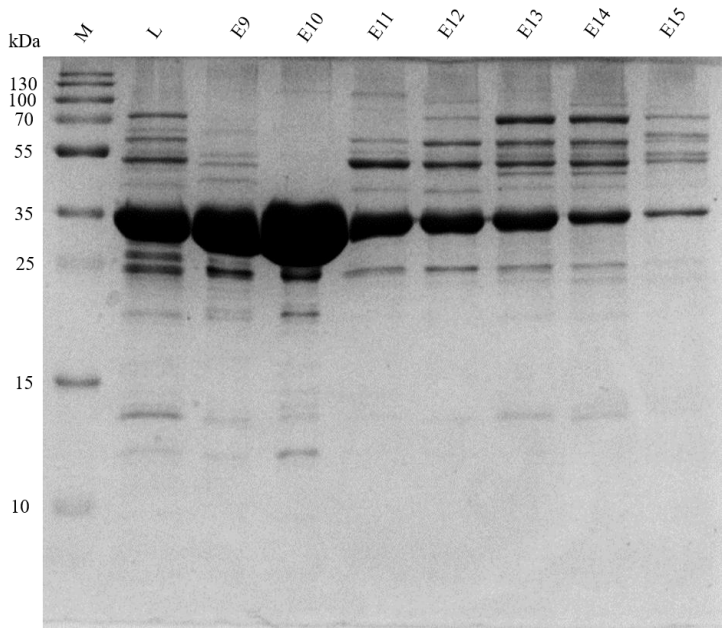

Figure 3.6: SDS PAGE after anion exchange chromatography. 15% SDS-PAGE analysis of anion exchange chromatography purification of bRBP3M4. M stands for Marker, L stands for Load, E stands for Elution fraction.

The fraction E10 was subsequently loaded on a SEC for the final polishing step (Figure 3.7 and 3.8).

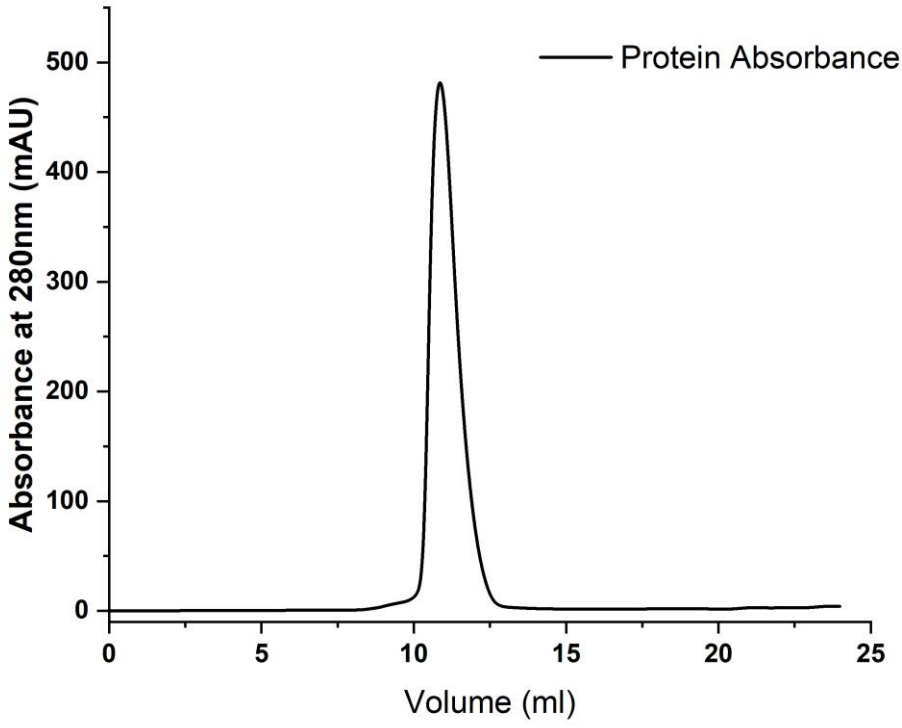

Figure 3.7: SEC chromatogram for bRBP3M4. Chromatogram of the bRBP3M4 on a Superdex 75 increase 10/300 GL column.

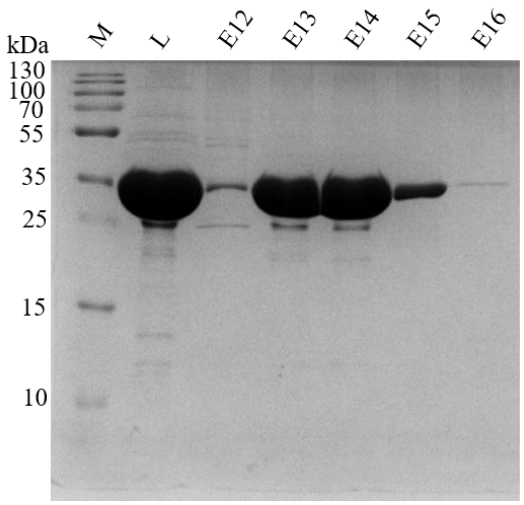

Figure 3.8: SDS PAGE of bRBP3M4 after SEC. 15% SDS-PAGE analysis of SEC chromatography purification of bRBP3M4. M stands for Marker, L stands for Load, E stands for Elution fraction.

On average, 3 mg of purified protein could be obtained per litre of LB media.

3.1.2 *Bos taurus* RBP3 Module 4 Circular dichroism

After SEC, the protein was diluted in 50 mM Tris-HCl pH 8.0, 2 mM DTT, 50 mM NaCl buffer until the concentration of 0.35 mg/ml. The spectra were acquired between 190 and 260 nm wavelengths. Two negative peaks at 209.5 nm and 218.5 nm show the molar ellipticity values [θ] of -40.01 deg·cm²·dmol⁻¹ and -36.39 deg·cm²·dmol⁻¹, respectively. A positive peak is present at 196 nm with the value of 30.73 deg·cm²·dmol⁻¹ (Figure 3.9).

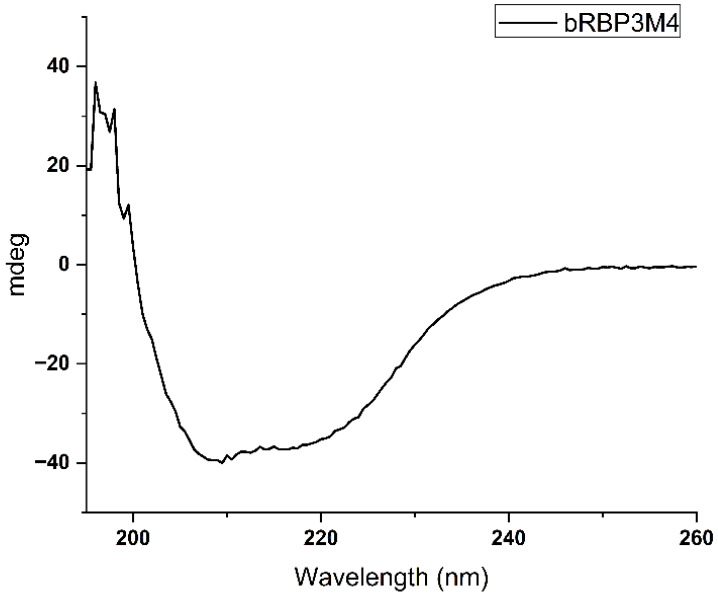

Figure 3.9: CD spectra for bRBP3M4.

The analysis of the data using the Bestsel software (Micsonai et al., 2018) showed that 21.9 % of bRBP3M4 residues form an α-helix structure, while 18.6% of the residues adopt a β-strand structure. The results are slightly different from the values predicted by the software Phyre 2.2 (Powell et al., 2025), which report 26% of residues in α-helix structure and 24% in a β-strand structure.

3.1.3 *Bos taurus* RBP3 Module 4 Fluorescence assay

The fluorescence enhancement assay was the technique selected for confirming the ability of bRBP3M4 to properly interact with the retinoids. The addition of the all-trans retinol to a solution containing 1 μM protein did not lead to a significant increase in the fluorescence enhancement compared to the all-trans retinol alone (control) (Figure 3.10). The fluorescence enhancement assay shows the inability of the recombinant construct to bind all-trans retinol.

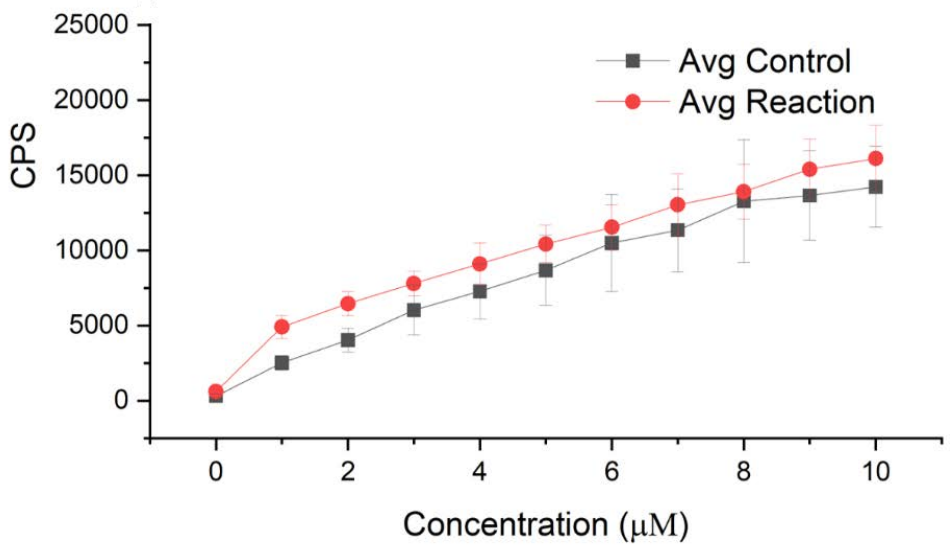

Figure 3.10: Fluorescence enhancement assay for bRBP3M4 with all-trans retinol.

3.2 *Sus scrofa* RBP3

3.2.1 *Bos taurus* and *Sus scrofa* RBP3 comparison

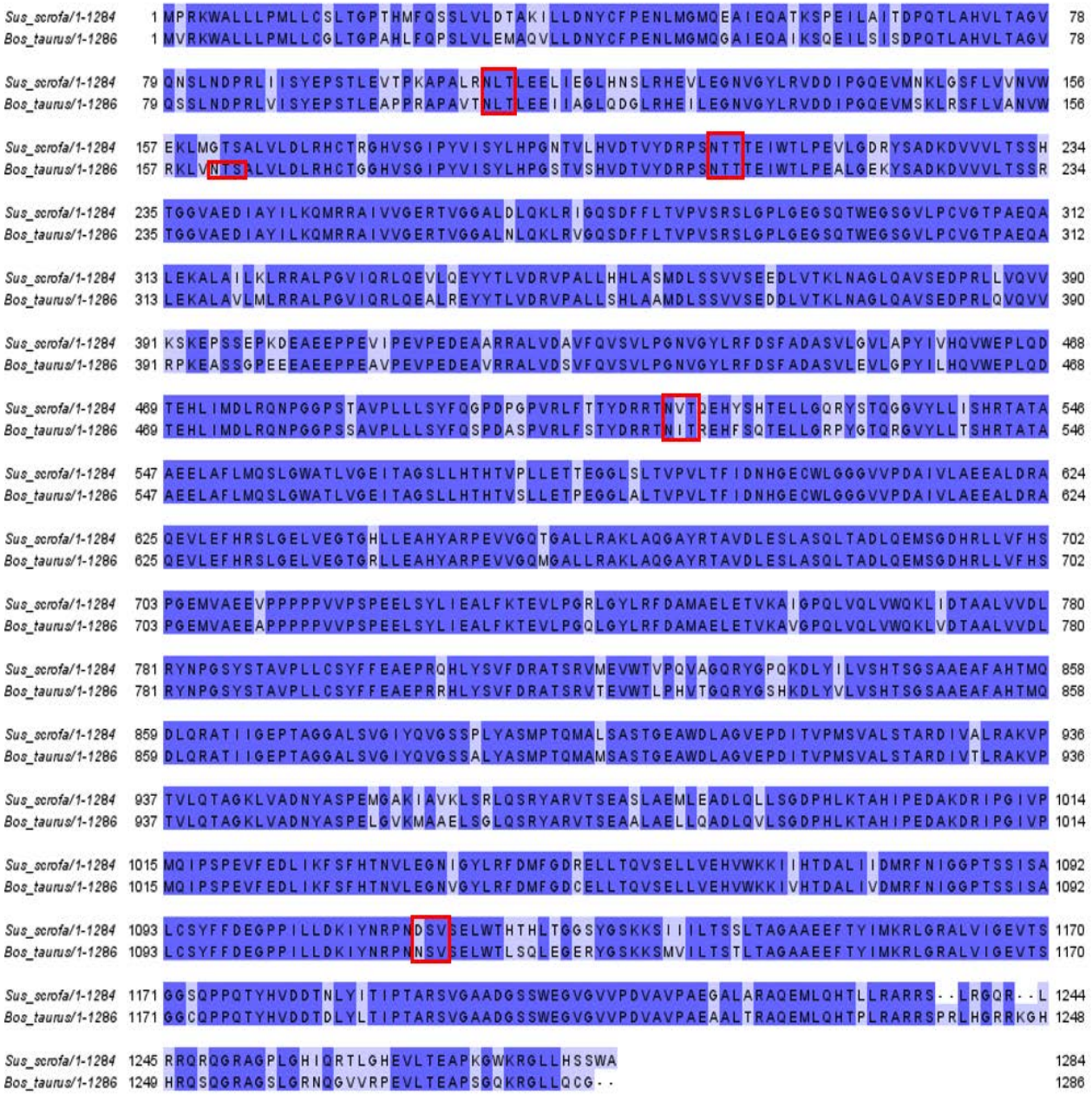

Figure 3.11: Sequence alignment of Sus scrofa (NCBI reference sequence: XP_020928418.1) and Bos taurus (NCBI reference sequence: NP_776589.1) RBP3. Predicted glycosylation sequons according to NetNGlyc (Gupta and Brunak, 2002) are marked in red boxes. Sequence alignment was made using the software Jalview (Waterhouse et al., 2009) and the embedded algorithm Clustal (Larkin et al., 2007).

Considering the inability to obtain a functional protein through recombinant expression of the single modules for X-ray diffraction, it has been decided to isolate the full-length protein from native sources in order to determine the structure through CryoEM. Initially, *Bos taurus* RBP3 was the preferred target; however, in order to increase the probability of obtaining a high resolution structure, *Sus scrofa*

RBP3 was included in the study, given the high percentage identity and the similar glycosylation pattern between the two orthologs (Figure 3.11).

3.2.2 Monoclonal antibody purification and validation

The monoclonal antibody mAb5 is secreted to the media during the hybridoma cells used growth. After concentration of the RPMI media, the desired antibody (mAb5) was purified through the use of an affinity chromatographic technique, leading to a single elution peak as shown in Figure 3.12.

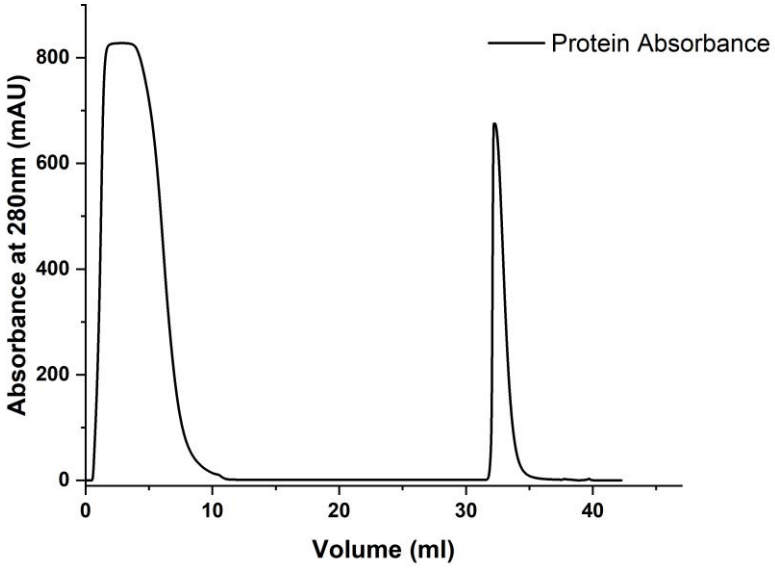

Figure 3.12: Affinity chromatography for the purification of mAb5. Chromatogram of the mAb5 on a HiTrap Protein G HP.

The purity was then assessed through an SDS-PAGE, where the bands corresponding to the heavy chains (50 kDa) and the light chains (25 kDa) are clearly visible (Figure 3.13).

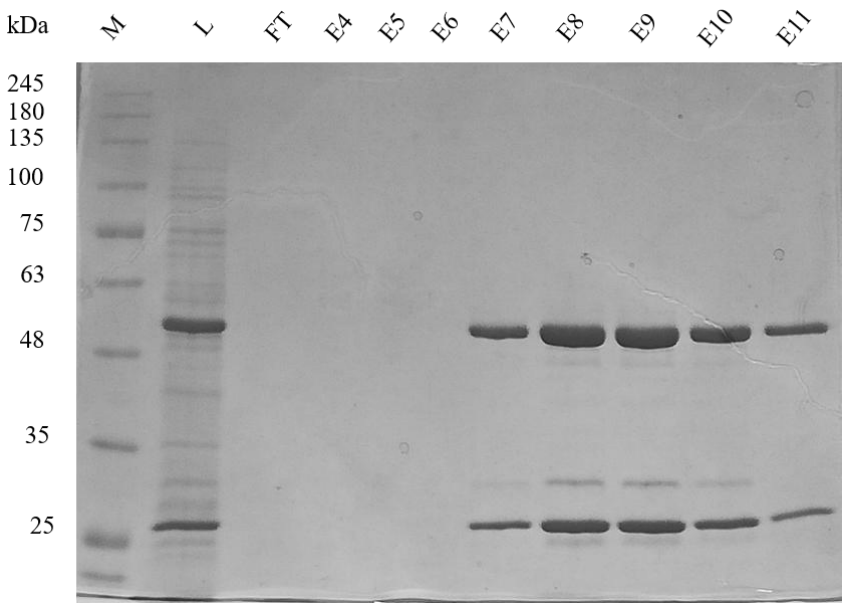

Figure 3.13: SDS-PAGE for mAb5 purification. 12% SDS-PAGE analysis of affinity chromatography purification of mAb5. M stands for Marker, L stands for Load, FT stands for Flow Through, E stands for Elution fraction.

In order to confirm the ability of the antibody to bind RBP3, a western blot analysis was performed (Figure 3.14).

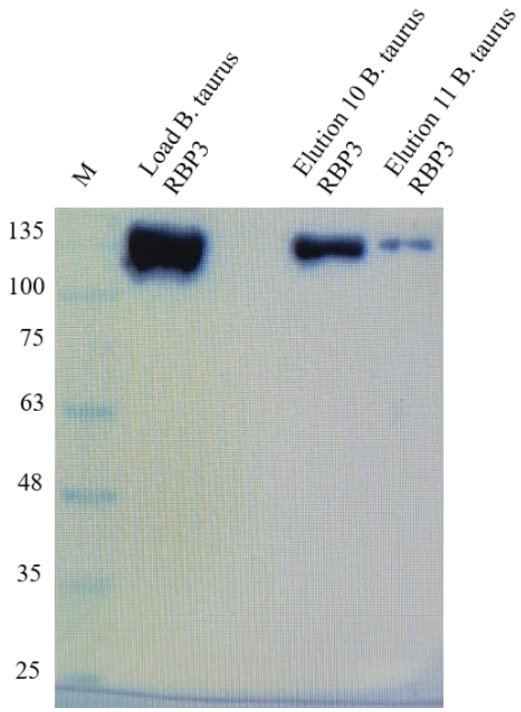

Figure 3.14: Western blot analysis of mAB5 against Bos taurus RBP3. Samples were resolved on a 10% SDS-PAGE. The blot was probed using the primary antibody mAb5 followed by goat anti-mouse IgG conjugated to HRP.

To test the ability to recognize folded RBP3 in solution, *Sus scrofa* RBP3 was incubated with the Fab of mAb5 (kind gift from Professor Palczewski's lab). The complex formation causes a shift in the retention volume of the elution peak from 11:46 to 10:98 in SEC (Figure 3.15), similarly to the result obtained by Sears and colleagues for the *Bos taurus* RBP3 (Sears et al., 2020).

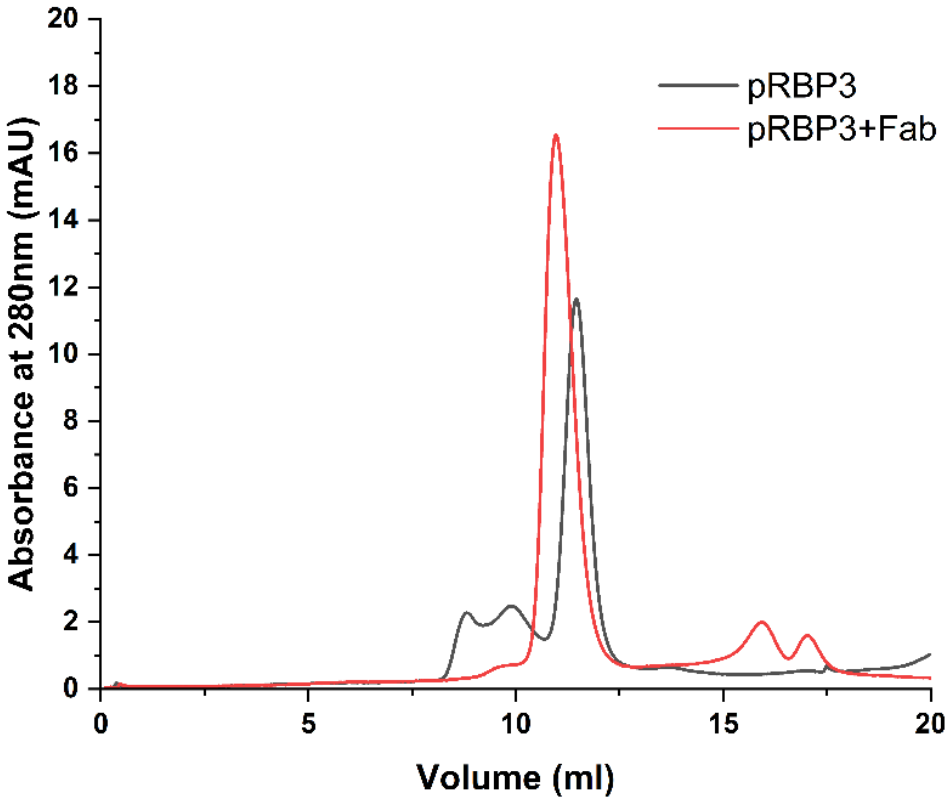

Figure 3.15: Overlapping chromatogram of Sus scrofa RBP3 SEC (pRBP3 in black) and Sus scrofa RBP3 incubated with Fab of mAb5 (pRBP3 plus Fab in red).

Of note, and perhaps not surprisingly, due to the high percentage identity between *Sus scrofa* and *Bos taurus* RBP3, mAb5 shows the ability to cross-react with *Sus scrofa* RBP3 as it was confirmed by western blot (Figure 3.16).

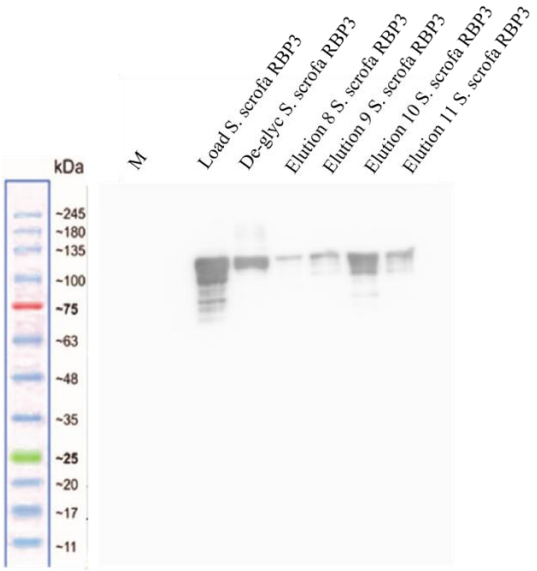

Figure 3.16: Western blot of Sus scrofa RBP3 against mAb5. Due to the limited sensitivity of the instrument, the protein marker is not visible, and the band size were estimated according to parallel experiment and distance run by the bands. Samples were resolved on a 10% SDS-PAGE. The blot was probed using the primary antibody mAb5 followed by goat anti-mouse IgG conjugated to HRP.

3.2.3 Full length RBP3 Purification

Due to easier accessibility, *Bos taurus* and *Sus scrofa* RBP3 were isolated. Both orthologs were purified from bovine and porcine retinas, respectively, using the same procedure. After stirring retinas in high salt buffer solution and two centrifugation rounds the protein was successfully purified through three chromatographic steps: ConA affinity chromatography allowed immediate removal of RBP3 from its natural environment, exploiting its glycosylation state, retaining only the glycosylated proteins (Figure 3.17), while all the non-glycosylated proteins are washed away.

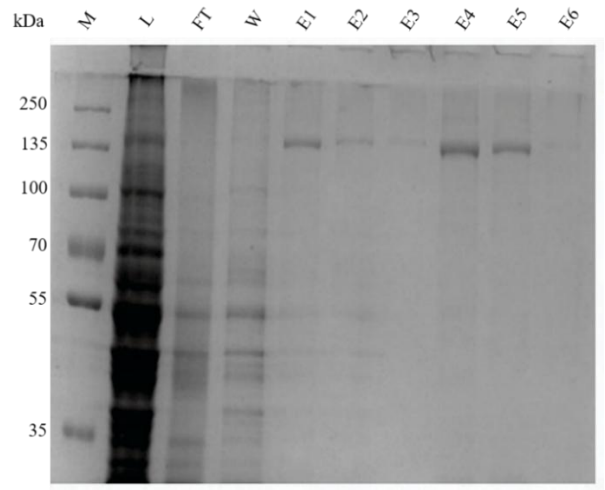

Figure 3.17: ConA affinity chromatography purification step for Sus scrofa RBP3 (Picture adapted from Kaushik et al., 2025B under the licence CC BY 4.0). *Bos taurus* RBP3 provided similar result (Data not shown). *10% SDS-PAGE analysis of affinity chromatography purification of Sus scrofa RBP3. M stands for Marker, L stands for Load, FT stands for Flow Through, W stands for Wash, E stands for Elution fraction.*

To further purify RBP3 and to prevent any harmful interactions with proteases present in the IPM, an anion exchange is used as an intermediate step (Figure 3.18 and 3.20A). This step also helps to remove fatty acid contaminants.

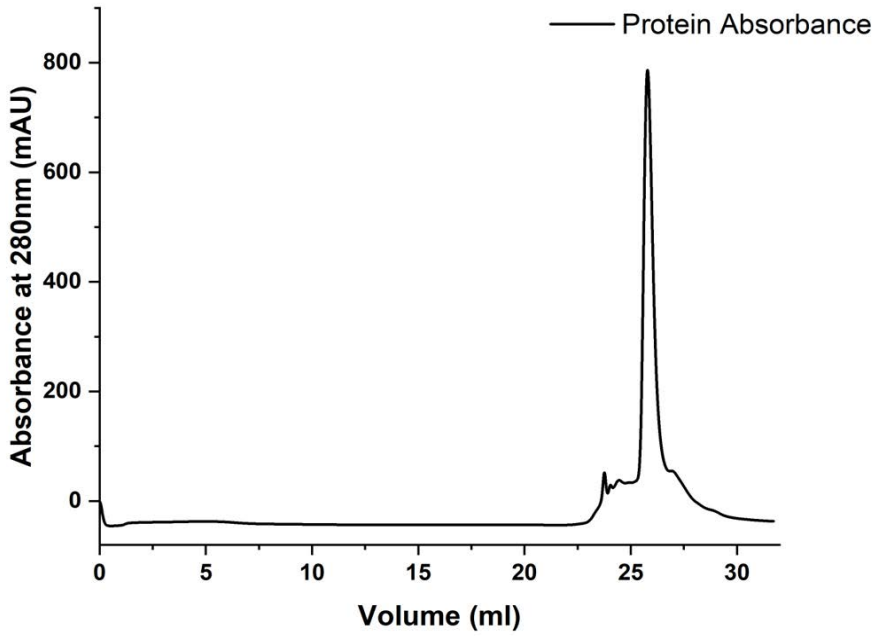

Figure 3.18: Anion exchange chromatogram of Sus scrofa RBP3. Chromatogram of anion exchange chromatography of Sus scrofa RBP3 using HiTrap Q HP column.

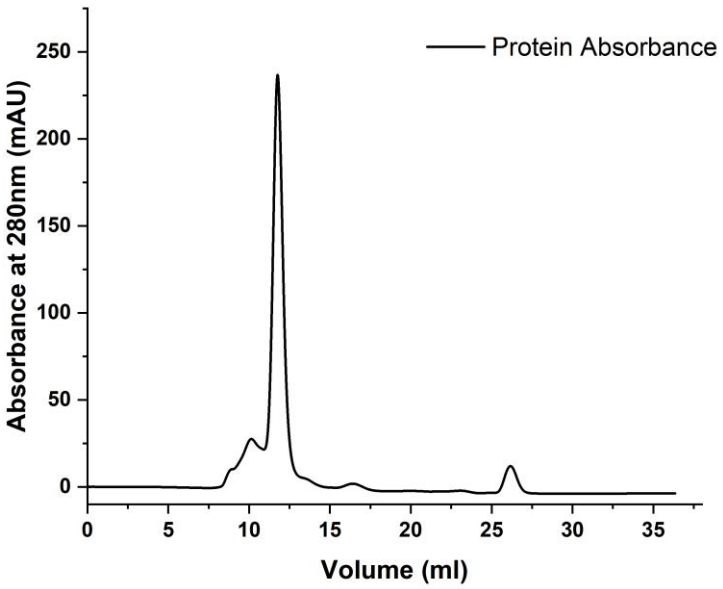

Figure 3.19: SEC for Sus scrofa RBP3. SEC chromatogram of Sus scrofa RBP3 using Superdex 200 increase 10/300 GL.

SEC was used for the final polishing step and for the separation of the oligomeric state, rendering a highly pure monomeric protein (Figure 3.19). During the whole purification procedure, RBP3's tendency to form aggregates was successfully limited by DTT and high NaCl concentration. DDM was used as a detergent during the last chromatographic step, its concentration (0.01%) never resulted in micelle formation. The purification process typically average yield oscillates between 2 and 2.5 mg from 600 pork eyes and 0.3 to 0.4 mg from 60 bovine eyes. *Sus scrofa* RBP3 is predicted to have four N-Glycan chains attached to the asparagine residues 107, 205, 513, and 1114. The purified protein was subjected to deglycosylation treatment performed using the enzyme PNGaseF. Its efficiency was evaluated by SDS-PAGE. When successful, a shift corresponding to 5 kDa was visible in the SDS-PAGE gel (Figure 3.20C). Three glycosylation asparagine residues (107, 513, 1014) were confirmed by mass spectrometry (data not shown). SEC allows a good separation of the oligomeric state of the protein, showing two different molecular weight peaks corresponding to aggregates and monomeric protein, respectively (Figure 3.19 and 3.20B).

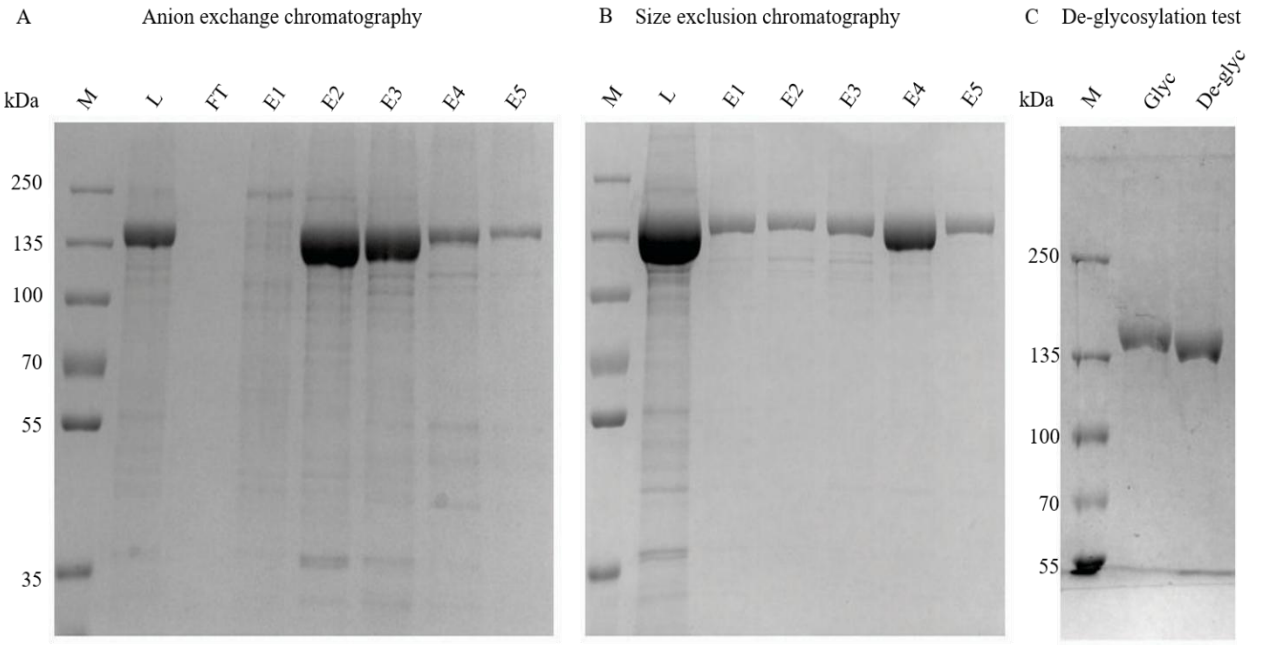

*Figure 3.20: Purification steps for Sus scrofa RBP3, M stands for Marker, L stands for Load, E stands for Elution fraction (*Picture adapted from Kaushik et al., 2025B under the licence CC BY 4.0*). A) 10% SDS-PAGE of Sus scrofa RBP3 performed after anion exchange chromatography. B) 10% SDS-PAGE of Sus scrofa RBP3 performed after SEC chromatography. C) 8% SDS-PAGE of glycosylated and de-glycosylated Sus scrofa RBP3.*

3.2.4 RBP3 biophysical characterization

In order to confirm that the protein conformation and functionality were not affected during the purification process, its functionality, ligand binding capacity, and ability to interact with retinoid molecules were tested through fluorescence binding assays. The ability of full-length RBP3 was

tested using tryptophan quenching, after the excitation at 280 nm it is visible an emission peak at 350 nm. The increase in all-trans retinol concentration causes a marked decrease in fluorescence emission peak at 350 nm, and a modest increase at 480 nm peak is visible (Figure 3.21A). Also, the titration with 11-cis retinal caused tryptophan quenching; however, the decrease at 350 nm is less marked, and a lower concentration is required for reaching the saturation point. Furthermore, there is no visible peak at 480 nm, given the non-fluorescence nature of 11-cis retinal (Figure 3.21B).

Glycan chains are known to reduce the flexibility of a glycosylated protein (Lee et al., 2015). Tryptophan fluorescence quenching assay was performed using a de-glycosylated version of *Bos taurus* RBP3; the de-glycosylation affected the binding properties of bovine RBP3, since de-glycosylated RBP3 requires less amount of all-trans retinol for reaching the saturation point (Cm) 0.3 µM) compared to the fully glycosylated protein (Cm 3.5 µM) (Figure 3.21C).

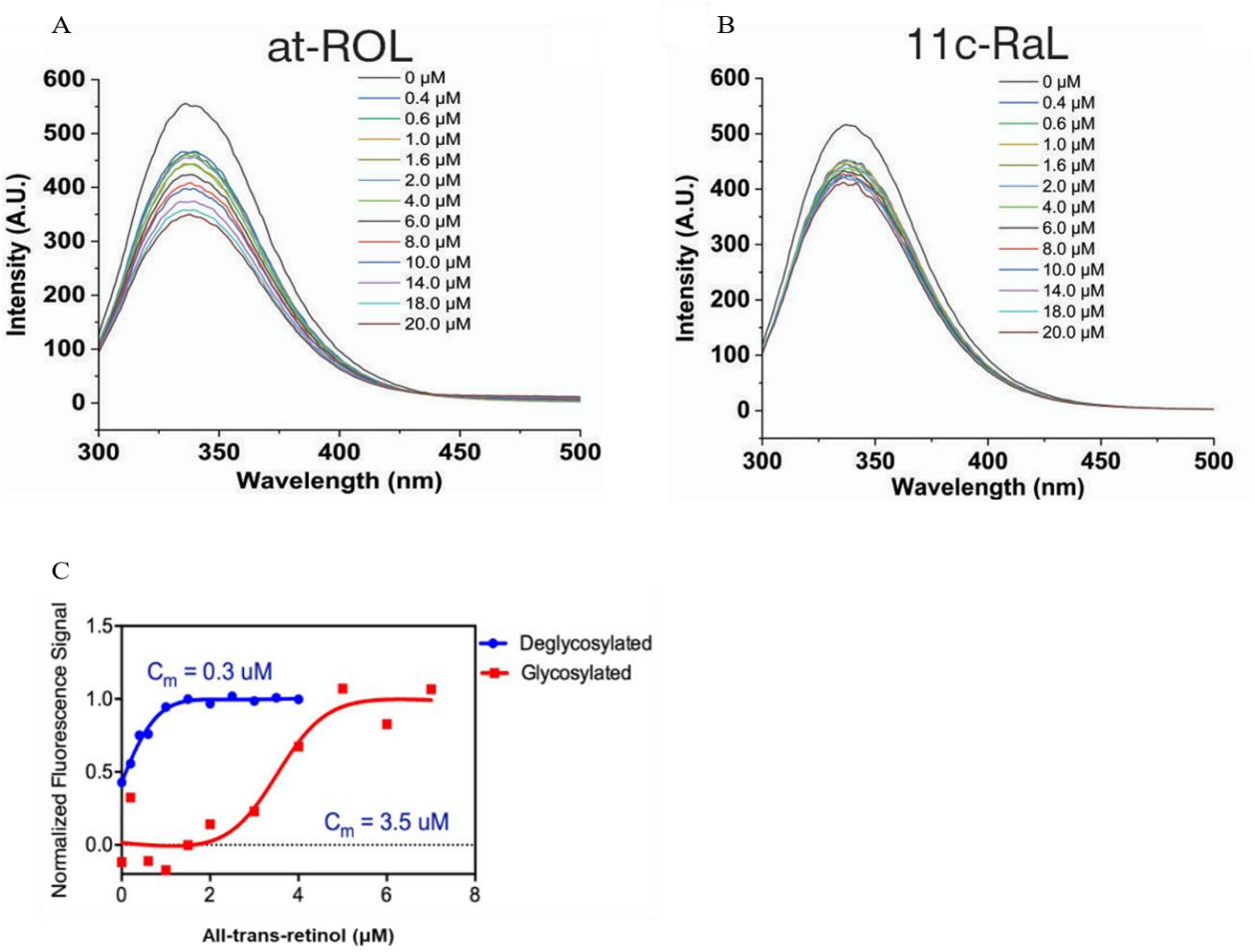

Figure 3.21: Biophysical characterization of native RBP3. A) Tryptophan fluorescence quenching assay using Sus scrofa RBP3 titrated with all-trans retinol (Picture taken from: Kaushik et al., 2025B under the licence CC BY 4.0). B) Tryptophan fluorescence quenching assay using Sus scrofa RBP3 titrated with 11-cis retinal (Picture taken from: Kaushik et al., 2025B under the licence CC BY 4.0). C) Normalized fluorescence signal for de-glycosylated and native Bos Taurus RBP3.

3.2.5 *Sus scrofa* RBP3 CryoEM structure

The first structure for the full length RBP3 in complex with a monoclonal antibody was published by Sears et al in 2020; the global resolution for this structure is 7.4 Å, leaving space for improvement (Sears et al., 2020). The effort of our work was focused on improving the resolution of this structure by testing different buffer compositions, blot conditions, and different grids in presence and absence of monoclonal antibody to increase the molecular weight and decrease the flexibility of the complex in order to obtain a better motion correction. Despite the protein exhibits a high degree of purity, homogeneity, and structural integrity, with no evidence of aggregation during negative staining analysis (data not shown), and despite the effort to find the right conditions, we were not able to obtain a suitable grid for Single Particle Analysis (SPA) using *Bos taurus* RBP3. Since it was not possible to collect particles for *Bos taurus* RBP3, it was decided to test *Sus scrofa* RBP3 ortholog. Given the ability to cross-react with the *Sus scrofa* ortholog of RBP3, the previously purified mAb5 was used for the grid preparation; however, its addition to *Sus scrofa* RBP3 was harmful to the particles and rendered no suitable grid for SPA. Trials continue then with the native protein without complexation with the antibody. After several attempts, testing different grids, different blotting conditions, and different reagents/additives, we were able to pinpoint that the detergent CHAPSO is playing a crucial role for rendering proper grids.

Using this information, we determined the optimal protein concentration, the grids were prepared containing apo *Sus scrofa* RBP3 as well as its complexes with 11-cis retinal all-trans retinol, and DHA. Screening these grids confirmed an appropriate distribution of particles (Table 2),

	Native *p*RBP3	pRBP3 + 11-cis retinal	pRBP3 +all-trans retinol	pRBP3+ DHA
Data collection processing				
Magnification	105000x	165000x	165000x	165000x
Voltage (kV)	300	200	200	200
Electron exposure ($e^-/Å^2$)	40	40	40	40
Defocus range (μm)	-1.4 to -3.0	-1.6 to -3.0	-1.6 to -3.0	-1.6 to -3.0
Physical pixel size (Å)	0.8336	0.783	0.783	0.783
Symmetry imposed	C1	C1	C1	C1
Initial particle images (n)	1903572	18582	15647	18027
Final particle images (n)	611246	n.a.	n.a.	n.a.
Map resolution (Å)	3.67			

FSC threshold	0.143			
Map resolution range (Å)	3.2 to 7.0(*)			
Refinement				
Model resolution (Å)	3.67			
FSC threshold	0.143			
Model composition	Apo- pRBP3			
Non-hydrogen atoms	8324			
Protein residues	1081			
Ligands	0			
B factors (Å^2)				
Protein	208.6 (Rigid = 75.1) (Flexible = 363.2)			
Ligand	n.a.			
R.m.s. deviations				
Bond lengths (Å)	0.003			
Bond angles (°)	0.546			
Validation				
MolProbity score	2.56			
Clash score	9.88			
Poor rotamers (%)	0.21			
Ramachandran plot				
Favoured (%)	96.01			
Allowed (%)	3.99			
Disallowed (%)	0			

Table 2: CryoEM data collection parameters and refinement and validation statistics. pRBP3 stands for *Sus scrofa* RBP3. Table taken from Kaushik et al., 2025B.

(n.a. = not applicable)

which could then be classified into distinct 2D groups (Figure 3.22). For the protein-ligand complexes, a ratio of 1:2 was used, to ensure saturation of all binding sites, and they were incubated for 1 minute before blotting.

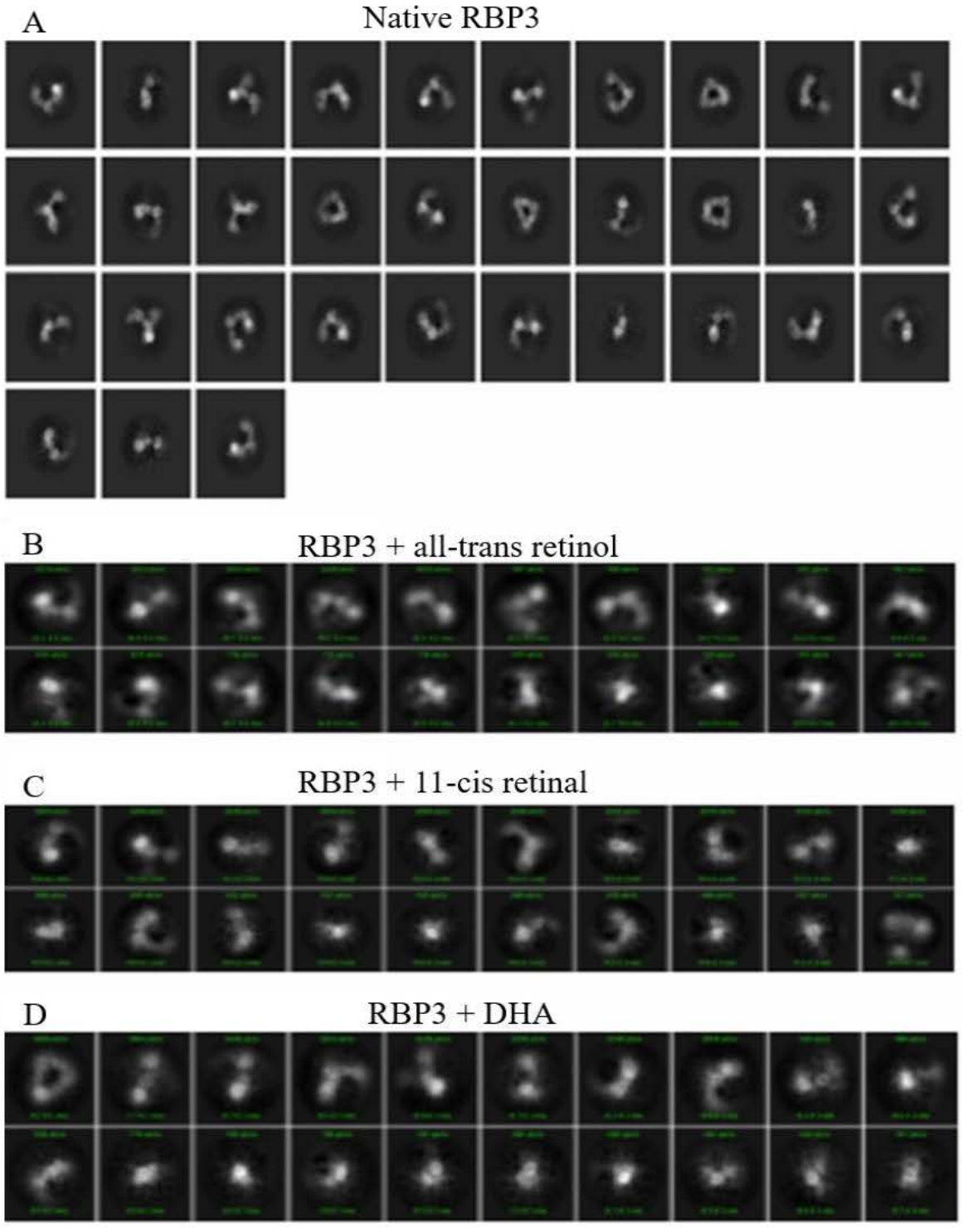

Figure 3.22: Sus scrofa RBP3 2D CryoEM classes. A) 2D classes for apo Sus scrofa RBP3. B) 2D classes of Sus scrofa RBP3 in complex with all-trans retinol. C) 2D classes of Sus scrofa RBP3 in complex with 11-cis retinal. D) 2D classes of Sus scrofa RBP3 in complex with DHA (Picture taken from Kaushik et al., 2025B supplementary material under the licence CC BY 4.0).

Interestingly, neither the apo form nor the complexes showed a significant presence of elongated particles similar to those described by Adler and colleagues in 1987 (Adler et al., 1987). Our results are in agreement with previous findings by Sears and colleagues; differences between the results presented in this thesis and Adler's findings are probably due to different experimental methodologies. Among the four datasets, only the one corresponding to the apo protein yielded the high-resolution data aimed at, and for this reason, it was the only one selected for further processing and analysis (Table 2).

A dataset was obtained using a *Titan Krios G3i* microscope operating at 300 kV. This dataset consisted of 23,971 micrographs, and it was subjected to multiple rounds of 2D classification, resulting in a total of 1.9 million particle images. Among these, 610,000 were selected for heterogeneous reconstruction and subsequent refinement. The resulting 2D particle views exhibited similarities to previously characterized *Bos taurus* RBP3 particles obtained by Sears and colleagues (Sears et al., 2020) and showed a preferential alignment in certain orientations. After reconstruction and refinement density map with an overall resolution of 4.5 Å was obtained.

The previously mentioned three-dimensional reconstruction rendered a density map that revealed a well-resolved central region of the protein, whereas the terminal regions exhibited a significant degree of structural flexibility, resulting in a lower local resolution value. This reconstructed density map was subsequently utilized to fit the computationally predicted AlphaFold model of *Sus scrofa* RBP3 (entry A0A287A908). The superimposition between the model and the experimental density was immediately evident, especially in the C-terminal portion of the protein, which corresponded precisely from Domain B within Module 2 of the four-module structure onwards (Figure 3.23). However, the positioning of Module 1 and Domain A of Module 2, required several adjustments, performed using the UCSF Chimera software (Pettersen et al., 2004) (Figure 3.23B, C). In order to get a good overlapping of these two structural portions inside the density map, it was necessary to apply a rotational transformation around the hinge region that connects Domains A and B within Module 2. This suggests that the flexibility observed in these regions may play a functional role in the protein's conformational changes (Figure 3.22).

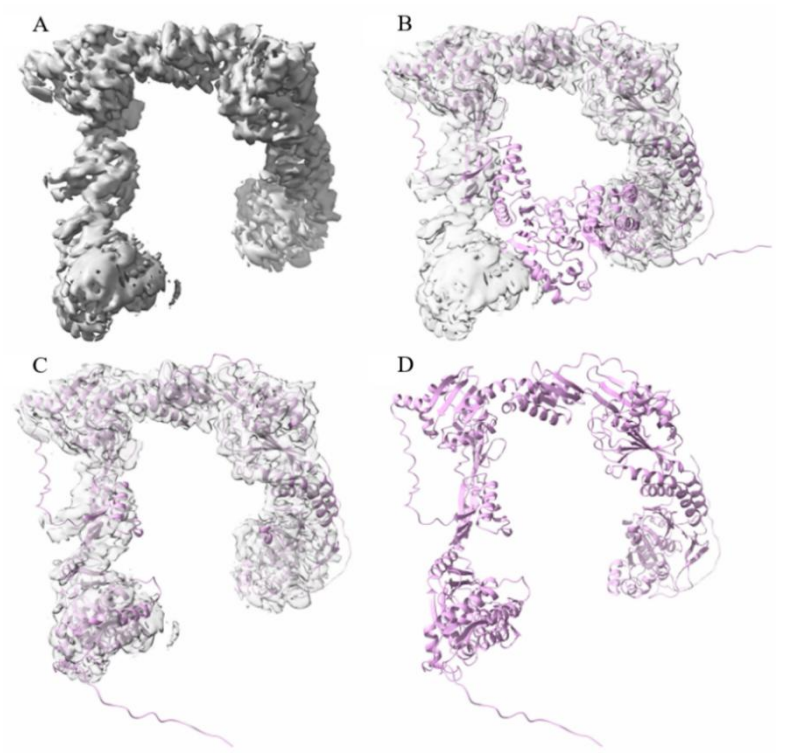

Figure 3.23: 3D reconstitution and AlphaFold model docking for Sus scrofa RBP3. A) "pi" shaped density map of Sus scrofa RBP3 at 3.67 Å resolution (EMD-50552). B) AlphaFold Sus scrofa RBP3 model docked into the map with a rigid-docking algorithm. C) Manual adjustment of Module 1 and domain A of Module 2 to fit the density. D) The initial protein model that was subjected to refinement (Picture taken from Kaushik et al., 2025B supplementary material under the licence CC BY 4.0.

The nominal resolution was improved thanks to a local refinement followed by a hetero refinement (Figure 3.23A and 3.24).

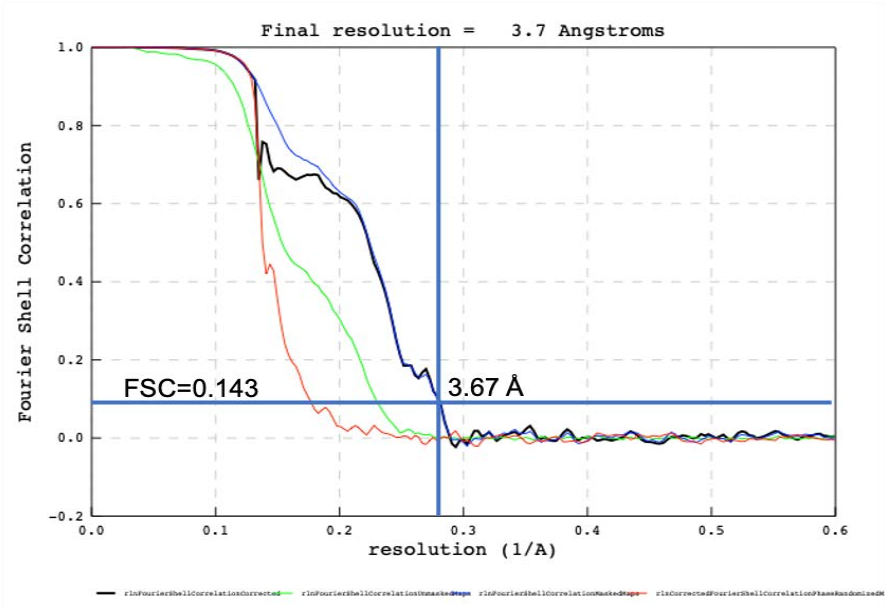

Figure 3.24: Graphs displaying the Fourier Shell Correlation (FSC) each line represents different computational conditions: phase-randomized masked half-maps (red), unmasked half-maps (green), masked half-maps (blue), final corrected FSC curve (black) (Picture taken from Kaushik et al., 2025B under the licence CC BY 4.0).

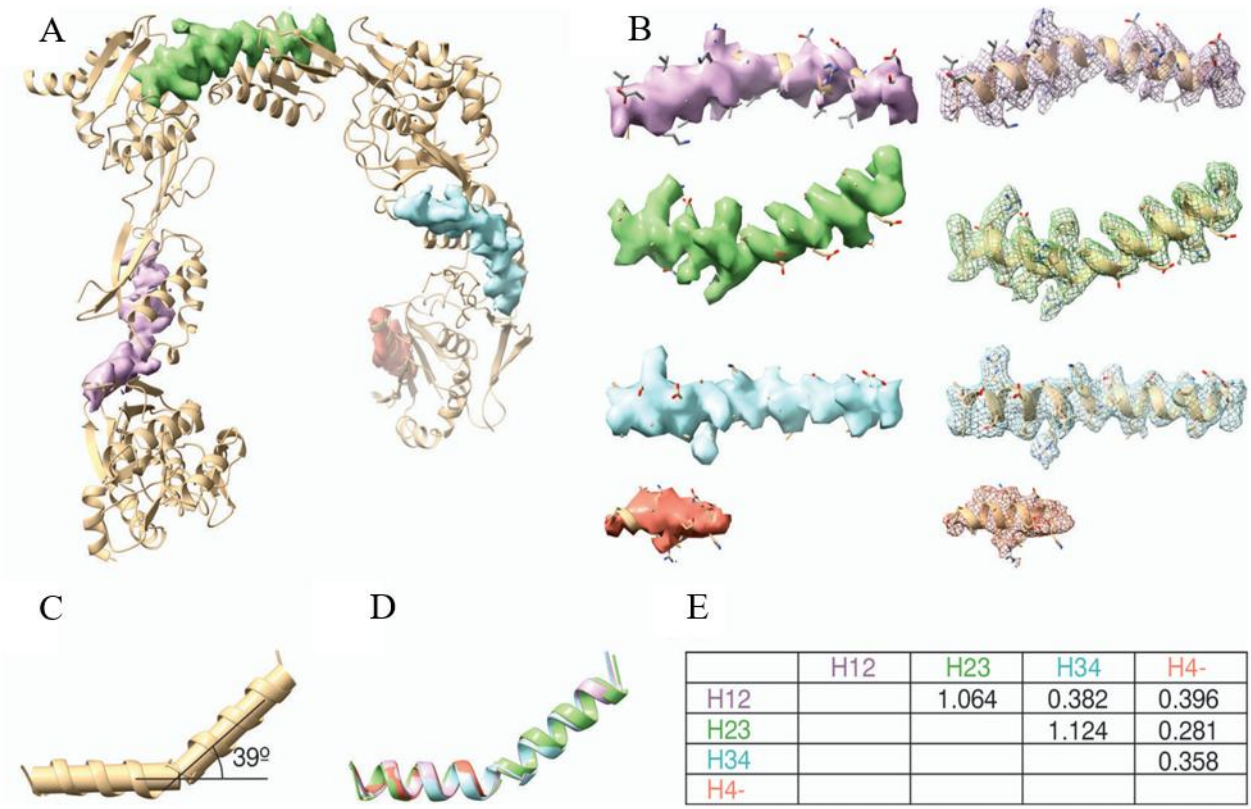

Figure 3.25: Modules connecting α-helices. A) Carton representation of Sus scrofa RBP3 showing coulomb potential map for the α-helices connecting modules. B) Cartoon model and Coulomb potential map for each of the connecting α-helices. C) Angle of the α-helix connecting Module 1 to Module 2. D) Superimposition of the three connecting α-helices. E) RMSD values of the three three connecting α-helices (Picture taken from Kaushik et al., 2025B under the licence CC BY 4.0).

The examination of the local resolution map (Figure 3.26) shows that the portion of the protein extending from domain B of Module 2 until the domain A of Module 4 present favorable parameters for de novo refinement. Unfortunately, the region corresponding to Module 1 until the domain A of Module 2 at the N-termini, and the domain B of Module 4 at the C-termini, permitted only rigid a body refinement approach. The resolution allows a clear identification of each of the four modules and the three connecting α-helices; altogether, they acquire a horseshoe conformation similar to the structure of *Bos taurus* RBP3 reported by Sears and colleagues in 2020 (Sears et al., 2020).

The modules are connected to each other through a long α-helix. The α-helices that connect the modules bend after three turns, showing an angle of 39°. Furthermore, when comparing their spatial alignment, these helices show a degree of structural overlap, quantified by a Root Mean Square Deviation (RMSD) ranging from 0.38 to 1.12 Å (Figure 3.25C, D) (Kaushik et al., 2025B). For the helix connecting the Modules 1 and 2 and the helix connecting the Module 3 and 4 the bend is occurring at the position of proline and/or glycine residues that appear to be conserved in the majorities of the vertebrates (data not shown) possibly suggesting a functional role for the flexibility

of the connecting helices. Analyzing the local resolution map (Figure 3.26), the region containing the whole Module 3 shows the best parameter for a structural analysis.

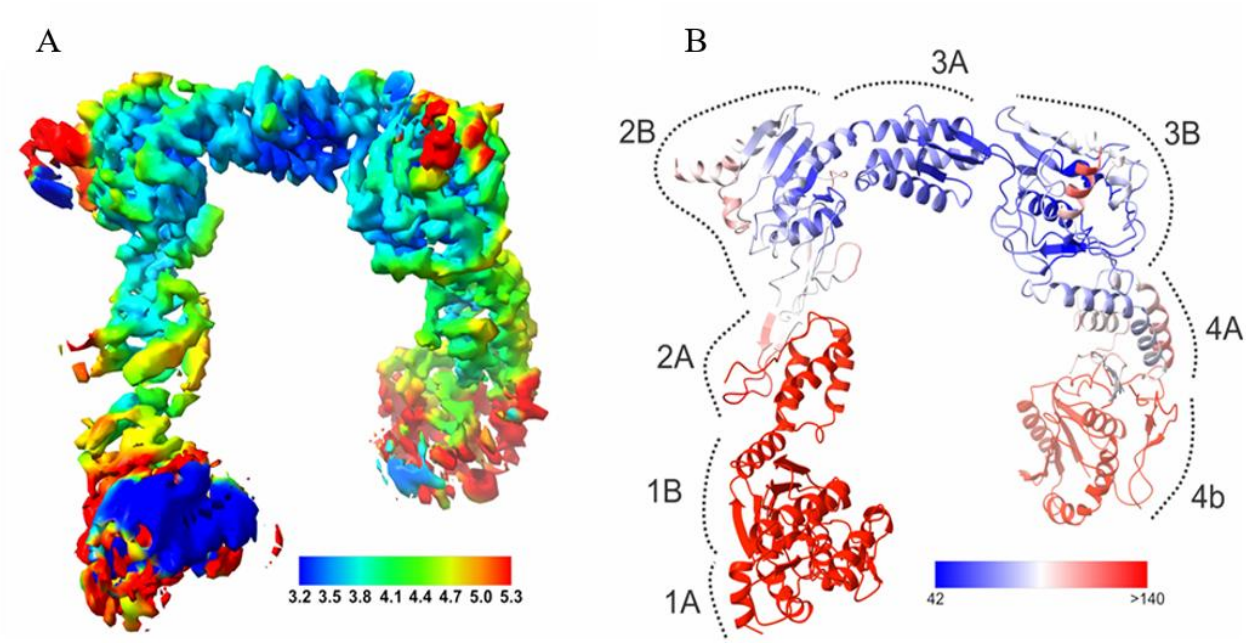

Figure 3.26: Sus scrofa RBP3 structure. A) The CryoEM density map was processed using a filter and it was coloured according to the local resolution. B) Cartoon representation of the refined atomic model of Sus scrofa RBP3 coloured by residue-averaged atomic B factor (Picture taken from Kaushik et al., 2025B under the licence CC BY 4.0).

Considering the high similarities between the four modules, they exhibit a high degree of spatial correspondence confirmed by the RMSD value, which ranges from 1.73 to 3.36 Å (Figure 3.27A, B) (Kaushik et al., 2025B). Despite some minor variations, the three-dimensional structures of the modules are very similar; therefore, the features of Module 3 can be inferred for the other modules.

Each module consists of a domain A (approximately 80 amino acids) and a domain B connected through a stretch of amino acids in a random coil conformation, not detectable in our Coulomb potential map due to the high flexibility. The domain A consists of three α-helices that continue with a β-turn and a short β-strand before the flexible stretch connecting with the domain B (Figure 3.27A). Two β-strands from domain B extending from domain B are paired antiparallel with the short β-strand of domain A and facing the three α-helices. Altogether, the three α-helices and the three β-

strands form a hydrophobic cavity, considered responsible for the binding of OA and other fatty acids (PDB ID: 4 LUR, Ghosh et al., 2015).

A

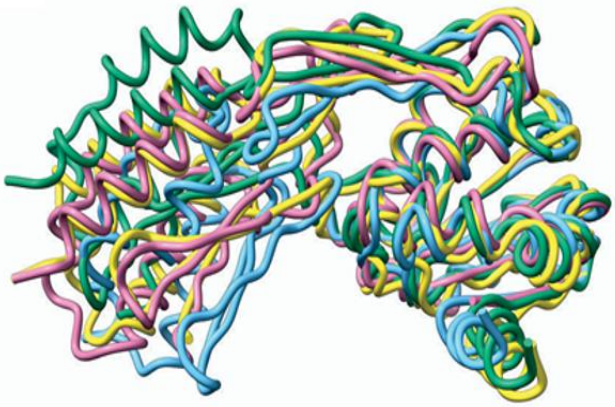

B

	M1	M2	M3	M4
M1		3.361	2.691	2.499
M2			2.581	2.869
M3				1.728
M4				

C

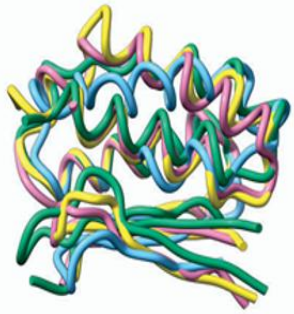

D

	A1	A2	A3	A4
A1		2.642	2.252	2.522
A2			1.291	1.713
A3				1.233
A4				

E

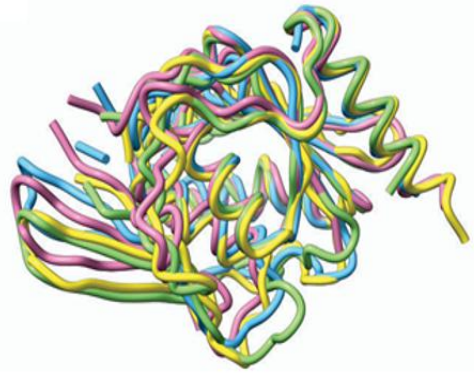

F

	B1	B2	B3	B4
B1		1.233	2.060	1.522
B2			1.395	1.549
B3				1.653
B4				

Figure 3.27: Superposition of Sus scrofa RBP3 modules and domains, and protein-topology structure. A) Superposition of the four Sus scrofa RBP3 modules. B) RMSD for the four modules. C) Superposition of the four domains A of Sus scrofa RBP3. D) RMSD for the four domains A. E) Superposition of the four domains B of Sus scrofa RBP3. F) RMSD of the four domains B. (Picture taken from Kaushik et al., 2025B under the licence CC BY 4.0).

Within the domain B, it is possible to visualize four α-helices forming a hydrophobic cavity with five β-strands that are located between the module-connecting α-helix and the four α-helices involved in the formation of the hydrophobic cavity (Figure 3.27E). The domain B contains five other β-strands, two of which extend from the domain B and are involved in the formation of the hydrophobic cavity

in the domain A. Between these two β-strands and the four α-helices of domain B's hydrophobic cavity, it is possible to recognize the hydrophobic cleft that separates the two domains.

Relative to the flexibility of the amino acid stretches that bridge the domains A and domains B in the four modules it is interesting to note the presence of consecutive proline residues that may play a role as hinge regions. In the bridges that connect the domain A and domain B of Module 3 there are five consecutive proline residues while in the in the bridges that connect the domain A and domain B of Module 4 there are two consecutive prolines in two cases, and they are at positions 1102-1103 and 1175-1176, the first pair appears to be exposed to the surrounding environment, although it remains in close proximity to the unresolved loop that spans the region between residues T1124 and K1135. Meanwhile, the second pair is situated on the loop that directly precedes the insertion of the two-stranded segment into domain A. It is however important to note that there are no consecutive proline residues in Module 1 of *Sus scrofa* RBP3, but they are present in *Homo sapiens* and *Bos taurus* RBP3 orthologs. RBP3 presents antioxidant activity (Gonzalez-Fernandez et al., 2014), which in the *Sus scrofa* ortholog is guaranteed by seven cysteine residues (C14, C40, C172, C304, C603, C795, C1094). Five out of seven cysteine residues are visible in our structure (Figure 3.28).

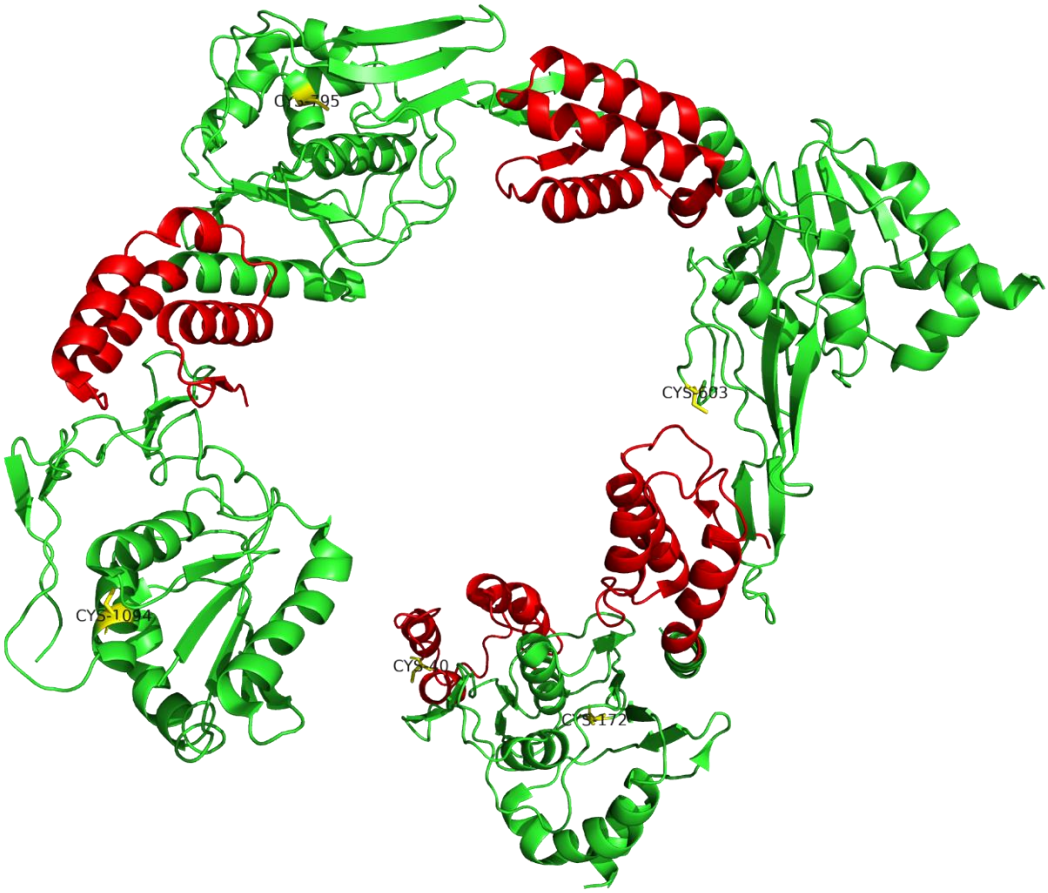

Figure 3.28: Cysteine positioning in Sus scrofa RBP3 cartoon representation, in red domains A, in green domains B and in yellow the cysteine residues, PDB ID: 9FRX (Kaushik et al., 2025B). Picture obtained using PyMol (Schrödinger, LLC).

And are located very distantly to each other form intraprotomer disulfide bonds, 2 cysteine residues are not visible in our structure because they are localized at the N-terminus portion of the protein (C14) and in the flexible amino acid stretch that connects the domain A and domain B of Module 1 (C304). Unfortunately, these regions are not visible in our structure due to their high flexibility; however, these residues are too distant to interact with other cystein residues for the formation of a disulfide bond (Kaushik et al., 2025B), witin the monomeric RBP3.

As previously mentioned, according to NetNGlyc (Gupta and Brunak, 2002), *Sus scrofa* RBP3 is predicted to have four N-Glycans chains attached to the asparagine residues 107, 205, 513, 1114. The residues 107 and 205 are located in Module 1; however, residue 107 is located on a missing loop not visible in our Coulomb potential map. The residues 205, 513, 1114 are situated in the Modules 1, 2, and 4, respectively, in particular, they localize on loops that connect two β-strands of domain B. It is interesting to note that by examining the three-dimensional structure of the modules, it is evident that the glycosylation sites are located in the same relative position within the structure of each glycosylated module (Figure 3.29). The fact that the position of the glycosylated residues is conserved amongst the three modules suggests that glycosylation may play a structural or functional role.

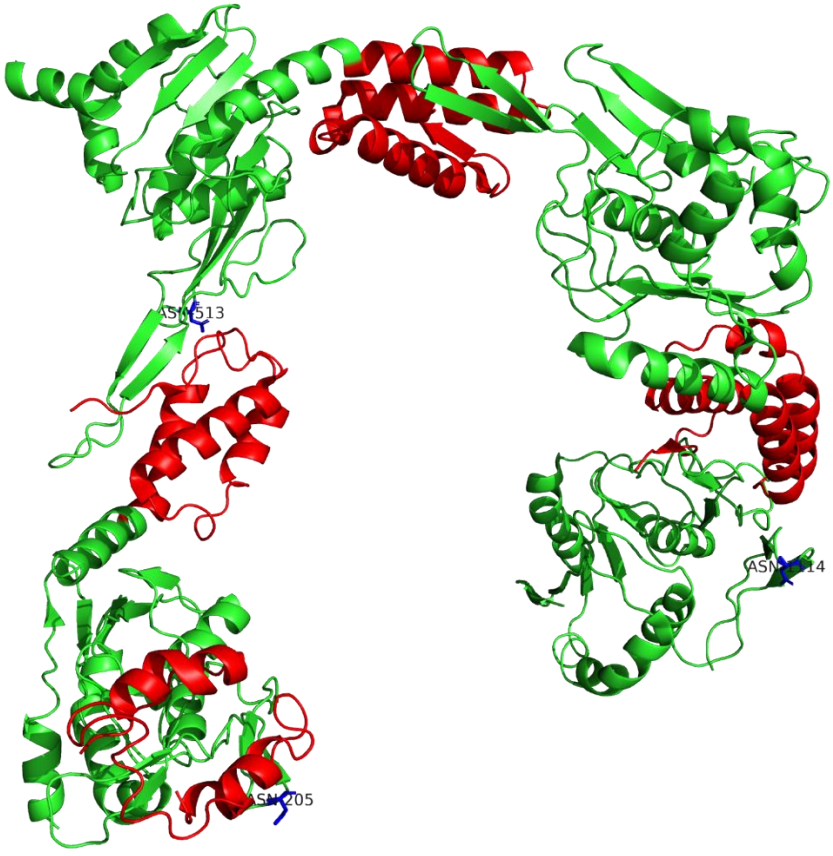

Figure 3.29: Sus scrofa RBP3 cartoon representation indicating the predicted glycosylation sites. In red domains A, in green domains B, in blue the asparagine residues predicted to be glycosylated, PDB ID: 9FRX. Picture obtained using PyMol (Schrödinger, LLC).

Structural homology search was performed using the DALI algorithm (Holm, 2020). A group of proteases exhibited the highest structural similarity scores for a peptidase derived from *Parabacteroides merdae* strain ATCC 43184, (PDB ID: 4L8K). Among these structurally similar proteases, some of the most interesting are: the chlamydial protease CPAF (PDB ID: 3DJA); a S41 protease originating from *Bacteroides fragilis* strain NCTC 9343, (PDB ID: YP_211611.1 PDB ID: 3K50); and Prc, which is a tail-specific protease (PDB ID: 6IQR) (Kaushik et al., 2025B).

The same structural homology search was also performed using domain A and domain B individually. When domain A is used; the proteases with the highest structural alignment scores are: photosystem II D1 C-terminal processing protease **(**PDB ID: 1FC6), tricorn protease (PDB ID: 1N6E). When the domain B is used as a query protein, the closest proteins are the carboxyl-terminal processing protease A, known as CtpA (PDB ID: 7RPQ), protease CtpB (PDB ID: 4C2C), and peptidase S41 (PDB ID: 6VBB).

3.2.6 *Sus scrofa* RBP3 structural features- implications in disease

Three retinal disease have been associated with RBP3: retinitis pigmentosa, myopia, and diabetic retinopathy (Georgiou et al., 2024; Li et al., 2013; Yokomizo et al., 2019). Autosomal recessive retinitis pigmentosa was diagnosed in four siblings carrying the homozygous missense mutation D1080N (den Hollander et al., 2009), on an aspartate residue that is located in domain B of Module 4. It was suggested by den Hollander and colleagues that: “The mutation Asp1080Asn may alter the conformation of the IRBP protein by disrupting a conserved salt bridge.” (den Hollander et al., 2009). The higher resolution of the *Sus scrofa* RBP3 structure reported here, indicates that the aspartate 1078 (corresponding to the aspartate 1080 of *Homo sapiens* RBP3 ortholog) is forming a salt bond with arginine 1080 (Figure 3.30); thus, the aspartate/asparagine mutation would disrupt this salt bond, possibly leading to the formation of another bond between asparagine 1082 and tyrosine 1044 (Kaushik et al., 2025B).

Few RBP3 mutations have been associated with inherited high myopia (Georgiou et al., 2024). They include several nonsense mutations that result in premature stop codons, leading to truncated forms of *Homo sapiens* RBP3 (Gln54Ter, Trp116Alafs*7, Trp211Ter, Tyr510Ter, Gln942Ter, Tyr1133Ter, Glu1152Ter). In addition to these truncated forms, other types of genetic mutations are also described, such as missense mutations, which cause single amino acid substitutions, and in-frame deletions, where one or more amino acids are removed without disrupting the open reading frame of the protein. The mutations reported by Georgiou and colleagues are: Arg170Gln, His505Leu, Leu540Pro, and Ala876Ser (Georgiou et al., 2024).

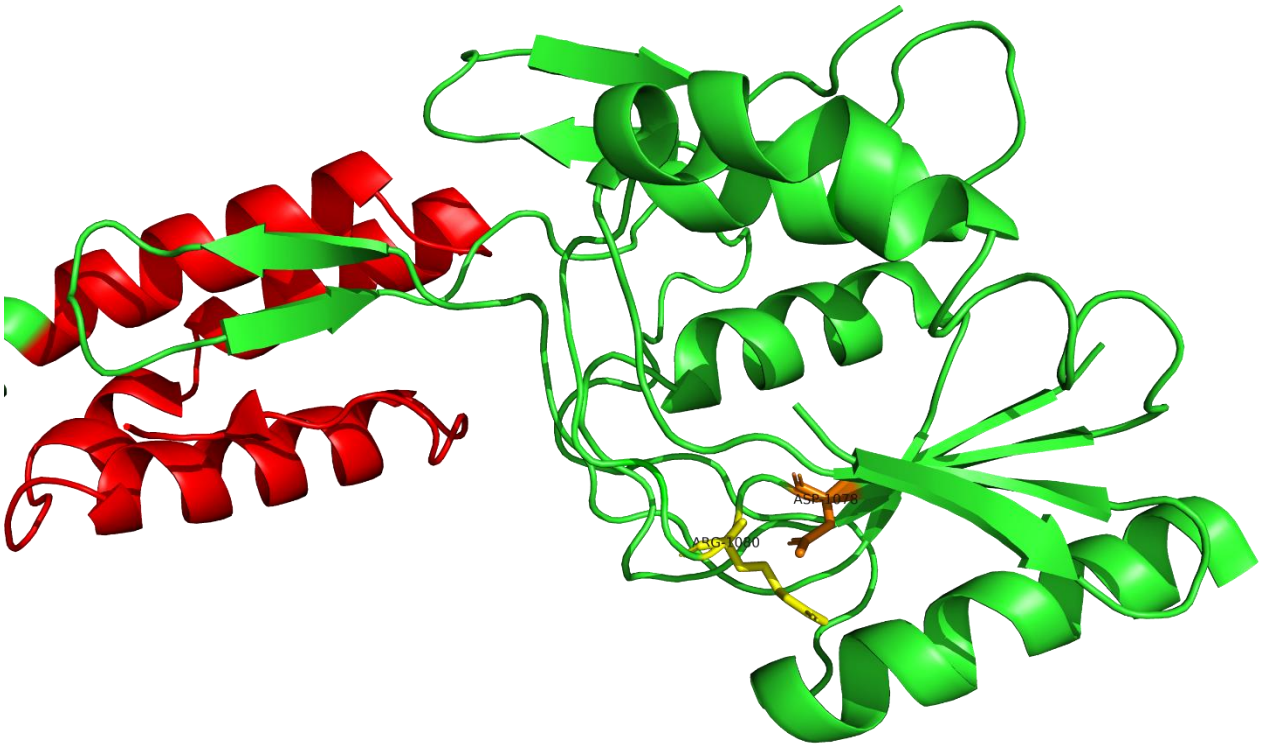

Figure 3.30: Sus scrofa RBP3 Module 4. In red domain A, in green domain B, in yellow the arginine residue 1081, in blue the aspartate residue 1078. PDB ID: 9FRX (Kaushik et al., 2025B). Picture obtained using PyMol (Schrödinger, LLC).

Arg170 is located in a loop of domain B of Module 1 that connects a β-strand and an α helix involved in the formation of the hydrophobic cavity, and it is exposed to the protein surface. His505Leu, 505 corresponds to Arg 503 in *Sus scrofa* sequence, is exposed at the protein surface, and it is located in a β-strand of domain B of Module2. Leu540Pro is located in another β-strand of domain B of Module2, it interacts with the α-helix that connects Module 2 to Module 3, and therefore it is not surface exposed. Ala876Ser is a surface residue, located in a loop of domain B of Module 3, interestingly, this residue is pointing toward the hydrophobic cleft between domain A and domain B of Module 3. The *in-frame* deletion, Phe278del in Module1 (not conserved *Bos taurus* nor in *Sus scrofa*) is the last of a stretch of three phenylalanine residues (*Sus scrofa* and *Bos taurus* have only two such phenylalanine residues) at the β-turn of the two-sheet insertion in domain A.

3.2.7 *Sus scrofa* RBP3 binding sites

The attempts to obtain a structure of RBP3 in complex with other ligands were not successful, however, considering the local resolution map of our structure it is possible to affirm that the region extending from the domain B of Module 2 until the domain A of Module 4 display a sufficiently high resolution for performing docking procedure aimed at identify the putative binding sites for retinoids and other allosteric factors. This allows not only to identify binding sites within a module, but also on the domain B – domain A, and domain A – domain B inter-module interfaces. For this purpose,

the entire rigid region was selected for the docking analysis and tested for 11-cis retinal, all-trans retinol, DHA, and OA. In our study, we opted to search 20 sites for each ligand which is significantly higher than what is expected in physiological conditions (Kaushik et al., 2025B). The rationale behind this decision was to select a high number of sites in order to use the different binding energies to discriminate between the weaker and stronger binding sites (Table 3) (Kaushik et al., 2025B).

	11-cis retinal	All-trans retinol	DHA	OA
Ligand 1	-9.8 (Cav 1)	-8.6 (Cav 1)	-9.0 (Cav 1)	-7.5 (Cav 1)
Ligand 2	-5.6 (Cleft 6)	-5.8 (Cleft 6)	-5.1 (Cleft 15)	-4.0 (Cleft 7)
Ligand 3	-7.1 (Cav 2)	-6.7 (Cav 2)	-6.6 (Cav 2)	-5.5 (Cav 2)
Ligand 4	-6.3 (Cleft 8)	-6.0 (Cleft 8)	-4.9 (Cleft 8)	-4.5 (Cleft 8)
Ligand 5	-5.8 (Cleft 3)	-6.0 (Cleft 3)	-4.7 (Cleft 3)	-4.1 (Cleft 3)
Ligand 6	-6.5 (Cleft 8)	-6.8 (Cleft 8)	-5.1 (Cleft 8)	-4.6 (Cleft 8)
Ligand 7	-5.5 (Cleft 4)	-5.2 (Cleft 4)	-4.8 (Cleft 4)	-3.7 (Cleft 5)
Ligand 8	-5.6 (Cleft 11)	-5.5 (Cleft 11)	-4.8 (Cleft 11)	-4.5 (Cleft 11)
Ligand 9	-5.5 (Cleft 10)	-5.4 (Cleft 10)	-4.4 (Cleft 10)	-4.2 (Cleft 10)
Ligand 10	-5.3 (Cleft 7)	-5.5 (Cleft 7)	-4.4 (Cleft 7)	-3.8 (Cleft 7)
Ligand 11	-4.9 (Cleft 13)	-5.1 (Cleft 13)	-4.4 (Cleft 16)	-4.1 (Cleft 13)
Ligand 12	-6.8 (Cleft 1)	-6.3 (Cleft 1)	-4.7 (Cleft 1)	-4.1 (Cleft 1)
Ligand 13	-5.5 (Cleft 12)	-6.0 (Cleft 12)	-5.2 (Cleft 12)	-4.0 (Cleft 12)
Ligand 14	-5.7 (Cleft 9)	-5.2 (Cleft 8)	-4.1 (Cleft 17)	-4.7 (Cleft 17)
Ligand 15	-7.4 (Cav 2)	-6.8 (Cav 2)	-5.6 (Cav 2)	-5.2 (Cav 2)
Ligand 16	-5.5 (Cleft 5)	-5.1 (Cleft 14)	-4.7 (Cleft 14)	-4.7 (Cleft 18)
Ligand 17	-7.2 (Cav 2)	-6.7 (Cav 2)	-5.9 (Cav 2)	-4.7 (Cav 2)
Ligand 18	-5.4 (Cleft 2)	-5.4 (Cleft 2)	-4.2 (Cleft 2)	-3.7 (Cleft 2)
Ligand 19	-5.7 (Cleft 10)	-6.2 (Cav 1)	-5.2 (Cleft 10)	-5.4 (Cav 1)
Ligand 20	-5.5 (Cleft 14)	-5.4 (Cleft 14)	-4.4 (Cleft 14)	-3.3 (Cleft 14)

Table 3: Binding energies of the studied ligands on *Sus scrofa* RBP3, expressed in kcal/mol, with the cavity/cleft localization of the ligands indicated in parentheses. Table taken from Kaushik et al., 2025B supplementary material.

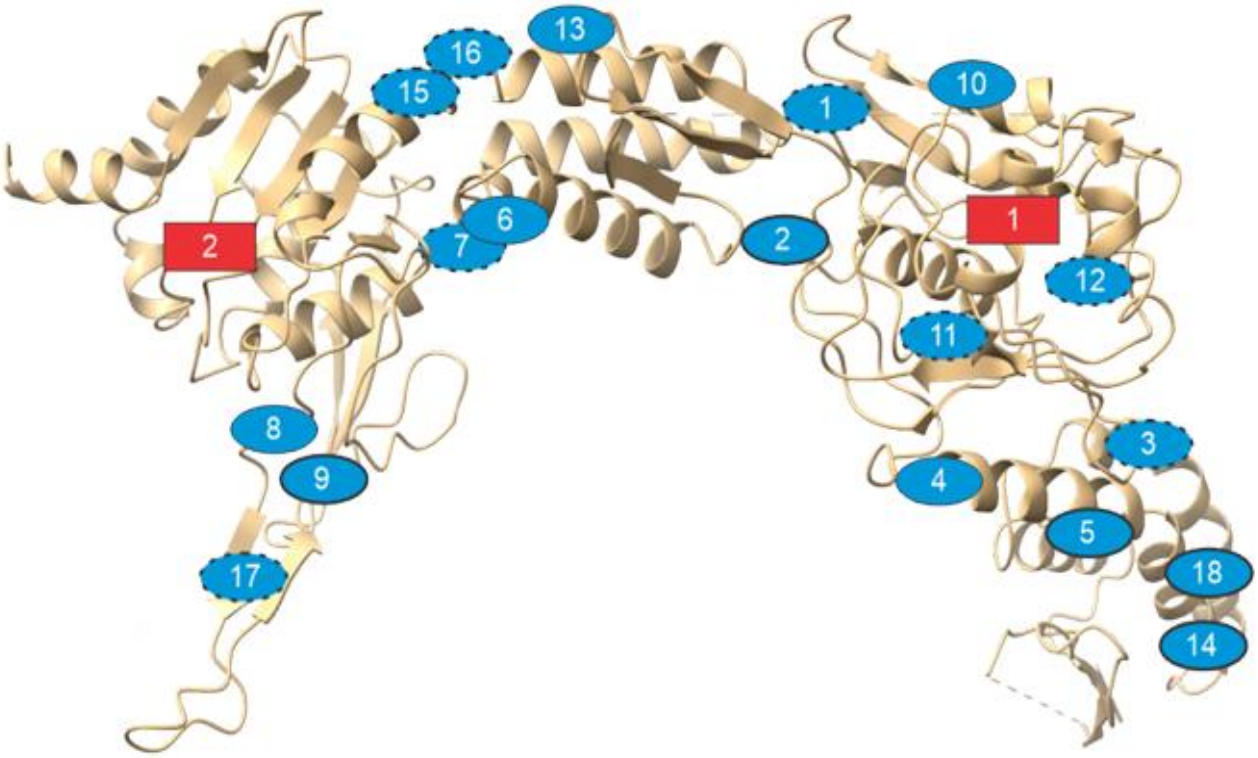

Figure 3.31: Portion of Sus scrofa RBP3 extending from domain B of Module 2 until domain A of domain 4. Numbers are indicating the binding sites identified by CB- dock. Red rectangles: hydrophobic cavities. Blue ellipsis: cleft. The continuous thick line encircling the ellipsis is indicating sites clearly visible on the surface, the dotted line encircling the ellipsis was used for indicating sites on hidden surfaces, and the continuous thin line encircling the ellipsis indicates sites that have features between the hidden and the visible sites (Picture taken from Kaushik et al., 2025B supplementary material under the licence CC BY 4.0).

In our study, out of the twenty putative binding sites, two are hydrophobic cavities and 18 are hydrophobic clefts (Figure 3.31) (Kaushik et al., 2025B). The strongest binding affinity is exhibited by the putative binding site localized in the hydrophobic cavity of domain B in Module 3 (Cavity 1, Figure 3.31), which displays a binding energy of -9.8 kcal/mol for 11-cis retinal-1 (Figure 3.32, Table 3). Within this cavity, the ligand appears to be enclosed and almost completely shielded from the external environment. Also, the domain B of Module 2 presents the same hydrophobic cavity localized in exactly the same region (Cavity 2). Cavity 2, as well as cavity 1, is capable of binding 11-cis retinal showing a binding energy of -7.1 kcal/mol (11-cis retinal-3); however, few minor differences between the two cavities relative to the binding mode are present. In cavity 2, the ligand is closer to the entrance of the cavity and not deeply inserted into the cavity. Furthermore, the polar moiety of the ligand is pointing outward rather than the inner of the cavity. The volume of cavity 2 (1939 $Å^3$) is slightly larger than the volume of cavity 1 (1807 $Å^3$). According to CB dock, there are two possible ways for cavity 2 to bind 11-cis retinal, in one case (11-cis retinal-15) is showing the tails of the ligand pointing toward the interior of the cavity. In the other binding mode, as shown by (as 11-cis retinal-3, and 11-cis retinal-17), the tails of the ligands are pointing outside of the cavity;

however, they are pointing toward different directions with binding energies of -7.1 and -7.2 kcal/mol, respectively. Thanks to CB dock it was possible to identify 18 hydrophobic clefts located on the surface of *Sus scrofa* RBP3 that can act as binding sites for hydrophobic ligands. Some of these clefts are placed on the interface between distinct RBP3 domains, and they display binding energies oscillating between -6.8 to -5.3 kcal/mol other hydrophobic clefts are entirely localized within a single domain, presenting binding energies ranging from -6.3 to -4.9 kcal/mol (Table 3). Clefts 1 and 2 are localized at the interface between the domain A and the domain B of Module 3, these surface-exposed hydrophobic regions are able to bind 11-cis retinal, specifically, they can bind 11-cis retinal-12 and 11-cis retinal-18 (Figure 3.32), respectively, with 11-cis retinal-12 displaying a binding energy of -6.8 kcal/mol. Another interesting region that possesses the ability to bind 11-cis retinal is localized between the domain B of the Module 3 and the domain A of the Module 4. This region presents three hydrophobic clefts (clefts 3-5) that are capable of binding 11-cis retinal, specifically 11-cis retinal-5, 11-cis retinal-7, and 11-cis retinal-16, respectively. The cleft 3 (11-cis retinal-5) is the one that is showing the higher affinity, showing binding energy of -5.8 kcal/mol. The hydrophobic clefts 6 and 7, which are almost overlapping, are located in the region between the domain B of Module 2 and the domain A of Module 3. These two clefts can bind 11-cis retinal (11-cis retinal-2 and 11-cis retinal-10, respectively). The cleft 6 (11-cis retinal-2) binds 11-cis retinal with stronger affinity (-5.6 kcal/mol) compared to the cleft 7 (Table 3). Interestingly, in the analogous region at the interface of domain B of the Module 2 and domain A of the Module 3, there are no hydrophobic cleft according to our docking analysis. Some of the hydrophobic clefts identified by our docking analysis are located within the single domains. In particular, the clefts 8 and 9 are located in the domain B of the Module 2, and they are capable to bind 11-cis retinal. Cleft 8 can bind two molecules of 11-cis retinal, specifically 11-cis retinal-4 and 11-cis retinal-6, with binding energies of -6.3 and -6.5 kcal/mol, respectively, while cleft 9 can accommodate 1 molecule of 11-cis retinal (11-cis retinal-14). A minor difference between the domain B of Module 2 and the domain B of Module 3 can be found, since the last one contains three hydrophobic clefts instead of two, unlike the domain B of Module 2, these three clefts (Clefts 10, 11,12) are completely distinct and not overlapping. Cleft 10 is able to bind two molecules of 11-cis retinal (11-cis retinal-9 and 11-cis retinal-19), showing binding energies of -5.5 and -5.7 kcal/mol, respectively. Clefts 11 and 12 are able to bind one molecule of 11-cis retinal each (11-cis retinal-8 and 11-cis retinal-13, respectively) with binding energies of -5.6 and -5.5 kcal/mol, respectively. Analyzing the hydrophobic clefts that are entirely located in a single domain, it is interesting to note that the domains A of the Modules 3 and 4 contain one cleft each (clefts 13 and 14 in Modules 3 and 4, respectively). The clefts 13 and 14 can accommodate 11-cis retinal with binding energies of -4.9 kcal/mol (11-cis retinal-11) and -5.5 kcal/mol, respectively (11-cis retinal-20).

The 11-cis retinal and the all-trans retinol share highly similar physical and chemical properties, given the similarity between the two molecules it is not surprising that CB-Dock 2 positions the all-trans retinol in the same cavities and clefts of 11-cis retinal; however, a few minor differences are visible. Cavity 1 represents the preferred binding site by both 11-cis retinal and all-trans retinol; however, they bind inside the cavity in a different way. Cavity 1 can accommodate all-trans retinol in two different ways (all-trans retinol-1 and all-trans retinol-19); however, unlike 11-cis retinal they are not deeply inserted into the hydrophobic cavity. All-trans retinol-1 is bound to the hydrophobic cavity with its aldehyde group directed toward the cavity entrance 2 and the β-ionone ring located inside the cavity. In contrast, all-trans retinol-19 has its β-ionone located near the cavity entrance 1 and the polar moiety resides inside the cavity (Figure 3.32A) showing binding energies of -8.6 and -6.2 kcal/mol, respectively. Cavity 2 has the ability to bind all-trans retinol; three different poses are suggested by our analysis with CB-Dock 2 (all-trans retinol-3, all-trans retinol-15, and all-trans retinol-17), in all of them, the all-trans retinol is positioned in a similar way, presenting its β-ionone ring placed at the cavity entrance 2. The binding energies for all-trans retinol all-trans retinol-3, all-trans retinol-15, and all-trans retinol-17 of -6.7, -6.8, and -6.7 kcal/mol, respectively (Figure 3.32B). Also, the hydrophobic clefts can bind all-trans retinol; cleft1 and cleft 2 are able to bind all-trans retinol-12 and all-trans retinol-18 in a manner similar to that in which they bind 11-cis retinal-18. The binding region is almost overlapping, and the β-ionone ring is placed in the same manner however the aldehyde group of the polar head is directed toward the domain A of the Module 3 instead of the domain B of the Module 3 as for 11-cis retinal-18. Cleft 4 is capable of binding all-trans retinol-7 with the binding energy of -5.2 kcal/mol; the pose of all-trans retinol is very similar to 11-cis retinal-7 since the β-ionone ring is completely overlapping, however, the polar moiety of the molecule is interacting with a different area of the cleft. The cleft 5 that is capable of binding 11-cis retinal is not recognized by CB-Dock 2 as a possible binding site for all-trans retinol; however, a region that connects the clefts 3 and 5 is identified as a possible binding site for all-trans retinol (all-trans retinol-5) with a binding energy of -6.0 kcal/mol. Cleft 6 is capable of binding 11-cis retinal (11-cis retinal-2) and all-trans retinol (all-trans retinol-2) with binding energies of -5.6 kcal/mol and -5.8 kcal/mol, respectively; however, the two ligands are positioned in a different manner in the hydrophobic cleft since the orientation of the two molecules is flipped. Cleft 7 is able to bind all-trans retinol (all-trans retinol-10) with a binding energy of -5.5 kcal/mol. In this cleft, the 11-cis retinal and all-trans retinol share the same orientation; however, the all-trans retinol molecule is slightly shifted since its β-ionone ring overlaps with the polar tail of the 11-cis retinal (11-cis retinal-10). Regarding the cleft 8, our docking analysis revealed three possible poses for all-trans retinol (all-trans retinol-4, all-trans retinol-6, and all-trans retinol-14). The pose adopted by all-trans retinol-6 and all-trans retinol-14 resembles the one

used by 11-cis retinal-4 and 11-cis retinal-6, while all-trans retinol-4 presents an orientation that is perpendicular to the ligands previously mentioned. Interestingly, the cleft 9 that is capable of binding 11-cis retinal-14 is not recognized by CB-Dock 2 as a putative binding site for all-trans retinol. Cleft 10, which can bind 11-cis retinal-9 and 11-cis retinal-19, can also bind all-trans retinol-9. The positioning of the ligand is very similar with the β-ionone ring, which shares almost the same localization; the minor difference is represented by the different orientation of the polar moiety of the ligands. All-trans retinol-8 and all-trans retinol-13 bind to the clefts 11 and 12, respectively, occupying the same regions of 11-cis retinal-8 and 11-cis retinal-13; the only difference is the flipped orientation of the ligands. The domain A of Module 3 contains the hydrophobic cleft 13, which is able to bind 11-cis retinal-11 and all-trans retinol-11 with binding energies of -4.9 kcal/mol and -5.1 kcal/mol, despite the two ligands are localized in the same cleft, they do not overlap with each other. The cleft 14 can accommodate 11-cis retinal-20 and all-trans retinol-16, showing different conformations for the polar tail of the ligands. Furthermore, also all-trans retinol-20 is localized in the cleft 14 similarly to all-trans retinol-16; the two ligands share the same position for their β-ionone rings; however, their polar moieties of the two ligands are directed in the opposite way.

DHA is an important allosteric factor for the regulation of RBP3 activity (Chen et al., 1996). In our docking analysis, we searched for 20 putative binding sites for this ligand. Overall, DHA shows results similar to all-trans retinol and 11-cis retinal; however, the binding energies are smaller. Cavity 1 represents the most significant site with a binding energy of -9.0 kcal/mol; DHA is deeply inserted into the hydrophobic cavity, similarly to 11-cis retinal-1 (Figure 3.32A). The most interesting differences between DHA and the retinoids examined are represented by the presence of two new clefts (clefts 15 and 16) that bind DHA with a binding energy oscillating between -5.1 kcal/mol and -4.4 kcal/mol; furthermore, cleft 6 is not recognized as a possible binding site for DHA.

The same search was performed for OA; again the cavity 1 was identified as the preferred site, showing two different binding modes: OA-1 and OA-19 with binding energies of -7.5 and -5.4 kcal/mol, respectively (Figure 3.32A, Table 3). The clefts 4 and 6 were not identified as putative binding sites for OA.

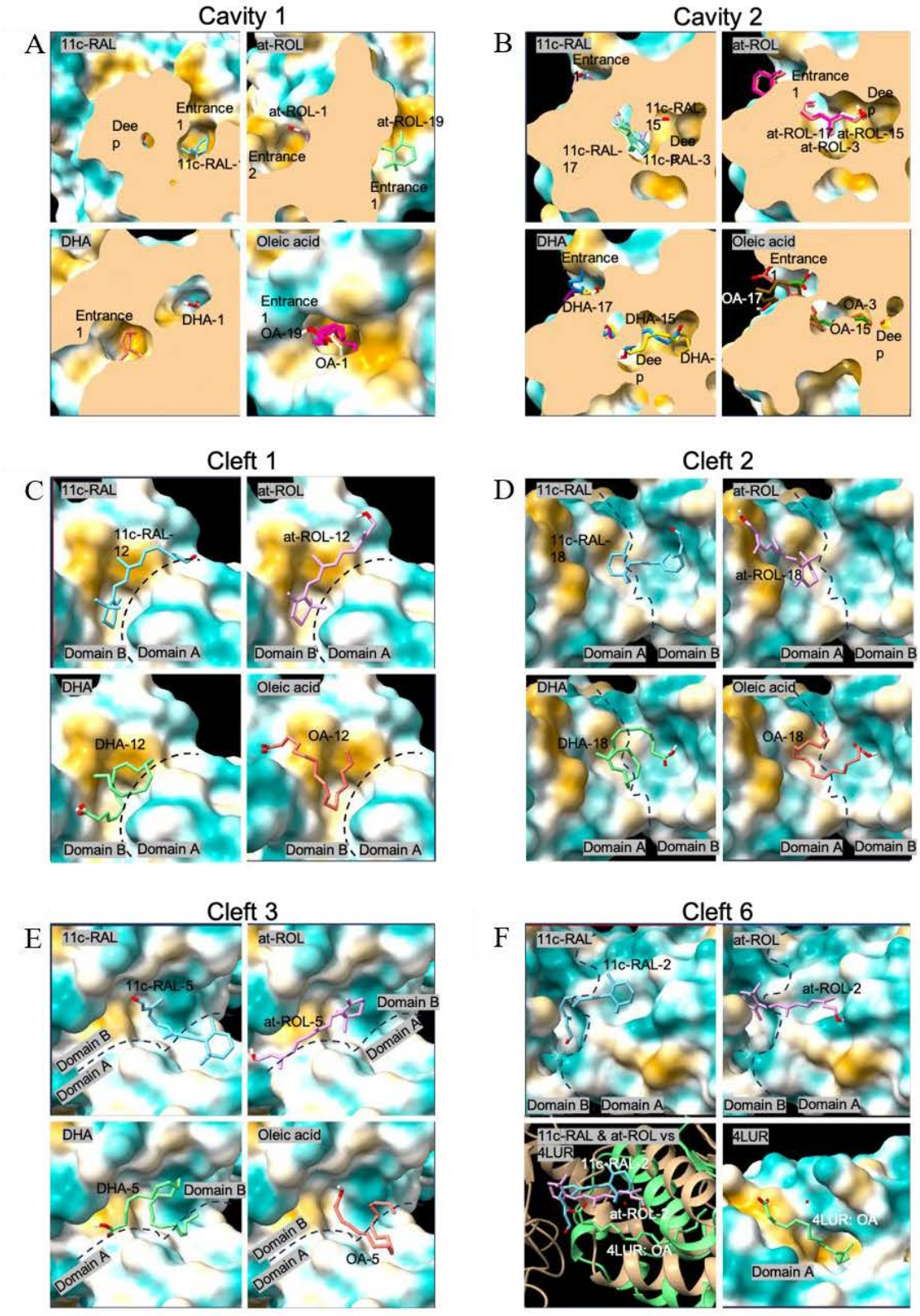

Figure 3.32*: Docking using the ligands:* 11-cis retinal, all-trans retinol, DHA *and* OA *in Sus scrofa RBP3 as receptor. (A–B) Hydrophobic cavities 1 and 2 located in domain B of* Sus scrofa RBP3. *(C–F) Hydrophobic clefts 1, 2, 3 and 6 localized at the interfaces of domain A and domain B of Sus scrofa RBP3, panel (F) is showing the aligned 4LUR structure and its* OA *ligand. The surface representation of Sus scrofa* RBP3 *is coloured according to relative hydrophobicity (golden colour the most lipophilic and dark cyan the most hydrophilic) (Picture taken from Kaushik et al., 2025B under the licence CC BY 4.0).*

3.2.8 *Sus scrofa* RBP3 SAXS measurement

In 1987, Adler and colleagues observed an extended conformation of *Bos taurus* RBP3 in their electron microscopy analysis (Adler et al., 1987). Despite the fact that we observed the extended conformation of *Sus scrofa* and *Bos taurus* RBP3 during the negative staining preparation, we were not able to obtain such extended conformation during the grid preparation for the CryoEM particle collection. In order to investigate the possibility of RBP3 to undergo such conformational changes, we decided to analyze the interaction of *Sus scrofa* RBP3 with the ligands using the Small-Angle X-ray Scattering (SAXS) technique. The SAXS measurements of apo RBP3 closely match the scattering curve we obtained from our CryoEM structure suggesting that *Sus scrofa* RBP3 consists of a stable monomer in solution and the R_g we obtained (5.22 ± 0.73 nm) is consistent with the atomic coordinates of *Bos taurus* RBP3 (PDB ID: 7JTI) reported by Sears and colleagues (Kaushik et al., 2025B). The P(R) distribution function shows a maximum linear dimension (Dmax) of 15.2 nm. The Kratky plot confirms that RBP3 adopts a globular conformation, additionally, the Guinier analysis confirms that the sample is monodisperse and do not display any sign of aggregation.

Sus scrofa RBP3 was titrated using four different ligands (11-cis retinal, all-trans retinol, OA, DHA). The titration with 11-cis retinal shows an increase in the Dmax value starting from 15.2 nm in the apo form until 19.87 nm in the presence of 8 µM 11-cis retinal, together with the increase in the Dmax value also a moderate increase of the is visible at higher concentration of the ligand ranging from 5.19 nm for the apo protein until 5.9 nm in presence of 8 µM 11-cis retinal (Table 4) consistently with a slight extension of the shape of the protein. Analyzing the Kratky plot for the protein in complex with 8 µM 11-cis retinal, the intensity ($q^2I(q)$) remains high for high q values, clearly indicating the flexibility induced by the ligand (Figure 3.33A).

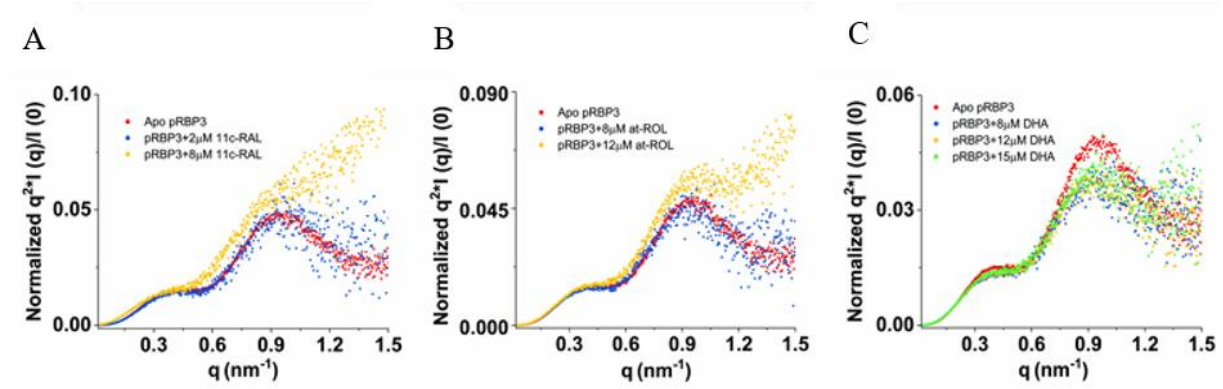

Figure 3.33: Kratky plots for RBP3 titrations. A) Kratky plot for Sus scrofa RBP3 titrated with 11-cis retinal. B) Kratky plot for Sus scrofa RBP3 titrated with all-trans-retinol. C) Kratky plot for Sus scrofa RBP3 titrated with DHA (Picture adapted from Kaushik et al.,2025B under the licence CC BY 4.0).

Samples	Apo-pRBP3	pRBP3 + 11c-RAL (2 µM)	pRBP3 + 11c-RAL (4 µM)	pRBP3 + 11c-RAL (8 µM)
Data collection parameters				
X-ray source	P12, DESY	P12, DESY	P12, DESY	P12, DESY
Detector	Pilatus6m	Pilatus6m	Pilatus6m	Pilatus6m
Wavelength (nm)	0.123	0.123	0.123	0.123
Exposure time Per frame (sec)	1	1	1	1
No. of frames collected	40	40	40	40
Concentration (mg/ml)	0.3	0.3	0.3	0.3
Measurement Temperature (°C)	20	20	20	20
Structural parameters				
I(0) [from Guinier]	27848±52.68	4286.01±25.75	5606.76±43.46	3654.01±24.71
Rg (nm) [from Guinier]	5.22±0.73	5.55±0.35	5.83±0.49	5.94±1.05
I(0) [from P(r)]	27830	4199	5487	3603
Rg (nm) [from P(r)]	5.19	5.34	5.68	5.90
Dmax (nm)	15.20	15.5	17.2	19.87
Modeling parameters				
Symmetry	P1	P1	P1	P1
Anisotropy	Unknown	Unknown	Unknown	Unknown
Modeling iterations	10	10	10	10
DAMMIF Chi^2	1.09	1.01	1.18	1.05

Table 4: taken from Kaushik et al., 2025B supplementary material. pRBP3 stands for *Sus scrofa* RBP3, 11c-RAL stands for 11-cis retinal.

The titration of *Sus scrofa* RBP3 with all-trans retinol gave similar results; the addition of all-trans retinol determined an increase in the Rg from 5.19 nm (apo protein) to 5.63 nm, and this parameter remained essentially unchanged with the increase of all-trans retinol concentration, while the Dmax showed a modest increase reaching the value of 18.07 nm. The minor fluctuations in the Rg value, coupled with a modest increase in the Dmax value, suggest that the overall mass of the protein remains stable, although some local extension at the periphery of the protein can determine an increase in the Dmax value (Table 5). Similarly, to what we have seen for RBP3 in the presence of 8 µM 11-cis

retinal, in the presence of 12 µM all-trans retinol, the Kratky plot shows that the intensity ($q^2I(q)$) remains high for high q values (Figure 3.33B), suggesting, analogously to 11-cis retinal, that also all-trans retinal is inducing higher structural flexibility.

Samples	pRBP3 + at-ROL (2 µM)	pRBP3 + at-ROL (8 µM)	pRBP3 + at-ROL (12 µM)
Data collection parameters			
X-ray source	P12, DESY	P12, DESY	P12, DESY
Detector	Pilatus6m	Pilatus6m	Pilatus6m
Wavelength (nm)	0.123	0.123	0.123
Exposure time Per frame (sec)	1	1	1
No. of frames collected	40	40	40
Concentration (mg/ml)	0.3	0.3	0.3
Measurement Temperature (°C)	20	20	20
Structural parameters			
I(0) [from Guinier]	4726.67±34.69	0.023±0.00013	0.03±0.00014
Rg (nm) [from Guinier]	5.77±0.52	5.65±0.78	5.73±1.03
I(0) [from P(r)]	4631	0.02	0.03
Rg (nm) [from P(r)]	5.63	5.78	5.66
Dmax (nm)	15.15	17.67	18.07
Modeling parameters			
Symmetry	P1	P1	P1
Anisotropy	Unknown	Unknown	Unknown
Modeling iterations	10	10	10
DAMMIF Chi^2	1.12	1.14	1.18

Table 5: taken from Kaushik et al., 2025B supplementary material. pRBP3 stands for *Sus scrofa* RBP3, at-ROL stands for all-trans retinol.

The titration with DHA displays R_g values obtained with Guinier analysis ranging from 5.83 nm to 6.15 nm indicating a modest extension in the protein conformation (Table 6). The P(R) function analysis gave R(g) values ranging from 5.67 nm to 5.92 nm clearly indicating that DHA binding is not causing major changes in the protein conformation (Table 6). Unlike All-trans retinol and 11-cis retinal, the Kratky plot does not show a plateau at high q values (Figure 3.33C).

Samples	pRBP3 + DHA (6 µM)	pRBP3 + DHA (8 µM)	pRBP3 + DHA (12 µM)	pRBP3 + DHA (15 µM)
Data collection parameters				
X-ray source	P12, DESY	P12, DESY	P12, DESY	P12, DESY
Detector	Pilatus6m	Pilatus6m	Pilatus6m	Pilatus6m
Wavelength (nm)	0.123	0.123	0.123	0.123
Exposure time Per frame (sec)	1	1	1	1
No. of frames collected	40	40	40	40
Concentration (mg/ml)	0.3	0.3	0.3	0.3
Measurement Temperature (°C)	20	20	20	20
Structural parameters				
I(0) [from Guinier]	0.027±0.00016	0.027±0.00012	0.028± 0.00011	0.025±0.00012
Rg (nm) [from Guinier]	5.94±0.34	6.15±0.51	5.91±0.73	5.83±0.87
I(0) [from P(r)]	0.03	0.03	0.03	0.03
Rg (nm) [from P(r)]	5.67	5.81	5.92	5.82
Dmax (nm)	17.5	17.67	22	19.09
Modeling parameters				
Symmetry	P1	P1	P1	P1
Anisotropy	Unknown	Unknown	Unknown	Unknown
Modeling iterations	10	10	10	10
DAMMIF Chi^2	1.3	1.37	1.14	0.92

Table 6: taken from Kaushik et al., 2025B supplementary material. pRBP3 stands for *Sus scrofa* RBP3.

The titration of *Sus scrofa* RBP3 with OA gave results comparable to DHA titration; however, the effect of the OA on the Dmax value (ranging from 18.09 to 19.17) is even more limited (Table 7).

Samples	pRBP3 + OA (2 µM)	pRBP3 + OA (6 µM)	pRBP3 + OA (10 µM)	pRBP3 + OA (15 µM)	pRBP3 + OA (20 µM)
Data collection parameters					
X-ray source	P12, DESY	P12, DESY	P12, DESY	P12, DESY	P12, DESY
Detector	Pilatus6m	Pilatus6m	Pilatus6m	Pilatus6m	Pilatus6m
Wavelength (nm)	0.123	0.123	0.123	0.123	0.123
Exposure time Per frame (sec)	1	1	1	1	1
No. of frames collected	40	40	40	40	40
Concentration (mg/ml)	0.3	0.3	0.3	0.3	0.3
Measurement Temperature (°C)	20	20	20	20	20
Structural parameters					
I(0) [from Guinier]	0.09±0.00048	0.068±0.00026	0.065±0.00029	0.092±0.00049	0.087±0.00052
Rg (nm) [from Guinier]	6.03±1.01	5.79±0.73	5.87±0.62	5.97±0.33	6.24±0.63
I(0) [from P(r)]	0.09	0.07	0.06	0.09	0.08
Rg (nm) [from P(r)]	5.91	5.72	5.78	5.91	6.01
Dmax (nm)	19.1	18.06	19.03	19.17	19.07
Modeling parameters					
Symmetry	P1	P1	P1	P1	P1
Anisotropy	Unknown	Unknown	Unknown	Unknown	Unknown
Modeling iterations	10	10	10	10	10
DAMMIF Chi^2	1.08	0.88	1.02	1.19	1.26

Table 7: taken from Kaushik et al., 2025B. pRBP3 stands for *Sus scrofa* RBP3.

The collected data were used to generate ab initio models with DAMMIF for the visualization of the protein conformation. The apo protein, as expected, presents the horseshoe conformation already visible in the CryoEM structure (Figure 3.34), however when the protein is presence of 11-cis retinal or all-trans retinol the protein adopts a slightly extended conformation (Figure 3.34A, B, C), although not comparable with the results provided by Adler and colleagues in 1987 for *Bos taurus* RBP3 (Adler et al., 1987; Kaushik et al., 2025B).

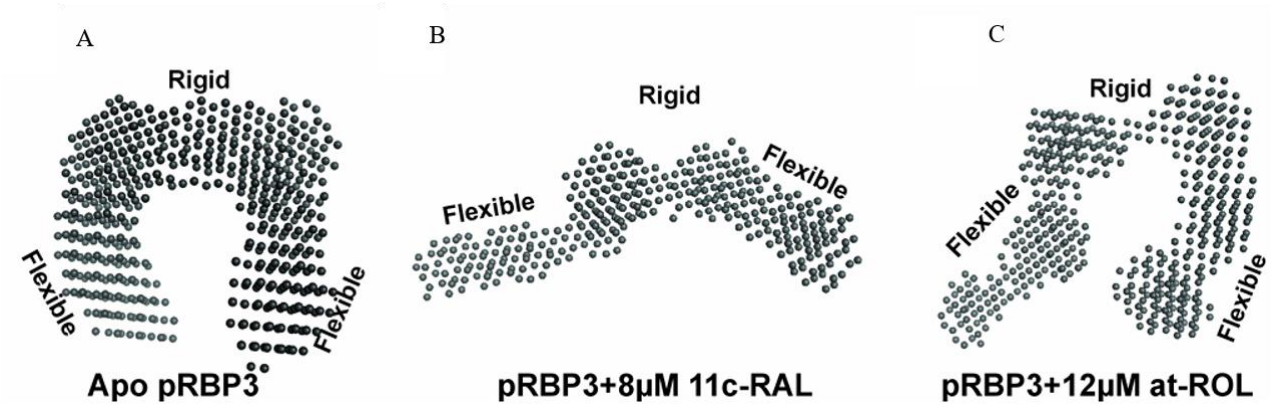

Figure 3.34: Conformational changes of Sus scrofa RBP3. A) Apo version of RBP3. B) RBP3 in complex with 11-cis retinal. C) RBP3 in complex with all-trans retinol (Picture adapted from Kaushik et al., 2025B under the licence CC BY 4.0).

4 Discussion

RBP3 plays a crucial role in the retinal physiology through its ability to bind retinoids. Despite its importance, the structural biology of RBP3 is still incomplete. In order to obtain the full structure of RBP3 and to identify the retinoid binding sites, two different approaches were used: the recombinant production of the single modules and the isolation of RBP3 from native sources for the CryoEM studies.

4.1 Recombinant modules

4.1.1 Expression and purification

Considering the intrinsic flexibility of the full-length RBP3, the expression of the recombinant modules and their crystallization represent the strategy for achieving the highest possible resolution. It is known from the literature that the expression of RBP3 modules posed several issues regarding the solubility and its recovery from inclusion bodies using urea (Baer et al., 1998). Furthermore, even when the RBP3 modules are recovered from inclusion bodies, their functionality cannot be restored completely (Baer et al., 1998). The solubility issues are not surprising if the glycosylated nature of RBP3 is taken into account and the impossibility for *E. coli* cells to introduce such post-translational modifications. Considering the fact that the N-linked glycan chains of RBP3 are not required for the folding process in the Golgi apparatus (Fong et al., 1984A), it is possible to speculate that one of the reasons why the N-glycans are conserved by evolution is to increase the solubility of the protein. For this reason, several constructs were cloned into the pGEX-6P-1 vector with a GST tag at the N-terminus of the construct in order to increase the solubility, mimicking the strategy adopted by Baer and colleagues (Baer et al., 1998). The presence of the GST tag clearly improved the expression of the constructs, which were totally absent when the histidine tag was used (Data not shown). Despite the presence of the GST tag, the majority of the constructs remained in the inclusion bodies, suggesting that although an increase in solubility, the *E. coli* translational apparatus is still incapable to provide the correct folding to the protein of interest, which may be due to the absence of specific eukaryotic chaperones that are not expressed by *E. coli*.

Notably, bRBP3M4 was partially soluble, and it was possible to obtain high yield and high purity of the sample through three chromatographic steps. A possible speculation to explain the partial solubility of Module 4 can be understood under the light of evolution. Proteins are evolutionarily pressured to avoid aggregation (Rousseau et al., 2006). Module 4 of RBP3 is the module that, more than the other modules, resembles the features of the old ancestral protein (Gonzalez-Fernandez et al., 2007). It is possible that Module 4 is retaining structural features that allow it to be expressed as

a single protein in the absence of other domains. In contrast, it is possible that the Modules 1, 2, and 3 may have not been selected to be stable as single proteins and other inter-Modules interactions are required for their folding.

The possible strategy to overcome the solubility issue relative to the expression of RBP3 modules may come from other heterologous expression systems that are able to introduce glycan chains to the protein, such as insect cells, yeast, or mammalian cell lines.

4.1.2 Circular dichroism

In order to test the folding state of the purified soluble fraction of bRBP3M4, a CD analysis was performed. The CD spectra of bRBP3M4 shows one positive peak at 196 nm, and 2 negative peaks at 209.5 nm and 218.5 nm. The spectrum is typical of folded proteins with a mixture of α-helix and β-strand. Although it is important to notice that the presence of Tris HCl is disturbing the signal from 190 to 200 nm, it is necessary to acknowledge that the signal of the positive peak is not as high as for proteins rich in α-helix, this may be caused by the presence of β-strands or random coil that attenuate the signal, suggesting that a fraction of the protein in solution may be misfolded. As mentioned before, the result obtained is slightly different from the in-silico prediction by the software Phyre 2.2 (Powell et al., 2025), however the CD spectra are comparable with the result showed by Nickerson and colleagues relative to the human RBP3 modules, unfortunately, only the range between 200 and 250 nm is shown in their paper (Nickerson et al., 1998).

4.1.3 Fluorescence enhancement

The fluorescence enhancement was used to test the ability of the recombinant constructs to bind all-trans retinol. The analysis clearly showed no difference between the control and the recombinantly produced M4 of *Bos taurus* RBP3, certifying the inability of the protein to bind the retinoids. It is possible to explain the failure considering that the *E. coli* does not possess the chaperones required for the proper folding of the protein of interest and their inability to introduce post-translational modifications such as glycosylation. Furthermore, it is possible that, although the GST-tag increases the solubility of the protein, reducing the formation of inclusion bodies, its steric hindrance may prevent the formation of weak transient interactions that play an essential role during the early stages of the folding process.

4.2 Full-length RBP3

4.2.1 Purification

The purification of the full-length RBP3 through three chromatographic steps rendered a highly pure sample with high yield for a protein isolated from native sources. Although the isolation procedure appears straightforward, the tendency of the protein to form aggregated complexes still represents the major issue, which is due to the disulfide bond formed by cysteine residues (Gonzalez-Fernandez et al., 2014). Since the analysis of our structure excludes the possibility of intra-protein disulfide bond, it is logical that the disulfide bonds are inter-protein. The proneness to aggregation is clearly visible in the SEC chromatogram, where two separated peaks show different retention time; however, when the fractions corresponding to the two different peaks are run on SDS-PAGE gel, they present the same band size, clearly indicating that the RBP3 proteins eluting with the first peak represent the aggregated fraction of the sample. The purification of *Sus scrofa* and *Bos taurus* RBP3 did not show any particular difference relative to the integrated area of the first peak, suggesting that the tendency to form aggregates is similar between the two orthologs although the bovine RBP3 contains three cysteine residues more than the porcine counterpart. The aggregation issue can be furtherly restrained by increasing the DTT concentration as suggested by Gonzalez-Fernandez and colleagues (Gonzalez-Fernandez et al., 2014).

4.2.2 RBP3 Biophysical characterization

The biophysical characterization, consisting of tryptophan quenching fluorescence assays, were performed in order to confirm the functionality of the protein and its ability to bind retinoids. The decrease in fluorescence emission at 338 nm, coupled with the modest increase at 480 nm, is compatible with the binding of all-trans retinol in a hydrophobic cavity, suggesting the conformation of the protein is retained. Also, the 11-cis retinal is causing tryptophan fluorescence quenching; however, the amount of retinoid required to reach the saturation is lower, suggesting the preference of RBP3 for 11-cis retinal rather than all-trans retinol. The decrease in the 350 nm peak obtained with 11-cis retinal is less marked compared to the one obtained with all-trans retinol; it is possible that 11-cis retinal is binding in a different pose that places itself in a slightly distant position from the tryptophan residues. Overall, the tryptophan quenching and the differences in binding between all-trans and 11-cis retinol suggest the ability of RBP3 to properly interact with retinoids.

It is of interest that the effect of the *Bos taurus* RBP3 de-glycosylation on the ligand binding is that the removal of the glycan chains decreases the concentration of all-trans retinol required for reaching the saturation point (Figure 3.21C). A possible interpretation for this result can be provided by taking

into account that the removal of the glycan chains leads to an increase in the flexibility of the protein, thus increasing the accessibility to the hydrophobic cavity responsible for the retinoids' binding.

4.2.3 RBP3 CryoEM structure

Thanks to single particle CryoEM analysis it was possible to obtain the high-resolution structure of the protein at 3.67 Å, this represents a substantial improvement from the previously published structure of *Bos taurus* RBP3 in complex with antibody (Sears et al., 2020) which allowed for the first time, the visualization of the overall architecture of RBP3 without providing the fine details of the structure.

A substantial improvement has also been achieved in the proposed atomic model, as it is demonstrated by the validation scores, indicating a lower clashscore, lower Ramachandran outliers, and lower sidechain outliers (Table 8).

	Sus scrofa RBP3	*Bos taurus* RBP3
Clashscore	10	22
Ramachandran outliers	0	0.9
Sidechain outliers	0.1	5.2

Table 8: Structure comparison between *Sus scrofa* RBP3 and *Bos taurus* RBP3 qualitatively

Sus scrofa RBP3 structure shares the same topology as the bovine ortholog published by Sears and colleagues; however, considering that the structure we propose did not require the presence of an antibody for reducing the flexibility of RBP3, it is possible to affirm that our model represents the native conformation of RBP3 more closely without potential bias induced by the complex with an antibody. Furthermore, the improved resolution coupled with better stereochemical parameters, allows the use of computational techniques such as docking. In particular, the region extending from the domain 2B to the domain 4A shows a higher local resolution. This allows the use of docking to identify putative binding sites not only within a specific module, but also in the boundary regions between the modules. Considering how the local resolution varies between the core region and the terminal portions, despite the substantial improvement, our structure still remains unsuitable for molecular dynamics experiments, not only for the high molecular weight, but especially because of the high flexibility of the N-terminal and C-terminal portions.

The attempts to determine the structure of RBP3 in complex with various ligands (e.g., DHA, all-trans retinol, 11-cis retinal) were hampered by the poor quality of the particles. After the 2D classification, the poor quality of the 2D classes appears clearly evident; for this reason, the datasets collected were not used for the 3D reconstruction. A possible explanation for the poor behavior of

the protein in the presence of the ligand can be provided by considering the high flexibility of the protein and the effects of the ligand on the conformation of the protein. Although the ligand binding is not able to induce an extensive conformational change, it still may induce flexibility in specific local regions of the protein. This behavior may cause particle misalignment leading to blurred images.

4.2.4 RBP3 structure – implications in disease

RBP3 is known to play a role in several pathological conditions, such as diabetic retinopathy and high myopia (Arno et al., 2015; Markand et al., 2016; Garcia-Ramirez et al., 2009). In some cases, its involvement appears to be more related to its concentration levels rather than the results of mutations in the amino acid sequence that may disrupt or alter the normal functionality of the protein. A clear example is provided by diabetic retinopathy, a disease in which there is an underproduction of RBP3 (Garcia-Ramirez et al., 2009). The overexpression of RBP3 counteracts the effects of the retinopathy (Chen et al., 2021) mitigating the effects of the hyperglycemia, slowing down the progression toward more severe stages (Yokomizo et al., 2019). Although the molecular mechanisms through which RBP3 is able to exert its protective role in diabetic retinopathy are still not completely elucidated, it is suggested that RBP3 binds GLUT1, decreasing glucose absorption by retinal cells (Yokomizo et al., 2019).

In 2009, a mutation in the RBP3 gene encoding for the mutant version D1080N, was found to be responsible for autosomal recessive retinitis pigmentosa (den Hollander et al., 2009). The mutation is responsible for the misfolding leading to accumulation of RBP3 in the endoplasmic reticulum and therefore blocking the secretion of the protein, in particular, the mutation is causing the formation of insoluble aggregates through disulfide bonds with cytotoxic effects (Li et al., 2013). Our structure can confirm the suggestion proposed by den Hollander and colleagues relative to a possible salt bond formed by the aspartate 1080 (den Hollander et al., 2009), we propose that this amino acid is interacting with arginine 1082, when the aspartate residue of the WT is replaced by asparagine it may form a new hydrogen bond with tyrosine 1044 (Kaushik et al., 2025B). As we suggest in our study (Kaushik et al., 2025B) this mutation can significantly alter the protein surface disturbing the proper interactions between RBP3 and the chaperone molecules of the endoplasmic reticulum blocking the secretion of the protein (Li et al., 2013). Furthermore, Li and colleagues described two cysteine residues (C304, C1175) that play a crucial role in the synthesis of non-secretory RBP3, causing aggregation and formation of insoluble complexes (Li et al., 2013). C304 is located on a flexible region that connects a β-strand of the domain B with the α-helix that connects the Module 1 with Module 2, *Homo sapiens* C1175 is replaced by a serine residue in *Sus scrofa* ortholog and it is located in the cleft between domain A and domain B. Analyzing our structure and considering the distance

between the aspartate 1080 and the two cysteine residues mentioned above it is possible to exclude a direct interactions between the three amino acids, we therefore suggest that the point mutation D1080N is not contributing directly to the incorrect formation of the disulfide bonds described by Li S and colleagues, however, it is possible to speculate that the accumulation of the misfolded mutant protein leads to high concentration levels that allows the formation of incorrect disulfide bonds (Li et al., 2013; Kaushik et al., 2025B). It is extremely important to notice that the residues aspartate 1080 and arginine 1082 belong to one of the five β-strands that form the architecture of the hydrophobic cavity of the domain B of the Module 4. Although the lateral groups of the amino acids mentioned above do not point inside the hydrophobic cavity, it is possible that they play a crucial role in the maintenance of the global architecture of the cavity. Notably, the β-strand where the aspartate 1080 resides corresponds to the amino acidic stretch identified as a possible ligand binding site of *Homo sapiens* RBP3 Module 1 by Rengarajan and colleagues (Rengarajan et al., 2001).

Although decreased expression of the RBP3 gene has been associated with high myopia (Getz et al., 2024), genetic mutations that alter the protein structure can cause the same issue (Georgiou et al., 2024). Amongst the several mutations associated with myopia described by Georgiou and colleagues, some of them are non-sense mutation resulting in shortened versions of RBP3 that are completely non-functional (Georgiou et al., 2024). Non-sense mutations such as Gln54Ter and Trp211Ter generates proteins that have not even Module 1 completed, however, Try510Ter encodes for a version of RBP3 with a complete Module 1 and the mutations Gln942Ter, Tyr1133Ter, and Glu1152 would still produce truncated proteins that contain at least three functional Modules. Although the single modules represent the functional units of RBP3, since each of them is capable of binding ligands (Nickerson et al., 1998), it is possible to speculate that the complete four-module protein is required for binding to specific cell receptors or another crucial biochemical/physiological function. Furthermore, although all the four modules are able to bind the retinoids and other ligands, they show different binding capacities (Lin et al., 1997) and as demonstrated by Yokomizo and colleagues the Module 1 of human RBP3 is better than other modules in inhibition of the 2-D-deoxy-D-glucose uptake, mimicking better the properties of the full-length RBP3 (Yokomizo et al., 2019).

Besides truncated versions, Georgiou and colleagues described a few interesting point mutations, including: Arg170Gln, Leu540Pro, and Ala876Ser (Georgiou et al., 2024). Arg170Gln, which is located on the same β-strand (this time in Module 1) as the Asp1080Asn mutation, and Leu540Pro, which is located on one of the five β-strands that make up the hydrophobic cavity of the domain B of Module 2. As we suggest in our paper, these mutations should be investigated using a similar methodology as the one used by Li et al in order to check the accumulation of the mutated RBP3 in

the endoplasmic reticulum (Li S et al., 2013). Ala876Ser is located in the hydrophobic cleft between Domain A and Domain B, a region that is identified as a putative binding site by our docking analysis. This mutation may compromise the ability to bind ligands through the introduction of a clash between the Serine hydroxyl group and the β-Ionone ring of the retinoid molecules since it reduces the distance of the interaction up to 3.0 Å, which is shorter compared to the 3.8 Å of the Cβ of the Alanine residue, this mutation may increase the probability of steric hindrance (Kaushik et al., 2025B).

4.2.5 Docking – *Sus scrofa* RBP3 ligand binding

Unfortunately, the major limitation of the 3.67 Å resolution structure we reported is that it is not possible to visualize the ligand binding sites occupied by the endogenous retinoid molecules interacting with RBP3. Two non-mutually exclusive explanations can be provided to describe why this occurred, although the 3.67 Å resolution may not be sufficiently high for the visualization of the retinoids it is necessary to acknowledge that during the purification procedure (in particular during the treatment with Concanavalin A) the majority of the endogenous retinoids are removed from their binding sites (Adler and Evans, 1983) therefore the absence of the retinoid ligands in our structure may be attributed to a low occupancy. Despite the above-mentioned limitations, our work represents the first structure with sufficiently high resolution to investigate the presence of possible binding sites in the boundary regions between the modules. Our docking analysis recognizes the hydrophobic cleft between domain A and domain B and the hydrophobic cavity within domain B previously described by Loew and Gonzalez-Fernandez (Loew and Gonzalez-Fernandez., 2002; Gonzalez-Fernandez et al., 2009). Beside the hydrophobic cleft described by Loew and Gonzalez-Fernandez in 2002 which correspond to the Cleft 2 of Module 3 in our analysis (Figure 3.31), we suggest another cleft located between the domains A and B (Cleft 1, Figure 3.31) can act as a binding site, both clefts can undergo conformational changes leading to a better accommodation of the ligands (Kaushik et al., 2025B). Interestingly, the binding energies for the retinoids (e.g., 11-Cis retinal, all-trans retinol) are stronger (-2.15 kcal/mol for Cleft 1, -1.45 kcal/mol for Cleft 2) compared to those for DHA and OA. This evidence may be of interest to explain the different affinities RBP3 shows toward different ligands. The clefts located between the modules (Cleft 6, 7, 13, 15, 16) are shallower and present slightly lower binding energies; however, the Cleft 15 may be a candidate for the binding of DHA with -5.1 kcal/mol binding energy.

Considering the highly similar topology between ligand binding hydrophobic cavity of CRALBP (PDB ID: 3HY5; He et al., 2009) and the domain B of RBP3, which consists of αβα sandwich (Kiser et al., 2014) (Figure 4.1), the prediction of the hydrophobic cavity of the domain B as a good candidate for retinoids binding site is somehow expected.

It is possible that several shallow hydrophobic clefts with lower binding energies identified by the docking analysis are not putative binding sites but act a “transient interaction points” that may regulate the protein activity.

Given the high number of putative binding sites/transient interaction points, it is possible to understand why the debate relative to binding sites of RBP3 is still open and why the number of binding sites reported in the literature varies greatly, as reported in paragraph 1.7.4.

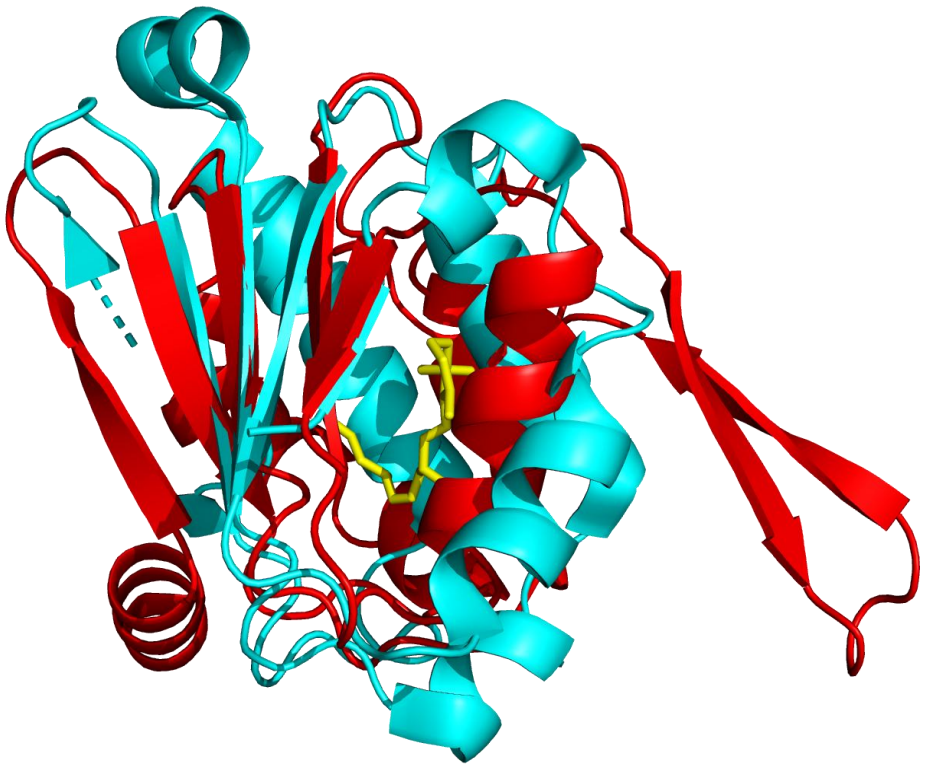

Figure 4.1: Superimposition between the Domain B of Sus scrofa Module 3 (in red) (PDB ID: 9FRX) with the amino acid stretch 141-225 of CRALBP (PDB ID: 3HY5) in cyan. In yellow the endogenous ligand 11-cis retinal coming from CRALBP. Picture obtained using PyMol (Schrödinger, LLC).

4.2.6 Ligand-induced conformational changes

The CryoEM local resolution map shows the high flexibility of the N-terminal portion (From domain of Module 1 to domain A of Module 2) and C-terminal portion (domain B of Module 4), this flexibility is confirmed by our SAXS experiment, furthermore it is possible to affirm that local flexibility induced by retinoid binding is higher than the flexibility induced by fatty acids binding as shown by the plateau of the Kratky plot. This may be due to the fact that retinoids and fatty acids are probably binding to different regions of the protein and they are exerting a different effect. The retinoid binding determined an extension of the protein, a different conformation of RBP3 was already observed by Adler and colleagues (Adler et al., 1987), however, as we have already stated in

our study: “the change, according to SAXS, is smaller than observed by negative staining EM or suggested by sedimentation analysis [44], where a 24 nm length was reported for the extended conformation, compared with our measured D_{max} of <20nm” (Kaushik et al., 2025B). Since our SAXS analysis is conducted in a protein-friendly solution and a less osmotic-stressing environment compared to the one performed by Adler and colleagues, we suggest our analysis offers a more physiologically relevant insight into RBP3 conformational changes. The biological meanings of these conformational changes are far from being explained; it is possible that they are required to expose specific epitopes of the protein that interact with membrane receptors present on the RPE or photoreceptor membranes. Furthermore, we are not the first group to speculate that the conformational changes of RBP3 may be related to a cooperative mechanism among the RBP3 modules (Lin et al., 1997). In the above cited paper, the binding capacity of the individually expressed single modules is higher than the binding capacity of the full-length protein containing all the four modules, referring to it as “lack of additivity”, suggesting a negative cooperativity mechanism in which the binding of one all-trans retinol molecule in one module causes a decrease in the binding affinity in other modules (Lin et al., 1997). Although the different binding capacities between the individually expressed modules and the full-length protein may be attributable to a different protein conformation (e.g., in the C-shape conformation not all the sites are already opened in contrast to the single modules) causing “lack of additivity”, it does not necessarily imply a negative cooperativity mechanism, it is still possible that a retinoid binding event is causing a conformational change (observed by SAXS analysis) that allows an easier access to the next binding site. However, the minimal extension caused by the binding event is not enough to get a completely open conformation; therefore, the full length protein, although slightly extended, is not able to acquire the same binding capacities as the sum of the four single modules. In conclusion, conformational changes may provide an explanation for the different number of binding sites reported in the literature when the single modules or the full-length protein were used.

5 Conclusion

The work presented here resulted in a significant improvement of RBP3 structure, which not only provides information on the overall architecture of the protein but also fine details relative to the junctions between the modules. The absence of a monoclonal antibody allows the structural characterization of the protein in a native conformation, providing information relative to the flexible portions of the protein.

Although it is still not possible to provide an unassailable and definitive model to explain how RBP3 functions, the results produced by SAXS analysis may provide helpful information to understand the ligand-binding-induced conformational changes and the allosteric regulation of the protein.

Unfortunately, it was not possible to produce good CryoEM datasets of the protein in complex with the ligands; thus, more efforts are required to investigate RBP3 complexes. Given the high number of putative binding sites, full-length RBP3 represent a complex system; for this reason, the analysis of the binding properties through biophysical assays such as fluorescence assays will likely fail in providing clear and unquestionable answers. A possible strategy to shed light on the function mechanism of RBP3 will likely require a dual approach: further investigation/optimization of the CryoEM studies of the full length protein in complex with the ligands, and the study of truncated recombinant proteins (e.g., modules and tandem modules) through crystallization and Nuclear Magnetic Resonance (NMR) using eukaryotic heterologous expression systems.

6 References

- Acharya, S., Foletta, V. C., Lee, J. W., Rayborn, M. E., Rodriguez, I. R., Young, W. S., 3rd, & Hollyfield, J. G. (2000). SPACRCAN, a novel human interphotoreceptor matrix hyaluronan-binding proteoglycan synthesized by photoreceptors and pinealocytes. *The Journal of biological chemistry*, *275*(10), 6945–6955. https://doi.org/10.1074/jbc.275.10.6945
- Acharya, S., Rayborn, M. E., & Hollyfield, J. G. (1998). Characterization of SPACR, a sialoprotein associated with cones and rods present in the interphotoreceptor matrix of the human retina: immunological and lectin binding analysis. *Glycobiology*, *8*(10), 997–1006. https://doi.org/10.1093/glycob/8.10.997
- Adler, A. J., Evans, C. D., & Stafford, W. F., 3rd (1985). Molecular properties of bovine interphotoreceptor retinol-binding protein. *The Journal of biological chemistry*, *260*(8), 4850–4855.
- Adler, A. J., & Evans, C. D. (1983). Rapid isolation of bovine interphotoreceptor retinol-binding protein. *Biochimica et biophysica acta*, *761*(3), 217–222. https://doi.org/10.1016/0304-4165(83)90068-5
- Adler, A. J., & Evans, C. D. (1985). Some functional characteristics of purified bovine interphotoreceptor retinol-binding protein. *Investigative ophthalmology & visual science*, *26*(3), 273–282.
- Adler, A. J., & Klucznik, K. M. (1982). Proteins and glycoproteins of the bovine interphotoreceptor matrix: composition and fractionation. *Experimental eye research*, *34*(3), 423–434. https://doi.org/10.1016/0014-4835(82)90088-4
- Adler, A. J., & Spencer, S. A. (1991). Effect of light on endogenous ligands carried by interphotoreceptor retinoid-binding protein. *Experimental eye research*, *53*(3), 337–346. https://doi.org/10.1016/0014-4835(91)90239-b
- Adler, A. J., Stafford, W. F., 3rd, & Slayter, H. S. (1987). Size and shape of bovine interphotoreceptor retinoid-binding protein by electron microscopy and hydrodynamic analysis. *The Journal of biological chemistry*, *262*(27), 13198–13203.
- Albini, A., Toffenetti, J., Zhu, Z., Chader, G. J., & Noonan, D. M. (1990). Hypomethylation of the interphotoreceptor retinoid-binding protein (IRBP) promotor and first exon is linked to expression of the gene. *Nucleic acids research*, *18*(17), 5181–5187. https://doi.org/10.1093/nar/18.17.5181

- Aliancy JF, Mamalis N. Crystalline Lens and Cataract. 2017 Aug 15. In: Kolb H, Fernandez E, Jones B, et al., editors. Webvision: The Organization of the Retina and Visual System [Internet]. Salt Lake City (UT): University of Utah Health Sciences Center; 1995-. Figure 2a. [A cartoon to show the...]. Available from: https://www.ncbi.nlm.nih.gov/books/NBK476171/figure/lens_cataract.F2a/
- Alvarez, R. A., Liou, G. I., Fong, S. L., & Bridges, C. D. (1987). Levels of alpha- and gamma-tocopherol in human eyes: evaluation of the possible role of IRBP in intraocular alpha-tocopherol transport. *The American journal of clinical nutrition*, *46*(3), 481–487. https://doi.org/10.1093/ajcn/46.3.481
- Ames J. B. (2022). Structural basis of retinal membrane guanylate cyclase regulation by GCAP1 and RD3. *Frontiers in molecular neuroscience*, *15*, 988142. https://doi.org/10.3389/fnmol.2022.988142
- Ames J. B. (2021). Structural Insights into Retinal Guanylate Cyclase Activator Proteins (GCAPs). *International journal of molecular sciences*, *22*(16), 8731. https://doi.org/10.3390/ijms22168731
- Anastasi G et al., (2007). Trattato di anatomia umana, volume III, Milano, Edi.Ermes, 2007,
- Arno, G., Hull, S., Robson, A. G., Holder, G. E., Cheetham, M. E., Webster, A. R., Plagnol, V., & Moore, A. T. (2015). Lack of Interphotoreceptor Retinoid Binding Protein Caused by Homozygous Mutation of RBP3 Is Associated With High Myopia and Retinal Dystrophy. *Investigative ophthalmology & visual science*, *56*(4), 2358–2365. https://doi.org/10.1167/iovs.15-16520
- Avesani, A., Marino, V., Zanzoni, S., Koch, K. W., & Dell'Orco, D. (2021). Molecular properties of human guanylate cyclase-activating protein 2 (GCAP2) and its retinal dystrophy-associated variant G157R. *The Journal of biological chemistry*, *296*, 100619. https://doi.org/10.1016/j.jbc.2021.100619
- Baer, C. A., Retief, J. D., Van Niel, E., Braiman, M. S., & Gonzalez-Fernandez, F. (1998). Soluble expression in E. coli of a functional interphotoreceptor retinoid-binding protein module fused to thioredoxin: correlation of vitamin A binding regions with conserved domains of C-terminal processing proteases. *Experimental eye research*, *66*(2), 249–262. https://doi.org/10.1006/exer.1997.0418
- Baker, S. A., & Kerov, V. (2013). Photoreceptor inner and outer segments. *Current topics in membranes*, *72*, 231–265. https://doi.org/10.1016/B978-0-12-417027-8.00007-6

- Bales TR, Lopez MJ, Clark J. Embryology, Eye. [Updated 2023 Mar 27]. In: StatPearls [Internet]. Treasure Island (FL): StatPearls Publishing; 2025 Jan-. Available from: https://www.ncbi.nlm.nih.gov/books/NBK538480/
- Barbieri, M., Carinci, P. (1997). *Embriologia* (2ª ed.). Milano: CSA Editrice Ambrosiana.
- Bazan, N. G., Reddy, T. S., Redmond, T. M., Wiggert, B., & Chader, G. J. (1985). Endogenous fatty acids are covalently and noncovalently bound to interphotoreceptor retinoid-binding protein in the monkey retina. *The Journal of biological chemistry*, *260*(25), 13677–13680.
- Beharry, S., Zhong, M., & Molday, R. S. (2004). N-retinylidene-phosphatidylethanolamine is the preferred retinoid substrate for the photoreceptor-specific ABC transporter ABCA4 (ABCR). *The Journal of biological chemistry*, *279*(52), 53972–53979. https://doi.org/10.1074/jbc.M405216200
- Berry, J., Frederiksen, R., Yao, Y., Nymark, S., Chen, J., & Cornwall, C. (2016). Effect of Rhodopsin Phosphorylation on Dark Adaptation in Mouse Rods. *The Journal of neuroscience : the official journal of the Society for Neuroscience*, *36*(26), 6973–6987. https://doi.org/10.1523/JNEUROSCI.3544-15.2016
- Besharse, J.C., Horst, C.J. (1990). The Photoreceptor Connecting Cilium A Model for the Transition Zone. In: Bloodgood, R.A. (eds) Ciliary and Flagellar Membranes. Springer, Boston, MA. https://doi.org/10.1007/978-1-4613-0515-6_15
- Betts-Obregon, B. S., Gonzalez-Fernandez, F., & Tsin, A. T. (2014). Interphotoreceptor retinoid-binding protein (IRBP) promotes retinol uptake and release by rat Müller cells (rMC-1) in vitro: implications for the cone visual cycle. *Investigative ophthalmology & visual science*, *55*(10), 6265–6271. https://doi.org/10.1167/iovs.14-14721
- Bill A. (1984). The circulation in the eye. In: Renkin EM, Michel CC, editors. Handbooak of Physiology: the Cardiovascular System IV: Microcirculation Part 2. Waverly Press; Baltimore: 1984. pp. 1001–1035.
- Boguslawski, J., Palczewska, G., Tomczewski, S., Milkiewicz, J., Kasprzycki, P., Stachowiak, D., Komar, K., Marzejon, M. J., Sikorski, B. L., Hudzikowski, A., Głuszek, A., Łaszczych, Z., Karnowski, K., Soboń, G., Palczewski, K., & Wojtkowski, M. (2022). In vivo imaging of the human eye using a 2-photon-excited fluorescence scanning laser ophthalmoscope. *The Journal of clinical investigation*, *132*(2), e154218. https://doi.org/10.1172/JCI154218
- Bok D. (1993). The retinal pigment epithelium: a versatile partner in vision. *Journal of cell science. Supplement*, *17*, 189–195. https://doi.org/10.1242/jcs.1993.supplement_17.27

- Bonilha, V. L., Finnemann, S. C., & Rodriguez-Boulan, E. (1999). Ezrin promotes morphogenesis of apical microvilli and basal infoldings in retinal pigment epithelium. *The Journal of cell biology*, *147*(7), 1533–1548. https://doi.org/10.1083/jcb.147.7.1533
- Bonilha, V. L., Rayborn, M. E., Bhattacharya, S. K., Gu, X., Crabb, J. S., Crabb, J. W., & Hollyfield, J. G. (2006). The retinal pigment epithelium apical microvilli and retinal function. *Advances in experimental medicine and biology*, *572*, 519–524. https://doi.org/10.1007/0-387-32442-9_72
- Boron W.F., Boulpaep EL. (2016). *Medical physiology* (3rd ed.). Philadelphia, PA: Elsevier.
- Borst, D. E., Redmond, T. M., Elser, J. E., Gonda, M. A., Wiggert, B., Chader, G. J., & Nickerson, J. M. (1989). Interphotoreceptor retinoid-binding protein. Gene characterization, protein repeat structure, and its evolution. *The Journal of biological chemistry*, *264*(2), 1115–1123.
- Boulton, M., Rózanowska, M., & Rózanowski, B. (2001). Retinal photodamage. *Journal of photochemistry and photobiology. B, Biology*, *64*(2-3), 144–161. https://doi.org/10.1016/s1011-1344(01)00227-5
- Bownds, D., & Brodie, A. E. (1975). Light-sensitive swelling of isolated frog rod outer segments as an in vitro assay for visual transduction and dark adaptation. *The Journal of general physiology*, *66*(4), 407–425. https://doi.org/10.1085/jgp.66.4.407
- Bridges, C. D., Liou, G. I., Alvarez, R. A., Landers, R. A., Landry, A. M., Jr, & Fong, S. L. (1986). Distribution of interstitial retinol-binding protein (IRBP) in the vertebrates. *The Journal of experimental zoology*, *239*(3), 335–346. https://doi.org/10.1002/jez.1402390305
- Bron AJ, et al. (1997) *Wolff's Anatomy of the Eye and Orbit*. 8th ed. / Anthony J. Bron, Ramesh C. Tripathi, Brenda J. Tripathi. London ; Chapman & Hall Medical, 1997. Print.
- Campbell, M., Humphries, P. (2013). The Blood-Retina Barrier. In: Cheng, C.Y. (eds) Biology and Regulation of Blood-Tissue Barriers. Advances in Experimental Medicine and Biology, vol 763. Springer, New York, NY. https://doi.org/10.1007/978-1-4614-4711-5_3
- Caporossi A, (2017). *Oftalmologia*. Padova: Piccin-Nuova Libraria.
- Carlson, A., & Bok, D. (1992). Promotion of the release of 11-cis-retinal from cultured retinal pigment epithelium by interphotoreceptor retinoid-binding protein. *Biochemistry*, *31*(37), 9056–9062. https://doi.org/10.1021/bi00152a049
- Carter-Dawson, L., Alvarez, R. A., Fong, S. L., Liou, G. I., Sperling, H. G., & Bridges, C. D. (1986). Rhodopsin, 11-cis vitamin A, and interstitial retinol-binding protein (IRBP) during retinal development in normal and rd mutant mice. *Developmental biology*, *116*(2), 431–438. https://doi.org/10.1016/0012-1606(86)90144-2

- Carter-Dawson, L., & Burroughs, M. (1989). Differential distribution of interphotoreceptor retinoid-binding protein (IRBP) around retinal rod and cone photoreceptors. *Current eye research*, *8*(12), 1331–1334. https://doi.org/10.3109/02713688909013914
- Carter-Dawson, L., & Burroughs, M. (1992). Interphotoreceptor retinoid-binding protein in the Golgi apparatus of monkey foveal cones. Electron microscopic immunocytochemical localization. *Investigative ophthalmology & visual science*, *33*(5), 1589–1594.
- Castano P et al., (1999) *Anatomia umana : per le Facoltà di farmacia e di scienze e per le scuole biomediche dirette a fini speciali*. 3a ristampa riv. e corr. Milano: Edi-ermes, 1999. Print.
- Chapot, C. A., Euler, T., & Schubert, T. (2017). How do horizontal cells 'talk' to cone photoreceptors? Different levels of complexity at the cone-horizontal cell synapse. *The Journal of physiology*, *595*(16), 5495–5506. https://doi.org/10.1113/JP274177
- Chen, C., Adler, L., 4th, Goletz, P., Gonzalez-Fernandez, F., Thompson, D. A., & Koutalos, Y. (2017). Interphotoreceptor retinoid-binding protein removes all-*trans*-retinol and retinal from rod outer segments, preventing lipofuscin precursor formation. *The Journal of biological chemistry*, *292*(47), 19356–19365. https://doi.org/10.1074/jbc.M117.795187
- Chen, J., Shao, Y., Sasore, T., Moiseyev, G., Zhou, K., Ma, X., Du, Y., & Ma, J. X. (2021). Interphotoreceptor Retinol-Binding Protein Ameliorates Diabetes-Induced Retinal Dysfunction and Neurodegeneration Through Rhodopsin. *Diabetes*, *70*(3), 788–799. https://doi.org/10.2337/db20-0609
- Chen, S., Wang, Q. L., Nie, Z., Sun, H., Lennon, G., Copeland, N. G., Gilbert, D. J., Jenkins, N. A., & Zack, D. J. (1997). Crx, a novel Otx-like paired-homeodomain protein, binds to and transactivates photoreceptor cell-specific genes. *Neuron*, *19*(5), 1017–1030. https://doi.org/10.1016/s0896-6273(00)80394-3
- Chen, X., Zhang, L., Sohn, E. H., Lee, K., Niemeijer, M., Chen, J., Sonka, M., & Abràmoff, M. D. (2012**A**). Quantification of external limiting membrane disruption caused by diabetic macular edema from SD-OCT. *Investigative ophthalmology & visual science*, *53*(13), 8042–8048. https://doi.org/10.1167/iovs.12-10083
- Chen, Y., Clarke, O. B., Kim, J., Stowe, S., Kim, Y. K., Assur, Z., Cavalier, M., Godoy-Ruiz, R., von Alpen, D. C., Manzini, C., Blaner, W. S., Frank, J., Quadro, L., Weber, D. J., Shapiro, L., Hendrickson, W. A., & Mancia, F. (2016). Structure of the STRA6 receptor for retinol uptake. *Science (New York, N.Y.)*, *353*(6302), aad8266. https://doi.org/10.1126/science.aad8266

- Chen, Y., Houghton, L. A., Brenna, J. T., & Noy, N. (1996). Docosahexaenoic acid modulates the interactions of the interphotoreceptor retinoid-binding protein with 11-cis-retinal. *The Journal of biological chemistry*, *271*(34), 20507–20515. https://doi.org/10.1074/jbc.271.34.20507
- Chen, Y., & Noy, N. (1994). Retinoid specificity of interphotoreceptor retinoid-binding protein. *Biochemistry*, *33*(35), 10658–10665. https://doi.org/10.1021/bi00201a013
- Chen, Y., Okano, K., Maeda, T., Chauhan, V., Golczak, M., Maeda, A., & Palczewski, K. (2012**B**). Mechanism of all-trans-retinal toxicity with implications for stargardt disease and age-related macular degeneration. *The Journal of biological chemistry*, *287*(7), 5059–5069. https://doi.org/10.1074/jbc.M111.315432
- Chen, Y., Saari, J. C., & Noy, N. (1993). Interactions of all-trans-retinol and long-chain fatty acids with interphotoreceptor retinoid-binding protein. *Biochemistry*, *32*(42), 11311–11318. https://doi.org/10.1021/bi00093a007
- Cioffi CL, (2020). Introduction: Overview of the Human Eye, Mammalian Retina, and the Retinoid Visual Cycle. In: Cioffi, C.L. (eds) Drug Delivery Challenges and Novel Therapeutic Approaches for Retinal Diseases. Topics in Medicinal Chemistry, vol 35. Springer, Cham. https://doi.org/10.1007/7355_2020_94
- Clark, S. J., Keenan, T. D., Fielder, H. L., Collinson, L. J., Holley, R. J., Merry, C. L., van Kuppevelt, T. H., Day, A. J., & Bishop, P. N. (2011). Mapping the differential distribution of glycosaminoglycans in the adult human retina, choroid, and sclera. *Investigative ophthalmology & visual science*, *52*(9), 6511–6521. https://doi.org/10.1167/iovs.11-7909
- Cmglee, 2019 – Own work, CC BY-SA 3.0, https://commons.wikimedia.org/w/index.php?curid=29924570.
- Cote, R. H., Gupta, R., Irwin, M. J., & Wang, X. (2022). Photoreceptor Phosphodiesterase (PDE6): Structure, Regulatory Mechanisms, and Implications for Treatment of Retinal Diseases. *Advances in experimental medicine and biology*, *1371*, 33–59. https://doi.org/10.1007/5584_2021_649
- Coughlin, B. A., Feenstra, D. J., & Mohr, S. (2017). Müller cells and diabetic retinopathy. *Vision research*, *139*, 93–100. https://doi.org/10.1016/j.visres.2017.03.013
- Cunningham, L. L., & Gonzalez-Fernandez, F. (2000). Coordination between production and turnover of interphotoreceptor retinoid-binding protein in zebrafish. *Investigative ophthalmology & visual science*, *41*(11), 3590–3599.

- Cunningham, L. L., & Gonzalez-Fernandez, F. (2003). Internalization of interphotoreceptor retinoid-binding protein by the Xenopus retinal pigment epithelium. *The Journal of comparative neurology*, *466*(3), 331–342. https://doi.org/10.1002/cne.10861
- Cunningham, L. L., Yang, L., & Gonzalez-fernandez, F. (1999). Interphotoreceptor retinoid-binding protein (IRBP) is rapidly cleared from the Xenopus interphotoreceptor matrix. *Experimental eye research*, *68*(4), 399–410. https://doi.org/10.1006/exer.1998.0633
- D'Ambrosio, D. N., Clugston, R. D., & Blaner, W. S. (2011). Vitamin A metabolism: an update. *Nutrients*, *3*(1), 63–103. https://doi.org/10.3390/nu3010063
- den Hollander, A. I., McGee, T. L., Ziviello, C., Banfi, S., Dryja, T. P., Gonzalez-Fernandez, F., Ghosh, D., & Berson, E. L. (2009). A homozygous missense mutation in the IRBP gene (RBP3) associated with autosomal recessive retinitis pigmentosa. *Investigative ophthalmology & visual science*, *50*(4), 1864–1872. https://doi.org/10.1167/iovs.08-2497
- Ding, J. D., Salinas, R. Y., & Arshavsky, V. Y. (2015). Discs of mammalian rod photoreceptors form through the membrane evagination mechanism. *The Journal of cell biology*, *211*(3), 495–502. https://doi.org/10.1083/jcb.201508093
- Dontsov, A., & Ostrovsky, M. (2024). Retinal Pigment Epithelium Pigment Granules: Norms, Age Relations and Pathology. *International journal of molecular sciences*, *25*(7), 3609. https://doi.org/10.3390/ijms25073609
- Duffy, M., Sun, Y., Wiggert, B., Duncan, T., Chader, G. J., & Ripps, H. (1993). Interphotoreceptor retinoid binding protein (IRBP) enhances rhodopsin regeneration in the experimentally detached retina. *Experimental eye research*, *57*(6), 771–782. https://doi.org/10.1006/exer.1993.1185
- Eberhardt, J., Santos-Martins, D., Tillack, A. F., & Forli, S. (2021). AutoDock Vina 1.2.0: New Docking Methods, Expanded Force Field, and Python Bindings. *Journal of chemical information and modeling*, *61*(8), 3891–3898. https://doi.org/10.1021/acs.jcim.1c00203
- Edward, D. P., & Kaufman, L. M. (2003). Anatomy, development, and physiology of the visual system. *Pediatric clinics of North America*, *50*(1), 1–23. https://doi.org/10.1016/s0031-3955(02)00132-3
- Edwards, R. B., & Adler, A. J. (2000). IRBP enhances removal of 11- cis -retinaldehyde from isolated RPE membranes. *Experimental eye research*, *70*(2), 235–245. https://doi.org/10.1006/exer.1999.0781
- Eggers, E. D., Mazade, R. E., & Klein, J. S. (2013). Inhibition to retinal rod bipolar cells is regulated by light levels. *Journal of neurophysiology*, *110*(1), 153–161. https://doi.org/10.1152/jn.00872.2012

- Eisenfeld, A. J., Bunt-Milam, A. H., & Saari, J. C. (1985). Immunocytochemical localization of interphotoreceptor retinoid-binding protein in developing normal and RCS rat retinas. *Investigative ophthalmology & visual science*, *26*(5), 775–778.
- Emsley, P., Lohkamp, B., Scott, W. G., & Cowtan, K. (2010). Features and development of Coot. *Acta crystallographica. Section D, Biological crystallography*, *66*(Pt 4), 486–501. https://doi.org/10.1107/S0907444910007493
- Ferrara, M., Lugano, G., Sandinha, M. T., Kearns, V. R., Geraghty, B., & Steel, D. H. W. (2021). Biomechanical properties of retina and choroid: a comprehensive review of techniques and translational relevance. *Eye (London, England)*, *35*(7), 1818–1832. https://doi.org/10.1038/s41433-021-01437-w
- Filipek, S., Stenkamp, R. E., Teller, D. C., & Palczewski, K. (2003). G protein-coupled receptor rhodopsin: a prospectus. *Annual review of physiology*, *65*, 851–879. https://doi.org/10.1146/annurev.physiol.65.092101.142611
- Fitzgerald, T. M. J., Gruener, G., & Mtui, E. (2012).*Neuroanatomia con riferimenti funzionali e clinici* (6ª ed.). Elsevier.
- Fong, S. L., & Bridges, C. D. (1988). Internal quadruplication in the structure of human interstitial retinol-binding protein deduced from its cloned cDNA. *The Journal of biological chemistry*, *263*(30), 15330–15334.
- Fong, S. L., & Fong, W. B. (1999). Elements regulating the transcription of human interstitial retinoid-binding protein (IRBP) gene in cultured retinoblastoma cells. *Current eye research*, *18*(4), 283–291. https://doi.org/10.1076/ceyr.18.4.283.5360
- Fong, S. L., Irimura, T., Landers, R. A., & Bridges, C. D. (1985). The carbohydrate of bovine interstitial retinol-binding protein. *Progress in clinical and biological research*, *190*, 111–128.
- Fong, S. L., Liou, G. I., Landers, R. A., Alvarez, R. A., & Bridges, C. D. (1984A). Purification and characterization of a retinol-binding glycoprotein synthesized and secreted by bovine neural retina. *The Journal of biological chemistry*, *259*(10), 6534–6542.
- Fong, S. L., Liou, G. I., Landers, R. A., Alvarez, R. A., Gonzalez-Fernandez, F., Glazebrook, P. A., Lam, D. M., & Bridges, C. D. (1984B). Characterization, localization, and biosynthesis of an interstitial retinol-binding glycoprotein in the human eye. *Journal of neurochemistry*, *42*(6), 1667–1676. https://doi.org/10.1111/j.1471-4159.1984.tb12758.x
- Franke, D., Petoukhov, M. V., Konarev, P. V., Panjkovich, A., Tuukkanen, A., Mertens, H. D. T., Kikhney, A. G., Hajizadeh, N. R., Franklin, J. M., Jeffries, C. M., & Svergun, D. I. (2017). *ATSAS 2.8*: a comprehensive data analysis suite for small-angle scattering from

macromolecular solutions. *Journal of applied crystallography*, *50*(Pt 4), 1212–1225. https://doi.org/10.1107/S1600576717007786

- Fung B. K. (1983). Characterization of transducin from bovine retinal rod outer segments. I. Separation and reconstitution of the subunits. *The Journal of biological chemistry*, *258*(17), 10495–10502.
- Furukawa, T., Ueno, A., & Omori, Y. (2020). Molecular mechanisms underlying selective synapse formation of vertebrate retinal photoreceptor cells. *Cellular and molecular life sciences : CMLS*, *77*(7), 1251–1266. https://doi.org/10.1007/s00018-019-03324-w
- Gandhi, S. Jain, S. (2015). The Anatomy and Physiology of Cornea. In: Cortina, M., de la Cruz, J. (eds) Keratoprostheses and Artificial Corneas. Springer, Berlin, Heidelberg. https://doi.org/10.1007/978-3-642-55179-6_3
- Gao, Y., Eskici, G., Ramachandran, S., Poitevin, F., Seven, A. B., Panova, O., Skiniotis, G., & Cerione, R. A. (2020). Structure of the Visual Signaling Complex between Transducin and Phosphodiesterase 6. *Molecular cell*, *80*(2), 237–245.e4. https://doi.org/10.1016/j.molcel.2020.09.013
- Garcia-Ramírez, M., Hernández, C., Villarroel, M., Canals, F., Alonso, M. A., Fortuny, R., Masmiquel, L., Navarro, A., García-Arumí, J., & Simó, R. (2009). Interphotoreceptor retinoid-binding protein (IRBP) is downregulated at early stages of diabetic retinopathy. *Diabetologia*, *52*(12), 2633–2641. https://doi.org/10.1007/s00125-009-1548-8
- Garlipp, M. A., & Gonzalez-Fernandez, F. (2013). Cone outer segment and Müller microvilli pericellular matrices provide binding domains for interphotoreceptor retinoid-binding protein (IRBP). *Experimental eye research*, *113*, 192–202. https://doi.org/10.1016/j.exer.2013.02.003
- Garlipp, M. A., Nowak, K. R., & Gonzalez-Fernandez, F. (2012). Cone outer segment extracellular matrix as binding domain for interphotoreceptor retinoid-binding protein. *The Journal of comparative neurology*, *520*(4), 756–769. https://doi.org/10.1002/cne.22773
- Gasteiger, E., Gattiker, A., Hoogland, C., Ivanyi, I., Appel, R. D., & Bairoch, A. (2003). ExPASy: The proteomics server for in-depth protein knowledge and analysis. *Nucleic acids research*, *31*(13), 3784–3788. https://doi.org/10.1093/nar/gkg563
- Georgiou, M., Fujinami, K., Robson, A. G., Fujinami-Yokokawa, Y., Shakarchi, A. F., Ji, M. H., Uwaydat, S. H., Kim, A., Kolesnikova, M., Arno, G., Pontikos, N., Mahroo, O. A., Tsang, S. H., Webster, A. R., & Michaelides, M. (2024). RBP3-Retinopathy-Inherited High Myopia and Retinal Dystrophy: Genetic Characterization, Natural History, and Deep

Phenotyping. *American journal of ophthalmology*, *258*, 119–129. https://doi.org/10.1016/j.ajo.2023.09.025

- Getz, T. E., Chrenek, M. A., Papania, J. T., Shelton, D. A., Markand, S., Iuvone, P. M., Kozmik, Z., Boatright, J. H., & Nickerson, J. M. (2024). Conditional Knockouts of Interphotoreceptor Retinoid Binding Protein Suggest Two Independent Mechanisms for Retinal Degeneration and Myopia. *Investigative ophthalmology & visual science*, *65*(6), 32. https://doi.org/10.1167/iovs.65.6.32
- Ghosh, D., Haswell, K. M., Sprada, M., & Gonzalez-Fernandez, F. (2015). Structure of zebrafish IRBP reveals fatty acid binding. *Experimental eye research*, *140*, 149–158. https://doi.org/10.1016/j.exer.2015.08.026
- Gonzalez-Fernandez, F., Baer, C. A., & Ghosh, D. (2007). Module structure of interphotoreceptor retinoid-binding protein (IRBP) may provide bases for its complex role in the visual cycle - structure/function study of Xenopus IRBP. *BMC biochemistry*, *8*, 15. https://doi.org/10.1186/1471-2091-8-15
- Gonzalez-Fernandez, F., Betts-Obregon, B., Yust, B., Mimun, J., Sung, D., Sardar, D., & Tsin, A. T. (2015). Interphotoreceptor retinoid-binding protein protects retinoids from photodegradation. *Photochemistry and photobiology*, *91*(2), 371–378. https://doi.org/10.1111/php.12416
- Gonzalez-Fernandez, F., Bevilacqua, T., Lee, K. I., Chandrashekar, R., Hsu, L., Garlipp, M. A., Griswold, J. B., Crouch, R. K., & Ghosh, D. (2009). Retinol-binding site in interphotoreceptor retinoid-binding protein (IRBP): a novel hydrophobic cavity. *Investigative ophthalmology & visual science*, *50*(12), 5577–5586. https://doi.org/10.1167/iovs.08-1857
- Gonzalez-Fernandez, F., Fong, S. L., Liou, G. I., & Bridges, C. D. (1985). Interstitial retinol-binding protein (IRBP) in the RCS rat: effect of dark-rearing. *Investigative ophthalmology & visual science*, *26*(10), 1381–1385.
- Gonzalez-Fernandez, F., & Healy, J. I. (1990). Early expression of the gene for interphotoreceptor retinol-binding protein during photoreceptor differentiation suggests a critical role for the interphotoreceptor matrix in retinal development. *The Journal of cell biology*, *111*(6 Pt 1), 2775–2784. https://doi.org/10.1083/jcb.111.6.2775
- Gonzalez-Fernandez, F., Landers, R. A., Glazebrook, P. A., Fong, S. L., Liou, G. I., Lam, D. M., & Bridges, C. D. (1984). An extracellular retinol-binding glycoprotein in the eyes of mutant rats with retinal dystrophy: development, localization, and biosynthesis. *The Journal of cell biology*, *99*(6), 2092–2098. https://doi.org/10.1083/jcb.99.6.2092

- Gonzalez-Fernandez, F., Sung, D., Haswell, K. M., Tsin, A., & Ghosh, D. (2014). Thiol-dependent antioxidant activity of interphotoreceptor retinoid-binding protein. *Experimental eye research*, *120*, 167–174. https://doi.org/10.1016/j.exer.2014.01.002
- Gonzalez-Fernandez, F., Van Niel, E., Edmonds, C., Beaver, H., Nickerson, J. M., Garcia-Fernandez, J. M., Campohiaro, P. A., & Foster, R. G. (1993). Differential expression of interphotoreceptor retinoid-binding protein, opsin, cellular retinaldehyde-binding protein, and basic fibroblastic growth factor. *Experimental eye research*, *56*(4), 411–427. https://doi.org/10.1006/exer.1993.1055
- Gospe, S. M., 3rd, Baker, S. A., Kessler, C., Brucato, M. F., Winter, J. R., Burns, M. E., & Arshavsky, V. Y. (2011). Membrane attachment is key to protecting transducin GTPase-activating complex from intracellular proteolysis in photoreceptors. *The Journal of neuroscience : the official journal of the Society for Neuroscience*, *31*(41), 14660–14668. https://doi.org/10.1523/JNEUROSCI.3516-11.2011
- Gulati, S., & Palczewski, K. (2023). Structural view of G protein-coupled receptor signaling in the retinal rod outer segment. *Trends in biochemical sciences*, *48*(2), 172–186. https://doi.org/10.1016/j.tibs.2022.08.010
- Guo, L. W., Hajipour, A. R., & Ruoho, A. E. (2010). Complementary interactions of the rod PDE6 inhibitory subunit with the catalytic subunits and transducin. *The Journal of biological chemistry*, *285*(20), 15209–15219. https://doi.org/10.1074/jbc.M109.086116
- Gupta, R., & Brunak, S. (2002). Prediction of glycosylation across the human proteome and the correlation to protein function. *Pacific Symposium on Biocomputing. Pacific Symposium on Biocomputing*, 310–322.
- Häggström M. (2014). Medical gallery of Mikael Häggström 2014. WikiJournal of Medicine, 1(2). https://doi.org/10.15347/wjm/2014.008.
- Hall J, E., Hall M,E. (2021). *Guyton and Hall textbook of medical physiology, 14th international edition,* (14). Philadelphia: Elsevier.
- Hargrave, P. A., Hamm, H. E., & Hofmann, K. P. (1993). Interaction of rhodopsin with the G-protein, transducin. *BioEssays : news and reviews in molecular, cellular and developmental biology*, *15*(1), 43–50. https://doi.org/10.1002/bies.950150107
- Hart NS. (2009). Retinal Photoreceptors. In: Binder, M.D., Hirokawa, N., Windhorst, U. (eds) Encyclopedia of Neuroscience. Springer, Berlin, Heidelberg. https://doi.org/10.1007/978-3-540-29678-2_5109
- Hayes, M. J., Burgoyne, T., Wavre-Shapton, S. T., Tolmachova, T., Seabra, M. C., & Futter, C. E. (2019). Remodeling of the Basal Labyrinth of Retinal Pigment Epithelial Cells With

Osmotic Challenge, Age, and Disease. *Investigative ophthalmology & visual science*, *60*(7), 2515–2524. https://doi.org/10.1167/iovs.19-26784

- He, X., Lobsiger, J., & Stocker, A. (2009). Bothnia dystrophy is caused by domino-like rearrangements in cellular retinaldehyde-binding protein mutant R234W. *Proceedings of the National Academy of Sciences of the United States of America*, *106*(44), 18545–18550. https://doi.org/10.1073/pnas.0907454106
- Heegaard, S., Jensen, O. A., & Prause, J. U. (1986). Structure and composition of the inner limiting membrane of the retina. SEM on frozen resin-cracked and enzyme-digested retinas of Macaca mulatta. *Graefe's archive for clinical and experimental ophthalmology = Albrecht von Graefes Archiv fur klinische und experimentelle Ophthalmologie*, *224*(4), 355–360. https://doi.org/10.1007/BF02150029
- Herman, K.G., Steinberg, R.H. (1982). Melanosome metabolism in the retinal pigmented epithelium of the opossum. *Cell Tissue Res.* **227**, 485–507 (1982). https://doi.org/10.1007/BF00204780
- Ho, M. T., Massey, J. B., Pownall, H. J., Anderson, R. E., & Hollyfield, J. G. (1989). Mechanism of vitamin A movement between rod outer segments, interphotoreceptor retinoid-binding protein, and liposomes. *The Journal of biological chemistry*, *264*(2), 928–935.
- Hollyfield, J. G., Fliesler, S. J., Rayborn, M. E., Fong, S. L., Landers, R. A., & Bridges, C. D. (1985A). Synthesis and secretion of interstitial retinol-binding protein by the human retina. *Investigative ophthalmology & visual science*, *26*(1), 58–67.
- Hollyfield, J. G., Varner, H. H., Rayborn, M. E., Liou, G. I., & Bridges, C. D. (1985B). Endocytosis and degradation of interstitial retinol-binding protein: differential capabilities of cells that border the interphotoreceptor matrix. *The Journal of cell biology*, *100*(5), 1676–1681. https://doi.org/10.1083/jcb.100.5.1676
- Holm L. (2020). Using Dali for Protein Structure Comparison. *Methods in molecular biology (Clifton, N.J.)*, *2112*, 29–42. https://doi.org/10.1007/978-1-0716-0270-6_3
- Hsieh, C. L., Yao, Y., Gurevich, V. V., & Chen, J. (2022). Arrestin Facilitates Rhodopsin Dephosphorylation *in Vivo*. *The Journal of neuroscience : the official journal of the Society for Neuroscience*, *42*(17), 3537–3545. https://doi.org/10.1523/JNEUROSCI.0141-22.2022
- Hurley, J. B., Spencer, M., & Niemi, G. A. (1998). Rhodopsin phosphorylation and its role in photoreceptor function. *Vision research*, *38*(10), 1341–1352. https://doi.org/10.1016/s0042-6989(97)00459-8

- Hussey, K. A., Hadyniak, S. E., & Johnston, R. J., Jr (2022). Patterning and Development of Photoreceptors in the Human Retina. *Frontiers in cell and developmental biology*, *10*, 878350. https://doi.org/10.3389/fcell.2022.878350
- Ichinose, T., & Habib, S. (2022). ON and OFF Signaling Pathways in the Retina and the Visual System. *Frontiers in ophthalmology*, *2*, 989002. https://doi.org/10.3389/fopht.2022.989002
- Imanishi, Y., Gerke, V., & Palczewski, K. (2004). Retinosomes: new insights into intracellular managing of hydrophobic substances in lipid bodies. *The Journal of cell biology*, *166*(4), 447–453. https://doi.org/10.1083/jcb.200405110
- Ishikawa, M., Sawada, Y., & Yoshitomi, T. (2015). Structure and function of the interphotoreceptor matrix surrounding retinal photoreceptor cells. *Experimental eye research*, *133*, 3–18. https://doi.org/10.1016/j.exer.2015.02.017
- Ivey, F. D., Taglia, F. X., Yang, F., Lander, M. M., Kelly, D. A., & Hoffman, C. S. (2010). Activated alleles of the Schizosaccharomyces pombe gpa2+ Galpha gene identify residues involved in GDP-GTP exchange. *Eukaryotic cell*, *9*(4), 626–633. https://doi.org/10.1128/EC.00010-10
- Jin, M., Li, S., Nusinowitz, S., Lloyd, M., Hu, J., Radu, R. A., Bok, D., & Travis, G. H. (2009). The role of interphotoreceptor retinoid-binding protein on the translocation of visual retinoids and function of cone photoreceptors. *The Journal of neuroscience : the official journal of the Society for Neuroscience*, *29*(5), 1486–1495.
- Johnson, L. V., Hageman, G. S., & Blanks, J. C. (1986). Interphotoreceptor matrix domains ensheath vertebrate cone photoreceptor cells. *Investigative ophthalmology & visual science*, *27*(2), 129–135.
- Kadomoto, S., Muraoka, Y., Uji, A., Ooto, S., Kawai, K., Ishikura, M., Nishigori, N., Akagi, T., & Tsujikawa, A. (2021). Human Foveal Cone and Müller Cells Examined by Adaptive Optics Optical Coherence Tomography. *Translational vision science & technology*, *10*(11), 17. https://doi.org/10.1167/tvst.10.11.17
- Kanai, M., Raz, A., & Goodman, D. S. (1968). Retinol-binding protein: the transport protein for vitamin A in human plasma. *The Journal of clinical investigation*, *47*(9), 2025–2044. https://doi.org/10.1172/JCI105889
- Kaneko A. (1979). Physiology of the retina. *Annual review of neuroscience*, *2*, 169–191. https://doi.org/10.1146/annurev.ne.02.030179.001125
- Kanow, M. A., Giarmarco, M. M., Jankowski, C. S., Tsantilas, K., Engel, A. L., Du, J., Linton, J. D., Farnsworth, C. C., Sloat, S. R., Rountree, A., Sweet, I. R., Lindsay, K. J., Parker, E. D.,

Brockerhoff, S. E., Sadilek, M., Chao, J. R., & Hurley, J. B. (2017). Biochemical adaptations of the retina and retinal pigment epithelium support a metabolic ecosystem in the vertebrate eye. *eLife*, *6*, e28899. https://doi.org/10.7554/eLife.28899

- Kasturi, N., Matalia, J. (2017). Anatomy of the Human Crystalline Lens. In: Chakrabarti, A. (eds) Posterior Capsular Rent. Springer, New Delhi. https://doi.org/10.1007/978-81-322-3586-6_2
- Kaushik, V., Dąbrowski, M., Gessa, L., Kumar, N., & Fernandes, H. (2025A). Corrigendum: Two-photon excitation fluorescence in ophthalmology: safety and improved imaging for functional diagnostics. *Frontiers in medicine*, *12*, 1572630. https://doi.org/10.3389/fmed.2025.1572630
- Kaushik, V., Gessa, L., Kumar, N., & Fernandes, H. (2023). Towards a New Biomarker for Diabetic Retinopathy: Exploring RBP3 Structure and Retinoids Binding for Functional Imaging of Eyes In Vivo. *International journal of molecular sciences*, *24*(5), 4408. https://doi.org/10.3390/ijms24054408
- Kaushik, V., Gessa, L., Kumar, N., Pinkas, M., Czarnocki-Cieciura, M., Palczewski, K., Nováček, J., & Fernandes, H. (2025B). CryoEM structure and small-angle X-ray scattering analyses of porcine retinol-binding protein 3. *Open biology*, *15*(1), 240180. https://doi.org/10.1098/rsob.240180
- Kawaguchi, R., Yu, J., Ter-Stepanian, M., Zhong, M., Cheng, G., Yuan, Q., Jin, M., Travis, G. H., Ong, D., & Sun, H. (2011). Receptor-mediated cellular uptake mechanism that couples to intracellular storage. *ACS chemical biology*, *6*(10), 1041–1051. https://doi.org/10.1021/cb200178w
- Kerschensteiner D. (2022). Feature Detection by Retinal Ganglion Cells. *Annual review of vision science*, *8*, 135–169. https://doi.org/10.1146/annurev-vision-100419-112009
- Kevany, B. M., & Palczewski, K. (2010). Phagocytosis of retinal rod and cone photoreceptors. *Physiology (Bethesda, Md.)*, *25*(1), 8–15. https://doi.org/10.1152/physiol.00038.2009
- Kiel JW. (2010). The Ocular Circulation. San Rafael (CA): Morgan & Claypool Life Sciences; 2010. Chapter 2, Anatomy. Available from: https://www.ncbi.nlm.nih.gov/books/NBK53329/
- Kiser, P. D., Golczak, M., Lodowski, D. T., Chance, M. R., & Palczewski, K. (2009). Crystal structure of native RPE65, the retinoid isomerase of the visual cycle. *Proceedings of the National Academy of Sciences of the United States of America*, *106*(41), 17325–17330. https://doi.org/10.1073/pnas.0906600106

- Kiser, P. D., Golczak, M., & Palczewski, K. (2014). Chemistry of the retinoid (visual) cycle. *Chemical reviews*, *114*(1), 194–232. https://doi.org/10.1021/cr400107q
- Kobat, S. G., & Turgut, B. (2020). Importance of Müller Cells. *Beyoglu eye journal*, *5*(2), 59–63. https://doi.org/10.14744/bej.2020.28290
- Koch, K. W., & Dell'Orco, D. (2015). Protein and Signaling Networks in Vertebrate Photoreceptor Cells. *Frontiers in molecular neuroscience*, *8*, 67. https://doi.org/10.3389/fnmol.2015.00067
- Koeppen BM, Stanton BA. (2018). "Berne & Levy Physiology". *7th ed* New Delhi: Elsevier, 2018. Text.
- Kolb H. (2005). Gross Anatomy of the Eye. 2005 May 1 [Updated 2024 Oct 10]. In: Kolb H, Fernandez E, Jones B, et al., editors. Webvision: The Organization of the Retina and Visual System [Internet]. Salt Lake City (UT): University of Utah Health Sciences Center; 1995-. Available from: https://www.ncbi.nlm.nih.gov/books/NBK11534/
- Kolb H. (1995). Roles of Amacrine Cells by Helga Kolb. In: Kolb H, Fernandez E, Jones B, et al., editors. Webvision: The Organization of the Retina and Visual System [Internet]. Salt Lake City (UT): University of Utah Health Sciences Center; 1995-. Available from: https://www.ncbi.nlm.nih.gov/books/NBK11539/
- Kolesnikov, A. V., Orban, T., Jin, H., Brooks, C., Hofmann, L., Dong, Z., Sokolov, M., Palczewski, K., & Kefalov, V. J. (2017). Dephosphorylation by protein phosphatase 2A regulates visual pigment regeneration and the dark adaptation of mammalian photoreceptors. *Proceedings of the National Academy of Sciences of the United States of America*, *114*(45), E9675–E9684. https://doi.org/10.1073/pnas.1712405114
- Kolesnikov, A. V., Tang, P. H., Parker, R. O., Crouch, R. K., & Kefalov, V. J. (2011). The mammalian cone visual cycle promotes rapid M/L-cone pigment regeneration independently of the interphotoreceptor retinoid-binding protein. *The Journal of neuroscience : the official journal of the Society for Neuroscience*, *31*(21), 7900–7909. https://doi.org/10.1523/JNEUROSCI.0438-11.2011
- Kono, M., & Crouch, R. K. (2010). In vitro assays of rod and cone opsin activity: retinoid analogs as agonists and inverse agonists. *Methods in molecular biology (Clifton, N.J.)*, *652*, 85–94. https://doi.org/10.1007/978-1-60327-325-1_4
- Kramer IM. (2015). *Signal transduction* (3rd ed.). Academic Press.
- Kutty, G., Duncan, T., Nickerson, J. M., Si, J. S., Van Veen, T., Chader, G. J., & Wiggert, B. (1994). Light deprivation profoundly affects gene expression of interphotoreceptor retinoid-

binding protein in the mouse eye. *Experimental eye research*, *58*(1), 65–75. https://doi.org/10.1006/exer.1994.1195

- Lai, R. K., Perez-Sala, D., Cañada, F. J., & Rando, R. R. (1990). The gamma subunit of transducin is farnesylated. *Proceedings of the National Academy of Sciences of the United States of America*, *87*(19), 7673–7677. https://doi.org/10.1073/pnas.87.19.7673
- Larkin, M. A., Blackshields, G., Brown, N. P., Chenna, R., McGettigan, P. A., McWilliam, H., Valentin, F., Wallace, I. M., Wilm, A., Lopez, R., Thompson, J. D., Gibson, T. J., & Higgins, D. G. (2007). Clustal W and Clustal X version 2.0. *Bioinformatics (Oxford, England)*, *23*(21), 2947–2948. https://doi.org/10.1093/bioinformatics/btm404
- Lee, B., Litt, M., & Buchsbaum, G. (1992). Rheology of the vitreous body. Part I: Viscoelasticity of human vitreous. *Biorheology*, *29*(5-6), 521–533. https://doi.org/10.3233/bir-1992-295-612
- Lee, H. S., Qi, Y., & Im, W. (2015). Effects of N-glycosylation on protein conformation and dynamics: Protein Data Bank analysis and molecular dynamics simulation study. *Scientific reports*, *5*, 8926. https://doi.org/10.1038/srep08926
- Lee, M., Li, S., Sato, K., & Jin, M. (2016). Interphotoreceptor Retinoid-Binding Protein Mitigates Cellular Oxidative Stress and Mitochondrial Dysfunction Induced by All-trans-Retinal. *Investigative ophthalmology & visual science*, *57*(4), 1553–1562. https://doi.org/10.1167/iovs.15-18551
- Li, S., Yang, Z., Hu, J., Gordon, W. C., Bazan, N. G., Haas, A. L., Bok, D., & Jin, M. (2013). Secretory defect and cytotoxicity: the potential disease mechanisms for the retinitis pigmentosa (RP)-associated interphotoreceptor retinoid-binding protein (IRBP). *The Journal of biological chemistry*, *288*(16), 11395–11406. https://doi.org/10.1074/jbc.M112.418251
- Liebschner, D., Afonine, P. V., Baker, M. L., Bunkóczi, G., Chen, V. B., Croll, T. I., Hintze, B., Hung, L. W., Jain, S., McCoy, A. J., Moriarty, N. W., Oeffner, R. D., Poon, B. K., Prisant, M. G., Read, R. J., Richardson, J. S., Richardson, D. C., Sammito, M. D., Sobolev, O. V., Stockwell, D. H., … Adams, P. D. (2019). Macromolecular structure determination using X-rays, neutrons and electrons: recent developments in Phenix. *Acta crystallographica. Section D, Structural biology*, *75*(Pt 10), 861–877. https://doi.org/10.1107/S2059798319011471
- Lin, Z. S., Fong, S. L., & Bridges, C. D. (1989). Retinoids bound to interstitial retinol-binding protein during light and dark-adaptation. *Vision research*, *29*(12), 1699–1709. https://doi.org/10.1016/0042-6989(89)90152-1

- Lin, Z. Y., Li, G. R., Takizawa, N., Si, J. S., Gross, E. A., Richardson, K., & Nickerson, J. M. (1997). Structure-function relationships in interphotoreceptor retinoid-binding protein (IRBP). *Molecular vision*, *3*, 17.
- Liou, G. I., Bridges, C. D., Fong, S. L., Alvarez, R. A., & Gonzalez-Fernandez, F. (1982). Vitamin A transport between retina and pigment epithelium--an interstitial protein carrying endogenous retinol (interstitial retinol-binding protein). *Vision research*, *22*(12), 1457–1467. https://doi.org/10.1016/0042-6989(82)90210-3
- Liou, G. I., Ma, D. P., Yang, Y. W., Geng, L., Zhu, C., & Baehr, W. (1989). Human interstitial retinoid-binding protein. Gene structure and primary structure. *The Journal of biological chemistry*, *264*(14), 8200–8206.
- Liou, G. I., Matragoon, S., Chen, D. M., Gao, C. L., Zhang, L., Fei, Y., Katz, M. L., & Stark, W. S. (1998). Visual sensitivity and interphotoreceptor retinoid binding protein in the mouse: regulation by vitamin A. *FASEB journal : official publication of the Federation of American Societies for Experimental Biology*, *12*(1), 129–138. https://doi.org/10.1096/fasebj.12.1.129
- Liou, G. I., Wang, M., & Matragoon, S. (1994). Timing of interphotoreceptor retinoid-binding protein (IRBP) gene expression and hypomethylation in developing mouse retina. *Developmental biology*, *161*(2), 345–356. https://doi.org/10.1006/dbio.1994.1036
- Liu, F., Lee, J., & Chen, J. (2021). Molecular structures of the eukaryotic retinal importer ABCA4. *eLife*, *10*, e63524. https://doi.org/10.7554/eLife.63524
- Liu, Y., Yang, X., Gan, J., Chen, S., Xiao, Z. X., & Cao, Y. (2022). CB-Dock2: improved protein-ligand blind docking by integrating cavity detection, docking and homologous template fitting. *Nucleic acids research*, *50*(W1), W159–W164. https://doi.org/10.1093/nar/gkac394
- Liz, M. A., Coelho, T., Bellotti, V., Fernandez-Arias, M. I., Mallaina, P., & Obici, L. (2020). A Narrative Review of the Role of Transthyretin in Health and Disease. *Neurology and therapy*, *9*(2), 395–402. https://doi.org/10.1007/s40120-020-00217-0
- Loew, A., & Gonzalez-Fernandez, F. (2002). Crystal structure of the functional unit of interphotoreceptor retinoid binding protein. *Structure (London, England : 1993)*, *10*(1), 43–49. https://doi.org/10.1016/s0969-2126(01)00698-0
- Lu, Y., Benedetti, J., & Yao, X. (2018). Light-Induced Length Shrinkage of Rod Photoreceptor Outer Segments. *Translational vision science & technology*, *7*(6), 29. https://doi.org/10.1167/tvst.7.6.29
- Lujan, B. J., Roorda, A., Croskrey, J. A., Dubis, A. M., Cooper, R. F., Bayabo, J. K., Duncan, J. L., Antony, B. J., & Carroll, J. (2015). DIRECTIONAL OPTICAL COHERENCE

TOMOGRAPHY PROVIDES ACCURATE OUTER NUCLEAR LAYER AND HENLE FIBER LAYER MEASUREMENTS. *Retina (Philadelphia, Pa.)*, *35*(8), 1511–1520.

- Majumder, A., Pahlberg, J., Muradov, H., Boyd, K. K., Sampath, A. P., & Artemyev, N. O. (2015). Exchange of Cone for Rod Phosphodiesterase 6 Catalytic Subunits in Rod Photoreceptors Mimics in Part Features of Light Adaptation. *The Journal of neuroscience : the official journal of the Society for Neuroscience*, *35*(24), 9225–9235. https://doi.org/10.1523/JNEUROSCI.3563-14.2015
- Markand, S., Baskin, N. L., Chakraborty, R., Landis, E., Wetzstein, S. A., Donaldson, K. J., Priyadarshani, P., Alderson, S. E., Sidhu, C. S., Boatright, J. H., Iuvone, P. M., Pardue, M. T., & Nickerson, J. M. (2016). IRBP deficiency permits precocious ocular development and myopia. *Molecular vision*, *22*, 1291–1308.
- Marmorstein A. D. (2001). The polarity of the retinal pigment epithelium. *Traffic (Copenhagen, Denmark)*, *2*(12), 867–872. https://doi.org/10.1034/j.1600-0854.2001.21202.x
- Masland R. H. (2001). The fundamental plan of the retina. *Nature neuroscience*, *4*(9), 877–886. https://doi.org/10.1038/nn0901-877
- Masland R. H. (2012). The neuronal organization of the retina. *Neuron*, *76*(2), 266–280.
- Mastronarde D. N. (2005). Automated electron microscope tomography using robust prediction of specimen movements. *Journal of structural biology*, *152*(1), 36–51. https://doi.org/10.1016/j.jsb.2005.07.007
- Mendez, A., Burns, M. E., Roca, A., Lem, J., Wu, L. W., Simon, M. I., Baylor, D. A., & Chen, J. (2000). Rapid and reproducible deactivation of rhodopsin requires multiple phosphorylation sites. *Neuron*, *28*(1), 153–164. https://doi.org/10.1016/s0896-6273(00)00093-3
- Mercer, A. J., & Thoreson, W. B. (2011). The dynamic architecture of photoreceptor ribbon synapses: cytoskeletal, extracellular matrix, and intramembrane proteins. *Visual neuroscience*, *28*(6), 453–471. https://doi.org/10.1017/S0952523811000356
- Mescher, A.L., York, New & San, Chicago & Athens, Francisco & Madrid, London & City, Mexico. (2018). Junqueira's Basic Histology, 15th edition, 2018.
- Micsonai, A., Wien, F., Bulyáki, É., Kun, J., Moussong, É., Lee, Y. H., Goto, Y., Réfrégiers, M., & Kardos, J. (2018). BeStSel: a web server for accurate protein secondary structure prediction and fold recognition from the circular dichroism spectra. *Nucleic acids research*, *46*(W1), W315–W322. https://doi.org/10.1093/nar/gky497
- Moakedi, Faezeh, "Structural and functional consequences of PDE6 prenylation in rod and cone photoreceptors" (2024). *Graduate Theses, Dissertations, and Problem Reports*. 12302. https://researchrepository.wvu.edu/etd/12302

- Moise, A. R., Golczak, M., Imanishi, Y., & Palczewski, K. (2007). Topology and membrane association of lecithin: retinol acyltransferase. *The Journal of biological chemistry*, *282*(3), 2081–2090. https://doi.org/10.1074/jbc.M608315200
- Molday, R. S., & Moritz, O. L. (2015). Photoreceptors at a glance. *Journal of cell science*, *128*(22), 4039–4045. https://doi.org/10.1242/jcs.175687
- Moore, B. A., Tyrell, L. P., Kamilar, J. M., Collin, S., Dominy, N. J., Hall, M. I., Heesy, C. P., Lisney, T. J., Loew, E. R., Moritz, G. L., Nava, S. S., Warrant, E., Shaw, K., & Fernandez-Juricic, E. (2017). Structure and function of regional specializations in the vertebrate retina. In J. H. Kaas, & G. Striedter (Eds.), *Evolution of nervous systems: The evolution of the nervous systems in nonmammalian vertebrates* (2nd ed., Vol. 1, pp. 351–372). Academic Press. https://doi.org/10.1016/B978-0-12-804042-3.00008-7
- Morgans C. W. (2000). Neurotransmitter release at ribbon synapses in the retina. *Immunology and cell biology*, *78*(4), 442–446. https://doi.org/10.1046/j.1440-1711.2000.00923.x
- Mustafi, D., Engel, A. H., & Palczewski, K. (2009). Structure of cone photoreceptors. *Progress in retinal and eye research*, *28*(4), 289–302. https://doi.org/10.1016/j.preteyeres.2009.05.003
- Napoli J. L. (2016). Functions of Intracellular Retinoid Binding-Proteins. *Sub-cellular biochemistry*, *81*, 21–76. https://doi.org/10.1007/978-94-024-0945-1_2
- Newcomer ME, Ong DE. (2013). Retinol Binding Protein and Its Interaction with Transthyretin. In: Madame Curie Bioscience Database [Internet]. Austin (TX): Landes Bioscience; 2000-2013. Available from: https://www.ncbi.nlm.nih.gov/books/NBK6223/#
- Ni, S., Khan, S., Jiménez-Villar, A., Pennesi, M. E., Huang, D., Jian, Y., & Chen, S. (2024). Optical Assessment of Photoreceptor Function Over the Macula. *Translational vision science & technology*, *13*(8), 41. https://doi.org/10.1167/tvst.13.8.41
- Nickerson, J. M., Frey, R. A., Ciavatta, V. T., & Stenkamp, D. L. (2006). Interphotoreceptor retinoid-binding protein gene structure in tetrapods and teleost fish. *Molecular vision*, *12*, 1565–1585.
- Nickerson, J. M., Li, G. R., Lin, Z. Y., Takizawa, N., Si, J. S., & Gross, E. A. (1998). Structure-function relationships in the four repeats of human interphotoreceptor retinoid-binding protein (IRBP). *Molecular vision*, *4*, 33.
- Noel, J. P., Hamm, H. E., & Sigler, P. B. (1993). The 2.2 A crystal structure of transducin-alpha complexed with GTP gamma S. *Nature*, *366*(6456), 654–663. https://doi.org/10.1038/366654a0

- Okajima, T. I., Pepperberg, D. R., Ripps, H., Wiggert, B., & Chader, G. J. (1989). Interphotoreceptor retinoid-binding protein: role in delivery of retinol to the pigment epithelium. *Experimental eye research*, *49*(4), 629–644. https://doi.org/10.1016/s0014-4835(89)80059-4
- Okajima, T. I., Pepperberg, D. R., Ripps, H., Wiggert, B., & Chader, G. J. (1990). Interphotoreceptor retinoid-binding protein promotes rhodopsin regeneration in toad photoreceptors. *Proceedings of the National Academy of Sciences of the United States of America*, *87*(17), 6907–6911. https://doi.org/10.1073/pnas.87.17.6907
- Palczewska, G., Boguslawski, J., Stremplewski, P., Kornaszewski, L., Zhang, J., Dong, Z., Liang, X. X., Gratton, E., Vogel, A., Wojtkowski, M., & Palczewski, K. (2020). Noninvasive two-photon optical biopsy of retinal fluorophores. *Proceedings of the National Academy of Sciences of the United States of America*, *117*(36), 22532–22543. https://doi.org/10.1073/pnas.2007527117
- Palczewska, G., Stremplewski, P., Suh, S., Alexander, N., Salom, D., Dong, Z., Ruminski, D., Choi, E. H., Sears, A. E., Kern, T. S., Wojtkowski, M., & Palczewski, K. (2018). Two-photon imaging of the mammalian retina with ultrafast pulsing laser. *JCI insight*, *3*(17), e121555. https://doi.org/10.1172/jci.insight.121555
- Palczewska, G., Wojtkowski, M., & Palczewski, K. (2023). From mouse to human: Accessing the biochemistry of vision in vivo by two-photon excitation. *Progress in retinal and eye research*, *93*, 101170. https://doi.org/10.1016/j.preteyeres.2023.101170
- Palczewski, K., & Kiser, P. D. (2020). Shedding new light on the generation of the visual chromophore. *Proceedings of the National Academy of Sciences of the United States of America*, *117*(33), 19629–19638. https://doi.org/10.1073/pnas.2008211117
- Palczewski, K., Kumasaka, T., Hori, T., Behnke, C. A., Motoshima, H., Fox, B. A., Le Trong, I., Teller, D. C., Okada, T., Stenkamp, R. E., Yamamoto, M., & Miyano, M. (2000). Crystal structure of rhodopsin: A G protein-coupled receptor. *Science (New York, N.Y.)*, *289*(5480), 739–745. https://doi.org/10.1126/science.289.5480.739
- Palczewski, K., Van Hooser, J. P., Garwin, G. G., Chen, J., Liou, G. I., & Saari, J. C. (1999). Kinetics of visual pigment regeneration in excised mouse eyes and in mice with a targeted disruption of the gene encoding interphotoreceptor retinoid-binding protein or arrestin. *Biochemistry*, *38*(37), 12012–12019. https://doi.org/10.1021/bi990504d
- Pandiyan, V. P., Nguyen, P. T., Pugh, E. N., Jr, & Sabesan, R. (2022). Human cone elongation responses can be explained by photoactivated cone opsin and membrane swelling and osmotic response to phosphate produced by RGS9-catalyzed GTPase. *Proceedings of the National*

Academy of Sciences of the United States of America, *119*(39), e2202485119. https://doi.org/10.1073/pnas.2202485119

- Parker, R., Wang, J. S., Kefalov, V. J., & Crouch, R. K. (2011). Interphotoreceptor retinoid-binding protein as the physiologically relevant carrier of 11-cis-retinol in the cone visual cycle. *The Journal of neuroscience : the official journal of the Society for Neuroscience*, *31*(12), 4714–4719. https://doi.org/10.1523/JNEUROSCI.3722-10.2011
- Parker, R. O., & Crouch, R. K. (2010). Retinol dehydrogenases (RDHs) in the visual cycle. *Experimental eye research*, *91*(6), 788–792. https://doi.org/10.1016/j.exer.2010.08.013
- Parker, R. O., Fan, J., Nickerson, J. M., Liou, G. I., & Crouch, R. K. (2009). Normal cone function requires the interphotoreceptor retinoid binding protein. *The Journal of neuroscience : the official journal of the Society for Neuroscience*, *29*(14), 4616–4621. https://doi.org/10.1523/JNEUROSCI.0063-09.2009
- Peng, Q., Li, J., Jiang, H., Cheng, X., Lu, Q., Zhou, S., Zhang, Y., Lv, S., Wan, S., Yang, T., Chen, Y., Zhang, W., Nan, W., Che, T., Li, Y., Liao, H & Zhang, J. (2024). Cryo-EM structures of human cone visual pigments. *bioRxiv*. DOI: 10.1101/2024.01.30.577689
- Pettersen, E. F., Goddard, T. D., Huang, C. C., Couch, G. S., Greenblatt, D. M., Meng, E. C., & Ferrin, T. E. (2004). UCSF Chimera--a visualization system for exploratory research and analysis. *Journal of computational chemistry*, *25*(13), 1605–1612. https://doi.org/10.1002/jcc.20084
- Phillips, T. S., Tsin, A. T., Reiter, R. J., & Malsbury, D. W. (1989). Retinoids in the bovine pineal gland. *Brain research bulletin*, *22*(2), 259–261. https://doi.org/10.1016/0361-9230(89)90051-8
- Pöge, M., Mahamid, J., Imanishi, S. S., Plitzko, J. M., Palczewski, K., & Baumeister, W. (2021). Determinants shaping the nanoscale architecture of the mouse rod outer segment. *eLife*, *10*, e72817. https://doi.org/10.7554/eLife.72817
- Politi, L. E., Lee, L., Wiggert, B., Chader, G., & Adler, R. (1989). Synthesis and secretion of interphotoreceptor retinoid-binding protein (IRBP) by isolated normal and rd mouse retinal photoreceptor neurons in culture. *Journal of cellular physiology*, *141*(3), 682–690. https://doi.org/10.1002/jcp.1041410329
- Porrello, K., Bhat, S. P., & Bok, D. (1991). Detection of interphotoreceptor retinoid binding protein (IRBP) mRNA in human and cone-dominant squirrel retinas by in situ hybridization. *The journal of histochemistry and cytochemistry : official journal of the Histochemistry Society*, *39*(2), 171–176. https://doi.org/10.1177/39.2.1987260

- Powell, H. R., Islam, S. A., David, A., & Sternberg, M. J. E. (2025). Phyre2.2: A Community Resource for Template-based Protein Structure Prediction. *Journal of molecular biology*, *437*(15), 168960. https://doi.org/10.1016/j.jmb.2025.168960
- Pugh, E. N., Jr, & Lamb, T. D. (1993). Amplification and kinetics of the activation steps in phototransduction. *Biochimica et biophysica acta*, *1141*(2-3), 111–149. https://doi.org/10.1016/0005-2728(93)90038-h
- Pugh E. N., Jr (2015). Photoreceptor disc morphogenesis: The classical evagination model prevails. *The Journal of cell biology*, *211*(3), 491–493. https://doi.org/10.1083/jcb.201510067
- Punjani, A., Rubinstein, J. L., Fleet, D. J., & Brubaker, M. A. (2017). cryoSPARC: algorithms for rapid unsupervised cryo-EM structure determination. *Nature methods*, *14*(3), 290–296. https://doi.org/10.1038/nmeth.4169
- Purves D, Augustine GJ, Fitzpatrick D, et al., editors. Neuroscience. 2nd edition. Sunderland (MA): Sinauer Associates; 2001. Anatomical Distribution of Rods and Cones. Available from: https://www.ncbi.nlm.nih.gov/books/NBK10848/
- Qtaishat, N. M., Wiggert, B., & Pepperberg, D. R. (2005). Interphotoreceptor retinoid-binding protein (IRBP) promotes the release of all-trans retinol from the isolated retina following rhodopsin bleaching illumination. *Experimental eye research*, *81*(4), 455–463. https://doi.org/10.1016/j.exer.2005.03.005
- Rajendran, R. R., Van Niel, E. E., Stenkamp, D. L., Cunningham, L. L., Raymond, P. A., & Gonzalez-Fernandez, F. (1996). Zebrafish interphotoreceptor retinoid-binding protein: differential circadian expression among cone subtypes. *The Journal of experimental biology*, *199*(Pt 12), 2775–2787. https://doi.org/10.1242/jeb.199.12.2775
- Reichenbach, A., & Bringmann, A. (2013). New functions of Müller cells. *Glia*, *61*(5), 651–678. https://doi.org/10.1002/glia.22477
- Remington, L,A., (2012) Chapter 4 - Retina,Editor(s): Lee Ann Remington, Clinical Anatomy and Physiology of the Visual System (Third Edition),Butterworth-Heinemann, 2012,Pages 61-92,ISBN 9781437719260, https://doi.org/10.1016/B978-1-4377-1926-0.10004-9. (https://www.sciencedirect.com/science/article/pii/B9781437719260100049)
- Rengarajan, K., Pohl, J., & Nickerson, J. (2001). Photoaffinity labeling of human IRBP with all-trans-retinoic acid. *Biochemical and biophysical research communications*, *284*(2), 268–274. https://doi.org/10.1006/bbrc.2001.4960
- Ripps, H., Peachey, N. S., Xu, X., Nozell, S. E., Smith, S. B., & Liou, G. I. (2000). The rhodopsin cycle is preserved in IRBP "knockout" mice despite abnormalities in retinal

structure and function. *Visual neuroscience*, *17*(1), 97–105. https://doi.org/10.1017/s095252380017110x

- Rizzolo, L. J., Peng, S., Luo, Y., & Xiao, W. (2011). Integration of tight junctions and claudins with the barrier functions of the retinal pigment epithelium. *Progress in retinal and eye research*, *30*(5), 296–323. https://doi.org/10.1016/j.preteyeres.2011.06.002
- Rodrigues, M. M., Hackett, J., Gaskins, R., Wiggert, B., Lee, L., Redmond, M., & Chader, G. J. (1986). Interphotoreceptor retinoid-binding protein in retinal rod cells and pineal gland. *Investigative ophthalmology & visual science*, *27*(5), 844–850.
- Röhlich P. (1975). The sensory cilium of retinal rods is analogous to the transitional zone of motile cilia. *Cell and tissue research*, *161*(3), 421–430. https://doi.org/10.1007/BF00220009
- Rohou, A., & Grigorieff, N. (2015). CTFFIND4: Fast and accurate defocus estimation from electron micrographs. *Journal of structural biology*, *192*(2), 216–221. https://doi.org/10.1016/j.jsb.2015.08.008
- Ross MH, Pawlina W, (2016). *Histology: a text and atlas with correlated cell and molecular biology*. Lippincott Williams & Wilkins. https://pa-core.lwwhealthlibrary.com/book.aspx?bookid=1316&sectionid=0
- Rousseau, F., Serrano, L., & Schymkowitz, J. W. (2006). How evolutionary pressure against protein aggregation shaped chaperone specificity. *Journal of molecular biology*, *355*(5), 1037–1047. https://doi.org/10.1016/j.jmb.2005.11.035
- Ruan, X., Liu, Z., Luo, L., & Liu, Y. (2020). The Structure of the Lens and Its Associations with the Visual Quality. *BMJ open ophthalmology*, *5*(1), e000459. https://doi.org/10.1136/bmjophth-2020-000459
- Rychlik W. (2007). OLIGO 7 primer analysis software. *Methods in molecular biology (Clifton, N.J.)*, *402*, 35–60. https://doi.org/10.1007/978-1-59745-528-2_2
- Saari, J. C., & Crabb, J. W. (2005). Focus on molecules: cellular retinaldehyde-binding protein (CRALBP). *Experimental eye research*, *81*(3), 245–246. https://doi.org/10.1016/j.exer.2005.06.015
- Saari, J. C., Teller, D. C., Crabb, J. W., & Bredberg, L. (1985). Properties of an interphotoreceptor retinoid-binding protein from bovine retina. *The Journal of biological chemistry*, *260*(1), 195–201.
- Sagoo, M. S., & Lagnado, L. (1997). G-protein deactivation is rate-limiting for shut-off of the phototransduction cascade. *Nature*, *389*(6649), 392–395. https://doi.org/10.1038/38750

- Salom, D., Padayatti, P. S., & Palczewski, K. (2013). Crystallization of G protein-coupled receptors. *Methods in cell biology*, *117*, 451–468. https://doi.org/10.1016/B978-0-12-408143-7.00024-4
- Santos, D., Foglia, L., Kiser, P. D., & Yu, A. (2025). The molecular mechanisms of visual chromophore release from cellular retinaldehyde-binding protein. *Structure (London, England : 1993)*, *33*(8), 1436–1445.e2. https://doi.org/10.1016/j.str.2025.04.018
- Sato, K., Li, S., Gordon, W. C., He, J., Liou, G. I., Hill, J. M., Travis, G. H., Bazan, N. G., & Jin, M. (2013). Receptor interacting protein kinase-mediated necrosis contributes to cone and rod photoreceptor degeneration in the retina lacking interphotoreceptor retinoid-binding protein. *The Journal of neuroscience : the official journal of the Society for Neuroscience*, *33*(44), 17458–17468. https://doi.org/10.1523/JNEUROSCI.1380-13.2013
- Sato, S., & Kefalov, V. J. (2024). The Retina-Based Visual Cycle. *Annual review of vision science*, *10*(1), 293–321. https://doi.org/10.1146/annurev-vision-100820-083937
- Schäfer, F., Seip, N., Maertens, B., Block, H., & Kubicek, J. (2015). Purification of GST-Tagged Proteins. *Methods in enzymology*, *559*, 127–139. https://doi.org/10.1016/bs.mie.2014.11.005
- Schneider, B. G., Papermaster, D. S., Liou, G. I., Fong, S. L., & Bridges, C. D. (1986). Electron microscopic immunocytochemistry of interstitial retinol-binding protein in vertebrate retinas. *Investigative ophthalmology & visual science*, *27*(5), 679–688.
- Sears, A. E., Albiez, S., Gulati, S., Wang, B., Kiser, P., Kovacik, L., Engel, A., Stahlberg, H., & Palczewski, K. (2020). Single particle cryo-EM of the complex between interphotoreceptor retinoid-binding protein and a monoclonal antibody. *FASEB journal : official publication of the Federation of American Societies for Experimental Biology*, *34*(10), 13918–13934. https://doi.org/10.1096/fj.202000796RR
- Semenova, E. M., & Converse, C. A. (2003). Comparison between oleic acid and docosahexaenoic acid binding to interphotoreceptor retinoid-binding protein. *Vision research*, *43*(28), 3063–3067. https://doi.org/10.1016/j.visres.2003.09.008
- Shaw, N. S., & Noy, N. (2001). Interphotoreceptor retinoid-binding protein contains three retinoid binding sites. *Experimental eye research*, *72*(2), 183–190. https://doi.org/10.1006/exer.2000.0945
- Shim, H., Chen, CK. (2012). G Protein Alpha Transducin. In: Choi, S. (eds) Encyclopedia of Signaling Molecules. Springer, New York, NY. https://doi.org/10.1007/978-1-4419-0461-4_587

- Singh, S., Srivastava, D., Boyd, K., & Artemyev, N. O. (2025). Structural and functional dynamics of human cone cGMP-phosphodiesterase important for photopic vision. *Proceedings of the National Academy of Sciences of the United States of America*, *122*(1), e2419732121. https://doi.org/10.1073/pnas.2419732121
- Sokke Rudraiah, P., Herbsleb, L., Salakova, M., Gröger, H., Steyer, A. M., Alves, F., Feldmann, C., & Walter, A. (2025). Combining Correlative Cryogenic Fluorescence and Electron Microscopy and Correlative Cryogenic Super-Resolution Fluorescence and X-Ray Tomography-Novel Complementary 3D Cryo-Microscopy Across Scales to Reveal Nanoparticle Internalization Into Cancer Cells. *Microscopy research and technique*, 10.1002/jemt.70071. Advance online publication. https://doi.org/10.1002/jemt.70071
- Solovei, I., Kreysing, M., Lanctôt, C., Kösem, S., Peichl, L., Cremer, T., Guck, J., & Joffe, B. (2009). Nuclear architecture of rod photoreceptor cells adapts to vision in mammalian evolution. *Cell*, *137*(2), 356–368. https://doi.org/10.1016/j.cell.2009.01.052
- Sparrow, J. R., Gregory-Roberts, E., Yamamoto, K., Blonska, A., Ghosh, S. K., Ueda, K., & Zhou, J. (2012). The bisretinoids of retinal pigment epithelium. *Progress in retinal and eye research*, *31*(2), 121–135. https://doi.org/10.1016/j.preteyeres.2011.12.001
- Sparrow, J. R., Wu, Y., Kim, C. Y., & Zhou, J. (2010). Phospholipid meets all-trans-retinal: the making of RPE bisretinoids. *Journal of lipid research*, *51*(2), 247–261. https://doi.org/10.1194/jlr.R000687
- Spencer, M., Detwiler, P. B., & Bunt-Milam, A. H. (1988). Distribution of membrane proteins in mechanically dissociated retinal rods. *Investigative ophthalmology & visual science*, *29*(7), 1012–1020.
- Standring S, (Ed.). (2020). *Gray's anatomy: The anatomical basis of clinical practice* (42ª ed.). Amsterdam: Elsevier.
- Steinhoff, J. S., Lass, A., & Schupp, M. (2021). Biological Functions of RBP4 and Its Relevance for Human Diseases. *Frontiers in physiology*, *12*, 659977. https://doi.org/10.3389/fphys.2021.659977
- Stenkamp, D. L., Calderwood, J. L., Van Niel, E. E., Daniels, L. M., & Gonzalez-Fernandez, F. (2005). The interphotoreceptor retinoid-binding protein (IRBP) of the chicken (Gallus gallus domesticus). *Molecular vision*, *11*, 833–845.
- Strauss O. (2005). The retinal pigment epithelium in visual function. *Physiological reviews*, *85*(3), 845–881. https://doi.org/10.1152/physrev.00021.2004

- Strauss O. (2014). Transport mechanisms of the retinal pigment epithelium to maintain of visual function. *Heat Mass Transfer* **50**, 303–313 (2014). https://doi.org/10.1007/s00231-013-1267-z
- Ţălu, Ş., & Nicoara, S. D. (2021). Malfunction of outer retinal barrier and choroid in the occurrence and progression of diabetic macular edema. *World journal of diabetes*, *12*(4), 437–452. https://doi.org/10.4239/wjd.v12.i4.437
- Taniguchi, T., Adler, A. J., Mizuochi, T., Kochibe, N., & Kobata, A. (1986). The structures of the asparagine-linked sugar chains of bovine interphotoreceptor retinol-binding protein. Occurrence of fucosylated hybrid-type oligosaccharides. *The Journal of biological chemistry*, *261*(4), 1730–1736.
- Taylor, A. W., Hsu, S., & Ng, T. F. (2021). The Role of Retinal Pigment Epithelial Cells in Regulation of Macrophages/Microglial Cells in Retinal Immunobiology. *Frontiers in immunology*, *12*, 724601. https://doi.org/10.3389/fimmu.2021.724601
- *The PyMOL Molecular Graphics System,* Version 3,0 Schrödinger, LLC.
- Tomczewski, S., Curatolo, A., Foik, A., Węgrzyn, P., Bałamut, B., Wielgo, M., Kulesza, W., Galińska, A., Kordecka, K., Gulati, S., Fernandes, H., Palczewski, K., & Wojtkowski, M. (2025). Photopic flicker optoretinography captures the light-driven length modulation of photoreceptors during phototransduction. *Proceedings of the National Academy of Sciences of the United States of America*, *122*(7), e2421722122. https://doi.org/10.1073/pnas.2421722122
- Trott, O., & Olson, A. J. (2010). AutoDock Vina: improving the speed and accuracy of docking with a new scoring function, efficient optimization, and multithreading. *Journal of computational chemistry*, *31*(2), 455–461. https://doi.org/10.1002/jcc.21334
- Tschanz, C. L., & Noy, N. (1997). Binding of retinol in both retinoid-binding sites of interphotoreceptor retinoid-binding protein (IRBP) is stabilized mainly by hydrophobic interactions. *The Journal of biological chemistry*, *272*(48), 30201–30207. https://doi.org/10.1074/jbc.272.48.30201
- Uehara, F., Matthes, M. T., Yasumura, D., & LaVail, M. M. (1990). Light-evoked changes in the interphotoreceptor matrix. *Science (New York, N.Y.)*, *248*(4963), 1633–1636. https://doi.org/10.1126/science.2194288
- Uhl A, Busch C, Marcel S, Veldhuis R. (2020). Handbook of Vascular Biometrics. 10.1007/978-3-030-27731-4.
- van Veen, T., Ekstrom, P., Wiggert, B., Lee, L., Hirose, Y., Sanyal, S., & Chader, G. J. (1988). A developmental study of interphotoreceptor retinoid-binding protein (IRBP) in single and

double homozygous rd and rds mutant mouse retinae. *Experimental eye research*, *47*(2), 291–305. https://doi.org/10.1016/0014-4835(88)90012-7

- van Wyk, M., Wässle, H., & Taylor, W. R. (2009). Receptive field properties of ON- and OFF-ganglion cells in the mouse retina. *Visual neuroscience*, *26*(3), 297–308. https://doi.org/10.1017/S0952523809990137
- Vishnivetskiy, S. A., Raman, D., Wei, J., Kennedy, M. J., Hurley, J. B., & Gurevich, V. V. (2007). Regulation of arrestin binding by rhodopsin phosphorylation level. *The Journal of biological chemistry*, *282*(44), 32075–32083. https://doi.org/10.1074/jbc.M706057200
- Wagenhorst, B. B., Rajendran, R. R., Van Niel, E. E., Hessler, R. B., Bukelman, A., & Gonzalez-Fernandez, F. (1995). Goldfish cones secrete a two-repeat interphotoreceptor retinoid-binding protein. *Journal of molecular evolution*, *41*(5), 646–656. https://doi.org/10.1007/BF00175823
- Waterhouse, A. M., Procter, J. B., Martin, D. M., Clamp, M., & Barton, G. J. (2009). Jalview Version 2--a multiple sequence alignment editor and analysis workbench. *Bioinformatics (Oxford, England)*, *25*(9), 1189–1191. https://doi.org/10.1093/bioinformatics/btp033
- Wensel, T. G., Zhang, Z., Anastassov, I. A., Gilliam, J. C., He, F., Schmid, M. F., & Robichaux, M. A. (2016). Structural and molecular bases of rod photoreceptor morphogenesis and disease. *Progress in retinal and eye research*, *55*, 32–51. https://doi.org/10.1016/j.preteyeres.2016.06.002
- Weston, A. E., Armer, H. E., & Collinson, L. M. (2009). Towards native-state imaging in biological context in the electron microscope. *Journal of chemical biology*, *3*(3), 101–112. https://doi.org/10.1007/s12154-009-0033-7
- Wiggert, B., Lal Kapoor, C., Lee, L., Somers, R. L., & Chader, G. J. (1988). Phosphorylation of interphotoreceptor retinoid-binding protein (IRBP). *Neurochemistry international*, *13*(1), 81–87. https://doi.org/10.1016/0197-0186(88)90106-4
- Wiggert, B., Lee, L., O'Brien, P. J., & Chader, G. J. (1984). Synthesis of interphotoreceptor retinoid-binding protein (IRBP) by monkey retina in organ culture: effect of monensin. *Biochemical and biophysical research communications*, *118*(3), 789–796. https://doi.org/10.1016/0006-291x(84)91464-5
- Wiggert, B., Lee, L., Rodrigues, M., Hess, H., Redmond, T. M., & Chader, G. J. (1986). Immunochemical distribution of interphotoreceptor retinoid-binding protein in selected species. *Investigative ophthalmology & visual science*, *27*(7), 1041–1049.

- Wilden U. (1995). Duration and amplitude of the light-induced cGMP hydrolysis in vertebrate photoreceptors are regulated by multiple phosphorylation of rhodopsin and by arrestin binding. *Biochemistry*, *34*(4), 1446–1454. https://doi.org/10.1021/bi00004a040
- Williams, C. J., Headd, J. J., Moriarty, N. W., Prisant, M. G., Videau, L. L., Deis, L. N., Verma, V., Keedy, D. A., Hintze, B. J., Chen, V. B., Jain, S., Lewis, S. M., Arendall, W. B., 3rd, Snoeyink, J., Adams, P. D., Lovell, S. C., Richardson, J. S., & Richardson, D. C. (2018). MolProbity: More and better reference data for improved all-atom structure validation. *Protein science : a publication of the Protein Society*, *27*(1), 293–315. https://doi.org/10.1002/pro.3330
- WILLMER E. N. (1949). Colour vision in the central fovea. *Documenta ophthalmologica. Advances in ophthalmology*, *3*, 194–213. https://doi.org/10.1007/BF00162603
- Wirth, A., Cavallacci, G., & Genovesi-Ebert, F. (1984). The advantages of an inverted retina. A physiological approach to a teleological question. *Developments in ophthalmology*, *9*, 20–28. https://doi.org/10.1159/000409800
- Wisard, J., Faulkner, A., Chrenek, M. A., Waxweiler, T., Waxweiler, W., Donmoyer, C., Liou, G. I., Craft, C. M., Schmid, G. F., Boatright, J. H., Pardue, M. T., & Nickerson, J. M. (2011). Exaggerated eye growth in IRBP-deficient mice in early development. *Investigative ophthalmology & visual science*, *52*(8), 5804–5811. https://doi.org/10.1167/iovs.10-7129
- Wolf G. (1998). Transport of retinoids by the interphotoreceptor retinoid-binding protein. *Nutrition reviews*, *56*(5 Pt 1), 156–158. https://doi.org/10.1111/j.1753-4887.1998.tb01743.x
- Wu, Q., Blakeley, L. R., Cornwall, M. C., Crouch, R. K., Wiggert, B. N., & Koutalos, Y. (2007). Interphotoreceptor retinoid-binding protein is the physiologically relevant carrier that removes retinol from rod photoreceptor outer segments. *Biochemistry*, *46*(29), 8669–8679. https://doi.org/10.1021/bi7004619
- Xie, T., Zhang, Z., Fang, Q., Du, B., & Gong, X. (2021). Structural basis of substrate recognition and translocation by human ABCA4. *Nature communications*, *12*(1), 3853. https://doi.org/10.1038/s41467-021-24194-6
- Xu, J., Dodd, R. L., Makino, C. L., Simon, M. I., Baylor, D. A., & Chen, J. (1997). Prolonged photoresponses in transgenic mouse rods lacking arrestin. *Nature*, *389*(6650), 505–509. https://doi.org/10.1038/39068
- Xu, J., Zhao, C., & Kang, Y. (2024). The Formation and Renewal of Photoreceptor Outer Segments. *Cells*, *13*(16), 1357. https://doi.org/10.3390/cells13161357

- Yadav, A. S., Rubinow, K. B., Zelter, A., Authement, A. K., Kestenbaum, B. R., Amory, J. K., & Isoherranen, N. (2025). Development and Validation of a Novel LC-MS/MS Based Proteomics Method for Quantitation of Retinol Binding Protein 4 (RBP4) and Transthyretin (TTR). *bioRxiv : the preprint server for biology*, 2025.02.27.640583. https://doi.org/10.1101/2025.02.27.640583
- Yokomizo, H., Maeda, Y., Park, K., Clermont, A. C., Hernandez, S. L., Fickweiler, W., Li, Q., Wang, C. H., Paniagua, S. M., Simao, F., Ishikado, A., Sun, B., Wu, I. H., Katagiri, S., Pober, D. M., Tinsley, L. J., Avery, R. L., Feener, E. P., Kern, T. S., Keenan, H. A., … King, G. L. (2019). Retinol binding protein 3 is increased in the retina of patients with diabetes resistant to diabetic retinopathy. *Science translational medicine*, *11*(499), eaau6627. https://doi.org/10.1126/scitranslmed.aau6627
- Yordi, S., Cakir, Y., Kalra, G., Cetin, H., Hu, M., Abraham, J., Reese, J., Srivastava, S. K., & Ehlers, J. P. (2024). Ellipsoid Zone Integrity and Visual Function in Dry Age-Related Macular Degeneration. *Journal of personalized medicine*, *14*(5), 543. https://doi.org/10.3390/jpm14050543
- Young, L. N., & Villa, E. (2023). Bringing Structure to Cell Biology with Cryo-Electron Tomography. *Annual review of biophysics*, *52*, 573–595. https://doi.org/10.1146/annurev-biophys-111622-091327
- Zang, J., & Neuhauss, S. C. F. (2021). Biochemistry and physiology of zebrafish photoreceptors. *Pflugers Archiv : European journal of physiology*, *473*(9), 1569–1585. https://doi.org/10.1007/s00424-021-02528-z
- Zeng, S., Zhang, T., Madigan, M. C., Fernando, N., Aggio-Bruce, R., Zhou, F., Pierce, M., Chen, Y., Huang, L., Natoli, R., Gillies, M. C., & Zhu, L. (2020). Interphotoreceptor Retinoid-Binding Protein (IRBP) in Retinal Health and Disease. *Frontiers in cellular neuroscience*, *14*, 577935. https://doi.org/10.3389/fncel.2020.577935
- Zhou, X. E., Melcher, K., & Xu, H. E. (2012). Structure and activation of rhodopsin. *Acta pharmacologica Sinica*, *33*(3), 291–299. https://doi.org/10.1038/aps.2011.171

7 Appendix 1

Primers were designed using the following softwares: Oligo 7 primer analysis software (Rychlik, 2007), ExPASY (Gasteiger et al., 2003).

For the cloning of the various constructs, the following codon optimized synthetic gene was used as a template:

>23_bRBP3_PreScission_pET-15b

Underlined the sequence coding for *Bos Taurus* RBP3

TTCTTGAAGACGAAAGGGCCTCGTGATACGCCTATTTTTATAGGTTAATGTCATGATAATAATGGTTTCTTAGACGTCAG
GTGGCACTTTTCGGGGAAATGTGCGCGGAACCCCTATTTGTTTATTTTTCTAAATACATTCAAATATGTATCCGCTCATG
AGACAATAACCCTGATAAATGCTTCAATAATATTGAAAAAGGAAGAGTATGAGTATTCAACATTTCCGTGTCGCCCTTAT
TCCCTTTTTTGCGGCATTTTGCCTTCCTGTTTTTGCTCACCCAGAAACGCTGGTGAAAGTAAAAGATGCTGAAGATCAGT
TGGGTGCACGAGTGGGTTACATCGAACTGGATCTCAACAGCGGTAAGATCCTTGAGAGTTTTCGCCCCGAAGAACGTTTT
CCAATGATGAGCACTTTTAAAGTTCTGCTATGTGGCGCGGTATTATCCCGTGTTGACGCCGGGCAAGAGCAACTCGGTCG
CCGCATACACTATTCTCAGAATGACTTGGTTGAGTACTCACCAGTCACAGAAAAGCATCTTACGGATGGCATGACAGTAA
GAGAATTATGCAGTGCTGCCATAACCATGAGTGATAACACTGCGGCCAACTTACTTCTGACAACGATCGGAGGACCGAAG
GAGCTAACCGCTTTTTTGCACAACATGGGGGATCATGTAACTCGCCTTGATCGTTGGGAACCGGAGCTGAATGAAGCCAT
ACCAAACGACGAGCGTGACACCACGATGCCTGCAGCAATGGCAACAACGTTGCGCAAACTATTAACTGGCGAACTACTTA
CTCTAGCTTCCCGGCAACAATTAATAGACTGGATGGAGGCGGATAAAGTTGCAGGACCACTTCTGCGCTCGGCCCTTCCG
GCTGGCTGGTTTATTGCTGATAAATCTGGAGCCGGTGAGCGTGGGTCTCGCGGTATCATTGCAGCACTGGGGCCAGATGG
TAAGCCCTCCCGTATCGTAGTTATCTACACGACGGGGAGTCAGGCAACTATGGATGAACGAAATAGACAGATCGCTGAGA
TAGGTGCCTCACTGATTAAGCATTGGTAACTGTCAGACCAAGTTTACTCATATATACTTTAGATTGATTTAAAACTTCAT
TTTTAATTTAAAAGGATCTAGGTGAAGATCCTTTTTGATAATCTCATGACCAAAATCCCTTAACGTGAGTTTTCGTTCCA
CTGAGCGTCAGACCCCGTAGAAAAGATCAAAGGATCTTCTTGAGATCCTTTTTTTCTGCGCGTAATCTGCTGCTTGCAAA
CAAAAAAACCACCGCTACCAGCGGTGGTTTGTTTGCCGGATCAAGAGCTACCAACTCTTTTTCCGAAGGTAACTGGCTTC
AGCAGAGCGCAGATACCAAATACTGTCCTTCTAGTGTAGCCGTAGTTAGGCCACCACTTCAAGAACTCTGTAGCACCGCC
TACATACCTCGCTCTGCTAATCCTGTTACCAGTGGCTGCTGCCAGTGGCGATAAGTCGTGTCTTACCGGGTTGGACTCAA
GACGATAGTTACCGGATAAGGCGCAGCGGTCGGGCTGAACGGGGGGTTCGTGCACACAGCCCAGCTTGGAGCGAACGACC
TACACCGAACTGAGATACCTACAGCGTGAGCTATGAGAAAGCGCCACGCTTCCCGAAGGGAGAAAGGCGGACAGGTATCC
GGTAAGCGGCAGGGTCGGAACAGGAGAGCGCACGAGGGAGCTTCCAGGGGGAAACGCCTGGTATCTTTATAGTCCTGTCG
GGTTTCGCCACCTCTGACTTGAGCGTCGATTTTTGTGATGCTCGTCAGGGGGGCGGAGCCTATGGAAAAACGCCAGCAAC
GCGGCCTTTTTACGGTTCCTGGCCTTTTGCTGGCCTTTTGCTCACATGTTCTTTCCTGCGTTATCCCCTGATTCTGTGGA
TAACCGTATTACCGCCTTTGAGTGAGCTGATACCGCTCGCCGCAGCCGAACGACCGAGCGCAGCGAGTCAGTGAGCGAGG
AAGCGGAAGAGCGCCTGATGCGGTATTTTCTCCTTACGCATCTGTGCGGTATTTCACACCGCATATATGGTGCACTCTCA
GTACAATCTGCTCTGATGCCGCATAGTTAAGCCAGTATACACTCCGCTATCGCTACGTGACTGGGTCATGGCTGCGCCCC
GACACCCGCCAACACCCGCTGACGCGCCCTGACGGGCTTGTCTGCTCCCGGCATCCGCTTACAGACAAGCTGTGACCGTC
TCCGGGAGCTGCATGTGTCAGAGGTTTTCACCGTCATCACCGAAACGCGCGAGGCAGCTGCGGTAAAGCTCATCAGCGTG
GTCGTGAAGCGATTCACAGATGTCTGCCTGTTCATCCGCGTCCAGCTCGTTGAGTTTCTCCAGAAGCGTTAATGTCTGGC
TTCTGATAAAGCGGGCCATGTTAAGGGCGGTTTTTTCCTGTTTGGTCACTGATGCCTCCGTGTAAGGGGGATTTCTGTTC
ATGGGGGTAATGATACCGATGAAACGAGAGAGGATGCTCACGATACGGGTTACTGATGATGAACATGCCCGGTTACTGGA
ACGTTGTGAGGGTAAACAACTGGCGGTATGGATGCGGCGGGACCAGAGAAAAATCACTCAGGGTCAATGCCAGCGCTTCG
TTAATACAGATGTAGGTGTTCCACAGGGTAGCCAGCAGCATCCTGCGATGCAGATCCGGAACATAATGGTGCAGGGCGCT
GACTTCCGCGTTTCCAGACTTTACGAAACACGGAAACCGAAGACCATTCATGTTGTTGCTCAGGTCGCAGACGTTTTGCA
GCAGCAGTCGCTTCACGTTCGCTCGCGTATCGGTGATTCATTCTGCTAACCAGTAAGGCAACCCCGCCAGCCTAGCCGGG
TCCTCAACGACAGGAGCACGATCATGCGCACCCGTGGCCAGGACCCAACGCTGCCCGAGATGCGCCGCGTGCGGCTGCTG
GAGATGGCGGACGCGATGGATATGTTCTGCCAAGGGTTGGTTTGCGCATTCACAGTTCTCCGCAAGAATTGATTGGCTCC
AATTCTTGGAGTGGTGAATCCGTTAGCGAGGTGCCGCCGGCTTCCATTCAGGTCGAGGTGGCCCGGCTCCATGCACCGCG
ACGCAACGCGGGGAGGCAGACAAGGTATAGGGCGGCGCCTACAATCCATGCCAACCCGTTCCATGTGCTCGCCGAGGCGG
CATAAATCGCCGTGACGATCAGCGGTCCAGTGATCGAAGTTAGGCTGGTAAGAGCCGCGAGCGATCCTTGAAGCTGTCCC
TGATGGTCGTCATCTACCTGCCTGGACAGCATGGCCTGCAACGCGGGCATCCCGATGCCGCCGGAAGCGAGAAGAATCAT
AATGGGGAAGGCCATCCAGCCTCGCGTCGCGAACGCCAGCAAGACGTAGCCCAGCGCGTCGGCCGCCATGCCGGCGATAA
TGGCCTGCTTCTCGCCGAAACGTTTGGTGGCGGGACCAGTGACGAAGGCTTGAGCGAGGGCGTGCAAGATTCCGAATACC

GCAAGCGACAGGCCGATCATCGTCGCGCTCCAGCGAAAGCGGTCCTCGCCGAAAATGACCCAGAGCGCTGCCGGCACCTG
TCCTACGAGTTGCATGATAAAGAAGACAGTCATAAGTGCGGCGACGATAGTCATGCCCCGCGCCCACCGGAAGGAGCTGA
CTGGGTTGAAGGCTCTCAAGGGCATCGGTCGAGATCCCGGTGCCTAATGAGTGAGCTAACTTACATTAATTGCGTTGCGC
TCACTGCCCGCTTTCCAGTCGGGAAACCTGTCGTGCCAGCTGCATTAATGAATCGGCCAACGCGCGGGGAGAGGCGGTTT
GCGTATTGGGCGCCAGGGTGGTTTTTCTTTTCACCAGTGAGACGGGCAACAGCTGATTGCCCTTCACCGCCTGGCCCTGA
GAGAGTTGCAGCAAGCGGTCCACGCTGGTTTGCCCCAGCAGGCGAAAATCCTGTTTGATGGTGGTTAACGGCGGGATATA
ACATGAGCTGTCTTCGGTATCGTCGTATCCCACTACCGAGATATCCGCACCAACGCGCAGCCCGGACTCGGTAATGGCGC
GCATTGCGCCCAGCGCCATCTGATCGTTGGCAACCAGCATCGCAGTGGGAACGATGCCCTCATTCAGCATTTGCATGGTT
TGTTGAAAACCGGACATGGCACTCCAGTCGCCTTCCCGTTCCGCTATCGGCTGAATTTGATTGCGAGTGAGATATTTATG
CCAGCCAGCCAGACGCAGACGCGCCGAGACAGAACTTAATGGGCCCGCTAACAGCGCGATTTGCTGGTGACCCAATGCGA
CCAGATGCTCCACGCCCAGTCGCGTACCGTCTTCATGGGAGAAAATAATACTGTTGATGGGTGTCTGGTCAGAGACATCA
AGAAATAACGCCGGAACATTAGTGCAGGCAGCTTCCACAGCAATGGCATCCTGGTCATCCAGCGGATAGTTAATGATCAG
CCCACTGACGCGTTGCGCGAGAAGATTGTGCACCGCCGCTTTACAGGCTTCGACGCCGCTTCGTTCTACCATCGACACCA
CCACGCTGGCACCCAGTTGATCGGCGCGAGATTTAATCGCCGCGACAATTTGCGACGGCGCGTGCAGGGCCAGACTGGAG
GTGGCAACGCCAATCAGCAACGACTGTTTGCCCGCCAGTTGTTGTGCCACGCGGTTGGGAATGTAATTCAGCTCCGCCAT
CGCCGCTTCCACTTTTTCCCGCGTTTTCGCAGAAACGTGGCTGGCCTGGTTCACCACGCGGGAAACGGTCTGATAAGAGA
CACCGGCATACTCTGCGACATCGTATAACGTTACTGGTTTCACATTCACCACCCTGAATTGACTCTCTTCCGGGCGCTAT
CATGCCATACCGCGAAAGGTTTTGCGCCATTCGATGGTGTCCGGGATCTCGACGCTCTCCCTTATGCGACTCCTGCATTA
GGAAGCAGCCCAGTAGTAGGTTGAGGCCGTTGAGCACCGCCGCCGCAAGGAATGGTGCATGCAAGGAGATGGCGCCCAAC
AGTCCCCCGGCCACGGGGCCTGCCACCATACCCACGCCGAAACAAGCGCTCATGAGCCCGAAGTGGCGAGCCCGATCTTC
CCCATCGGTGATGTCGGCGATATAGGCGCCAGCAACCGCACCTGTGGCGCCGGTGATGCCGGCCACGATGCGTCCGGCGT
AGAGGATCGAGATCTCGATCCCGCGAAATTAATACGACTCACTATAGGGGAATTGTGAGCGGATAACAATTCCCCTCTAG
AAATAATTTTGTTTAACTTTAAGAAGGAGATATACCATGGGCAGCAGCCATCATCATCATCATCACAGCAGCGGCCTGGT
GCCGCGCGGCAGC
ATGGTGCGTAAGTGGGCGCTGCTGCTGCCGATGCTGCTGTGCGGTCTGACCGGTCCGGCGCACCTGTTCCAACCGAGCCT
GGTGCTGGAAATGGCGCAGGTTCTGCTGGACAACTACTGCTTTCCGGAGAACCTGATGGGCATGCAGGGTGCGATCGAAC
AAGCGATTAAAAGCCAGGAGATCCTGAGCATTAGCGACCCGCAAACCCTGGCGCATGTGCTGACCGCGGGTGTTCAGAGC
AGCCTGAACGATCCGCGTCTGGTGATCAGCTACGAACCGAGCACCCTGGAGGCGCCGCCGCGTGCGCCGGCGGTTACCAA
CCTGACCCTGGAGGAAATCATTGCGGGTCTGCAAGACGGCCTGCGTCACGAAATCCTGGAGGGCAACGTGGGTTATCTGC
GTGTTGACGATATTCCGGGTCAGGAAGTGATGAGCAAGCTGCGTAGCTTCCTGGTTGCGAACGTGTGGCGTAAACTGGTG
AACACCAGCGCGCTGGTTCTGGATCTGCGTCATTGCACCGGTGGCCATGTGAGCGGCATCCCGTACGTTATTAGCTACCT
GCATCCGGGTAGCACCGTTAGCCACGTGGACACCGTTTACGATCGTCCGAGCAACACCACCACCGAGATCTGGACCCTGC
CGGAAGCGCTGGGCGAGAAGTATAGCGCGGACAAAGATGTGGTTGTGCTGACCAGCAGCCGTACCGGTGGCGTTGCGGAA
GACATCGCGTACATTCTGAAGCAGATGCGTCGTGCGATTGTTGTTGGTGAACGTACCGTGGGTGGCGCGCTGAACCTGCA
AAAACTGCGTGTTGGCCAGAGCGATTTCTTTCTGACCGTTCCGGTGAGCCGTAGCCTGGGTCCGCTGGGTGAAGGTAGCC
AAACCTGGGAGGGCAGCGGTGTGCTGCCGTGCGTTGGTACCCCGGCGGAACAGGCGCTGGAGAAGGCGCTGGCGGTGCTG
ATGCTGCGTCGTGCGCTGCCGGGTGTTATCCAGCGTCTGCAAGAAGCGCTGCGTGAGTACTATACCCTGGTGGACCGTGT
GCCGGCGCTGCTGAGCCACCTGGCGGCGATGGATCTGAGCAGCGTTGTGAGCGAAGACGATCTGGTTACCAAGCTGAACG
CGGGTCTGCAGGCTGTGAGCGAAGACCCGCGTCTGCAGGTTCAAGTTGTGCGTCCGAAAGAGGCGAGCAGCGGTCCGGAG
GAAGAGGCGGAAGAGCCGCCGGAAGCGGTTCCGGAAGTGCCGGAAGATGAGGCGGTGCGTCGTGCGCTGGTTGACAGCGT
TTTCCAAGTTAGCGTGCTGCCGGGCAACGTTGGTTACCTGCGTTTCGACAGCTTTGCGGATGCGAGCGTGCTGGAAGTGC
TGGGTCCGTATATCCTGCACCAAGTGTGGGAACCGCTGCAGGACACCGAGCACCTGATTATGGATCTGCGTCAAAATCCG
GGTGGTCCGAGCAGCGCGGTGCCGCTGCTGCTGAGCTATTTTCAAAGCCCGGATGCGAGCCCGGTTCGTCTGTTTAGCAC
CTATGATCGTCGTACCAACATCACCCGTGAACACTTCAGCCAAACCGAGCTGCTGGGTCGTCCGTACGGCACCCAGCGTG
GTGTTTATCTGCTGACCAGCCACCGTACCGCGACCGCGGCGGAAGAGCTGGCGTTTCTGATGCAGAGCCTGGGTTGGGCG
ACCCTGGTGGGCGAAATTACCGCGGGTAGCCTGCTGCACACCCACACCGTTAGCCTGCTGGAAACCCCGGAGGGTGGCCT
GGCGCTGACCGTTCCGGTGCTGACCTTCATCGATAACCACGGCGAGTGCTGGCTGGGTGGCGGTGTTGTGCCGGACGCGA
TTGTGCTGGCGGAAGAGGCGCTGGATCGTGCGCAGGAAGTGCTGGAGTTTCACCGTAGCCTGGGTGAACTGGTTGAGGGC
ACCGGTCGTCTGCTGGAAGCGCATTATGCGCGTCCGGAAGTGGTGGGTCAAATGGGTGCGCTGCTGCGTGCGAAGCTGGC
GCAGGGTGCGTATCGTACCGCGGTTGATCTGGAAAGCCTGGCGAGCCAACTGACCGCGGACCTGCAGGAGATGAGCGGCG
ATCACCGTCTGCTGGTGTTCCACTCTCCGGGTGAAATGGTTGCGGAGGAAGCGCCGCCGCCGCCGCCGGTTGTGCCGAGC
CCGGAAGAGCTGAGCTACCTGATCGAAGCGCTGTTCAAAACCGAGGTGCTGCCGGGCCAACTGGGTTATCTGCGTTTTGA
CGCGATGGCGGAACTGGAGACCGTGAAGGCGGTTGGTCCGCAGCTGGTGCAACTGGTTTGGCAGAAACTGGTGGACACCG
CGGCGCTGGTTGTGGATCTGCGTTACAATCCGGGTAGCTATAGCACCGCGGTTCCGCTGCTGTGCAGCTACTTCTTTGAA
GCGGAGCCGCGTCGTCACCTGTATAGCGTGTTCGATCGTGCGACCAGCCGTGTGACCGAGGTTTGGACCCTGCCGCACGT
TACCGGCCAGCGTTACGGTAGCCACAAAGACCTGTATGTTCTGGTTAGCCACACCAGCGGCAGCGCGGCGGAAGCGTTTG
CGCACACCATGCAGGATCTGCAACGTGCGACCATCATTGGTGAACCGACCGCGGGCGGTGCGCTGAGCGTGGGCATCTAC
CAAGTTGGTAGCAGCGCGCTGTATGCGAGCATGCCGACCCAAATGGCGATGAGCGCGAGCACCGGTGAAGCGTGGGACCT

GGCGGGTGTGGAGCCGGACATCACCGTTCCGATGAGCGTTGCGCTGAGCACCGCGCGTGACATTGTTACCCTGCGTGCGA
AGGTGCCGACCGTTCTGCAAACCGCGGGTAAACTGGTGGCGGATAACTACGCGAGCCCGGAACTGGGCGTTAAGATGGCG
GCGGAGCTGAGCGGTCTGCAGAGCCGTTATGCGCGTGTGACCAGCGAAGCGGCGCTGGCGGAGCTGCTGCAGGCGGACCT
GCAAGTTCTGAGCGGCGATCCGCACCTGAAGACCGCGCACATCCCGGAGGACGCGAAAGATCGTATTCCGGGTATTGTGC
CGATGCAAATCCCGAGCCCGGAAGTTTTCGAGGACCTGATTAAATTCAGCTTTCACACCAACGTGCTGGAAGGTAATGTG
GGTTACCTGCGTTTTGACATGTTTGGTGATTGCGAGCTGCTGACCCAAGTGAGCGAGCTGCTGGTTGAGCACGTTTGGAA
GAAAATCGTGCACACCGACGCGCTGATTGTTGATATGCGTTTTAACATCGGCGGTCCGACCAGCAGCATTAGCGCTTTAT
GCAGCTACTTCTTTGACGAAGGTCCGCCGATCCTGCTGGATAAGATTTATAACCGTCCGAACAACAGCGTGAGCGAGCTG
TGGACCCTGAGCCAGCTGGAAGGCGAGCGTTACGGTAGCAAGAAAAGCATGGTTATTCTGACCAGCACCCTGACCGCGGG
TGCGGCGGAAGAGTTCACCTATATCATGAAACGTCTGGGCCGTGCGCTGGTGATTGGTGAAGTTACCAGCGGCGGTTGCC
AGCCGCCGCAAACCTACCACGTTGACGATACCGACCTGTATCTGACCATTCCGACCGCGCGTAGCGTGGGTGCGGCGGAC
GGTAGCAGCTGGGAGGGCGTTGGTGTTGTTCCGGATGTGGCGGTGCCGGCGGAAGCGGCGCTGACCCGTGCGCAGGAGAT
GCTGCAACATACCCCGCTGCGTGCGCGTCGTAGCCCGCGTCTGCACGGCCGTCGTAAGGGTCACCACCGTCAAAGCCAAG
GTCGTGCGGGTAGCCTGGGTCGTAACCAAGGTGTTGTTCGTCCGGAAGTGCTGACCGAGGCGCCGAGCGGTCAAAAACGT
GGTCTGCTGCAGTGCGGC ttaGAAGTGCTGTTTCAGGGTCCGTAA
TAACTAGCATAACCCCTTGGGGCCTCTAAACGGGTCTTGAGGGGTTTTTTGCTGAAAGGAGGAACTATATCCGGATATCC
CGCAAGAGGCCCGGCAGTACCGGCATAACCAAGCCTATGCCTACAGCATCCAGGGTGACGGTGCCGAGGATGACGATGAG
CGCATTGTTAGATTTCATACACGGTGCCTGACTGCGTTAGCAATTTAACTGTGATAAACTACCGCATTAAAGCTTATCGA
TGATAAGCTGTCAAACATGAGAA

Protein sequence *Bos taurus* RBP3

>NP_776589.1 retinol-binding protein 3 precursor [Bos taurus]
MVRKWALLLPMLLCGLTGPAHLFQPSLVLEMAQVLLDNYCFPENLMGMQGAIEQAIKSQEILSISDPQTL
AHVLTAGVQSSLNDPRLVISYEPSTLEAPPRAPAVTNLTLEEIIAGLQDGLRHEILEGNVGYLRVDDIPG
QEVMSKLRSFLVANVWRKLVNTSALVLDLRHCTGGHVSGIPYVISYLHPGSTVSHVDTVYDRPSNTTTEI
WTLPEALGEKYSADKDVVVLTSSRTGGVAEDIAYILKQMRRAIVVGERTVGGALNLQKLRVGQSDFFLTV
PVSRSLGPLGEGSQTWEGSGVLPCVGTPAEQALEKALAVLMLRRALPGVIQRLQEALREYYTLVDRVPAL
LSHLAAMDLSSVVSEDDLVTKLNAGLQAVSEDPRLQVQVVRPKEASSGPEEEAEEPPEAVPEVPEDEAVR
RALVDSVFQVSVLPGNVGYLRFDSFADASVLEVLGPYILHQVWEPLQDTEHLIMDLRQNPGGPSSAVPLL
LSYFQSPDASPVRLFSTYDRRTNITREHFSQTELLGRPYGTQRGVYLLTSHRTATAAEELAFLMQSLGWA
TLVGEITAGSLLHTHTVSLLETPEGGLALTVPVLTFIDNHGECWLGGGVVPDAIVLAEEALDRAQEVLEF
HRSLGELVEGTGRLLEAHYARPEVVGQMGALLRAKLAQGAYRTAVDLESLASQLTADLQEMSGDHRLLVF
HSPGEMVAEEAPPPPPVVPSPEELSYLIEALFKTEVLPGQLGYLRFDAMAELETVKAVGPQLVQLVWQKL
VDTAALVVDLRYNPGSYSTAVPLLCSYFFEAEPRRHLYSVFDRATSRVTEVWTLPHVTGQRYGSHKDLYV
LVSHTSGSAAEAFAHTMQDLQRATIIGEPTAGGALSVGIYQVGSSALYASMPTQMAMSASTGEAWDLAGV
EPDITVPMSVALSTARDIVTLRAKVPTVLQTAGKLVADNYASPELGVKMAAELSGLQSRYARVTSEAALA
ELLQADLQVLSGDPHLKTAHIPEDAKDRIPGIVPMQIPSPEVFEDLIKFSFHTNVLEGNVGYLRFDMFGD
CELLTQVSELLVEHVWKKIVHTDALIVDMRFNIGGPTSSISALCSYFFDEGPPILLDKIYNRPNNSVSEL
WTLSQLEGERYGSKKSMVILTSTLTAGAAEEFTYIMKRLGRALVIGEVTSGGCQPPQTYHVDDTDLYLTI
PTARSVGAADGSSWEGVGVVPDVAVPAEAALTRAQEMLQHTPLRARRSPRLHGRRKGHHRQSQGRAGSLG
RNQGVVRPEVLTEAPSGQKRGLLQCG

7.1 *Bos taurus* RBP3 Module 1 cloning

Bos taurus RBP3 Module 1 protein sequence underlined

>NP_776589.1 retinol-binding protein 3 precursor [Bos taurus]
MVRKWALLLPMLLCGLTGPAHLFQPSLVLEMAQVLLDNYCFPENLMGMQGAIEQAIKSQEILSISDPQTL
AHVLTAGVQSSLNDPRLVISYEPSTLEAPPRAPAVTNLTLEEIIAGLQDGLRHEILEGNVGYLRVDDIPG
QEVMSKLRSFLVANVWRKLVNTSALVLDLRHCTGGHVSGIPYVISYLHPGSTVSHVDTVYDRPSNTTTEI
WTLPEALGEKYSADKDVVVLTSSRTGGVAEDIAYILKQMRRAIVVGERTVGGALNLQKLRVGQSDFFLTV
PVSRSLGPLGEGSQTWEGSGVLPCVGTPAEQALEKALAVLMLRRALPGVIQRLQEALREYYTLVDRVPAL
LSHLAAMDLSSVVSEDDLVTKLNAGLQAVSEDPRLQVQVVRPKEASSGPEEEAEEPPEAVPEVPEDEAVR
RALVDSVFQVSVLPGNVGYLRFDSFADASVLEVLGPYILHQVWEPLQDTEHLIMDLRQNPGGPSSAVPLL
LSYFQSPDASPVRLFSTYDRRTNITREHFSQTELLGRPYGTQRGVYLLTSHRTATAAEELAFLMQSLGWA
TLVGEITAGSLLHTHTVSLLETPEGGLALTVPVLTFIDNHGECWLGGGVVPDAIVLAEEALDRAQEVLEF
HRSLGELVEGTGRLLEAHYARPEVVGQMGALLRAKLAQGAYRTAVDLESLASQLTADLQEMSGDHRLLVF

HSPGEMVAEEAPPPPPVVPSPEELSYLIEALFKTEVLPGQLGYLRFDAMAELETVKAVGPQLVQLVWQKL
VDTAALVVDLRYNPGSYSTAVPLLCSYFFEAEPRRHLYSVFDRATSRVTEVWTLPHVTGQRYGSHKDLYV
LVSHTSGSAAEAFAHTMQDLQRATIIGEPTAGGALSVGIYQVGSSALYASMPTQMAMSASTGEAWDLAGV
EPDITVPMSVALSTARDIVTLRAKVPTVLQTAGKLVADNYASPELGVKMAAELSGLQSRYARVTSEAALA
ELLQADLQVLSGDPHLKTAHIPEDAKDRIPGIVPMQIPSPEVFEDLIKFSFHTNVLEGNVGYLRFDMFGD
CELLTQVSELLVEHVWKKIVHTDALIVDMRFNIGGPTSSISALCSYFFDEGPPILLDKIYNRPNNSVSEL
WTLSQLEGERYGSKKSMVILTSTLTAGAAEEFTYIMKRLGRALVIGEVTSGGCQPPQTYHVDDTDLYLTI
PTARSVGAADGSSWEGVGVVPDVAVPAEAALTRAQEMLQHTPLRARRSPRLHGRRKGHHRQSQGRAGSLG
RNQGVVRPEVLTEAPSGQKRGLLQCG

Forward primer 1

In bold restriction site for BamH1

Underlined: portion annealing to the gene

5” TTT TTT **GGA TCC** gcg cac ctg ttc caa ccg agc 3”

Tm: 66°C.

Reverse primer 1

In bold restriction site for Xho1

In blue: stop codon

Underlined: portion annealing to the gene

5” TTT TTT **CTC GAG** CTA acg cag cat cag cac cgc cag 3”

Tm: 67°C.

Expected insert size: 912 bp

Expected protein size 32.9 kDa + 25.5 kDa (GST tag) = 58.4 kDa

7.2 *Bos taurus* RBP3 Module 2 cloning

Bos taurus RBP3 Module 2 protein sequence underlined

>NP_776589.1 retinol-binding protein 3 precursor [Bos taurus]
MVRKWALLLPMLLCGLTGPAHLFQPSLVLEMAQVLLDNYCFPENLMGMQGAIEQAIKSQEILSISDPQTL
AHVLTAGVQSSLNDPRLVISYEPSTLEAPPRAPAVTNLTLEEIIAGLQDGLRHEILEGNVGYLRVDDIPG
QEVMSKLRSFLVANVWRKLVNTSALVLDLRHCTGGHVSGIPYVISYLHPGSTVSHVDTVYDRPSNTTTEI
WTLPEALGEKYSADKDVVVLTSSRTGGVAEDIAYILKQMRRAIVVGERTVGGALNLQKLRVGQSDFFLTV
PVSRSLGPLGEGSQTWEGSGVLPCVGTPAEQALEKALAVLMLRRALPGVIQRLQEALREYYTLVDRVPAL

LSHLAAMDLSSVVSEDDLVTKLNAGLQAVSEDPRLQVQVVRPKEASSGPEEEAEEPPEAVPEVPEDEAVR
RALVDSVFQVSVLPGNVGYLRFDSFADASVLEVLGPYILHQVWEPLQDTEHLIMDLRQNPGGPSSAVPLL
LSYFQSPDASPVRLFSTYDRRTNITREHFSQTELLGRPYGTQRGVYLLTSHRTATAAEELAFLMQSLGWA
TLVGEITAGSLLHTHTVSLLETPEGGLALTVPVLTFIDNHGECWLGGGVVPDAIVLAEEALDRAQEVLEF
HRSLGELVEGTGRLLEAHYARPEVVGQMGALLRAKLAQGAYRTAVDLESLASQLTADLQEMSGDHRLLVF
HSPGEMVAEEAPPPPPVVPSPEELSYLIEALFKTEVLPGQLGYLRFDAMAELETVKAVGPQLVQLVWQKL
VDTAALVVDLRYNPGSYSTAVPLLCSYFFEAEPRRHLYSVFDRATSRVTEVWTLPHVTGQRYGSHKDLYV
LVSHTSGSAAEAFAHTMQDLQRATIIGEPTAGGALSVGIYQVGSSALYASMPTQMAMSASTGEAWDLAGV
EPDITVPMSVALSTARDIVTLRAKVPTVLQTAGKLVADNYASPELGVKMAAELSGLQSRYARVTSEAALA
ELLQADLQVLSGDPHLKTAHIPEDAKDRIPGIVPMQIPSPEVFEDLIKFSFHTNVLEGNVGYLRFDMFGD
CELLTQVSELLVEHVWKKIVHTDALIVDMRFNIGGPTSSISALCSYFFDEGPPILLDKIYNRPNNSVSEL
WTLSQLEGERYGSKKSMVILTSTLTAGAAEEFTYIMKRLGRALVIGEVTSGGCQPPQTYHVDDTDLYLTI
PTARSVGAADGSSWEGVGVVPDVAVPAEAALTRAQEMLQHTPLRARRSPRLHGRRKGHHRQSQGRAGSLG
RNQGVVRPEVLTEAPSGQKRGLLQCG

Forward primer 2

In bold restriction site for BamH1

Underlined: portion annealing to the gene

In light blue: nucleotides mutated to prevent hairpin formation

5” TTT TTT **GGA TCC** gca gtg ctg atg ctt cgt cg 3”

Tm: 61°C.

Reverse primer 2

In bold restriction site for Xho1

In blue: stop codon

In green: portion annealing to the gene

5” TTT TTT **CTC GAG** CTA acg gtg aaa ctc cag cac ttc ctg c 3”

Tm: 65°C.

Expected insert size: 945 bp

Expected protein size 34.58 kDa + 25.5 kDa (GST tag) = 60.08 kDa

7.3 *Bos taurus* RBP3 Module 3 cloning

Bos taurus RBP3 Module 3 protein sequence underlined

>NP_776589.1 retinol-binding protein 3 precursor [Bos taurus]
MVRKWALLLPMLLCGLTGPAHLFQPSLVLEMAQVLLDNYCFPENLMGMQGAIEQAIKSQEILSISDPQTL
AHVLTAGVQSSLNDPRLVISYEPSTLEAPPRAPAVTNLTLEEIIAGLQDGLRHEILEGNVGYLRVDDIPG
QEVMSKLRSFLVANVWRKLVNTSALVLDLRHCTGGHVSGIPYVISYLHPGSTVSHVDTVYDRPSNTTTEI
WTLPEALGEKYSADKDVVVLTSSRTGGVAEDIAYILKQMRRAIVVGERTVGGALNLQKLRVGQSDFFLTV
PVSRSLGPLGEGSQTWEGSGVLPCVGTPAEQALEKALAVLMLRRALPGVIQRLQEALREYYTLVDRVPAL
LSHLAAMDLSSVVSEDDLVTKLNAGLQAVSEDPRLQVQVVRPKEASSGPEEEAEEPPEAVPEVPEDEAVR
RALVDSVFQVSVLPGNVGYLRFDSFADASVLEVLGPYILHQVWEPLQDTEHLIMDLRQNPGGPSSAVPLL
LSYFQSPDASPVRLFSTYDRRTNITREHFSQTELLGRPYGTQRGVYLLTSHRTATAAEELAFLMQSLGWA
TLVGEITAGSLLHTHTVSLLETPEGGLALTVPVLTFIDNHGECWLGGGVVPDAIVLAEEALDRAQEVLEF
HRSLGELVEGTGRLLEAHYARPEVVGQMGALLRAKLAQGAYRTAVDLESLASQLTADLQEMSGDHRLLVF
HSPGEMVAEEAPPPPPVVPSPEELSYLIEALFKTEVLPGQLGYLRFDAMAELETVKAVGPQLVQLVWQKL
VDTAALVVDLRYNPGSYSTAVPLLCSYFFEAEPRRHLYSVFDRATSRVTEVWTLPHVTGQRYGSHKDLYV
LVSHTSGSAAEAFAHTMQDLQRATIIGEPTAGGALSVGIYQVGSSALYASMPTQMAMSASTGEAWDLAGV
EPDITVPMSVALSTARDIVTLRAKVPTVLQTAGKLVADNYASPELGVKMAAELSGLQSRYARVTSEAALA
ELLQADLQVLSGDPHLKTAHIPEDAKDRIPGIVPMQIPSPEVFEDLIKFSFHTNVLEGNVGYLRFDMFGD
CELLTQVSELLVEHVWKKIVHTDALIVDMRFNIGGPTSSISALCSYFFDEGPPILLDKIYNRPNNSVSEL
WTLSQLEGERYGSKKSMVILTSTLTAGAAEEFTYIMKRLGRALVIGEVTSGGCQPPQTYHVDDTDLYLTI
PTARSVGAADGSSWEGVGVVPDVAVPAEAALTRAQEMLQHTPLRARRSPRLHGRRKGHHRQSQGRAGSLG
RNQGVVRPEVLTEAPSGQKRGLLQCG

Forward primer 3

In bold restriction site for BamH1

Underlined: portion annealing to the gene

5” TTT TTT **GGA TCC** ttt ttt gga tcc cgt agc ctg ggt gaa ctg gtt gag g 3”

Tm: 66°C.

Reverse primer 3

In bold restriction site for Xho1

In blue: stop codon

Underlined: portion annealing to the gene

5” TTT TTT **CTCGAG** CTA cac ctt cgc acg cag ggt aac aat gtc 3”

Tm: 66°C.

Expected insert size: 912 bp

Expected protein size 32.83 kDa + 25.5 kDa (GST tag) = 58.33 kDa

7.4 *Bos taurus* RBP3 Module 4 cloning

Bos taurus RBP3 Module 4 protein sequence underlined

>NP_776589.1 retinol-binding protein 3 precursor [Bos taurus]
MVRKWALLLPMLLCGLTGPAHLFQPSLVLEMAQVLLDNYCFPENLMGMQGAIEQAIKSQEILSISDPQTL
AHVLTAGVQSSLNDPRLVISYEPSTLEAPPRAPAVTNLTLEEIIAGLQDGLRHEILEGNVGYLRVDDIPG
QEVMSKLRSFLVANVWRKLVNTSALVLDLRHCTGGHVSGIPYVISYLHPGSTVSHVDTVYDRPSNTTTEI
WTLPEALGEKYSADKDVVVLTSSRTGGVAEDIAYILKQMRRAIVVGERTVGGALNLQKLRVGQSDFFLTV
PVSRSLGPLGEGSQTWEGSGVLPCVGTPAEQALEKALAVLMLRRALPGVIQRLQEALREYYTLVDRVPAL
LSHLAAMDLSSVVSEDDLVTKLNAGLQAVSEDPRLQVQVVRPKEASSGPEEEAEEPPEAVPEVPEDEAVR
RALVDSVFQVSVLPGNVGYLRFDSFADASVLEVLGPYILHQVWEPLQDTEHLIMDLRQNPGGPSSAVPLL
LSYFQSPDASPVRLFSTYDRRTNITREHFSQTELLGRPYGTQRGVYLLTSHRTATAAEELAFLMQSLGWA
TLVGEITAGSLLHTHTVSLLETPEGGLALTVPVLTFIDNHGECWLGGGVVPDAIVLAEEALDRAQEVLEF
HRSLGELVEGTGRLLEAHYARPEVVGQMGALLRAKLAQGAYRTAVDLESLASQLTADLQEMSGDHRLLVF
HSPGEMVAEEAPPPPPVVPSPEELSYLIEALFKTEVLPGQLGYLRFDAMAELETVKAVGPQLVQLVWQKL
VDTAALVVDLRYNPGSYSTAVPLLCSYFFEAEPRRHLYSVFDRATSRVTEVWTLPHVTGQRYGSHKDLYV
LVSHTSGSAAEAFAHTMQDLQRATIIGEPTAGGALSVGIYQVGSSALYASMPTQMAMSASTGEAWDLAGV
EPDITVPMSVALSTARDIVTLRAKVPTVLQTAGKLVADNYASPELGVKMAAELSGLQSRYARVTSEAALA
ELLQADLQVLSGDPHLKTAHIPEDAKDRIPGIVPMQIPSPEVFEDLIKFSFHTNVLEGNVGYLRFDMFGD
CELLTQVSELLVEHVWKKIVHTDALIVDMRFNIGGPTSSISALCSYFFDEGPPILLDKIYNRPNNSVSEL
WTLSQLEGERYGSKKSMVILTSTLTAGAAEEFTYIMKRLGRALVIGEVTSGGCQPPQTYHVDDTDLYLTI
PTARSVGAADGSSWEGVGVVPDVAVPAEAALTRAQEMLQHTPLRARRSPRLHGRRKGHHRQSQGRAGSLG
RNQGVVRPEVLTEAPSGQKRGLLQCG

Forward primer 4

In bold restriction site for BamH1

Underlined: portion annealing to the gene

5” TTT TTT **GGA TCC** cgt gcg aag gtg ccg acc 3”

Tm: 65°C.

Reverse primer 4

In bold restriction site for Xho1

In blue: stop codon

Underlined: portion annealing to the gene

5” TTT TTT **CTC GAG** CTA cgg ggt atg ttg cag cat ctc ctg 3”

Tm: 64°C.

Expected insert size: 906 bp

Expected protein size 32.83 kDa + 25.5 kDa (GST tag) = 58.33 kDa

7.5 *Bos taurus* RBP3 tandem Modules M1M2 cloning

Bos taurus RBP3 tandem Modules M1M2 protein sequence underlined

>NP_776589.1 retinol-binding protein 3 precursor [Bos taurus]
MVRKWALLLPMLLCGLTGPAHLFQPSLVLEMAQVLLDNYCFPENLMGMQGAIEQAIKSQEILSISDPQTL
AHVLTAGVQSSLNDPRLVISYEPSTLEAPPRAPAVTNLTLEEIIAGLQDGLRHEILEGNVGYLRVDDIPG
QEVMSKLRSFLVANVWRKLVNTSALVLDLRHCTGGHVSGIPYVISYLHPGSTVSHVDTVYDRPSNTTTEI
WTLPEALGEKYSADKDVVVLTSSRTGGVAEDIAYILKQMRRAIVVGERTVGGALNLQKLRVGQSDFFLTV
PVSRSLGPLGEGSQTWEGSGVLPCVGTPAEQALEKALAVLMLRRALPGVIQRLQEALREYYTLVDRVPAL
LSHLAAMDLSSVVSEDDLVTKLNAGLQAVSEDPRLQVQVVRPKEASSGPEEEAEEPPEAVPEVPEDEAVR
RALVDSVFQVSVLPGNVGYLRFDSFADASVLEVLGPYILHQVWEPLQDTEHLIMDLRQNPGGPSSAVPLL
LSYFQSPDASPVRLFSTYDRRTNITREHFSQTELLGRPYGTQRGVYLLTSHRTATAAEELAFLMQSLGWA
TLVGEITAGSLLHTHTVSLLETPEGGLALTVPVLTFIDNHGECWLGGGVVPDAIVLAEEALDRAQEVLEF
HRSLGELVEGTGRLLEAHYARPEVVGQMGALLRAKLAQGAYRTAVDLESLASQLTADLQEMSGDHRLLVF
HSPGEMVAEEAPPPPPVVPSPEELSYLIEALFKTEVLPGQLGYLRFDAMAELETVKAVGPQLVQLVWQKL
VDTAALVVDLRYNPGSYSTAVPLLCSYFFEAEPRRHLYSVFDRATSRVTEVWTLPHVTGQRYGSHKDLYV
LVSHTSGSAAEAFAHTMQDLQRATIIGEPTAGGALSVGIYQVGSSALYASMPTQMAMSASTGEAWDLAGV
EPDITVPMSVALSTARDIVTLRAKVPTVLQTAGKLVADNYASPELGVKMAAELSGLQSRYARVTSEAALA
ELLQADLQVLSGDPHLKTAHIPEDAKDRIPGIVPMQIPSPEVFEDLIKFSFHTNVLEGNVGYLRFDMFGD
CELLTQVSELLVEHVWKKIVHTDALIVDMRFNIGGPTSSISALCSYFFDEGPPILLDKIYNRPNNSVSEL
WTLSQLEGERYGSKKSMVILTSTLTAGAAEEFTYIMKRLGRALVIGEVTSGGCQPPQTYHVDDTDLYLTI
PTARSVGAADGSSWEGVGVVPDVAVPAEAALTRAQEMLQHTPLRARRSPRLHGRRKGHHRQSQGRAGSLG
RNQGVVRPEVLTEAPSGQKRGLLQCG

Forward primer 1

In bold restriction site for BamH1

Underlined: portion annealing to the gene

5” TTT TTT **GGA TCC** gcg cac ctg ttc caa ccg agc 3”

Tm: 66°C.

Reverse primer 2

In bold restriction site for Xho1

In blue: stop codon

Underlined: portion annealing to the gene

5” TTT TTT **CTC GAG** CTA acg gtg aaa ctc cag cac ttc ctg c 3”

Tm: 65°C.

Expected insert size: 1839 bp

Expected protein size 66.7 kDa + 25.5 kDa (GST tag) = 92.2 kDa

7.6 *Bos taurus* RBP3 tandem Modules M2M3 cloning

Bos taurus RBP3 tandem Modules M2M3 protein sequence underlined

>NP_776589.1 retinol-binding protein 3 precursor [Bos taurus]
MVRKWALLLPMLLCGLTGPAHLFQPSLVLEMAQVLLDNYCFPENLMGMQGAIEQAIKSQEILSISDPQTL
AHVLTAGVQSSLNDPRLVISYEPSTLEAPPRAPAVTNLTLEEIIAGLQDGLRHEILEGNVGYLRVDDIPG
QEVMSKLRSFLVANVWRKLVNTSALVLDLRHCTGGHVSGIPYVISYLHPGSTVSHVDTVYDRPSNTTTEI
WTLPEALGEKYSADKDVVVLTSSRTGGVAEDIAYILKQMRRAIVVGERTVGGALNLQKLRVGQSDFFLTV
PVSRSLGPLGEGSQTWEGSGVLPCVGTPAEQALEKALAVLMLRRALPGVIQRLQEALREYYTLVDRVPAL
LSHLAAMDLSSVVSEDDLVTKLNAGLQAVSEDPRLQVQVVRPKEASSGPEEEAEEPPEAVPEVPEDEAVR
RALVDSVFQVSVLPGNVGYLRFDSFADASVLEVLGPYILHQVWEPLQDTEHLIMDLRQNPGGPSSAVPLL
LSYFQSPDASPVRLFSTYDRRTNITREHFSQTELLGRPYGTQRGVYLLTSHRTATAAEELAFLMQSLGWA
TLVGEITAGSLLHTHTVSLLETPEGGLALTVPVLTFIDNHGECWLGGGVVPDAIVLAEEALDRAQEVLEF
HRSLGELVEGTGRLLEAHYARPEVVGQMGALLRAKLAQGAYRTAVDLESLASQLTADLQEMSGDHRLLVF
HSPGEMVAEEAPPPPPVVPSPEELSYLIEALFKTEVLPGQLGYLRFDAMAELETVKAVGPQLVQLVWQKL
VDTAALVVDLRYNPGSYSTAVPLLCSYFFEAEPRRHLYSVFDRATSRVTEVWTLPHVTGQRYGSHKDLYV
LVSHTSGSAAEAFAHTMQDLQRATIIGEPTAGGALSVGIYQVGSSALYASMPTQMAMSASTGEAWDLAGV
EPDITVPMSVALSTARDIVTLRAKVPTVLQTAGKLVADNYASPELGVKMAAELSGLQSRYARVTSEAALA
ELLQADLQVLSGDPHLKTAHIPEDAKDRIPGIVPMQIPSPEVFEDLIKFSFHTNVLEGNVGYLRFDMFGD
CELLTQVSELLVEHVWKKIVHTDALIVDMRFNIGGPTSSISALCSYFFDEGPPILLDKIYNRPNNSVSEL
WTLSQLEGERYGSKKSMVILTSTLTAGAAEEFTYIMKRLGRALVIGEVTSGGCQPPQTYHVDDTDLYLTI
PTARSVGAADGSSWEGVGVVPDVAVPAEAALTRAQEMLQHTPLRARRSPRLHGRRKGHHRQSQGRAGSLG
RNQGVVRPEVLTEAPSGQKRGLLQCG

Forward primer 2

In bold restriction site for BamH1

Underlined: portion annealing to the gene

In light blue: nucleotides mutated to prevent hairpin formation

5” TTT TTT **GGA TCC** gca gtg ctg atg ctt cgt cg 3”

Tm: 61°C.

Reverse primer 3

In bold restriction site for Xho1

In blue: stop codon

Underlined: portion annealing to the gene

5” TTT TTT **CTCGAG** CTA cac ctt cgc acg cag ggt aac aat gtc 3”

Tm: 66°C.

Expected insert size: 1839 bp

Expected protein size 67.2 kDa + 25.5 kDa (GST tag) = 92.7 kDa

7.7 *Bos taurus* RBP3 tandem Modules M3M4 cloning

Bos taurus RBP3 Module 3 protein sequence underlined

>NP_776589.1 retinol-binding protein 3 precursor [Bos taurus]
MVRKWALLLPMLLCGLTGPAHLFQPSLVLEMAQVLLDNYCFPENLMGMQGAIEQAIKSQEILSISDPQTL
AHVLTAGVQSSLNDPRLVISYEPSTLEAPPRAPAVTNLTLEEIIAGLQDGLRHEILEGNVGYLRVDDIPG
QEVMSKLRSFLVANVWRKLVNTSALVLDLRHCTGGHVSGIPYVISYLHPGSTVSHVDTVYDRPSNTTTEI
WTLPEALGEKYSADKDVVVLTSSRTGGVAEDIAYILKQMRRAIVVGERTVGGALNLQKLRVGQSDFFLTV
PVSRSLGPLGEGSQTWEGSGVLPCVGTPAEQALEKALAVLMLRRALPGVIQRLQEALREYYTLVDRVPAL
LSHLAAMDLSSVVSEDDLVTKLNAGLQAVSEDPRLQVQVVRPKEASSGPEEEAEEPPEAVPEVPEDEAVR
RALVDSVFQVSVLPGNVGYLRFDSFADASVLEVLGPYILHQVWEPLQDTEHLIMDLRQNPGGPSSAVPLL
LSYFQSPDASPVRLFSTYDRRTNITREHFSQTELLGRPYGTQRGVYLLTSHRTATAAEELAFLMQSLGWA
TLVGEITAGSLLHTHTVSLLETPEGGLALTVPVLTFIDNHGECWLGGGVVPDAIVLAEEALDRAQEVLEF
HRSLGELVEGTGRLLEAHYARPEVVGQMGALLRAKLAQGAYRTAVDLESLASQLTADLQEMSGDHRLLVF
HSPGEMVAEEAPPPPPVVPSPEELSYLIEALFKTEVLPGQLGYLRFDAMAELETVKAVGPQLVQLVWQKL
VDTAALVVDLRYNPGSYSTAVPLLCSYFFEAEPRRHLYSVFDRATSRVTEVWTLPHVTGQRYGSHKDLYV
LVSHTSGSAAEAFAHTMQDLQRATIIGEPTAGGALSVGIYQVGSSALYASMPTQMAMSASTGEAWDLAGV
EPDITVPMSVALSTARDIVTLRAKVPTVLQTAGKLVADNYASPELGVKMAAELSGLQSRYARVTSEAALA
ELLQADLQVLSGDPHLKTAHIPEDAKDRIPGIVPMQIPSPEVFEDLIKFSFHTNVLEGNVGYLRFDMFGD
CELLTQVSELLVEHVWKKIVHTDALIVDMRFNIGGPTSSISALCSYFFDEGPPILLDKIYNRPNNSVSEL
WTLSQLEGERYGSKKSMVILTSTLTAGAAEEFTYIMKRLGRALVIGEVTSGGCQPPQTYHVDDTDLYLTI
PTARSVGAADGSSWEGVGVVPDVAVPAEAALTRAQEMLQHTPLRARRSPRLHGRRKGHHRQSQGRAGSLG
RNQGVVRPEVLTEAPSGQKRGLLQCG

Forward primer 3

In bold restriction site for BamH1

Underlined: portion annealing to the gene

5” TTT TTT **GGA TCC** ttt ttt gga tcc cgt agc ctg ggt gaa ctg gtt gag g 3”

Tm: 66°C.

Reverse primer 4

In bold restriction site for Xho1

In blue: stop codon

Underlined: portion annealing to the gene

5” TTT TTT **CTC GAG** CTA cgg ggt atg ttg cag cat ctc ctg 3”

Tm: 64°C.

Expected insert size: 1803 bp

Expected protein size 65.06 kDa + 25.5 kDa (GST tag) = 90.56 kDa

8 Appendix 2

OCT is a powerful technique that allows the detection of changes in photoreceptor morphology. Upon light stimulus, photoreceptors undergo a fast elongation and shrinkage process along the axial direction (Lu et al., 2018; Pandiyan et al., 2022).

PDE6 is a peripheral membrane protein localized in the membrane of photoreceptor's discs, it presents two catalytic subunits of 100 kDa each (Guo et al., 2010; Cote et al., 2022). Light activation of PDE6 induces a conformational change leading to an extension of PDE6 by up to 30 Å (Gulati and Palczewski, 2023).

Taking into account that *Mus musculus* ROS contain about 900 discs, and that PDE6 can elongate up to 30 Å, a simple multiplication of the two values can explain the photoreceptor extension upon light stimulus, leading to the hypothesis that PDE6 conformational changes may be responsible for photoreceptor extension (Gulati and Palczewski, 2023; Tomczewski et al., 2025).

We have used several techniques to study the morphology of the photoreceptors and their change following light stimulus and PDE6 activation.

8.1 Methods

8.1.1 Retinal samples for TEM

Eyes were obtained through enucleation of Wild-Type (WT) mice, subjected to ultrathin sectioning followed by staining with contrast reagents. Imaging was performed at the Nencki Institute of Experimental Biology in Warsaw.

8.1.2 ROS extraction and grids preparation

Eyes were obtained through enucleation of Wild-Type (WT) mice and quickly placed in pre-cooled Kuhn's buffer (1 mM 2, 0.1 mM Mg(OAc) EDTA, 67 mM KH_2PO_4, pH 7.0, 1 mM DTT) at 4°C (Salom et al., 2013). After removal of the cornea, lens, and vitreous; the retina and the RPE were detached. After cutting the optical nerve, the retina was transferred to a microcentrifuge tube and vigorously vortexed to allow the detachment of ROS. The sample was centrifuged for 60 seconds at 100 RCF at 4°C, and the supernatant was then available for plunge-freezing (Pöge et al., 2021). In total, 3 µl of ROS samples were blotted on a Quantifoil Cu 200 mesh, holycarbon film R2/1 by plunge-freezing in liquid ethane using Vitroblot.

8.1.3 Cryo-Soft X-Ray Tomography

After the addition of fiducials, the grids prepared according to the procedure described in 8.1.2 were used for data collection through Cryo Soft X-Ray Tomography (CryoSXT) at Diamond Light Source (Oxfordshire UK).

8.1.4 CryoET

The grids prepared according to the procedure described in 8.1.2 were used for lamellas preparation with cryo-FIB milling, the grids were then analysed with a Titan Krios 300 kv at CEITEC (Brno, Czech Republic).

8.2 Results

TEM represented a powerful tool for structural studies, providing structural information relative to the disc organization in the OS. The high resolution allows for the detection of inter-discs' distance changes, possibly caused by PDE6 conformational changes; however, it is necessary to take into account the deviation from the native state imposed by chemical fixation and dehydration (Weston et al., 2009) (Figure 8.1). Images have been collected for dark and light adapted ROS, and also in the presence or absence of PDE inhibitors.

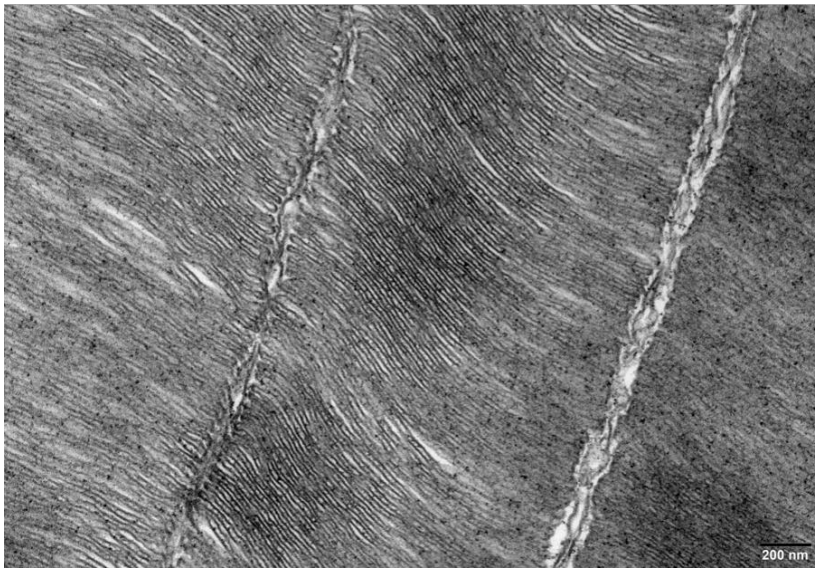

Figure 8.1: Picture of Mus musculus ROS obtained through TEM, showing the discs stacking.

CryoSXT allows for investigating the internal organization of the OS discs in a near native state; however, the low resolution does not allow for studying the minimal morphological changes caused by the small movements of the molecular component (Sokke Rudraiah et al., 2025) (Figure 8.2).

Figure 8.2: Picture of Mus musculus ROS obtained through CryoSXT, showing the discs stacking.

More recently, CryoET has emerged as a powerful tool for structural cell biology. If higher resolution is needed in order to gain details relative to the molecular component driving the morphological changes in photoreceptors, CryoET can be considered as the elective technique since it does not require chemical treatment of the sample, thus the morphology of the cell is preserved in a near native state (Young and Villa, 2023) (Figure 8.3).

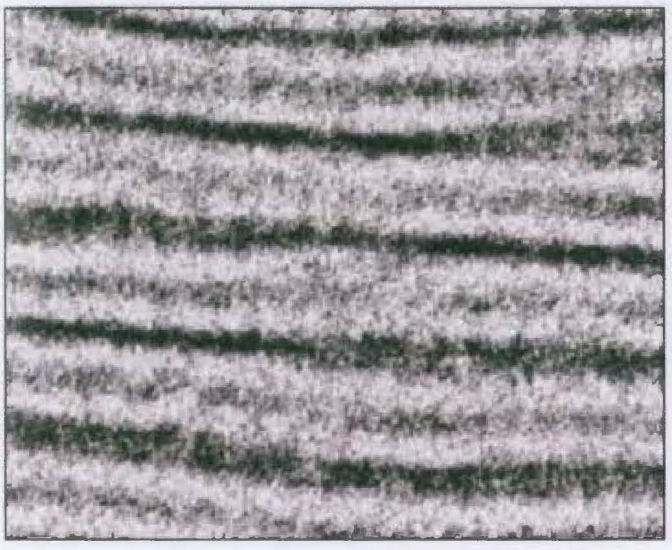

Figure 8.3: Picture of Mus musculus ROS obtained through CryoET showing discs' membranes.

These preliminary results shows that the above mentioned techniques can be used to investigate the morphological changes of photoreceptors; however, they present advantages and disasvantages, therefore they should be regarded as complementary. Their combination would increase the reliability of future results.